Nucleotide regulation of AMP-activated protein kinase

Elizabeth Ann Underwood

A thesis submitted for the degree of Doctor of Philosophy
October 2012

Division of Molecular Structure,
MRC National Institute for Medical Research, London

Division of Biosciences,
UCL, London

I, Elizabeth Ann Underwood, confirm that the work presented in this thesis is my own. Where information has been derived from other sources, I confirm that this has been indicated in the thesis.

Abstract

AMP-activated protein kinase (AMPK) acts as the cell's master energy regulator, sensing and maintaining the concentration of ATP in a narrow range irrespective of energy demand. This kinase has received significant attention as a drug-target for type-2 diabetes, obesity and cancer. Although historically the AMP:ATP ratio has been considered the signal for AMPK activation, we have recently demonstrated that ADP is likely to be an important physiological regulator of AMPK in both mammals and yeast.

The binding of adenine nucleotides and staurosporine to the full-length $\alpha 1\beta 1\gamma 1$ heterotrimer, both phosphorylated and unphosphorylated, is described. Binding was monitored through displacement of fluorescently labelled nucleotides (coumarin-AXP), either via direct coumarin excitation or Forster Resonance Energy Transfer (FRET) in which tryptophan residues were excited. Mg.ATP was found to bind more weakly than ADP, a feature which is likely key to AMPK regulation.

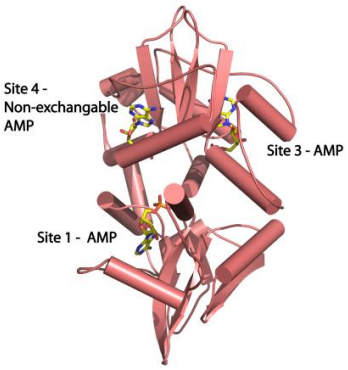

A β-Nicotinamide adenine dinucleotide (NADH) coupled spectrophotometric assay was used to monitor AMPK kinetics and its regulation by nucleotides. NADH binds at Site-1, within the γ-subunit (pictured right), and competes with allosteric activation by AMP, but not the protective effect of AMP/ADP against αT172 dephosphorylation. Therefore it seems that AMP binding at Site-1 mediates allostery whilst AMP/ADP binding at Site-3 affords protection against dephosphorylation. In order to explore this idea further, AXP binding constants were used to model binding site occupancies over the concentration ranges used *in vitro.* The modelling demonstrates that, *in vitro,* Site-1 is occupied by AMP and Site-3 by AMP/ADP in a manner consistent with their assigned regulatory functions. This modelling study was also extended to consider *in vivo* binding site occupancy.

It was important to verify that coumarin-ADP bound in a homologous fashion to ADP, specifically in the same exchangeable binding pockets. X-ray crystallography was used to determine the structure of a truncated form of AMPK in complex with coumarin-ADP. This structure is compared to an ADP-bound form.

SNF1 is the *Saccharomyces cerevisiae* AMPK ortholog. The binding of nucleotides to SNF1, and its regulation by ADP, was also characterised. As with the mammalian enzyme AXP bound at two exchangeable sites, and interacted with Mg.ATP more weakly than ADP.

Acknowledgments

First, I must thank Steve Martin without whom this thesis, and the work it contains, would literally not have been possible. His support, guidance and friendship over the past three years has been invaluable. I could not have wished for a better mentor.

I must also thank Steve Gamblin for giving me the opportunity to work in his lab, for his help and direction, and for giving me so much freedom during my time at the NIMR.

I extend this thanks to the rest of the Gamblin ~~empire~~ lab, past and present. Especially Bing Xiao, Matt Sanders and Richard Heath with whom I have worked, in parallel, on AMPK. They have offered me a lot of practical advice, listened to my chattering, but perhaps most importantly, have become good friends.

To the members of Molecular Structure and Physical Biochemistry, the cohort of students that I started with (Dan, Darren, Leonard, Sorrel, Christina), those which have come and gone (Alice, Jo, Mateo, Laura, James, Aylin, Gem, Kat, Lucy), the people who periodically ask "so, how goes the science?" (Sarah, Sarah, Ross, Cath, Avneet, Julz, Kelly, Kate, Caroline, Jen) and anyone else that I temporarily forget; thank-you for being such good friends to me.

To my parents (Mike and Di) and brothers (Charles and Matt) I hope that you know how much your *favourite* daughter/sister loves you all, and how grateful I am for your support over the past 25 years (or at least the bits my younger brothers were around for).

Finally, thanks to those who were brave enough to proof-read my thesis (Smartin, Gamblin, Dave Carling and Matt), and to those who are just about to venture in. I owe you all a pint.

Cheers,
Lizzi (aka Bob)

October 2012

Publications

Work described in this thesis has been presented in the following publications:

Xiao, B.*, Sanders, M. J.*, Underwood, E.*, Heath, R.*, Mayer, F. V.*, Carmena, D., Jing, C., Walker, P. A., Eccleston, J. F., Haire, L. F., Saiu, P., Howell, S. A., Aasland, R., Martin, S. R., Carling, D., and Gamblin, S. J. (2011) **Structure of mammalian AMPK and its regulation by ADP**, *Nature 472*, 230-233.

(*1*)

Mayer, F. V.*, Heath, R.*, Underwood, E.*, Sanders, M. J.*, Carmena, D., McCartney, R. R., Leiper, F. C., Xiao, B., Jing, C., Walker, P. A., Haire, L. F., Ogrodowicz, R., Martin, S. R., Schmidt, M. C., Gamblin, S. J., and Carling, D. (2011) **ADP regulates SNF1, the Saccharomyces cerevisiae homolog of AMP-activated protein kinase**, *Cell Metabolism 14*, 707-714.

(*2*)

***** These authors contributed equally to the work.

Abbreviations

ACC	Acetyl-CoA Carboxylase
AD	Alzheimer's Disease
AICAR	Aminoimidazole-4-carboxamide ribotide
AID	Autoinhibitory domain
ADP	Adenosine Diphosphate
AID	Autoinhibitory Domain
Aq	Aqueous
AgRP	Agouti-Related Peptide
AMP	Adenosine Monophosphate
AMPK	Adenosine Monophosphate-activated Protein Kinase
ATP	Adenosine Triphosphate
AU	Absorbance Unit
CaMKKβ	Calmodulin-dependent protein Kinase Kinaseβ
CPT1	Carnitine palmitoyltransferase 1
CD	Circular Dichroism
CCD	Charge-Coupled Device
C-ADP	(7-diethylaminocoumarin-3-carbonylamino)-3'-deoxyadenosine 5'diphosphate
C-ATP	(7-diethylaminocoumarin-3-carbonylamino)-3'-deoxyadenosine 5'triphosphate
CBS	Cystathionine-β-synthase
CIDEA	Cell-death Inducing DFFA-like Effector A
CLC2	Chloride Channel 2
CNTF	Ciliary Neurotrophic Factor
COX2	Cyclooxygenase-2
CPT1	Carnitine Palmitoyltransferase 1
Cr	Creatine
CREB	cAMP Response Element-Binding *protein*
CRTC-1	cAMP-Regulated Transcriptional Co-activator-1
DLS	Dynamic Light Scattering
DNA	Deoxyribonucleic acid
DNP	2,4-dinitrophenol
DR	Dietary Restriction
DUB	Deubiquitinating enzymes
EDTA	Ethylenediaminetetraacetic acid
EF2	Elongation Factor 2
EM	Electron Microscopy
ER	Endoplasmic Reticulum
FABP	Fatty Acid Binding Protein
FAS	Fatty Acid Synthase
FAT	Fatty Acid Translocase
FRET	Förster Resonance Energy Transfer
GAP	Guanosine triphosphate Activating Protein

GBD	Glycogen Binding Domain
GLUT	Glucose Transporter
GP	Glycogen Phosphorylase
GPAT	Glycerol-3-phosphate acyl-transferase
GS	Glycogen Synthase
GSK-3	Glycogen Synthase Kinase 3
GST	Glutathione S-transferase
HDAC5	Histone Deacetylase 5
HNF-4α	Hepatic Nuclear Factor 4 α
HPLC	High Performance Liquid Chromatography
HSL	Hormone-Sensitive Lipase
HMGR	3-hydroxy-3-methyl-glutaryl-CoA reductase
IC	Inhibitory Concentration
IGF-1	Insulin-like Growth Factor-1
IMAC	Immobilised Metal ion Affinity Chromatography
IMPDH	IMP-dehydrogenase
IRS-1	Insulin Receptor Substrate-1
IPTG	Isopropyl β-D-1-thiogalactopyranoside
LB	Luria-Bertoni
LDH	Lactate Dehydrogenase
LKB1	Liver kinase B1
MCD	Malonyl-CoA Decarboxylase
MALLS	Multiangle Laser Light Scattering
MEF	Myocyte Enhancer Factor
MES	2-(N-morpholino)ethanesulfonic acid
MO25	Mouse protein 25
MPD	2-methyl-2,4-pentanediol
MRW	Mean Residue Weight
mTOR	Mammalian Target of Rapamycin
MW	Molecular Weight
NADH	Nicotinamide Adenine Dinucleotide
NADPH	Nicotinamide Adenine Dinucleotide Phosphate
nd	not determined
NE	Non-Exchangeable
NF$\kappa\beta$	Nuclear Factor kappa-light-chain-enhancer of activated B cells
NMR	Nuclear Magnetic Resonance
NPY	Neuropeptide Y
NRF	Nuclear Respiratory Factors
OD	Optical Density
PCr	Phosphocreatine
PDB	Protein Data Bank
PEG	Polyethylene Glycol
PEP	Phosphoenol Pyruvate

PFK2	Phosphofructose kinase-2
PGC-1 α	Proliferator-activated receptor gamma coactivator-1 α
PK	Pyruvate Kinase
PKA	Protein Kinase A
POMC	Proopiomelanocortin
PP2C	Protein Phosphatase 2C
RBS	Ribosome Binding Site
ROS	Reactive Oxygen Species
SAK1	SNF1 Activating Kinase-1
SD	Standard Deviation
SDS-PAGE	Sodium Dodecyl Sulfate-Polyacrylamide Gel Electrophoresis
SEC	Size-Exclusion Chromatography
SHREBP1c	Sterol Regulatory Element Binding Protein 1c
SNF1	Sucrose-NonFermenting 1
SNP	Single Nucleotide Polymorphism
STRE	Stress Response Element
TCEP	Tris(2-carboxyethyl)phosphine
TLS	Translation, Libration and Screw
TSC1/TSC2	Tuberous Sclerosis 1/2 Complex
ULK1	Unc-51-Like Kinase
UV	Ultraviolet
WPWS	Wolff-Parkinson-White Syndrome
ZMP	AICAR 5'-monophosphate

Table of Contents

List of Figures

List of Tables

Chapter 1: Introduction

1.1 AMPK

AMP-activated protein kinase (AMPK) has frequently been dubbed 'the cellular fuel sensor' and has more recently been referred to as a 'whole-body energy gauge' (*3, 4*). Broadly speaking, AMPK is responsible for activating catabolic pathways and inhibiting anabolic systems during periods of metabolic stress. It is ubiquitously expressed throughout the body, activated by phosphorylation and catalytically active as a Ser/Thr kinase (Figure 1). It produces immediate effects through targeted phosphorylation of substrates such as acetyl-CoA Carboxylase (ACC) (*3*), and in the longer term downstream effectors of AMPK regulate transcription and progression through the cell cycle (*5*).

AMPK was first named in 1988, with reference to its most potent activator AMP. It previously appeared under various guises, including 3-hydroxy-3-methylglutaryl-CoA reductase (HMGR) kinase (*5*). Activation of AMPK via a phosphorylation cascade was amongst the first to be described.

AMPK is conserved throughout the entire eukaryotic kingdom, with homologues found in mammals, fungi and plants (*5*). Of particular note is the *Saccharomyces cerevisiae* ortholog, *s*ucrose-*n*on*f*ermenting 1 (SNF1). The study of SNF1 was important in isolating the upstream AMPK kinases, and in structural characterisation of the heterotrimeric complex. Convergence of the yeast and mammalian studies in 1994 marked the creation of the AMPK family (*6*).

AMPK is a heterotrimeric complex composed of a ~63kDa α catalytic subunit, a ~30kDa β scaffolding subunit and a regulatory 36-63kDa γ subunit (Figure 2). All three subunits, present in 1:1:1 ratio are required for stable complex formation. In mammals, there are two isoforms of α, two of β and three of γ, each encoded by a single gene, therefore a total of 12 different complexes are theoretically possible (*7*).

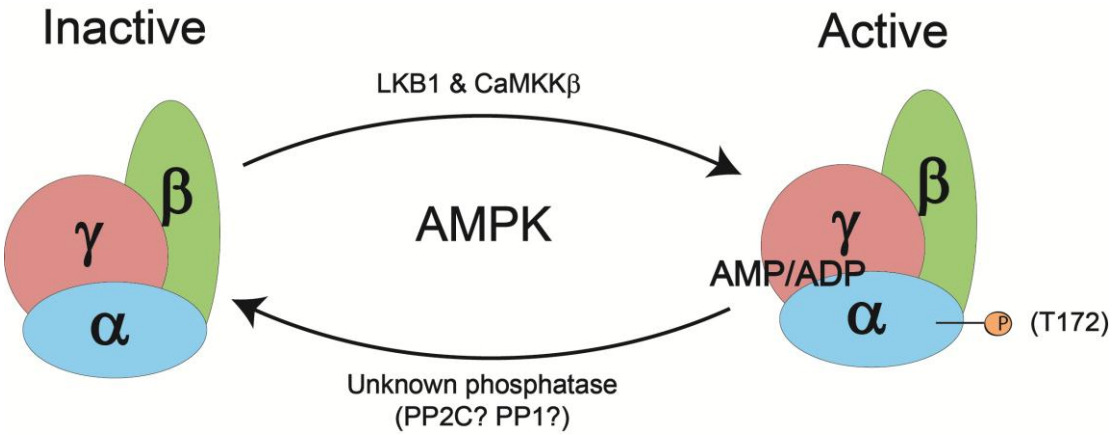

Figure 1: **AMPK operates as part of a futile cycle.**

Phosphorylation of the heterotrimeric AMPK by upstream kinases at αT172 results in an active kinase complex. Dephosphorylation by the relevant phosphatases returns the protein to an inactive state. Adenine nucleotides bind to the γ-subunit. AMP allosterically activates AMPK, whilst both AMP and ADP protect αT172 from dephosphorylation.

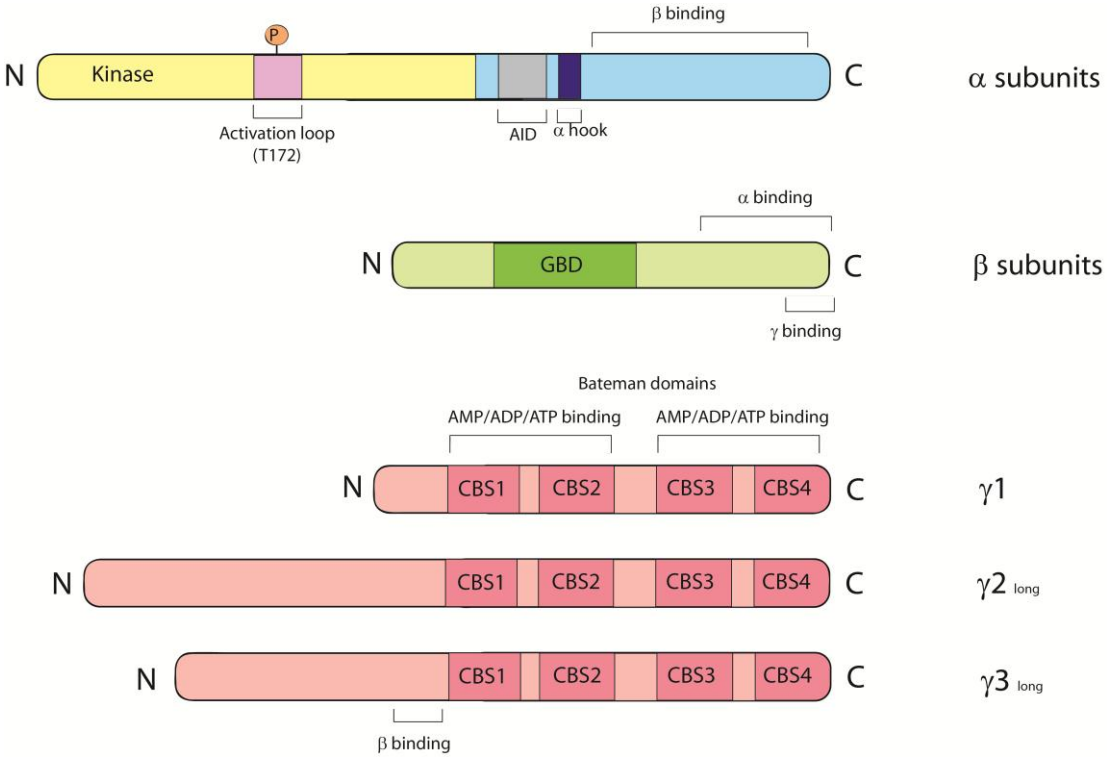

Figure 2: Domain schematic of AMPK subunits.

The mammalian isoforms of α1/α2 and β1/β2 are very similar and a general example for each is shown here. Abbreviations: AID: autoinhibitory domain, GBD: glycogen binding domain (also referred to as the carbohydrate binding module), CBS: cystathionine β-synthase domain.

Figure 3: Schematic diagram of AMPK activation and its effects on downstream targets. AMPK activation acts to replenish cellular ATP supplies, playing a central role as a regulator of both lipid and glucose metabolism and of protein levels, cell growth and turnover. Taken from www.cellsignal.com/reference/pathway/AMPK.

1.2 AMPK activity

Any metabolic stress which inhibits ATP production or which accelerates ATP consumption will lead to shifts in the cellular nucleotide ratios, and therefore to AMPK activation. AMPK acts to limit ATP consuming pathways and promote ATP producing pathways in order to restore ATP concentrations to basal levels during periods of cellular stress. Whole body genetic deletion of AMPK activity in mouse models results in embryonic lethality, highlighting the importance of this enzyme in mammals (*8*).

Numerous AMPK phosphorylation targets have been identified (Figure 3) which have far reaching effects throughout the cell. Here, the role of AMPK on carbohydrate metabolism, lipid metabolism, protein synthesis, cell growth and apoptosis are considered further.

1.2.1 Carbohydrate Metabolism

Glucose is the major cellular energy source in most tissues (although not in cardiac tissue), and glucose homeostasis is therefore regulated in a number of ways; the rate of glucose uptake from the blood, glycolytic rate, glycogen metabolism and through gluconeogenesis in the liver. AMPK regulates all of these processes and examples of each are given.

In addition to the glucose gradient, it is the expression of glucose transporters (GLUTs) and their localisation to cellular membranes which regulates the uptake of glucose from the blood. AMPK activity regulates glucose uptake in at least four ways:

1) In response to insulin signalling or energetic stress GLUT4 is translocated to the plasma membrane facilitating rapid glucose uptake (*9*). AMPK activity stimulates this translocation, predominantly in skeletal and cardiac muscle tissue, but perhaps also in adipocytes (*10-12*). AMPK's role is insulin independent, and it is therefore not involved

with maintaining glucose homeostasis through the classic regulatory pathway (*13, 14*). Although AMPK is activated in response to muscle contraction (see Section 1.5.3.3).

2) AMPK also affects glucose transportation via phosphorylation of Rab GTPases AS160 and TBC1D1 which associate with 14-3-3 proteins promoting GLUT4 vesicle recycling (*15, 16*).
3) AMPK phosphorylation of insulin receptor substrate-1 (IRS-1) on S789 prevents inhibitory phosphorylation of IRS-1 by JNK, IKK and S6 kinase. AMPK phosphorylation of IRS-1 also stimulates downstream activation of the Akt/AS160 pathway. Overall, this increases the sensitivity of the cell to an insulin stimulus, thereby increasing glucose uptake (*17, 18*).
4) AMPK indirectly increases transcription of the GLUT4 gene through phosphorylation of proliferator-activated receptor gamma coactivator-1 α (PGC-1α) and sequestering of histone deacetylase 5 (HDAC5) from the nucleus. This results in increased activity of the transcription factor, myocyte enhancer factor (MEF), known to upregulate the GLUT4 gene (*19, 20*).

Glycogen homeostasis is maintained by glycogen synthase (GS) which extends polymer chains and glycogen phosphorylase (GP) which breaks them down. AMPK directly phosphorylates GS causing inactivation and an acute drop in glycogen synthesis (*21*). Counter intuitively, chronic AMPK activation (via naturally occurring mutations or pharmacological treatment – Sections 1.3.4 and 1.5.2.3) actually increases glycogen synthesis, through increased glucose uptake and therefore production of glucose-6-phosphate, an allosteric activator of GS (*22*). This suggests that AMPK may have an inhibitory/activatory effect on glycogen synthesis dependent on the level of AMPK activation.

Glycolysis, a key metabolic step which sees glucose converted to pyruvate, is controlled by phosphofructokinase 2 (PFK2). AMPK phosphorylation of PFK2 S466 (cardiac and inducible isoforms only) causes increased production of fructose-2,6-diphosphate, an allosteric activator of PFK1, and ultimately an increase in the rate of glycolysis in cardiac tissue (*23, 24*). Through activation of PFK and increased glycolytic rate AMPK is key in mounting the cellular response to energetic stress, e.g. anaerobic exercise, anoxia and ischemia.
A recent proteomics screen identified 12 *in vitro* substrates of AMPK in the brain, many of which were related to glycolysis, although further investigation is required to understand the significance of this *in vivo* (*25*).

Gluconeogenesis is a metabolic pathway present in hepatocytes which produces glucose from non-carbohydrate carbon sources such as lactate and glycerol. It has been demonstrated in knock-out mouse models that AMPK activation in the liver inhibits gluconeogenesis and therefore reduces release of glucose into the blood. This effect is mediated through transcriptional regulation of gluconeogenic enzymes, for example;

1) Inhibition of the transcription factor hepatic nuclear factor 4α (HNF-4α) (*26-28*).
2) Phosphorylation of CREB coactivator CRTC2 resulting in export to the cytosol where it can no longer bind CREB and regulate transcription of gluconeogenic genes (*29-31*).

AMPK activation aims to increase glucose availability to stressed cells, thus increasing their fuel supplies and ultimately restoring the ATP concentration to basal levels. Clearance of glucose from the blood is an important goal of anti-type-2 diabetes drugs, suggesting that AMPK is a good candidate for treatment of this disorder.

1.2.2 Lipid Metabolism

Although carbohydrates are considered the cellular energy source of choice, in times of starvation lipid metabolism is important to maintain a consistent fuel supply to cells. The balance between carbohydrate and lipid metabolism is carefully controlled. AMPK influences the uptake and synthesis of fatty acids and mitochrondrial β-oxidation (the breakdown of fatty acids to acetyl-CoA).

The uptake of fatty acids into cells is mediated by fatty acid translocase (FAT/CD36) and fatty acid binding protein (FABP). Aminoimidazole-4-carboxamide ribotide (AICAR) is an AMPK activator; following its administration AMPK has been shown to stimulate fatty acid uptake, although the mechanism behind these effects (be it direct phosphorylation or transcriptional regulation) remains unclear (*32, 33*).

Following entry into the cell, fatty acids are converted to active fatty acyl-CoA which can either enter the mitochondrial β-oxidation pathway for conversion to acetyl-CoA, or be stored. ACC catalyses the conversion of acetyl-CoA to malonyl-CoA and was one of the first AMPK substrates to be identified (*34*). There are two isoforms of ACC, the cytosolic ACC1 and the mitochondrial ACC2, which are phosphorylated and therefore inhibited by AMPK at S80 and S221, respectively. Malonyl-CoA is a substrate for fatty acid synthesis, it is also an allosteric inhibitor of carnitine palmitoyltransferase 1 (CPT1) which regulates fatty acid transport into the mitochondria for oxidation. By inhibiting ACC, AMPK decreases malonyl-CoA inhibition of CPT1 and thus increases fatty acid breakdown in the mitochondria (*35*).

Malonyl-CoA concentrations are also regulated by malonyl-CoA decarboxylase (MCD). Increased MCD activity, regulated by AMPK phosphorylation, increases the rate of fatty acid oxidation (*36*). AMPK also negatively regulates the ACC and fatty acid synthase (FAS) genes, through down-regulation of the transcription factor SREBP1c (*37-40*). Additionally AMPK may directly phosphorylate and inactivate FAS (*41*).

AMPK stimulates mitochondrial biogenesis through regulation of transcription factors and co-activators including PGC-1α and nuclear respiratory factors (NRF). The mitochondria are the cellular location of fatty acid breakdown and oxidative respiration and it is therefore clear how increased mitochondrial capacity is beneficial in the restoration of cellular energy balance (*42*).

Triglycerides are important molecules in the storage and transportation of energy. AMPK activation has been shown to decrease both liver and plasma triglyceride levels in mouse models (*43*). AMPK directly inactivates *in vitro*:

1) Glycerol-3-phosphate acyl-transferase (GPAT), a rate limiting enzyme in the synthesis of triglycerides (*44*).
2) Hormone-sensitive lipase (HSL) which hydrolyses triglycerides to free fatty acids (*44*).

HMGR catalysis is the rate-limiting enzyme in cholesterol synthesis. Its inhibition is correlated with decreased ATP concentrations, an effect mediated by phosphorylation of HMGR S871 by AMPK (*45*). Phosphorylation is thought to disrupt the interface between HMGR and NADPH (*46*). HMGR was one of the first AMPK targets to be discovered (along with ACC) (*34*).

AMPK increases fatty acid uptake and breakdown, and reduces the activity of triglyceride and cholesterol synthesis pathways in response to metabolic stresses. Stimulation of these downstream effects is important in reversing the effects of obesity.

1.2.3 Protein Synthesis

The synthesis of proteins is an energetically costly process. When a cell is placed under metabolic stress AMPK acts to inhibit transcription/translation in various ways (summarised in Figure 4).

One central regulator of protein metabolism is the kinase mammalian target of rapamycin (mTOR). This enzyme promotes ribosome biogenesis and therefore increases the rate of translation through activation of the ribosomal S6 kinases (S6K1 and S6K2). mTOR also phosphorylates 4E-binding protein (4E-BP1) allowing formation of translation-initiation complexes (*47*). mTOR and AMPK have antagonistic activities, it is therefore unsurprising that AMPK inhibits the activation of mTOR (and therefore protein synthesis):

1) AMPK phosphorylates the tuberous sclerosis 1/2 complex (TSC1/TSC2), a guanosine triphosphate activating proteins (GAP), enhancing their activity. This inactivates Rheb GTPases which function to activate mTOR (*48*).
2) AMPK phosphorylation of the protein raptor causes it to bind 14-3-3 proteins, excluding it from the complex and inhibiting the activity of mTOR (*49*).

Elongation factor 2 (eEF-2) is responsible for the translocation of the peptidyl-tRNA complexes through the ribosome. AMPK inhibits protein synthesis through activation of eEF-2 kinase which goes on to inhibit eEF-2 activity (*50*).

Additionally, there are many documented cases of AMPK phosphorylation influencing the activity of transcription factors and their binding proteins, leading to decreases in mRNA production which will obviously affect the rate of protein synthesis. There are also reports of decreased RNA polymerase I activity through AMPK phosphorylation of proteins found in the transcription initiation complex (*51*).

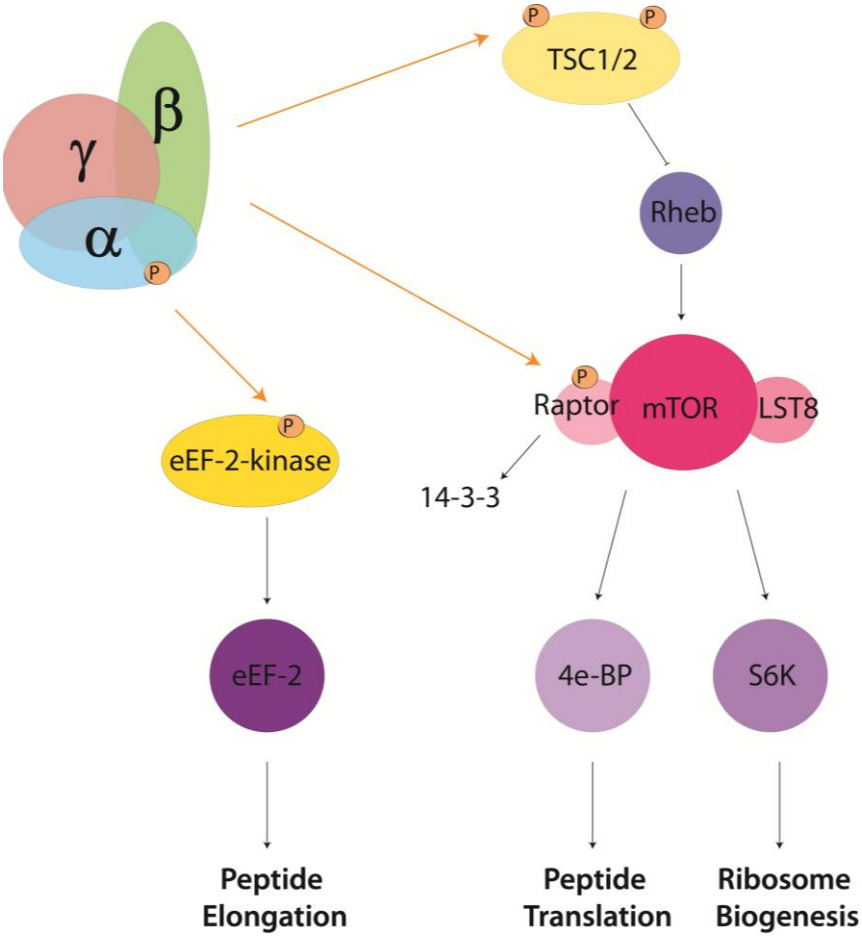

Figure 4: AMPK inhibition of protein synthesis.

1) AMPK activates eEF-2-kinase, resulting in inactivation of eEF-2 and translational processes. 2) AMPK phosphorylation of TSC1/2 inhibits Rheb, resulting in decreased activation of the mTOR complex, 3) AMPK phosphorylation of Raptor results in binding to 14-3-3 proteins and excludes it from the mTOR complex. Inhibition of the mTOR complex results in reduced peptide translation and ribosome biogenesis through 4e-BP and S6K (*46*). Orange arrows; AMPK phosphorylation

1.2.4 Cell Growth and Apoptosis

The balance between cell survival and cell death (apoptosis) is tightly controlled. AMPK activity is thought to have both pro- and anti-apoptotic effects in various tissues and in response to various signals, a number of examples are outlined here.

Pro-apoptotic:

1) In addition to its roles in protein metabolism mTOR has downstream anti-apoptotic effects through Ulk1. Therefore inhibition of mTOR activation by AMPK is pro-apoptotic.
2) Overactivation of AMPK via glutamate signalling in neuronal tissues results in apoptosis (*52, 53*).
3) AMPK stabilises p53, a major proapoptotic protein, via Ser15 phosphorylation (*54*).

Anti-apoptotic

1) In endothelial cells AMPK reduces reactive oxygen species (ROS), through increased expression of uncoupling protein 2, perhaps through AMPK regulation of PGC1α, and through suppression of NADPH oxidase (*55*).
2) Activation of AMPK α1, but not α2 decreased apoptosis through nuclear factor kappa-light-chain-enhancer of activated B cells (NF$\kappa\beta$) mediated transcription of B-cell lymphoma-2 (Bcl-2) and survivin in endothelial cells (*55*). Bcl-2 and survivin are anti-apoptotic factors, which inhibit entry into the caspase cascade.

Cell growth and proliferation are energetically costly; therefore AMPK acts to inhibit them directly.

1) Cells treated with low glucose or transfected with constitutively active AMPK are arrested in the G1/S phase through a p53-dependent mechanism (*56, 57*).
2) AMPK may regulate cell growth by reducing the cytoplasmic level of the RNA-binding protein HuR which is essential for stabilising mRNA cell cycle regulators, including several cyclins (*58*).
3) AMPK activates the TSC1/2 complex (Figure 4) which, via its role in mTOR regulation, has a well-documented tumour suppressor function. TSC1/2 is thought to restrict both cell growth and proliferation (*59*).

AMPK regulation of cell division and apoptosis suggest that it has the potential to influence the progression of tumour formation, and that it may be a worthy drug-candidate in this capacity (discussed further in Section 1.3.3). Since AMPK has both pro- and anti-apoptotic effects in some tissues and under certain conditions it is important to understand the underlying molecular pathways which are being stimulated.

1.3 AMPK in Health and Disease

A coherent understanding of how the body maintains its energy balance might facilitate new health care strategies. AMPK is involved in sustaining energy balance by responding to hormonal and nutrient signals in skeletal muscle, heart, adipose tissue, liver, pancreatic β cells and the brain (specifically the hypothalamus) (*3*).

In Section 1.2 I described the impact of AMPK activation at a cellular level, on glucose and lipid metabolism, protein production, apoptosis and cell growth (Figure 3). Given the central role of AMPK signalling in the regulation of cellular energy homeostasis it follows that it can influence the balance between healthy and disease states. Now I consider the impact of AMPK on different tissues types and at a whole-body level, focusing on; the metabolic syndrome, obesity, type-2 diabetes, cancer, Wolf-Parkinson-White Syndrome (WPWS), cardiac function, Alzheimer's disease and ageing. A number of pharmacological agents, described in detail in Section 1.5.2.3, are referred to throughout this section on health and disease.

1.3.1 Obesity

Obesity, the accumulation of excess body fat, is increasingly prevalent in the western and developing world. A person is considered obese if they have a body mass index (BMI) greater than 30kg/m^2. Obesity is a risk factor in many other chronic physical and mental disorders and is central to the metabolic syndrome. This is broadly defined as including glucose intolerance, insulin resistance, central obesity, high blood cholesterol and hypertension. It is a risk factor for both diabetes and cardiovascular disease. The metabolic syndrome varies in prevalence between sexes, countries and age groups; for example a survey in Iran showed the prevalence was less than 10% for both men and women in the 20-29 year age group, rising to 38% and 67% respectively in the 60-69 year age group (*60, 61*).

Various studies have shown AMPK activity contributes to the pathophysiology of obesity, in both beneficial and detrimental fashions. AMPK activity in peripheral tissues acts to increase glucose uptake/metabolism, fatty acid oxidation etc. as described in Section 1.2. It has been suggested that AMPK signalling is suppressed with obesity and therefore that therapeutic AMPK activation may be beneficial in its treatment. In heart, skeletal muscle and liver tissue AMPK activity is reduced in most genetic models of rodent obesity, but no differences in the levels of activation are observed in animals made obese by a high-fat diet (described in (*46*)). In obese humans, muscle AMPK activity appears to be unaltered (*62*), suggesting that down regulation of AMPK is not a signal which precedes the onset of obesity.

In contrast, A-769662 (a direct AMPK activator) treatment of obese (*ob/ob*) mice increases AMPK activity and reduces body-weight (*43*). This suggests that whilst AMPK signalling in obese individuals is not compromised, activation of AMPK might still be exploited as a treatment for obesity.

AMPK activity in the brain plays a key role in the regulation of food intake and therefore affects weight-gain. AMPK activity in the hypothalamus integrates endocrine, nutrient and neuropeptide signals to influence the feeding response of the organism. Fasting and refeeding result in activation and inhibition of hypothalamic AMPK respectively (*63*). It is the changes in nutrient and hormone levels associated with the feeding state of an organism which produce these fluctuations in AMPK activity; for example the anorexigenic (inhibit feeding) adipokine, leptin, inhibits the pathway, whilst the orexigenic (promote feeding) adipokines, adiponectin and ghrelin, are stimulatory (See Section 1.5.3.4) (*63*). AMPK activity causes alterations in neuropeptide expression and therefore the action of hypothalamic neurones (e.g. agouti-related peptide (AgRP),

neuropeptide Y (NPY) and proopiomelanocortin (POMC)). In general, stimulation of hypothalamic AMPK results in feeding and weight gain whilst inhibition results in weight loss (*64*). However, deletion of AMPKα2 in POMC neurons caused mice to increase in body weight and fat content, whilst its deletion in AgRP neurons produced a lean phenotype (*65*). POMC and AgRP neurones produce orexigenic and anorexigenic signals respectively. The ultimate role of AMPK in the progression of obesity is therefore cell-type dependent and far from fully understood.

AMPK activity in the hypothalamus is an attractive target for anti-obesity drugs. This presents something of a challenge because to be effective, drugs must be designed to inhibit AMPK in the brain and thereby act to combat obesity, but be null/activatory in peripheral tissues in order to be anti-diabetic.

1.3.2 Type-2 Diabetes

Diabetes mellitus is a chronic condition caused by high-levels of circulating blood glucose; this occurs when the pancreas fails to produce sufficient insulin or when the body is unable to respond to the hormone correctly. Whilst genetic factors and ethnic origin play a role in the development of type-2 diabetes, the major risk factors are those of the metabolic syndrome (described in Section 1.3.1).

As discussed in Section 1.2.1 AMPK increases glucose uptake through stimulation of GLUT4 transcription and translocation to the cell membranes, increasing cellular sensitivity to insulin signals, increasing the glycolytic rate, and decreasing hepatic gluconeogenesis. Therefore activation of AMPK acts to clear glucose from the blood, which is the ultimate goal of anti-diabetic drugs.

Indirect activators such as exercise and metformin (a prominent type-2 diabetes pharmaceutical), are thought to activate AMPK by increasing cellular AMP/ADP

concentrations, and reduce the symptoms of the metabolic syndrome (*66, 67*). Metformin is thought to reduce glucose blood plasma concentrations by inhibiting gluconeogenesis through AMPK, although this has recently been challenged by a number of genetic models (see Section 1.5.3.2) (*66*). AICAR treatment of rodent and human tissue samples, and in diabetic mouse models, increases glucose uptake primarily through increased GLUT4 expression and translocation (for example Halseth *et al* (2002)(*68*)). The magnitude of AICAR stimulated glucose transport is dependent on nutritional status and muscle fibre type (reviewed in (*69*)). AICAR treatment of insulin-resistant mouse models results in increased clearance of glucose from the blood plasma, and the effects are therefore insulin independent (*70*).

AMPK activators combat the symptoms of the metabolic syndrome and type-2 diabetes, and for this reason pharmaceutical companies are interested in developing direct activators, such as A-769662. The treatment of obese (*ob/ob*) mice with A-769662, reduced plasma glucose, body weight, plasma/liver triglyceride levels and decreased transcription of gluconeogenic genes (*43*). This and other AMPK activators are discussed in greater detail in Sections 1.5.2 and 1.5.3.

1.3.3 Cancer

The malignant phenotype of cancer cells is characterised by increased lipid production, DNA and protein synthesis, and cell proliferation and migration. The role of AMPK in the regulation of cell growth and apoptosis is described in Section 1.2.4 and obviously suggests a potential link between AMPK and cancer. Additionally, AMPK acts to reduce the activity of anabolic pathways which ultimately reduces cell growth. AMPK activation appears to be generally anti-proliferative, although it may have varied effects dependent on cell-type and stimulus. Some examples are highlighted here.

Tumour Suppressor

Patients treated with metformin, thought to activate AMPK, show a 30% reduction in cancer deaths compared to a control group (*71*). Additionally AMPK activators including AICAR and A-769662 confer increased resistance to tumour formation in both cell lines and animal models (*72-74*).

The role of AMPK in breast cancer is the best studied (*75*). AMPK expression and signalling is significantly reduced in primary breast cancer tissue samples (*76*). Metformin-treated breast cancer patients show reduced levels of the proliferation marker Ki-67. Ki-67 is a nuclear protein that is associated with ribosomal RNA transcription; its expression is strictly associated with cell proliferation (*77*). Genome wide studies of metformin treated breast cancer cell lines highlight inhibition of both ribosomal proteins, and mitosis-related gene family members e.g. kinesins, tubulins, histones, and auroras, consistent with decreased proliferation (*75*).

Other natural AMPK activators (listed in Table 3) have been shown to suppress growth of breast cancers through decreased cyclooxygenase-2 (COX2) expression (*75*). COX2 is key in the conversion of arachidonic acid to the signalling molecule prostaglandin, and is often upregulated in cancer tissue.

Tumour Promoter

Cancerous tissue rapidly proliferates and therefore always exists in a state of metabolic stress. During specific stages of tumorigenesis, AMPK activation could confer an advantage to tumour cells through its role in increasing glycolytic rate, combating hypoxia, nutrient shortage and apoptosis (*78, 79*). One example of this was recently reported, knocking out AMPK or its upstream kinase (LKB1) results in increased cancer cell death in response to glucose deprivation. In α1 AMPK knock-out cells, NADPH concentrations are

reduced due to glucose deprivation and reduced glycolysis/oxidative respiration, the resulting cellular stress leads to apoptosis. AMPK acts to increase fatty acid oxidation and provide an alternative route through which NADPH can be produced, thereby increasing cancer cell survival (*80*).

It is probable that the role of AMPK in cancer cell metabolism, growth and proliferation operates in a context dependent fashion, perhaps with varied effects over the course of tumorigenesis. Therefore, potentially, both AMPK activators and inhibitors could be beneficial in cancer treatment.

1.3.4 Cardiac Function and Wolf-Parkinson-White Syndrome (WPWS)

AMPK is a key regulator of energy metabolism in the heart; myocardial tissue has high energy requirements met through a combination of fatty acid and glucose metabolism, both processes are regulated by AMPK (described in Section 1.2). AMPK is activated in response to increased cardiac work (e.g. during exercise), a similar effect having been demonstrated in skeletal muscle (see Section 1.5.3.3) (*81*). In the event of ischemia AMPK is rapidly activated, increasing fatty acid oxidation, glycolysis and glucose uptake (*82*). Whilst this protects the heart from ischemic shock in the short term, prolonged activation of AMPK and its downstream effects (e.g. fatty acid metabolism) may result in inhibition of glucose oxidation and therefore decreased cardiac efficiency (*82*).

WPWS is a form of cardiac hypertrophy categorised as a pre-excitation syndrome. A number of point mutations have been identified in the AMPK γ2 subunit which cause abnormal glycogen accumulation and cardiac conductivity, resulting in WPWS (Table 1)(*83*). Although these mutations may ultimately be fatal, they affect only a few hundred people

from a limited number of families (*83*). Increased glycogen content in animals harbouring similar mutations was originally observed in the skeletal muscle of Hampshire pigs, and subsequently in the cardiac tissue of transgenic mouse models harbouring human-disease containing mutations (*83, 84*).

No γ2 complexes have yet been crystallised, but when the equivalent mutations are mapped onto the γ1 structure they predominantly reside near AXP binding sites or are key phosphate interacting residues (*46*). These mutants, in general, increase basal AMPK activity and decrease sensitivity to AMP activation, although some discrepancies in their activities have been reported (*83, 85, 86*). Altered nucleotide binding to these mutants has also been reported (Peter Saiu – PhD Thesis) (*86*). Additionally AMPK is known to localise to and be inhibited by glycogen, therefore increased glycogen concentrations in cardiac tissue may lead to misregulation of the enzyme (*83*). However, all in all, it is not clear how dysregulation of AMPK leads to the WPWS cardiac phenotype.

Mutation in human γ2	Equivalent residue in γ1	Effect on regulation
R302Q	R69	Yes
L351 Insertion	R117-E118	No
H383R	H150	Yes
R384T	R151	Yes
T400N	T167	Yes
Y487H	Y254	nd
N488I	N255	nd
E506K	E273	nd
R531G/Q	R298	Yes
S548P	S315	nd

Table 1: WPWS point mutations.

The mutations in human γ2 that are associated with WPWS are given along with their corresponding residues in rat γ1. Their effects on AMP regulation, based on *in vitro* studies, are shown. This table is adapted from Xiao *et al* (2007) and Faith Mayer (PhD Thesis) (*87*).

1.3.5 Alzheimer's Disease (AD)

Metabolic stress is associated with the pathogenesis of Alzheimer's disease (AD) (*88*). In fact, a decline in glucose metabolism is an early diagnostic marker of AD.

AD is a form of dementia which affects an estimated 24 million people worldwide, with the majority of sufferers being over 65 years old. A number of genetic components which act as risk factors for the development of AD have been characterised. The pathological traits of the disease are amyloid $\alpha\beta$ plaques and neurofibrillary tangles in the brain. Tau, a microtubule-associated protein, is the major constituent of neurofibrillary tangles; these are hyperphosphorylated, insoluble protein aggregates which disrupt the structure and function of the neuron. The extent of tau tangle formation is more closely associated with the severity of AD than $\alpha\beta$ plaques (*89*).

Proteins related to insulin signalling, including insulin, insulin-like growth factor-1 (IGF-1), their receptors and downstream substrates e.g. insulin receptor substrate-1/2, are significantly reduced in the neurons of AD sufferers and therefore these cells are insulin resistant (*90*). It is this which results in abnormal glucose uptake. The concentrations of GLUT1 and GLUT3 glucose transporters are also reduced on the neuronal cell membranes of AD patients (*91*), thus the glucose supply to these neurones is decreased resulting in 'starvation'. AMPK activation has been shown to excite glutamate neurones, stimulating glucose uptake by increasing the translocation of glucose transporters (GLUT3) to the membrane and upregulation of their expression (*52*). AMPK therefore provides a secondary way for neurons to regulate glucose uptake, a mechanism that could be exploited for AD treatment.

Whilst AMPK activity stimulates glucose uptake, it remains unclear what role it may play in plaque and tangle formation:

1) Immunohistochemical staining has shown AMPK localised to hyperphosphorylated pre-tangle structures, and mature tangle-like structure, suggesting AMPK may be involved in their formation. AMPK phosphorylates tau protein at numerous sites (*92, 93*).
2) Tau is acetylated in tangle structures, reducing trafficking to the proteasome, SIRT1 reduces this acetylation and AMPK potently activates SIRT1, thus the degradation of tau is enhanced.
3) AMPK inhibits GSK3β *in vitro* which is a known tau kinase (*94*).
4) AICAR treatment of rat neurons inhibited tau phosphorylation (*95*).
5) AMPK activation via AICAR, resveratrol and quercetin treatments decreased the deposition of amyloid plaques (perhaps through increased autophagy) in both cultured cells and mice models (*96-98*).

The roles of AMPK in the progression of neurodegenerative diseases is closely linked with its regulation of cellular metabolism, although unique roles in tangle and plaque progression are emerging. AMPK has been implicated as both a neuroprotective and neurodegenerative factor in non-AD neuronal cell lines (*46*). Perhaps the most convincing evidence comes from AMPK α2 knock-out mice which have reduced neuronal death in response to stroke, suggesting that AMPK activation is pro-apoptotic and neurodegenerative (*99*). This remains an interesting area of study in the AMPK field.

1.3.6 Ageing

There are several studies which suggest that AMPK activation via phosphorylation declines with age (*100-103*). This appears to parallel many metabolic changes associated with age such as the prevalence of AD, obesity and the metabolic syndrome. The mechanism for this decrease in AMPK activity is unknown but might be due to increased dephosphorylation by phosphatases; ceremides (sphingosine and fatty acids – mostly found in the cell membrane

but known to also be signalling molecules) inhibit AMPK signalling by increasing the activity of PP2A. Ceramide concentrations are significantly increased in brain regions susceptible to the pathological changes of AD, in obese and diabetic patients and in the elderly (*104-106*).

Autophagy is important in the regulation of ageing and several age-related degenerative diseases (*90*), it is the process by which cellular components are degraded through the lysosomal system. AMPK inhibits mTOR, the main inhibitor of autophagy (see Section 1.2.3). AMPK also directly activates unc-51-like kinase (ULK1) the mammalian autophagy initiating kinase (*107, 108*). AMPK also regulates autophagy in response to stress/exercise in order to recycle nutrients for metabolic breakdown (*46, 109*).

Dietary restriction (DR) is known to extend lifespan in a wide range of species. DR in *Caenorhabditis elegans* results in AMPK activation through increased AMP/ADP concentrations and subsequent phosphorylation of the FOXO/DAF-16 transcription factor (*110*). FOXO/DAF-16 upregulates genes involved in detoxification of reactive oxygen species (ROS) and therefore reduces progression to apoptosis. The authors showed that lifespan is increased in transgenic worms in which AMPK is constitutively active, demonstrating that AMPK activation is responsible for this ageing effect (*110*).

AMPK activation increases the lifespan of *C.elegans* through inhibition of the cAMP-regulated transcriptional co-activator-1 (CRTC-1)/CREB signalling pathway (*111*). Chronic activation of this pathway is associated with insulin resistance, hyperglycaemia and inflammation (*112*). Whilst there is a wide range of CREB target genes, only a subset are activated by the CRTC-1/CREB pathway, notably a number of genes involved with endoplasmic reticulum (ER) stress. ER stress is a known feature of AD pathology, ageing and

the metabolic syndrome (*90*). Increased AMPK activation combats this cellular stress and reduces stimulation of apoptosis.

Both genetic and pharmaceutical inhibition of mTOR and its downstream effector S6K, has been shown to increase lifespan in *S.cerevisiae*, *C.elegans* and *Drosophila melanogaster* (*113, 114*). As described in Section 1.2.3 AMPK activity decreases mTOR activity through decreased Rheb activation and exclusion of Raptor from the mTOR complex.

Transgenic S6K knockout mice have both increased lifespan and AMPK activity (*114*). However double S6K and AMPK knockout transgenic mice do not have increased lifespan, suggesting that the interplay between AMPK and mTOR/S6K in regulation of ageing is more complex than originally thought.

Some studies suggest that AMPK signalling regulates lifespan, perhaps by improving general health. Mice treated with metformin have extended lifespans through increased AMPK activity (*115*). With so many factors being implicated in the regulation of lifespan it is perhaps unsurprising to find a link between AMPK and these pathways. Further studies on higher organisms will elucidate the mechanism through which AMPK activation increases life-span. This is certainly an interesting 'side-effect' of AMPK activators prescribed primarily in the treatment of metabolic disorders.

1.3.7 Concluding Remark

A number of downstream targets of AMPK and their implications on human health have been described. AMPK has recently been linked to the regulation of, amongst others, cell polarity, ion influx, circadian rhythms, inflammation and bile-acid metabolism, and in the progression of stroke, atherosclerosis and vascular dysfunction (*46, 90, 116*). It has been said that "…it can seem like AMPK is involved in regulating every biochemical pathway conceivable!"(*116*).

1.4 The αβγ Heterotrimer

There is evidence that some of the downstream effects of AMPK phosphorylation are isoform dependent. I will now consider the two α, two β and three γ subunits at a molecular level, and highlight what is known about their differences and similarities.

Through alternate initiation and splicing there are additional transcripts to those covered in this section. There are also a number of Single Nucleotide Polymorphisms (SNPs) mapped to the seven AMPK genes, the physiological effects of which are largely undetermined (*46*).

1.4.1 Overall architecture

Although the complex as a whole has not been crystallised, in 2011 the Gamblin laboratory published the structure of an active mammalian α1β2γ1 complex missing only the β-subunit Glycogen Binding Domain (GBD) (Figure 5).

The domain structure of the αβγ subunits is shown in Figure 2. The C-terminal region of the β-subunit forms a β-sheet structure that serves as a binding platform for both the α and γ subunits (Figure 5 - green). The βγ interface comprises mainly hydrogen bonding (Figure 5 - green/pink); whilst the βα interface consists mainly of hydrophobic interactions (Figure 5 - green/light blue). The γ-subunit forms a distinctive, pseudosymmetric structure which binds nucleotides and is resistant to protease treatment (Figure 5- pink). The γ-subunit interacts with the α-subunit through the α-hook structure which forms a lid over one of the nucleotide binding sites (Figure 5 – dark blue). The N-terminal α-kinase comprises a classic kinase fold, and interacts with the β-subunit with a surface area of 1100Å^2 (Figure 5 - yellow).

Implications of the various interactions between the regulatory domain and α-kinase are touched upon in this introduction and are considered in more detail throughout the thesis.

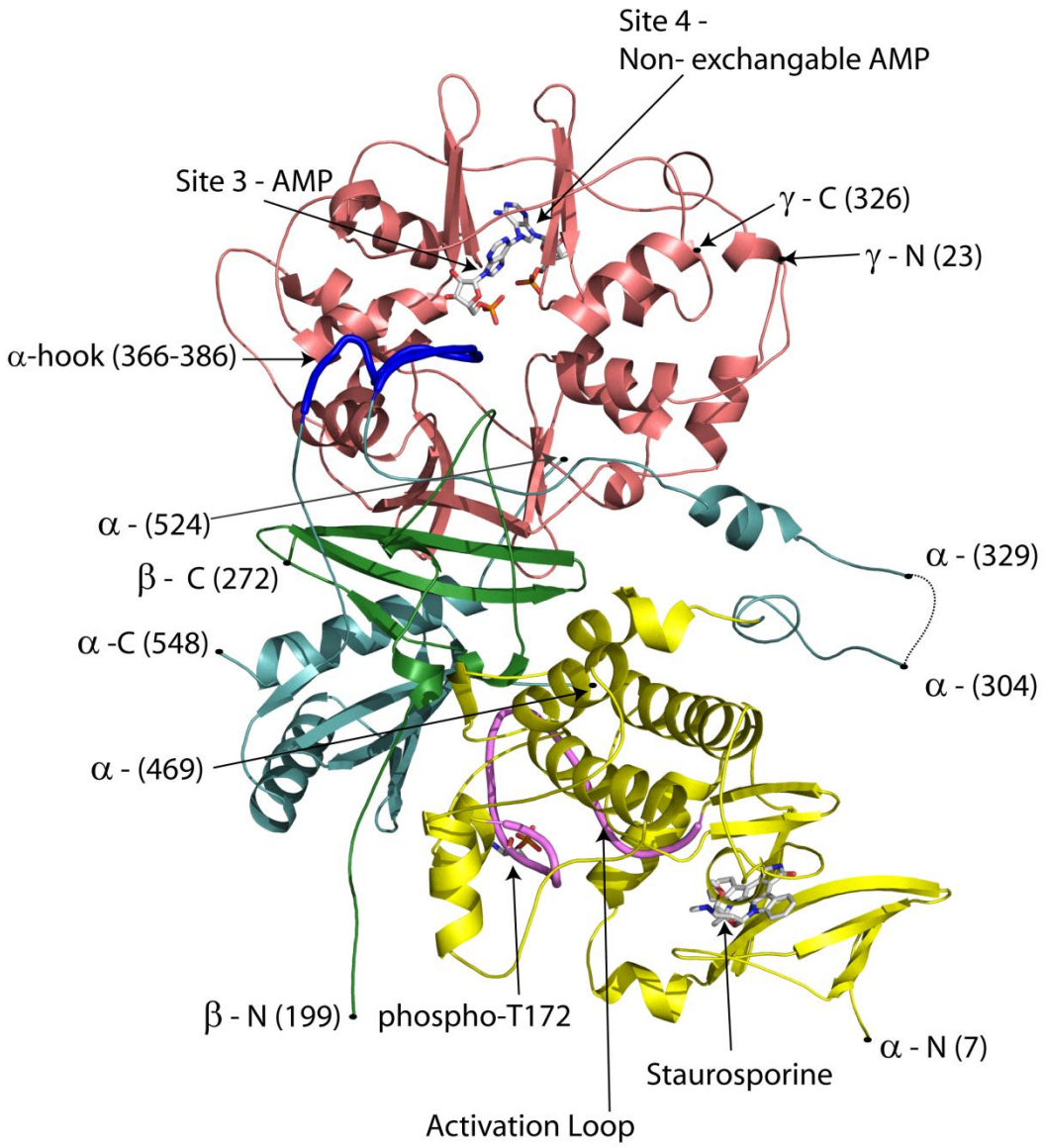

Figure 5: Structure of α1β2(ΔGBD)γ1 AMPK.

Ribbon representation of a mammalian complex ($\alpha 1_{1\text{-}469,524\text{-}548}\beta 2_{187\text{-}272}\gamma 1$): yellow; α kinase domain, pink; γ regulatory domain, blue; α subunit, green; β subunit missing the GBD. The complex is bound to two AMPs, and staurosporine, all shown in stick representation. The α-hook and activation (T) loop of the kinase domain are shown in heavier lines and coloured dark blue and purple respectively. The phosphorylated αT172 residue is indicated. PDB ID: 2Y94. (*1*)

1.4.2 The α subunit

The α-subunit is catalytically active as a Ser/Thr protein kinase and possesses a highly conserved N-terminal kinase domain and more divergent C-terminal regulatory region (Figure 2). There are two mammalian α isoforms encoded by two separate genes. Following identification of the second α isoform that is more ubiquitously expressed, the initial isoform identified in liver was termed α2 and the new isoform α1 (*117*). AMPK is activated by phosphorylation of a conserved threonine residue (αT172) on the kinase T-loop, and inactivated through dephosphorylation (Figure 1).

Although α1 is widely expressed, it is α2 which is predominant in skeletal and cardiac muscle, suggesting divergent roles for the two isoforms. For example, following rigorous exercise only α2 containing heterotrimers (α2β2γ3) are activated in skeletal muscle (*118, 119*), whilst both isoforms contribute equally to activity in the liver (*120*).

Immunofluorescence and western blotting studies have shown that α1 localises to the cytoplasm whilst α2 is present in both the cytoplasm and the nucleus, suggesting a potential role for it in transcriptional regulation (*121*). This difference is due to the presence of a nuclear localisation signal on the α2 subunit, there is also evidence for a nuclear export signal at the C-terminal of the α-subunit (*122, 123*). It has been shown that α2, but not α1, regulates gene transcription in response to external glucose in pancreatic cells (*124*). More work is necessary to fully understand the signals which stimulate the cellular redistribution of the α2 subunit.

Both isoforms have similar specific activities and only subtle differences in substrate specificity. α2 containing complexes appear to be more sensitive to allosteric activation by

AMP and dephosphorylation by phosphatases, thus allowing modulation of the AMPK response in an isoform specific way (*120*).

The α N-terminal region ($\alpha_{1\text{-}278}$) is sufficient for catalytic activity and produces a classic kinase fold (*125*). The active site is positioned in a cleft between two lobes, the smaller of which is composed predominantly of β-sheet structure. The larger lobe is 63% α-helical in mammalian AMPK and mediates substrate binding, activation and catalysis (*126*). In the structure of an inactive (unphosphorylated) form of human α2 (Figure 6 - PDB ID: 2H6D) conserved elements are visible, including the catalytic loop in the large lobe which runs from His-133 through to Glu-143 and the invariant Asp residue, αD157, required for catalysis (*126*). In the active structure shown in Figure 6 the phosphorylated αT172 residue is clearly visible and is bound in a pocket created by tandem Arg-Asp residues from the kinase as seen in related structures (*125*). The activation loop is also well-defined and its conformation is stabilised through interaction with the β subunit (Figure 5 and Figure 6). It is hypothesised that promotion of kinase binding to the regulatory fragment upon AMP/ADP binding to the γ domain mediates protection of the activation loop from dephosphorylation by phosphatases (described in Section 4.4.2.1)(*1*).

Several papers describe an autoinhibitory domain (AID), spanning around 70 residues C-terminal to the α-kinase domain. This is an established mechanism for the regulation of other kinases, specifically those to which AMPK is evolutionarily related (*127*). The inactive states of truncated Snf1 kinases have been crystallised (*128, 129*); however it is not clear if the interface between the kinase and regulatory subunits demonstrated in Xiao *et al* (2011)(*1*) could accommodate the formation of the AID. It could be that this structure operates to downregulate kinase activity when the kinase domain is dissociated from the regulatory fragment prior to dephosphorylation.

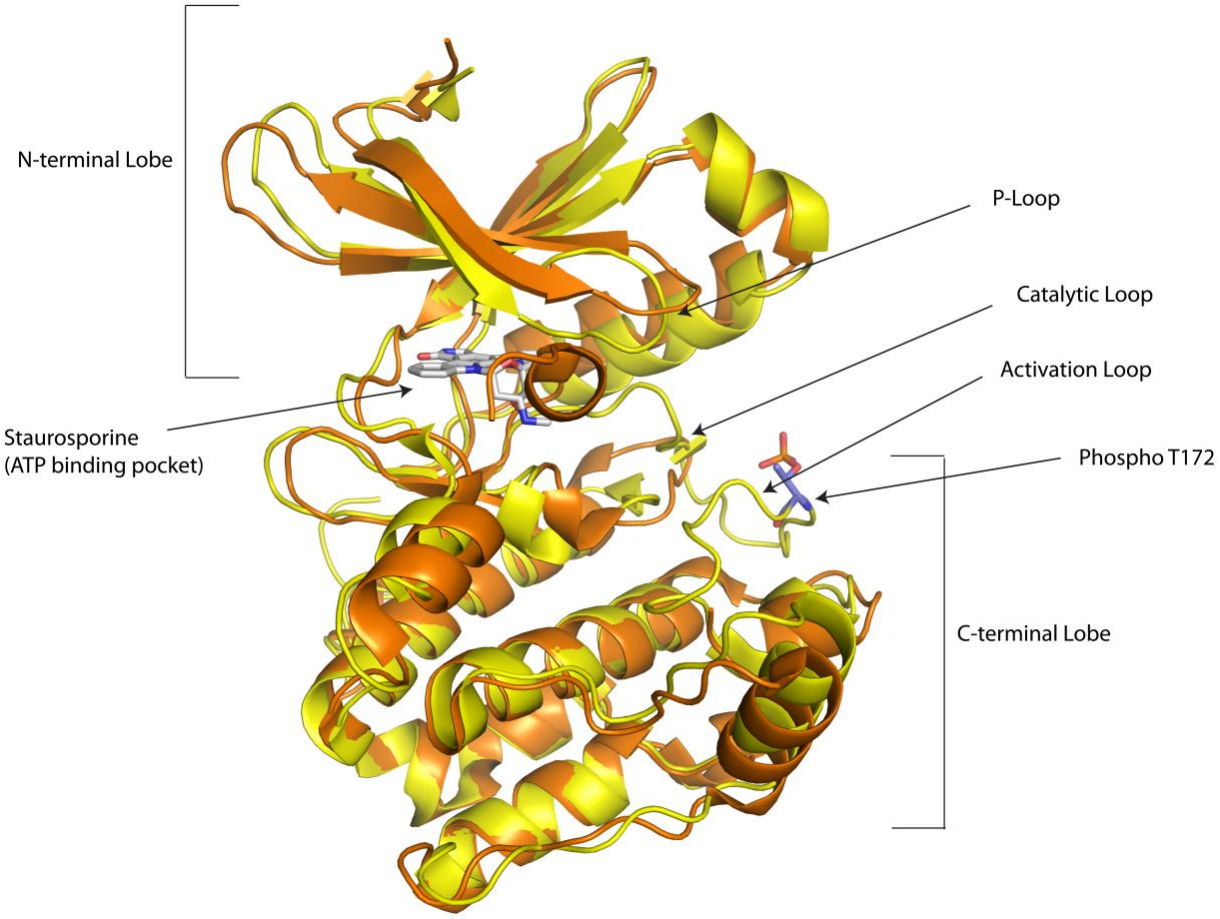

Figure 6: Overlay of inactive (orange) and phosphorylated (yellow) AMPK kinase domain structures.

The active form is complexed with staurosporine (white – stick representation). A number of conserved structural elements are labelled. PDB ID: 2Y94 (active), 2H6D (inactive).

1.4.3 The β subunit

There are two β isoforms; which share around 70% amino acid sequence identity and a similar domain structure (Figure 2)(*130*). Heterotrimers containing β1 or β2 subunits have been shown to have similar levels of activity but different cellular localisation (*131*). In mouse myoblasts α2β1 complexes are anchored to the mitochondrial membrane whereas α2β2 complexes translocate to the nucleus (*122*). In terms of tissue distribution, β1 is expressed very highly in the liver (rodent models) where it is present in almost all AMPK complexes. About 50% of complexes in skeletal muscle contain β2, and have been implicated in exercise induced AMPK activity (*119, 131*).

The β-subunit undergoes significant post-translational modification, including myristoylation and phosphorylation which are important in regulation (see Sections 1.5.1.3 and 1.5.1.4) (*132, 133*).

In 2003 a Glycogen Binding Domain (GBD) was identified on the β subunit (Figure 7), through which allosteric inhibition of AMPK activity by glycogen is mediated (see Section 1.5.2.2) (*134, 135*). Rat β1 GBD comprises a compact β-sandwich, formed from two anti-parallel β-sheets, homologous to carbohydrate branching enzymes and starch binding domains (*136*). In this crystal structure the GBD is complexed to β-cyclodextrin (Figure 7), bound through an extensive network of hydrophobic stacking interactions between the protein and five glucose units (*137*). β-cyclodextrin is not a natural AMPK ligand and it may therefore not accurately mimic physiological sugar-binding.
A second structure of the *S.cerevisiae* AMPK homolog identified a potential interface between the GBD and γ-subunit involving a number of residues from the γ-subunit CBS2 (Figure 8). The residues within the hydrophobic core of the interface are conserved in mammalian AMPKs, suggesting that they might play an important role in the structure or regulation

of the protein. However, the position of the GBD in the yeast structure would sterically clash with the kinase domain in the active AMPK structure (these structures are shown in Figure 5 and Figure 8). This raises the intriguing possibility that only one domain (the kinase or the GBD) can bind to the regulatory fragment at any time.

The GBD is flexibly linked to the rest of the heterotrimer, at least in certain conditions. Two observations support this idea; 1) full-length AMPK protein crystals contain no density for the GBD, 2) NMR reveals the independent tumbling of a small domain tethered to the rest of the complex, the resonances of which correspond to the GBD (Personal Communication – Bing Xiao). Perhaps *in vivo* this allows tethering of the protein to glycogen, without hindering substrate access to the kinase domain.

The GBD and its autophosphorylation is required for small molecule (e.g. A-769662) activation of the complex (discussed further in Section 1.5.2.3). Therefore it is certainly both an interesting and open question as to how the GBD interacts with the rest of the heterotrimer.

1.4.4 The γ subunit

There are 3 γ isoforms (*138*), and a fourth variant of γ2 termed $\gamma2_{short}$ (*139*). The γ-subunit is formed of four cystathionine beta synthase (CBS) motifs arranged as two Bateman domains. CBS motifs from AMPK and other proteins have been shown to bind adenosine-containing ligands such as AMP and ATP (*86, 140*). Competitive binding of AXPs to the γ subunit allows the protein to respond to changes in cellular energy status (see Section 1.5.2).

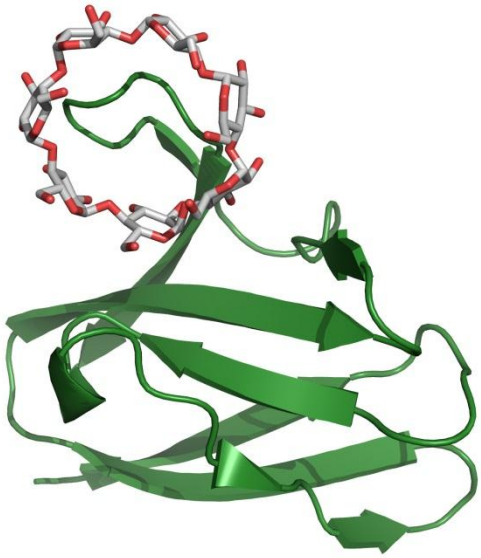

Figure 7: Complex of β1 $_{68\text{-}163}$ 'GBD' bound by β-cyclodextrin.

β-cyclodextrin (white – stick representation) binds the GBD, forming an extensive network of hydrophobic stacking interactions. PDB ID: 1Z0M.

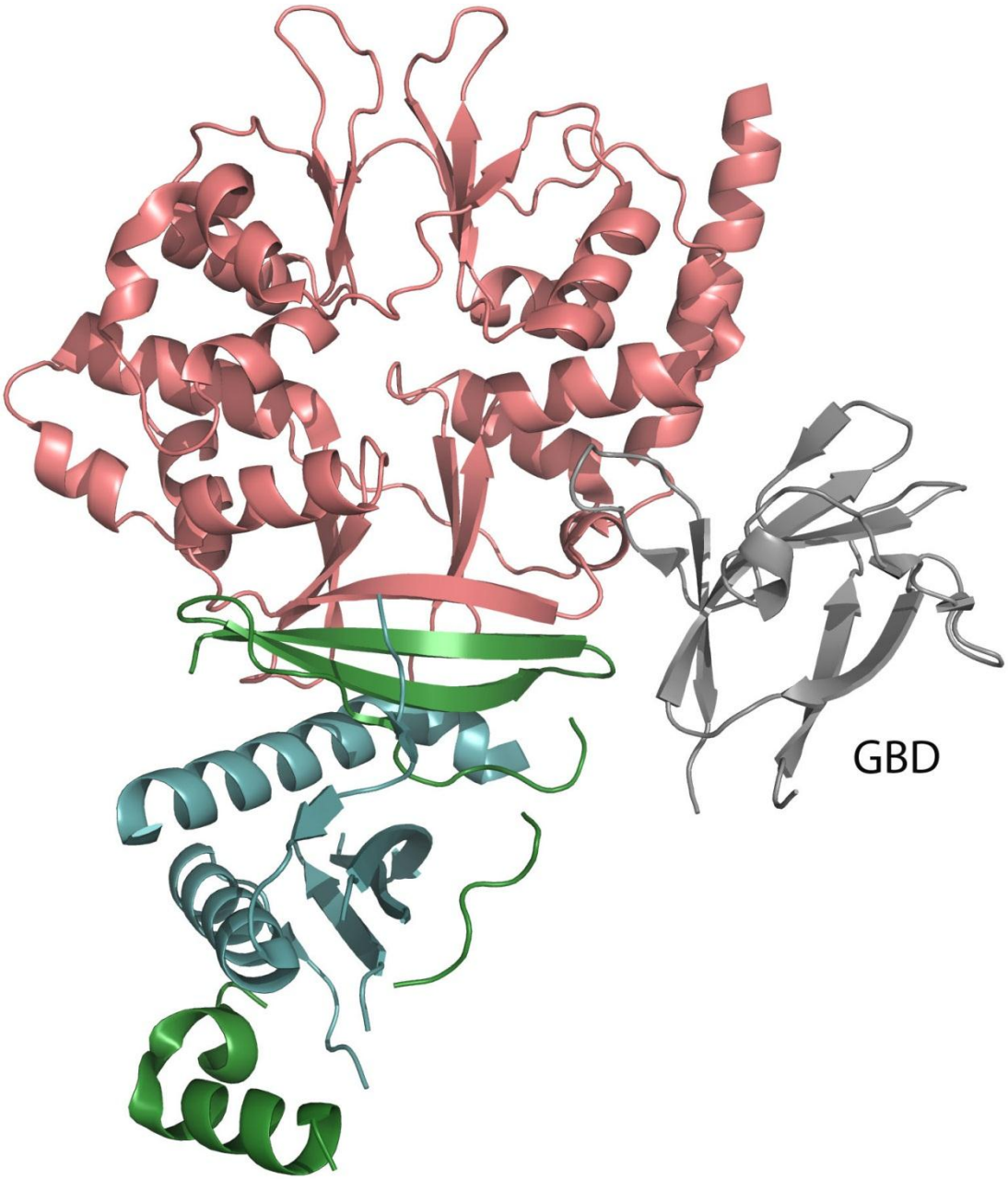

Figure 8: Structure of Snf1$_{398-633}$ Sip2$_{154-415}$ Snf4.

Snf4-γ (pink), Sip2-β (green), Sip2 GBD (grey and labelled), Snf1-α (blue). The GBD predominantly forms an interface with the γ-subunit. PDB ID: 2QLV.

γ1 and γ2 are expressed in a wide number of tissues, while γ3 is only found in skeletal muscle (*138*). In most tissues 80-90% of AMPK heterotrimers contain γ1, 10-20% γ2 and any remaining complexes contain γ3. Exceptions include the brain and the testis where the three isoforms are present in about equal amounts (*139*). In the central nervous system γ1 containing heterotrimers have a predominantly nuclear localisation relative to those containing γ2 (*141*). Differences in the cellular localisation and tissue distribution suggest that the isoforms may have different functional roles.

The γ-subunit is, structurally, the best investigated of the three subunits. Crystal structures are available for full-length *Schizosaccharomyces pombe* Snf4 (*142*), *S.cerevisiae* Snf4 (*2, 143*) and mammalian γ1 (*1, 87, 144*). The structures display similar topologies; the four CBS motifs generate an elliptical disc of ~60Å across and 30Å deep (*145*). A pair of adjacent CBS motifs produce helix/β-hairpin/helix structural elements (Figure 9) which are termed Bateman domains (*126*). The four CBS motifs in the γ-subunit therefore potentially generate four nucleotide binding sites, labelled Sites 1-4 following the numbering of the CBS motifs (Figure 10) (see Section 1.5.2). All four sites are located between pairs of adjacent helix-loop strands; in three of the four sites, the three which bind AXP, an Asp residue is positioned on one helix such that it forms interactions with the 2', 3' hydroxyl groups of the AXP ribose moiety. The adenine rings are sandwiched between β-strands and make various hydrophobic interactions. The phosphates are positioned in the solvent accessible core of the γ-subunit and their charge neutralised through electrostatic interactions with the protein (*146*). The four CBS motifs contribute different numbers of basic residues for interaction with the phosphates (e.g. CBS2 contributes H151, R152 and K170 whilst CBS3 contributes none), for this reason there is a high degree of connectivity between the binding sites.

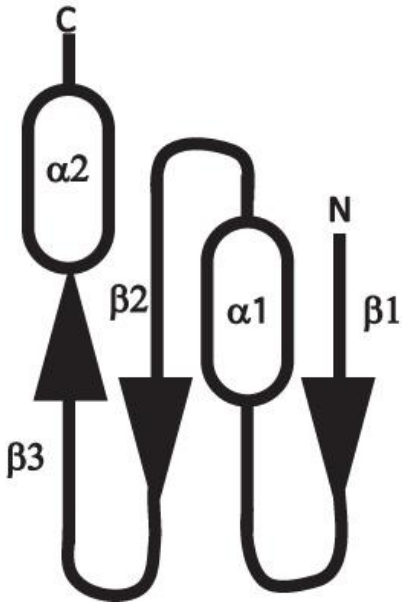

Figure 9: The Topology of the CBS domain.

β-strands are numbered β1-3 and α-helices numbered α1 and α2 (*145*).

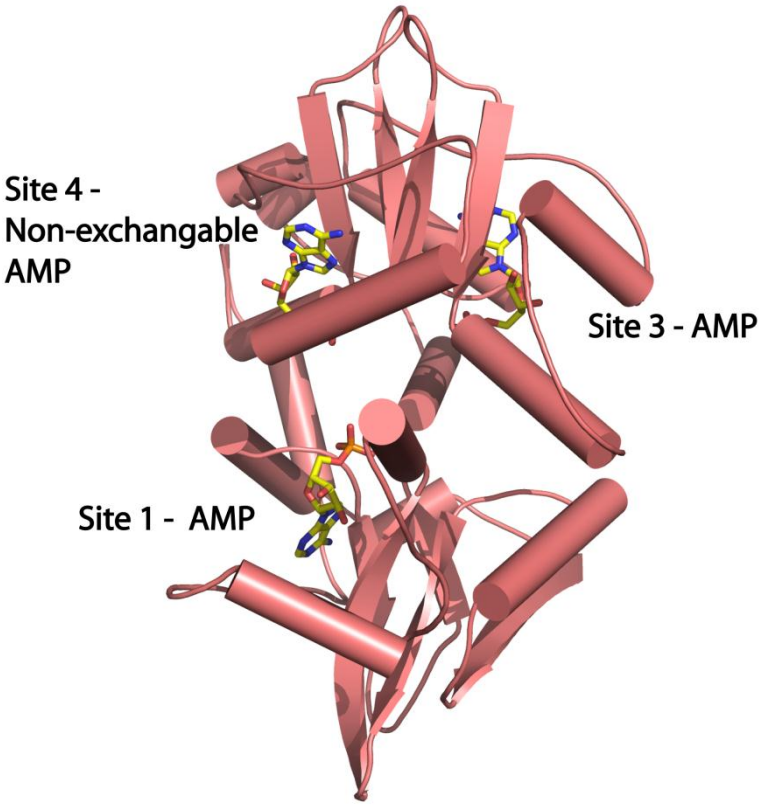

Figure 10: Structure of the AMPK γ-subunit.

Ribbon representation of the mammalian γ subunit with three bound AMP molecules. Site-4 is non-exchangeably bound, whilst Site-1 and Site-3 are exchangeable with ADP/ATP. PDB ID: 2V8Q. (*87*).

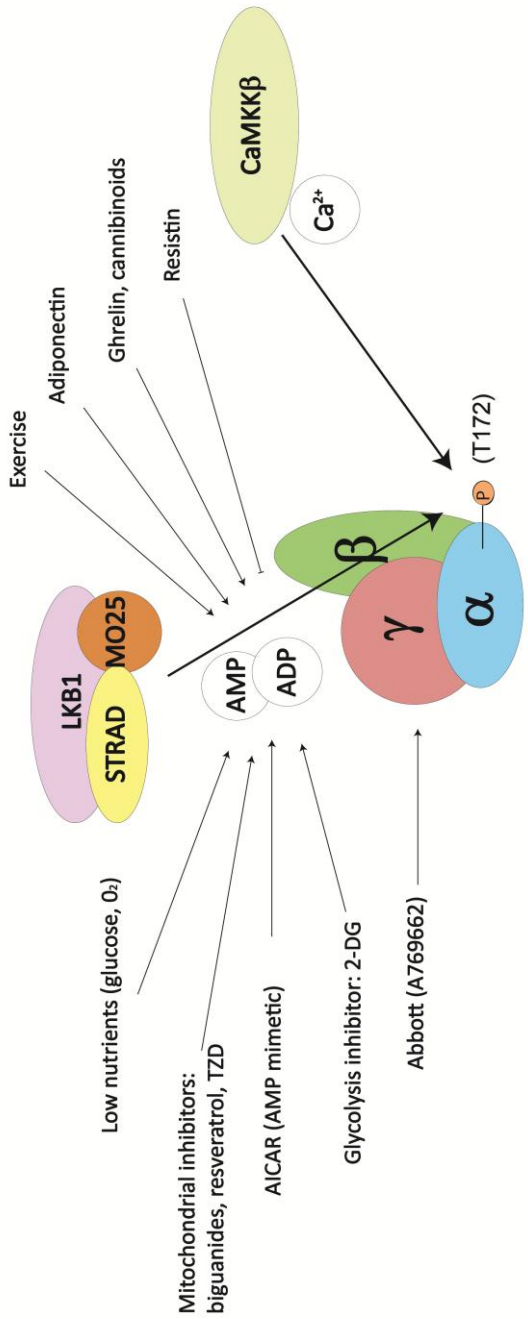

Figure 11: The AMPK signalling pathway.

AMPK is activated in response to increases in cellular AMP and ADP concentrations deriving from a variety of physiological stresses, or the presence of pharmacological inducers. LKB1 and CaMKKβ are AMPK's upstream kinases, and phosphorylate αT172.

1.5 Regulation of AMPK

The primary event in AMPK activation is the phosphorylation of αT172 on the T-loop of the α-kinase domain by its upstream kinases. However, many other factors contribute to the complexity of AMPK regulation; dephosphorylation, autophosphorylation, myristoylation, ubiquitination, acetylation, nucleotide binding, glycogen binding, pharmacological/small molecule activation and endocrinological activation (summarised in Figure 11).

1.5.1 Post Translational Modifications

1.5.1.1 αT172 phosphorylation by upstream kinases

The kinase protein family is one of the largest in existence; phosphorylation-based activation cascades allow extracellular signals to be conferred to a broad but specific range of cellular targets. Phosphorylation of αT172 increases activity by approximately 1000-fold (*7*). For a long time the identity of the upstream AMPK kinase(s) remained elusive, but through sequence homology with yeast enzymes two candidates were identified, Ca^{2+}/calmodulin-dependent protein kinase kinase (CaMKKβ) and Liver Kinase B1 (LKB1) (*147*).

Direct AMPK αT172 phosphorylation by LKB1 purified from liver extract has been demonstrated (*148, 149*). LKB1 is thought to be the predominant upstream AMPK kinase in most tissues. Cell lines lacking LKB1 expression e.g. HeLa cells, and those expressing dominant negative forms are unresponsive to AMPK activation mediated be changes in adenine nucleotide concentrations (AMPK still responds to calcium) (*148-150*). A number of LKB1 related mouse models have demonstrated the importance of a functional LKB1 complex in the regulation of metabolism and in the prevention of tumour formation (*151*). LKB1 also activates a number of AMPK related protein kinases, many of

which are thought to be involved with maintenance of cell polarity and progression through the cell cycle (*152, 153*) (*154*).

Deletion of LKB1 in skeletal or cardiac muscle only reduced the activation of α2 containing complexes, suggesting that LKB1 may not operate through α1-containing complexes (*155, 156*). Mutations in LKB1 are linked to Peutz-Jeghers syndrome, an inherited predisposition to cancer (*7*). The adverse effects of aberrant LKB1 activity are mediated through AMPK and other AMPK related kinases.

CaMKKβ phosphorylation of αT172 *in vitro* has been demonstrated (*157*). Overexpression of CaMKKβ and treatment with Ca^{2+} ionophores increases AMPK activity, whilst treatment with CaMKKβ inhibitors or siRNA decreases AMPK activation (*158, 159*).

In pancreatic cells AMPK appears to be regulated in a Ca^{2+}-dependent manner, in fact most conditions which activate AMPK also increase intracellular Ca^{2+} concentrations (e.g. muscle contraction, mitochondrial uncoupling and oxidative stress) (*160*). CaMKKβ is weakly expressed in liver, where LKB1 is the predominant AMPK kinase, however it is highly expressed in neuronal tissue. K^{+}-induced depolarisation of rat cerebro-cortical slices has been shown to activate AMPK in an AMP independent manner, highlighting an important tissue-specific role for CaMKKβ and an additional regulatory point for AMPK (*159*).

More recently a third upstream AMPK kinase, Tak1, was proposed. This kinase phosphorylates αT172 *in vitro* (*161*), but subsequent data suggested that Tak1 may simply function upstream of LKB1 (*162*). It remains unclear whether this kinase plays a role in the activation of AMPK *in vivo*.

1.5.1.2 Dephosphorylation by phosphatases

The ratio of phosphorylated to unphosphorylated AMPK depends upon the relative activity of the upstream kinases and phosphatases. LKB1 is constitutively active; therefore it is predominantly the rate of the phosphatase which influences this equilibrium. The rate of dephosphorylation is decreased by binding of AMP/ADP to the γ-subunit (discussed further in Section 1.5.2) (*1*).

Members of the phosphoprotein phosphatases (PP1 and PP2A) and metal-dependent protein phosphatases (PP2C, PPM1E and PPMF1) families have been shown to dephosphorylate AMPK *in vitro* but the physiologically relevant phosphatase(s) have not yet been demonstrated in humans (*163, 164*).

The *S.cerevisiae* AMPK homolog, SNF1, is dephosphorylated by a PP1 family phosphatase Glc7 complexed with a regulatory subunit, Reg1 (discussed further in Appendix 1.1.4). In pancreatic β-cells, PP1 and the regulatory subunit R6 have been implicated in glucose-induced AMPK dephosphorylation (*165*). A direct interaction between the β-subunit GBD and R6 was identified, which is homologous to the interaction between SNF1 and Reg1 in the yeast system (*165*). It may be the regulatory subunits associated with the various phosphatases which dictates their ability to dephosphorylate AMPK.

Increased expression of PP2A and PP2C, leading to decreased AMPK activity, may be an important feature of AMPK regulation. For example, glucose and palmitate appear to regulate AMPK activity via increased PP2A activity, and α–lipoic acid regulates AMPK activity through modulation of PP2C levels (see Section 1.5.3.4) (*166, 167*).

It remains to be seen if a single major AMPK phosphatase exists *in vivo,* or if contributions from several candidates are responsible for inactivation of AMPK in a stimulus/localisation dependent fashion.

1.5.1.3 Other phosphorylation sites

In addition to phosphorylation on the critical αT172 residue, a number of secondary phosphorylation sites on the α and β subunits have been identified. These sites are both autophosphorylated and phosphorylated by other kinases (*132, 150*).

A large number of putative phosphorylation sites at the C-terminus of the α-subunit have been proposed. These sites are within the region which interacts with the other subunits suggesting phosphorylation could regulate heterotrimer formation. Additionally, phosphorylation at these sites may regulate AMPK activation. For example, α1 S485 and α2 S491 phosphorylation is correlated with decreased AMPK activity in cardiac tissue in response to insulin treatment (*168, 169*). Akt (PKB) phosphorylates S485 *in vitro* and PKA phosphorylates this residue in cell-based assays in response to elevated cAMP levels (*170*). PKA is also thought to phosphorylate α1 S173 which may inhibit αT172 phosphorylation through steric hindrance (*171*). Recently p70S6 kinase was found to phosphorylate α2 S491, an effect which is integral to the inhibition of AMPK in the hypothalamus in response to leptin (see Section 1.5.3.4) (*172*).

Four native phosphorylation sites have been identified on the β1 subunit of AMPK, located at S24/25, S108 and S182, (*164, 173, 174*). Complexes with a truncated β subunit or with a mutated autophosphorylation site, β1 S108A, are insensitive to A-769662 stimulation, suggesting some role of this phosphorylation in the action of pharmacological agents (discussed in Section 1.5.2.3) (*173*). A reduction in the AMP regulation of AMPK in S108A mutants has also been reported in cells, suggesting a place for β-subunit phosphorylation in regulation of the heterotrimer (*175*).

1.5.1.4 Myristoylation

N-myristoylation of proteins can play a number of different roles in complex stabilisation and the targeting and binding of proteins to membranes (*176*). Both β-subunits are co-translationally N-myristoylated (*132*). A proportion of cellular AMPK is membrane associated, *in vitro* AMPK appears to become membrane associated in response to AMP and nutrient stress (*133*). Disruption of the myristoylation site, through mutation, results in localisation throughout the cytoplasm and increased recovery of AMPK from the soluble cell fraction (*132, 175*).

Myristoylation has also been reported to affect regulation of AMPK by nucleotides and its activity. A decrease in basal AMPK activity is observed when the β1 subunit is myristoylated, suggesting this modification is important in maintaining an inactive AMPK state (*133, 175*). Recent *in vitro* studies have suggested a role for myristoylation in up-regulation of αT172 phosphorylation by AMPK kinases in response to AMP and ADP (*133, 177*). The authors suggest that AMPK is regulated through a myristoyl switch, in which the myristoyl group interacts with a hydrophobic pocket and reduces the phosphorylation of αT172 by upstream kinases, activatory signals (AMP/ADP) release the repression and result in membrane association of the complex (*178*).

However, AMP does not promote αT172 phosphorylation of AMPK purified from rat liver (and therefore myristoylated) (*179*). It therefore remains to be seen whether myristoylation has a regulatory role in addition to its role in localising AMPK to membranes.

1.5.1.5 Ubiquitination and acetylation

The addition of ubiquitin chains to proteins has, historically, been thought to mediate targeting of the protein to the proteasome for degradation, although more recently it has been demonstrated that it plays an important regulatory role akin to protein phosphorylation. There is only limited evidence that AMPK is regulated by ubiquitination.

The ubiquitin ligase, cell-death inducing DFFA-like effector a (CIDEA), expression levels are inversely correlated with basal metabolic rate. This complex is thought to ubiquitinate AMPK targeting it for proteasomal degradation. In CIDEA knock-out mice AMPK activity and stability is increased, suggesting ubiquitination plays an inhibitory role in AMPK regulation (*180*).

The α1 subunit has been found to be ubiquitinated in the presence of deubiquitininating enzymes (DUB) inhibitors. The polyubiquitin chains are predominantly Lys29 and Lys33 linked suggesting that they play a role in direct AMPK regulation rather than in targeting AMPK for degradation (*181*).

Protein acetylation is a further regulatory mechanism employed by cells. There are only limited reports of AMPK acetylation; HDAC1 and p300 control the reversible acetylation of the α-subunit. Deacetylation is thought to increase the affinity of AMPK for LKB1 and therefore increase activation through αT172 phosphorylation (*182*). Further studies are required to determine whether acetylation affects phosphorylation state and nucleotide regulation directly.

There are multiple ways that AMPK is post-translationally modified. The fact that phosphorylation is the most well-established, does not mean that it is the most important; it will therefore be interesting to see how the interplay between the many modifications mediates AMPK activity.

1.5.2 Direct Regulators

1.5.2.1 Nucleotide Regulation

The characteristics of AXP binding to the γ-subunit varies between homologues (Table 2). The mammalian γ1 isoform binds three nucleotides, one of which is a non-exchangeable AMP (as described in Section 1.4.4)(Figure 10). In the mammalian structure Site-1 and 3 can bind exchangeably, Site-4 is non- exchangeably bound by AMP and Site-2 is empty. The lack of binding at Site-2 has been suggested to be due to a natural Asp to Arg mutation at a position that might be involved in AXP binding (*146*).

S.pombe and *S.cerevisiae* structures suggest that Site-4 (equivalent to the non-exchangeable site in AMPK) binds AXPs exchangeably. In the case of *S.pombe* it has also been observed that ADP can bind Site-2 (equivalent to the empty site in AMPK). Nucleotide occupancy of the four potential binding sites, in different species, is summarised in Table 2.

The current consensus is that AMPK responds to the AMP/ADP:ATP ratio of the cell and thus acts as an 'energy gauge' (*3*). In the early days of AMPK research, the enzyme was thought to respond to ADP activation, but further investigation suggested that AMP was a much more potent activator and that the original results were caused by adenylate kinase contamination.

AMP allosterically activates the phospho-form of the kinase on average about 2-4 fold (*174*) (*7*). The γ2 isoform is the most sensitive to allosteric activation by AMP, followed by γ1 and γ3. Differing sensitivities to regulation may allow for greater variation in the AMPK response. It is unclear how nucleotide binding at the exchangeable sites produces allosteric activation of the catalytic domain but both exchangeable sites competitively bind AMP/ADP/ATP.

In contrast to previous structures, two co-crystallisation experiments of truncated AMPK in complex with AXP recently revealed a 5^{o} rotation of the Bateman domains with respect to one another in the presence of ATP as opposed to AMP. This may explain the allosteric activation of AMPK by AMP. However the complexes contained β1 (ATP) and β2 (AMP), suggesting, perhaps, some influence of the β-subunit on the structure of the γ (*144*).

In the ATP-bound structure, the previously termed 'non-exchangeable' Site-4 was occupied by ATP, as was Site-1, however Site-3 was unoccupied. The displacement of the 'permanent' AMP by ATP in the crystal, which has not been shown in solution, might well account for the rearrangement of the Bateman domains.

Two further regulatory roles of AMP are 1) the protection of αT172 from dephosphorylation by phosphatases, and 2) promotion of phosphorylation of αT172 by upstream kinases (an effect which is dependent on myristoylation state)(discussed in Section 1.5.1.4) (*177*). Recently the Gamblin/Carling/Kemp laboratories demonstrated that both regulatory effects are additionally mediated by ADP (*1, 177*).

1.5.2.2 Glycogen Regulation

Glycogen is a highly branched glucose polymer, which forms large cytoplasmic particles. AMPK plays a key role in the regulation of glycogen metabolism (discussed in Section 1.2.1). Indeed aberrant AMPK activity results in glycogen storage disease in skeletal and cardiac tissues (discussed in Section 1.3.4).

The localisation of AMPK to the periphery of glycogen particles has been observed via electron microscopy, in cell-based systems, and in cell-free systems (*136, 183, 184*). Glycogen is thought to bind the GBD at the same interface as β-cyclodextrin (Figure 7). Conserved residues in this interface include β1 W100, K126, W133, L146 and T148, and they appear to be involved in AMPK association with glycogen (*134, 136, 185*).

High levels of skeletal muscle glycogen have been shown to allosterically inhibit AMPK activation in response to either pharmacological treatment or exercise *in vivo* (*186, 187*). Allosteric inhibition and reduced αT172 phosphorylation of AMPK by glycogen granules has been observed *in vitro* and in cell-free assays (*134, 135*). This effect appears to be dependent on the level of glycogen chain branching, and some polysaccharides containing branch point structures were found to inhibit AMPK more potently than others (*134*).

In this model, AMPK is thought to interact with glycogen in two ways; 1) Glycogen branch points (α1→6 linked) are only accessible during times of cellular energy shortage when the structures are broken down to release glucose; AMPK is inhibited, acting as a feedback mechanism allowing rapid re-synthesis of glycogen when environmental glucose concentrations increase. 2) Interactions of AMPK with the reducing ends of linear chains (α1→4 linked) localises AMPK to glycogen particles and in close proximity to some of its targets (e.g. GS), but does not regulate the protein directly (*134, 135*).

Of course the real difficulty in identifying the natural ligand which mediates AMPK regulation by glycogen is the intrinsic heterogeneity of glycogen preparations. However, it is clear that the interaction between AMPK and glycogen is not simply a localisation effect, but also involves effects on the enzyme's regulation.

	Site-1	Site-2	Site-3	Site-4	Ref
Mammalian AMPK	AMP/ADP/ATP/Mg.ATP/NADH ATP/AMP	-	AMP/ADP/ATP/Mg.ATP AMP	AMP (NE) ATP/AMP	(*1, 87*) (*144*)
S.pombe	-	ADP	-	AMP/ADP/ATP	(*142, 188*)
S.cerevisiae	-		-	ADP/AMP/NADH AMP?	(*2*) (*189*)

Table 2: Site occupancy by nucleotides.

The data was compiled from numerous crystal structures of mammalian and yeast γ subunits as referenced in the table. (NE: non-exchangeable).

1.5.2.3 Pharmacological agents

The activation of AMPK has a number of beneficial effects in the treatment of type-2 diabetes (discussed in Section 1.3) and for this reason pharmaceutical companies have pursued the development of small molecule activators of AMPK.

In an experimental setting, AICAR has been widely used as an AMPK activator. AICAR is a nucleoside which, upon cellular uptake, is converted to AICAR 5'-monophosphate (ZMP) by adenosine kinase. ZMP mimics the activatory effects of AMP, albeit with lower potency (*190, 191*). Short-term AICAR treatment does not alter the cellular adenine nucleotide concentrations; however, over prolonged periods the accumulation of ZTP may inhibit AMPK (*192, 193*). ZMP is not a specific AMPK activator as it interacts with other AMP-binding proteins, for example stimulating GP and inhibiting fructose-1,6-bisphosphate (*194, 195*). For this reason it is not practical as a pharmaceutical agent.

In 2003 a specific AMPK activator A-769662 was shown to activate both recombinant and partially purified heart and liver AMPK (*43*). Its administration to obese (*ob/ob)* mice improves several aspects of type-2 diabetes and the metabolic syndrome; reducing plasma glucose and triglyceride levels, increasing fatty acid utilisation, decreasing liver fat area and triglyceride concentration, and decreasing overall body weight (*43*). A-769662 was most concentrated in the liver and plasma tissues, suggesting that it is possible to target drugs to specific tissues dependent on delivery mechanism/concentration administered (*43*).

A-769662 both allosterically activates and protects αT172 from dephosphorylation via a mechanism distinct from that of AMP/ADP (*43, 173, 196*). The compound more potently activates β1-containing complexes, suggesting some isoform specificity.

β-subunit truncations and β S108A phosphorylation site mutation results in a loss of AMPK activation, suggesting that the activity somehow requires this subunit (*173, 197*). Interestingly A-769662 did not compete with sugar binding to the GBD (*134*).

For three reasons A-769662 is not an ideal pharmaceutical agent;

1) A-769662 was delivered to mice models via intraperitoneal injection (although oral administration has been demonstrated), this is not practical in a clinical setting since type-2 diabetes and obesity are chronic disorders treated regularly over long periods (*43*).
2) Skeletal muscle is an important drug target in the treatment of type-2 diabetes. A-769662 did not activate AMPK in this tissue, where the β2 isoform is predominant.
3) Recently it has been suggested that A-769662 may have additional targets to AMPK (e.g. Na^+K^+- ATPase). Thus, A-769662 may not be a specific AMPK activator (*198, 199*).

Therefore, there is considerable interest in designing a more potent, direct AMPK activator for *in vivo* applications.

Salicylate, the breakdown product of aspirin, has recently been shown to directly activate AMPK both allosterically and through protection of αT172 against dephosphorylation. The regulatory effect of salicylate competes with A-769662 activation in a concentration dependent manner; it is both more potent in β1 containing heterotrimers, and absent in S108A mutants. Taken together, this suggests that binding to the same AMPK site might be responsible for activation by both A-769662 and salicylate (*200*). In order for AMPK activation to be achieved *in vivo* it is possible that a high-dose would need to be administered, however it is an intriguing possibility that the anti-cancer effects of aspirin may be mediated through AMPK.

Whilst activation of AMPK in most tissues is beneficial in the treatment of type-2 diabetes, its activation in the hypothalamus may increase the feeding response of the organism

resulting in obesity. Therefore specific inhibitors of AMPK activity may also be interesting drug candidates. Compound C acts as a reversible AMPK inhibitor, competing for binding with Mg.ATP in the α-kinase domain (*66*). Although Compound C has some AMPK selectivity, it has been shown to inhibit a range of other kinases and biological processes (*201*). Furthermore, the apparent inhibition of AICAR activation is due to disruption of AICAR cellular uptake, suggesting that Compound C may not be a direct inhibitor (*202*).

1.5.3 Indirect Regulators

1.5.3.1 Natural Compounds

It appears that a number of naturally occurring compounds activate AMPK indirectly resulting in anti-obesity and anti-cancer phenotypes consistent with AMPK stimulation (Table 3) (described in Section 1.3). Many of these compounds are thought to increase the cellular AMP:ATP ratio through inhibition of mitochondrial ATP production (*203*). One exception is quercetin which has been shown to decrease expression levels of the PP2C phosphatase thereby increasing the activity of AMPK (*204*). It will be interesting to ascertain which of the downstream effects of these compounds are mediated through AMPK.

1.5.3.2 Metformin and thiazolidinediones

Metformin is a prominent type-2 diabetes pharmaceutical agent. The main site of metformin action is the liver where it suppresses gluconeogenic and lipogenic gene expression (*46*).

Metformin inhibits Complex I of the respiratory chain and thereby indirectly activates AMPK through increasing cellular AMP/ADP concentrations (*66, 67*). Studies utilising γ-subunit mutants demonstrate that AMP/ADP binding is necessary for metformin mediated AMPK activation (*205*).

More recently it has been shown that cultured hepatocytes carrying α1 and α2 or LKB1 knock-out mutations show decreased glucose output in response to metformin treatment, suggesting that the effect may in part be AMPK-independent (*206*). Whilst this suggests that control of heptatic gluconeogenesis by metformin may not be AMPK-mediated, it does not negate the fact that AMPK is activated in a metformin dependent fashion (*207*). Therefore other beneficial effects of metformin treatment may still act through AMPK.

Thiazolidinediones bind to the nuclear hormone receptor PPAR-γ, which is predominantly expressed in the adipose tissue but also in the skeletal muscle, liver and macrophages (*46*). The thiazolidinediones improve heptatic insulin sensitivity but do not reduce lipid content, and they activate AMPK in cardiac and skeletal muscle through increasing AMP/ADP concentrations (*46, 208, 209*). Chronic thiazolidinedione treatment may ultimately increase AMPK activity through increased adiponectin production (see Section 1.5.3.4)(*210*).

1.5.3.3 Exercise

During exercise AMPK is activated in an intensity- and time-dependent manner throughout skeletal muscle (*118, 211-213*). Different AMPK isoforms appear to be differentially regulated in response to exercise, with the $\alpha 2\beta 2\gamma 3$ heterotrimer being primarily activated (*119*). Small increases in the cellular AMP:ATP ratio are observed in response to exercise (*155*); it is therefore this and increases in AMP/ADP concentration which activate AMPK. Additionally increased Ca^{2+} concentrations activate CaMKKβ, and therefore AMPK (*160*). It seems likely that this is the basis of many of the health benefits associated with regular exercise, for example through increasing GLUT4 expression and therefore insulin sensitivity as well as increased mitochondrial capacity/density (*19, 42, 214*). Therefore AMPK may mediate, at least in part, the beneficial health effects of exercise.

Compound	Origin	Reference
Curcumin	Principal curcuminoid of the spice turmeric	(*215*)
5-fluorouricil	Chemotherapy drug	(*216*)
Epigallocatechin gallate	Most abundant catechin in tea	(*217, 218*)
Genistein	Isoflavone found in a number of plants	(*216*)
Capsaicin	Active component of chili peppers	(*219*)
p-HPEA-EDA	A phenolic compound of virgin olive oil	(*220*)
Catechin	Component of green tea extract	(*217*)
Quercetin	Flavonoid found in fruits, vegetables, leaves and grains	(*221*)
Resveratrol	Found in the skins of red grapes	(*222*)
Berberine	Plant extract	(*223*)
Various	Nutmeg extract	(*224*)
Ginsenosides	Ginseng	(*225*)

Table 3: Naturally occurring AMPK activators.

A number of compounds have been shown to indirectly activate AMPK through increasing cellular AMP/ADP levels. These compounds, their origin and the relevant references are shown.

1.5.3.4 Endocrine regulation of AMPK

Hormones are secreted into the blood stream from endocrine glands and influence whole-body homeostasis. A number of hormones and cytokines play roles in the progression of the metabolic syndrome and have been shown to regulate AMPK.

Leptin is secreted by the adipose tissue; it is an anorexigenic hormone which targets the hypothalamus. Obese (*ob/ob)* knock-out mice are severely overweight and diabetic (*226, 227*). Through AMPK stimulation, leptin increases the oxidation of fatty acids, increases glucose uptake and prevents the accumulation of lipids in skeletal muscle. Increased αT172 phosphorylation does not appear to correspond to elevated AMP/ADP concentrations suggesting that another mechanism activates AMPK and therefore it remains unclear how leptin activates AMPK (*228, 229*). Chronic leptin treatment required an intact sympathetic nervous system and appeared to increase expression of α2 and β2 AMPK subunits (*63, 229*). In the hypothalamus leptin signalling reduces AMPK activity and decreases food intake through altered neuropeptide expression (*63*). Recently α2 S491 phosphorylation by p70S6K kinase, acting downstream of PI3K-AKT, was found to underlie AMPK inhibition in the hypothalamus. Using S491A mutants this phosphorylation site was shown to be integral to leptin signalling in both cell-based systems and in mouse models (*172*). This suggests that there may be multiple factors which contribute to AMPK inhibition in addition to αT172 dephosphorylation.

Adiponectin is also secreted from the adipose tissue and has a complementary/additive effect to leptin; increasing glucose uptake and fatty acid oxidation whilst decreasing gluconeogenesis (*18, 230*). The levels of this hormone are often decreased in obese and type-2 diabetic humans, compounding the deleterious effects of these diseases (*231*).

AMPK is integral to adiponectin signalling in the skeletal muscle where dominant-negative expression results in a loss of all downstream effects of adiponectin (*232*). AMPK is also activated in the hypothalamus, stimulating food intake (*233*). It appears that this is due to both an increase in AMP and Ca^{2+} concentrations, although the exact mechanism through which adiponectin stimulates these changes remains unclear (*230, 234, 235*). Consistent with LKB1 and CaMKKβ dependent activation, LKB1 knock-out blunts but does not abolish adiponectin signalling in hepatocytes (*236*).

Ghrelin is an orexigenic hormone which acts on the hypothalamus to stimulate food intake, through binding to its G-coupled receptor, it raises Ca^{2+} concentrations and activates AMPK via CaMKKβ (*237, 238*). It is this AMPK activity which, if inhibited pharmacologically, would be beneficial in combating the obesity epidemic.

Oestrogen, androgens, IL-6 and resistin have also been linked to AMPK activity (*46*). Several factors including ciliary neurotrophic factor (CNTF) and α-lipoic acid, inhibit AMPK signalling in the hypothalamus thereby reducing food intake, whilst stimulating AMPK activity in peripheral tissues (i.e. increasing fatty acid oxidation and glucose uptake) (*239-242*). TNFα downregulates AMPK and reduces fatty acid oxidation through increased activity of PP2C (*242-244*). α-lipoic acid stimulates AMPK in the skeletal muscle, and inhibits AMPK in the hypothalamus, through regulation of PP2C (*46*).

A plethora of hormones and cytokines have been shown to regulate AMPK, cementing the enzyme as a key regulator of whole-body metabolism, and as a valuable drug-target in the treatment of multiple diseases.

1.5.4 Concluding Remark

AMPK is regulated in multiple ways both directly and indirectly; it is therefore an important point of integration in the transduction of signals through the cell and in coordinating complex cellular responses to both external and internal stimuli. This thesis focuses on the regulation of mammalian AMPK and the *S.cerevisiae* ortholog, SNF1, by ADP.

1.6 Aims

This project aims to further the understanding of how AMPK is regulated by nucleotide binding to the heterotrimer specifically:

1) To determine the affinities of AXP for the AMPK γ-subunit, and for the equivalent Snf4 subunit of the *S.cerevisiae* homolog.
2) To confirm the AXP γ-subunit sites at which fluorescently labelled nucleotides bind (used in (1)),via X-ray crystallography.
3) To monitor AMPK/SNF1 kinetics and regulation by nucleotide using a coupled spectrophotometric assay.
4) To model the occupancy of AMPK/SNF1 binding sites by AXP based upon the K_d values determined in (1). Firstly, given the conditions of the *in vitro* assay performed in (3), and secondly given intracellular AXP concentrations.

Chapter 2: Methods

General methods of molecular biology, protein expression and protein purification are covered in this Chapter. Specific biophysical and X-ray crystallographic methods are described within the relevant Chapters.

2.1 Molecular Biology

2.1.1 DNA constructs

All vectors were kindly provided by Dr Richard Heath and Dr Matthew Sanders (NIMR).

AMPK

A tricistronic vector containing all three AMPK subunits (N-terminal hexahistidine (His)- α, β and γ) with a commercial pET3d backbone was used for expression in *E.coli*. The polycistronic vector was constructed from individual monocistronic vectors by repetitive cycles of restriction enzyme digestion and ligation as described in Neumann *et al* (*245*). Each subunit has an individual ribosome binding site (RBS), transcription was driven through a T7 promoter, and the vector carried an ampicillin resistance gene.

Full length AMPK: *Human $\alpha1\beta1\gamma1$*

Truncated AMPK: *Rat $\alpha1_{396-548}$, human $\beta2_{187-272}$, rat $\gamma1$*

SNF1

A pETDuet-1 vector (Novagen) carrying Snf4 (γ) and the His-Snf1 (α) subunits and a pRSFDuet-1 vector (Novagen) carrying the Gal83 (β) subunit were co-transformed for the expression of SNF1 in *E.coli.* The vectors carried ampicillin and kanamycin resistance genes respectively; transcription was driven through a T7 promoter.

Full length SNF1: *Snf1, Gal83, Snf4*

Site Directed mutagenesis

Site-directed mutants were generated using the QuikChange site-directed mutagenesis kit (Strategene) according to the manufacturer's protocol.

CaMKKβ

CaMKKβ was expressed from a pET DUET-1 vector (Novagen) from which N-terminally His-tagged CaMKKβ was expressed in *E.coli* cells (*158*).

2.1.2 Bacterial strains

JM109 Competent Cells (Sigma); F′ (traD36*,* *pro*AB+ *lac*I^q, Δ(*lac*Z)M15*)* *end*A1 *rec*A1*hsd*R17(r_k^-, m_k^+) *mcr*A *sup*E44 λ^- *gyr*A96 *rel*A1 Δ*(lacproAB) thi*-1. This competent cell line is a general purpose cloning strain used to generate high quality plasmid DNA. Vectors were transformed (as described in Section 2.1.5), single colonies picked into 10ml LB containing the relevant antibiotic, grown overnight at 37^oC 200rpm (revolutions per minute), and purified using a QIAprep Spin Miniprep Kit (Qiagen) as per the manufacturer's instructions.

XL10-Gold® Ultracompetent Cells (Stratagene); Tet^r Δ(*mcrA*)*183* Δ(*mcrCB-hsdSMR-mrr*)*173* *endA1 supE44 thi-1 recA1 gyrA96 relA1 lac*Hte [F′ *proAB lacI*^{q}ZΔ*M15* Tn*10* (Tet^r) Amy Cam^r]. This competent cell line was used to produce plasmids generated during mutagenesis. The Hte phenotype increases transformation efficiency.

One Shot® BL21 Star™ (DE3) Chemically Competent *E. coli* (Invitrogen); F^- *ompT hsdS*B F^- *ompT hsdS*B (rB^-mB^-) *gal dcm rne131* (DE3). Competent cells were used for the expression of recombinant proteins. The DE3 designation means the strain contains the λ DE3 lysogen

which carries the gene for the T7 RNA polymerase under the control of the *lac*UV5 promoter. Isopropyl β-D-1-thiogalactopyranoside (IPTG) is a lactose analogue which relieves repression of the *lac*UV*5* promoter through clearence of the Lac repressor. This allows expression of T7 RNA polymerase, and therefore transcription of the gene of interest, controlled by a T7 promoter.

Ampicillin (100mg/ml stock) and kanamycin (50mg/ml) were prepared as stock solutions in ddH_2O and stored at -20^oC. Ampicillin and kanamycin were used at a final concentration of 100μg/ml and 50μg/ml respectively.

2.1.3 Agarose gel electrophoresis

DNA preperations were analysed by electrophoresis on a 1% agarose gel made with tris-acetate-EDTA (TAE) buffer containing 0.2μg/ml ethidium bromide for 40minutes at 140V. DNA loading buffer was added to DNA at a ratio of 1:5. DNA was visualised by exposure to UV radiation and the size of DNA fragments was determined through comparison with standard markers (Bioline Hyperladder I).

2.1.4 DNA sequencing

DNA was sequenced by GATC biotech following the company guidelines.

2.1.5 Transformation

Bacterial transformation is the process whereby competent cells take up DNA molecules from the external environment. *In vitro* this technique is used to introduce plasmids carrying a gene of interest to a chemically competent cell-line. 50-1000ng of plasmid DNA (see Section 2.1.1) was added to a single aliquot of *E.coli* competent cells (see Section 2.1.2) and incubated on ice for 10minutes. The DNA:cell solution was heat shocked at 42^{o}C for 45 seconds and immediately returned to ice for 2 minutes. Cells recovered in 250μl SOC media (2%(*w/v*) tryptone, 0.5% yeast extract, 0.05% NaCl, 20mM glucose) at 37^{o}C, and subsequently 30μl was plated on agar plates of the appropriate antibiotic resistance. Plates were incubated overnight at 37^{o}C.

2.2 Protein biochemistry

2.2.1 Protein expression

A single bacterial colony from an agar plate (see Section 2.1.5) was picked into 10ml of Luria Bertani medium (LB - 1% (*w/v*) tryptone, 0.5% yeast extract, 0.5% (*w/v*) NaCl) containing the appropriate antibiotic. The starter culture was incubated at 37^{o}C, 200rpm for around 5hours. For each subsequent 750ml 'large-scale' culture 250μl of the starter culture was plated onto an agar plate of the appropriate antibiotic and incubated overnight at 37^{o}C. Cells were suspended by washing each plate with 10ml of LB-antibiotic and pooling the resulting cultures. 7.5ml of this 'small scale' culture was used to inoculate 750ml of LB containing the appropriate antibiotic, and 'large-scale' cultures were incubated at 37^{o}C, 200rpm until the optical density at 600nm (OD_{600}) was 1.2. The cells were induced with 1mM IPTG and incubated overnight at 25^{o}C, 200rpm. Cells were pelleted by centrifugation at 4000rpm, 4^{o}C for 30minutes and the supernatant discarded, the pellet was washed with 0.9% NaCl and repelleted as before. Cells were stored at -20^{o}C until cell lysis (see Section 2.2.2).

2.2.2 Cell Lysis

Cells were prepared as described in 2.2.1, thawed on ice and resuspended in an appropriate volume of lysis buffer (>5ml per gram of cells)(50mM Tris.HCl pH 8.0, 300mM NaCl, 20mM Imidazole, 0.5mM tris(2-carboxyethyl)phosphine (TCEP), 1mM $MgCl_2$, 25 units Benzonase nuclease (Merck) and 1 cOmplete, EDTA-free Protease Inhibitor Cocktail Tablet (Roche) per 50ml of lysis buffer). Cells were lysed on ice by sonication (Branson Sonifier 450) at 50% power 90second pulses with 30sec rest for a total of 14minutes. The lysate was centrifuged at 25,000rpm, 4^{o}C, for 45minutes, the supernatant was kept on ice, pooled and passed through a 0.45micron filter.

2.2.3 Protein Purification

2.2.3.1 Nickel affinity purification

Immobilised metal ion affinity chromatography (IMAC) is based on the principle that certain divalent metal ions (such as Ni^{2+}) strongly coordinate amino acids, particularly histidine. The introduction of a poly-histidine tag to the protein of interest (see Section 2.1.1) allows these overexpressed proteins to selectively bind the column whilst un-tagged proteins are washed away.

Nickel affinity purification was performed using a 5ml HisTrap HP column (GE healthcare). The column was equilibrated with binding buffer (50mM Tris.HCl pH 8.0, 300mM NaCl, 20mM imidazole, 0.5mM TCEP), the filtered lysis applied and then washed with binding buffer using a P1 pump at a flow rate of 2ml/min. Bound protein was eluted using an AKTAprime, flow rate 2ml/min, with a gradient of 0-100% elution buffer (50mM Tris.HCl pH 8.0, 300mM NaCl, 300mM Imidazole, 0.5mM TCEP) over a volume of 100ml; 5ml fractions were collected throughout. Samples of the lysis, flow through, wash and fractions were taken for analysis on an SDS-PAGE gel (see Section 2.2.6). The best fractions were pooled for further purification.

2.2.3.2 Ion exchange chromatography

Ion exchange chromatography separates proteins based on differences in charge. The pI of a protein is the pH at which the protein carries no net electrical charge, at a pH above its pI the protein carries a net negative charge and vice versa. Full length $\alpha 1\beta 1\gamma 1$ has a pI of 6.7, (crystallography construct: Rat $\alpha 1_{\ 396\text{-}548}$, human $\beta 2_{187\text{-}272}$, rat $\gamma 1$ pI 7.9) (SNF1: Snf1 Gal83 Snf4 pI 5.6). In all cases a HiTrap mono-Q HP column (anionic exchange)(GE healthcare) was used since the buffer pH was higher than the protein's pI. The column was equilibrated and the sample diluted with a low-salt buffer (50mM Tris, 100mM NaCl). The sample was then loaded using a P1 pump at a flow rate of 2ml/min, and the column washed. Bound protein was eluted using an AKTAprime, flow rate 2ml/min, with a gradient of 0-100% high-salt elution buffer (50mM Tris.HCl pH 8.0, 1M NaCl, 0.5mM TCEP) over a volume of 100ml; 5ml fractions were collected throughout. Samples of the fractions were taken for analysis on an SDS-PAGE gel (see Section 2.2.6). The best fractions were pooled for further purification.

2.2.3.3 Size exclusion chromatography

Size exclusion chromatography separates molecules based on their size, larger molecules pass through the column quicker than smaller molecules which are retarded by passing through the porous beads which make up the column. A Superdex 200 gel filtration column (GE healthcare), volume 120ml, was equilibrated with gel filtration buffer (50mM Tris.HCl pH 8.0, 300mM NaCl, 1mM TCEP) on a AKTAprime at a flow rate of 1ml/min. The 5ml sample was injected onto the column and eluted into 2ml fractions. Samples were collected for analysis by SDS-PAGE. The best fractions were pooled for further purification or phosphorylation (Section 2.2.4).

2.2.4 *In vitro* phosphorylation

After gel filtration the best fractions were pooled and the concentration measured (see Section 2.2.7). The samples were phosphorylated through incubation with (final concentrations); 2.5mM $MgCl_2$, 0.5mM AMP and 0.5mM ATP. 1mg of CaMKKβ (purified in house) was added for every 100mg protein. The sample was left overnight (16-17hours) at 25°C and repurified as in Section 2.2.3.3. A sample of unphosphorylated protein was retained for SDS-PAGE (see Section 2.2.6) and mass spectrometry analysis.

2.2.5 His-tag cleavage

After gel filtration the best fractions were pooled and the concentration measured (see Section 2.2.7). 1mg of His-3C (kindly provided by Dr Vangelis Christodoulou, NIMR) was added for every 100mg AMPK/SNF1, and the sample incubated at 20°C for 2hours. The sample was repurified as in Section 2.2.3.3. A sample of uncleaved protein was retained for SDS-PAGE analysis (see Section 2.2.6).

2.2.6 Sodium Dodecyl sulphate-Polyacrylamide Gel Electrophoresis (SDS-PAGE)

5µl of NuPAGE LDS Sample Buffer (Invitrogen) was added to 15µl aliquots of protein sample, and heated at 90°C for 3minutes. Protein samples and Mark 12 protein standards (Invitrogen) were loaded onto a NuPAGE 4-12% Bis-Tris Gels (Invitrogen). Gels were run at 180V for 35minutes in NuPAGE MES SDS Running buffer (Invitrogen). Protein bands were visualised by staining with InstantBlue (Novexin), a Coomassie based staining solution.

2.2.7 Determination of protein concentration

The pooled protein fractions were concentrated using a Vivaspin 20 (Sartorius), 100K, centrifuged at 4000prm until the desired concentration was achieved. The concentration was measured using UV-vis spectrophotometry. The samples absorbance was measured at a wavelength of 280nm using a Nanodrop Spectrometer (ND-1000) or Jasco V-550 UV-Vis spectrophotometer. The protein concentration was calculated as described by the Beer Lambert equation:

$$A = \varepsilon \times C \times L$$

Where: A = absorbance; ε = extinction coefficient ($M^{-1}cm^{-1}$); C = concentration (M); L = pathlength (cm). Protein extinction coefficients were determined using the ExPASy ProtParam tool available online or using published extinction coefficients.

2.2.8 Dynamic Light Scattering (DLS)

DLS measures the size distribution of molecules in an aqueous solution; it is a measure of the heterogeneity of a protein sample. 30μl of 0.6mg/ml sample was centrifuged at 10,000xg, 20^{o}C, for 30minutes. A Viscotek-802 DLS with Omnisize 3.0 Software was used to perform 10 scans per sample and subsequently taking an average. Protein samples for which the calculated molecular weight did not exceed 20% of the expected size, and the polydispersity was less than 20% were considered optimum samples for crystallisation trials.

Chapter 3: Nucleotide binding to AMPK

3.1 Abstract

AMP, ADP and Mg.ATP binding to the γ-subunit of AMPK regulates the catalytic activity of the α-kinase. Binding constants for the interactions between nucleotides and full-length active (phosphorylated on αT172) AMPK have not previously been defined.

In this Chapter the binding of AXP to the full-length α1β1γ1 heterotrimer, both phosphorylated and unphosphorylated, is described. Binding was monitored through displacement of fluorescently labelled nucleotides, either through direct coumarin excitation or Forster Resonance Energy Transfer (FRET) from excitation of intrinsic tryptophan residues.

AMPK binds nucleotides exchangeably at two sites, one (Site-1) with significantly higher affinity than the other (Site-3). Mg.ATP binds competitively but with weaker affinity than the regulatory nucleotides, AMP and ADP. Binding of nucleotides to a number of γ-subunit mutants and the interaction between the α-kinase active site and staurosporine (an inhibitor) was also characterised.

Various biophysical techniques (CD, MALLS) were utilised to ensure the protein samples were of a high quality, and highlighted some interesting differences between the phosphorylated and unphosphorylated AMPK species.

3.2 Introduction

3.2.1 Previous reports of nucleotide binding to AMPK

The γ-subunit of AMPK comprises four CBS motifs, arranged in two Bateman domains (as described in Chapter 1). The role of CBS motifs as adenosine-nucleotide binding modules was first demonstrated in 2004 (*86*). Scott *et al* cloned and purified GST fusions of a number of CBS motifs both in isolation and as tandem repeats from AMPK γ2, γ1 and γ3, IMPDH2, CLC2 and CBS itself. Ligand binding assays were performed by incubation of various concentrations of [^{14}C]AMP or [γ-^{32}P]ATP with CBS constructs and measurement of bound radioactivity by scintillation counting. This study showed that AMPK proteins bound both AMP and ATP competitively. The γ1 CBS 1-4 construct bound AMP and ATP at two sites with K_d values of 20μM (AMP) and 119μM (ATP). The binding curves were analysed assuming two identical AXP binding sites were present, and that binding of AXP at the sites was cooperative. The constructs containing γ2 CBS Sites-1-4 bound 2 molecules of AXP with strong positive cooperativity (Hill coefficient = 2), whilst this was also observed for the γ1 construct the extent of cooperativity was less. These authors observed no effect of $MgCl_2$ on ATP binding (*86*). Two nucleotide molecules were still found to bind to a number of WPWS point mutants introduced into the γ2 construct, but with reduced affinity.

Scott *et al* (2004) established that the γ-subunit of AMPK is the key to α-kinase regulation by nucleotides. However the K_d values were determined based on interactions between the isolated Bateman domains and AXPs and not the intact heterotrimeric AMPK. In 2007, the Gamblin laboratory published the crystal structure of an AMPK truncate which included the complete γ1 subunit (as described in Section 1.4.4) (*87*). This structure confirmed adenosine-nucleotides exchangeably bound the AMPK γ-subunit with a stoichiometry of 2:1 (the third observed AMP being non-exchangeable). At the same time K_d values for

nucleotide interactions with the truncate were reported. Fluorescently-labelled reporters, mant-ATP and mant-AMP, bound with a stoichiometry of 2:1 and with affinities of 4μM and 10μM respectively. Competition assays provided K_d values of 12.5μM and 24.5μM for ATP and AMP respectively. The binding data were analysed assuming the AXP binding sites were independent and identical. No effect of $MgCl_2$ on ATP binding was reported (*87*). Using the same fluorescent reporters, equilibrium dissociation constants for AMP/ADP/ATP binding to a number of WPWS mutations (R69Q, H150R, R298G) in the truncated AMPK construct were determined and suggested weaker binding at both sites (Peter Saiu – PhD Thesis).

A similar but more powerful approach, in which fluorescently-labelled nucleotides were used to probe the interactions between AXP and AMPK is described in this Chapter. The remainder of the introduction focuses on fluorescence, the development of fluorescence AXP reporters, and FRET.

3.2.2 Fluorescence

The absorption of a photon by a fluorophore causes an electronic transition from a ground state to a higher energy excited state. The excess energy in the electronically excited states will eventually be lost by vibrational relaxation and internal conversion until the lowest vibrational level of the first excited state is reached. As the species returns to the ground state a photon is emitted, and it is this which we term fluorescence. The transitions between energy states are often represented in Jablonski diagrams (Figure 12). Loss of energy via a radiative pathway (of which fluorescence is an example) is competitive with other non-radiative pathways such as release of heat, interactions with solvent molecules, collisions with other molecules or resonance transfer to other chromophores. These non-radiative processes are sensitive to solvent properties, temperature and pH, and for this reason fluorescence intensity is also affected by these parameters.

Upon binding a protein, a fluorescent ligand will often experience a change in environment from an aqueous solvent to a partially hydrophobic binding pocket. In many cases this will result in changes in fluorescence emission intensity and emission maximum. Monitoring this change offers one way to characterise the interactions between small molecule ligands and proteins. The small amounts of sample required and the short data collection times involved make optical methods particularly useful in this area.

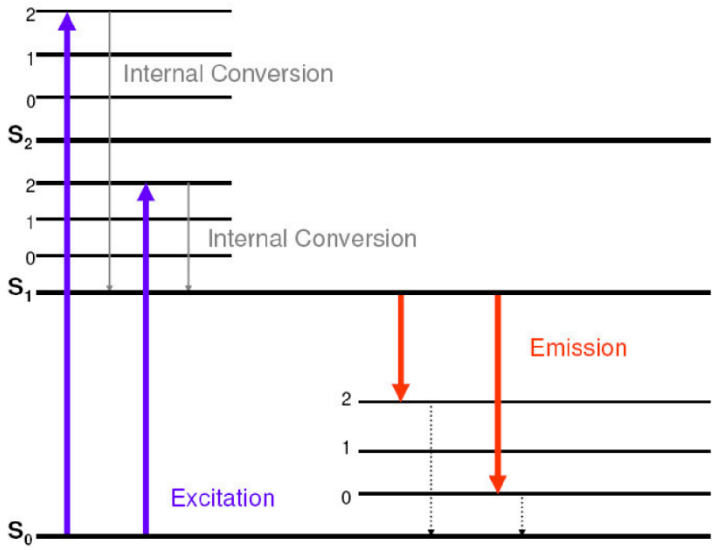

Figure 12: Jablonski diagram.

A photon is absorbed upon excitation causing an electronic transition from the ground state (S_0) to an excited state ($S_{1\text{-}2}$). Excess energy is lost via internal conversion, when the lowest vibrational state of the excited state is reached (S_1) a photon is emitted to return the species to S_0. The species may return to one of multiple vibrational states of S_0.

3.2.3 Fluorescent nucleotide derivatives

Nucleotides bind to a wide range of proteins. Such interactions are fundamental to many cellular processes, and many techniques have been developed to study the kinetic and equilibrium constants which describe them. The use of fluorescent nucleotide derivatives to monitor AXP binding to proteins is widespread owing to its high sensitivity (*246*).

Adenine nucleotides consist of an adenine ring, ribose sugar, and the relevant number of phosphates (Figure 13a). Fluorescent nucleotide analogues with high extinction coefficients, good quantum yields (greater than 0.1) and absorption bands at longer wavelengths than endogenous backgrounds (i.e. mid-UV and longer) have been synthesised and date from the 1970's (*247*). Many such compounds are commercially available. When designing a nucleotide derivative it is important to consider the choice of fluorophore, the linker which connects it to the nucleotide and the likelihood of non-specific binding (*247*).

There are many nucleotide derivatives, a few of which are described here. The purine ring system can be modified, producing so-called 'etheno' nucleotides (Figure 13a). These derivatives are not strongly sensitive to changes in environment and therefore measurements are often made using fluorescence anisotropy. They are often found to alter the rate and equilibrium constants for nucleotide-protein interactions.

Modifications which do not alter the purine ring system but instead conjugate a fluorophore to the ribose moiety, at the 2'- and/or 3'-hydroxyl positions, often mimic more closely their parent nucleotides. In the case of myosin, other nucleoside triphosphatases and AMPK these hydroxyl groups project from the nucleotide binding site away from the protein so

that the fluorophore lies on or near the surface of the protein (Section 5.4)(*246*). In this position it often acts as a good reporter of binding.

2'(3')-O-methylanthraniloyl (mant) derivatives of adenine nucleotides (Figure 13c) have been used to study many nucleotide-binding proteins, including AMPK. The mant fluorophore was chosen for its small size, and sensitivity to changes in environment (typically 2-3 fold enhancement in fluorescence upon binding to proteins) (*87*).

Webb *et al* (2003) synthesised nine coumarin-labelled nucleotides with various lengths and types of linkers and described their properties. One particular analogue (Figure 13d) shows a 17-fold enhancement of fluorescence upon binding actomyosin. They conclude that 'coumarin fluorophores provide a compromise between the wavelength and good environmental sensitivity of their fluorescence'. Such coumarin-labelled nucleotides have been used previously to measure ADP release from actomyosin (*248*). The large fluorescence enhancement upon protein binding make these coumarin-AXP's (C-AXP) much more sensitive than mant-AXP's in the study of nucleotide interaction with AMPK.

In addition to chemically synthesised fluorescent reporters other naturally occurring molecules can be used to the same end. NADH contains an ADP moiety in which the β-phosphate is linked to a second ribose and nicotinamide group (Figure 13e).

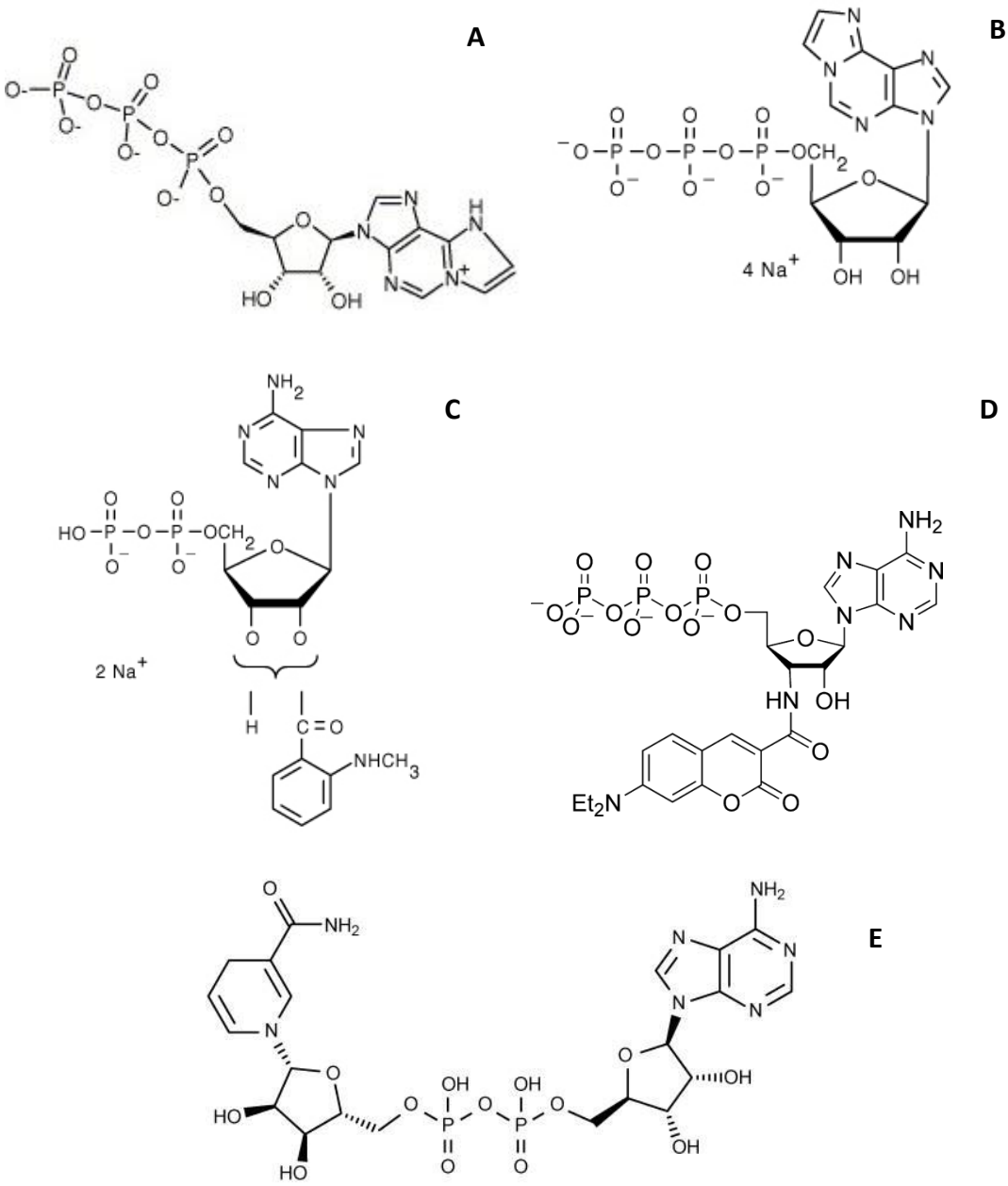

Figure 13: Examples of fluorescently-labelled nucleotides.

A) 1,N^6-ethenoadenosine 5'-triphosphate (ε-ATP);

B) 2'-(or-3')-*O*-(trinitrophenyl)adenosine 5'-diphosphate;

C) 2'-(or-3')-*O*-(*N*-methylanthraniloyl)adenosine 5'-diphosphate;

D) 3’-(7-diethylaminocoumarin-3-carbonylamino)-3’-deoxy-AXP;

E) Nicotinamide adenine dinucleotide

3.2.4 Förster Resonance Energy Transfer (FRET)

Tyrosine, phenylalanine and tryptophan residues are intrinsically fluorescent; all three are excited at wavelengths in the near-UV region (250-300nm). Phenylalanine fluorescence is only observed in proteins lacking both tryptophan and tyrosine. The fluorescence of proteins containing tryptophan and tyrosine is generally dominated by contributions from tryptophan residues, even though the two residues have similar quantum yields. Although this is partly due to the fact that tryptophan has the larger extinction coefficient (fluorescence intensity is proportional to the product of extinction coefficient and quantum yield) the major effect is the loss of tyrosine excited state energy through energy transfer to tryptophan.

It is possible to measure equilibrium dissociation constants for the interaction between a fluorophore and a protein by monitoring FRET between 'donor' tryptophan residues, excited at 290nm, and the 'acceptor' fluorophores from which emission is observed. Electronic excitation energy is transferred through nonradiative dipole-dipole coupling from one fluorophore to another over distances that may extend to 30Å or more. The efficiency of energy transfer depends upon the sixth power of the distance between the fluorophores and upon their relative orientation (*249*). The overlap between the emission of the donor and the absorption of the acceptor must also be considered (*247*). The use of a FRET-based approach to study protein-ligand interactions is an established technique.

In the case of C-AXP binding to AMPK there are 11 potential 'donor' tryptophan residues in full-length human $\alpha 1\beta 1\gamma 1$, two of which are in the γ–subunit. There are also two 'acceptor' C-AXP's binding in the two exchangeable sites of the γ-subunit as determined by direct excitation experiments (Section 3.4.3.1) and observed in the crystal structure of a truncate bound to C-ADP (Chapter 5).

3.3 Methods

3.3.1 Binding experiments

In the analysis of each set of binding data, efforts to confirm stoichiometry of the interaction were initially undertaken, data were then fitted to the models described in the following sections.

In the case of 2:1 interactions data were analysed assuming two independent (non-cooperative), non-identical nucleotide binding sites, to which binding of fluorescent ligand is not necessarily optically equivalent.

3.3.1.1 1:1 interactions

The interaction of a protein (P) with a ligand (L) to form a simple 1:1 complex (PL) is represented by the following scheme:

$$P + L \underset{}{\overset{K_d}{\rightleftharpoons}} PL$$

with the dissociation constant, K_d, defined as $K_d = \frac{[P][L]}{[PL]}$

For any mixture of P and L the observed fluorescence signal (F_{OBS}) is given by:

$$F_{OBS} = F_P[P] + F_L[L] + F_{PL}[PL]$$

Equation 1

where $[X_0]$, $[X]$, and F_X represent the total concentration, the equilibrium concentration, and the molar fluorescence coefficient of species X. A non-linear least-squares fit to equation (1) with [PL] calculated using equation (2) yields the K_d for the interaction and the F_X values.

$$[PL] = \frac{\left(K_d + [P_0] + [L_0]\right) - \sqrt{\left(K_d + [P_0] + [L_0]\right)^2 - 4[P_0][L_0]}}{2}$$

Equation 2

3.3.1.2 2:1 interactions

In the case of 2:1 interactions, when the ligand (L) binds to two sites on a protein (P) the following completely general scheme is appropriate:

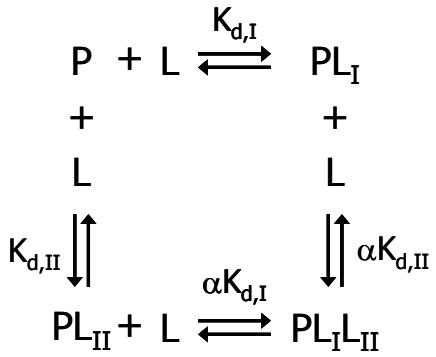

The dissociation constants for the two sites are defined as:

$$K_{d,I} = \frac{[P][L]}{[PL_I]} \qquad K_{d,II} = \frac{[P][L]}{[PL_{II}]}$$

where α is a 'cooperativity factor' which is used to account for the fact that binding at one site may increase ($\alpha < 1$) or decrease ($\alpha > 1$) the affinity of the ligand for the other site. For any mixture of P and L the observed fluorescence signal (F_{OBS}) is given by:

$$F_{OBS} = F_P[P] + F_L[L] + F_{PL_I}[PL_I] + F_{PL_{II}}[PL_{II}] + F_{PL_IL_{II}}[PL_IL_{II}]$$

Equation 3

A non-linear least squares fit to equation (3) yields the K_d values for the interaction and the F_X values. In this case the concentrations are calculated in the following way. The free ligand concentration is given by the root of the following equation:

$$C_3[L]^3 + C_2[L]^2 + C_1[L] + C_0 = 0$$

where the coefficients are:

$$C_3 = \alpha$$
$$C_2 = -\alpha[L_0] + K_{d,I} + K_{d,II} + 2\alpha[P_0]$$
$$C_1 = -[L_0]K_{d,I} - [L_0]K_{d,II} + K_{d,I}K_{d,II} + [P_0]K_{d,I} + [P_0]K_{d,II}$$
$$C_0 = -[L_0]K_{d,I}K_{d,II}$$

[P] can then be obtained from equation (4)

$$[P] = \frac{K_{d,I}K_{d,II}([L_0] - [L])}{K_{d,I}[L] + K_{d,II}[L] + 2\alpha[L]^2}$$

Equation 4

When [P] and [L] are known $[PL_I]$ and $[PL_{II}]$ can be obtained from the expressions for the K_ds and $[PL_IL_{II}]$ from equation (5)

$$[PL_IL_{II}] = \frac{\alpha[L]^2[P]}{K_{d,I}K_{d,II}}$$

Equation 5

3.3.1.3 Competition/displacement

When two ligands (L and N) compete for binding to a single site on a protein (P) the following scheme is appropriate:

$$P + L \overset{K_{d,L}}{\rightleftharpoons} PL$$

$$P + N \overset{K_{d,N}}{\rightleftharpoons} PN$$

The dissociation constants for the two ligands are defined as:

$$K_{d,L} = \frac{[P][L]}{[PL]} \qquad K_{d,N} = \frac{[P][N]}{[PN]}$$

For any mixture of P, L and N the observed fluorescence signal (F_{OBS}) is given by**:**

$$F_{OBS} = F_P[P] + F_L[L] + F_N[N] + F_{PL}[PL] + F_{PN}[PN]$$

Equation 6

A non-linear least squares fit to equation (6) yields the K_d values for the interaction and the F_X values. If the protein and the displacing ligand (N) are non-fluorescent, as is usually the case, then $F_N = F_{PN} = F_P = 0$. For this system the concentrations are calculated in the following way. The free protein concentration is given by the root of the following equation:

$$C_3[P]^3 + C_2[P]^2 + C_1[P] + C_0 = 0$$

where the coefficients are:

$$C_3 = 1$$
$$C_2 = -[P_0] + K_{d,L} + K_{d,N} + [L_0] + [N_0]$$
$$C_1 = -[P_0]K_{d,L} - [P_0]K_{d,N} + K_{d,L}K_{d,N} + [L_0]K_{d,N} + [N_0]K_{d,L}$$
$$C_0 = -[P_0]K_{d,L}K_{d,N}$$

[PL] and [PN] can then be calculated from equations (7) and (8) and the remaining concentrations from the expressions for the K_ds or from conservation of mass (e.g., [L] = [L_0] - [PL]).

$$[\mathrm{PL}] = \frac{[\mathrm{L_0}][\mathrm{P}]}{\mathrm{K_{d,L}} + [\mathrm{P}]}$$

Equation 7

$$[\mathrm{PN}] = \frac{[\mathrm{N_0}][\mathrm{P}]}{\mathrm{K_{d,N}} + [\mathrm{P}]}$$

Equation 8

3.3.1.4 General Materials

Unless otherwise noted all binding measurements were performed at 20^{o}C in 25mM Tris, 1mM TCEP, 100mM NaCl (pH 8) (standard buffer). All fluorescence measurements were made using a Jasco FP-6300 spectrofluorimeter equipped with a ETC-273T Peltier temperature controller. Quartz cuvettes with 3mm and 5mm path lengths were from Hellma. C-AXP's were kind gifts from Dr Martin Webb. ATP, ADP, AMP and NADH were purchased from Sigma and staurosporine from LC laboratories. The concentrations of all stock solutions were determined using published extinction coefficients.

3.3.1.5 Staurosporine binding titrations

Uncorrected fluorescence emission spectra of staurosporine and its complexes with AMPK were recorded at 20^{o}C (unless otherwise specified) in 20% isopropanol (standard buffer). An excitation wavelength of 335nm (bandwidth 2.5nm) was used and emission scanned from 360-500nm (bandwidth 10nm; sensitivity high). Staurosporine has a characteristic emission spectrum with maxima at 378nm and 396nm, the intensity ratio of these peaks is

shifted upon AMPK binding. Binding of staurosporine was monitored through titration of AMPK into a staurosporine solution (0.06μM) mixed by gentle pipetting. The stoichiometry of the interaction was 1:1 (as described in results section) and the binding data were therefore analysed using non-linear least-squares fits to equation (1). In a titration of staurosporine (L) with AMPK (P) $F_P = 0$ and F_L can be estimated from the fluorescence signal observed from the staurosporine solution prior to the addition of AMPK.

3.3.1.6 NADH binding titrations

Uncorrected fluorescence emission spectra of NADH and its complexes with AMPK were recorded at 20^{o}C (unless otherwise specified) in standard buffer. An excitation wavelength of 340nm (bandwidth 2.5nm) was used and emission scanned from 400-550nm (bandwidth 10nm). Free (uncomplexed) NADH has an emission maximum at 462nm. In the presence of saturating AMPK the fluorescence intensity is increased by 3-6 fold depending on the AMPK construct and is blue shifted to 438nm. Binding of NADH was monitored through titration of AMPK into a NADH solution (8μM), mixed by gentle pipetting. The stoichiometry was 1:1 therefore the binding data were analysed using non-linear least-squares fits to equation (1). In a titration of NADH (L) with AMPK (P) $F_P = 0$ and F_L can be estimated from the fluorescence signal observed from the NADH solution prior to the addition of AMPK.

3.3.1.7 Coumarin labelled AXP binding titrations

Uncorrected fluorescence emission spectra of the coumarin analogues of AXP (C-ATP, C-ADP: 3'-(7-diethylaminocoumarin-3-carbonylamino)-3'-deoxyadenosine 5' di- and triphosphate) and its complexes with AMPK were recorded at 20^{o}C (unless otherwise specified) in standard buffer. C-ATP and C-ADP have emission maxima at 479nm (with excitation at 430nm). In the presence of excess AMPK the emission maxima are blue shifted to ~ 470nm and the fluorescence intensity is increased. The stoichiometry of the interactions (2:1) was

confirmed using 'close to stoichiometric' titrations in no salt, 7^{o}C conditions. C-AXP binding data were therefore analysed using non-linear least-squares fits to equation (3). When C-AXP (L) is titrated with AMPK (P) there are six parameters to be determined since F_P = 0 and F_L can be determined from the fluorescence signal observed from C-AXP alone. In order to simplify the analysis we assumed that $F_{PL_IL_{II}} = F_{PL_I} + F_{PL_{II}}$ and that α =1 (i.e., that the binding is non-cooperative). $K_{d,I}$, $K_{d,II}$ and F_{PL_I}/F_L and $F_{PL_{II}}/F_L$ were estimated.

3.3.1.8 AXP binding titrations

Displacement assays of 1) NADH and 2) C-AXP with AMP, ADP and ATP (with and without Mg^{2+}) were used to determine K_d values for adenine nucleotides. Contamination of stock ATP/ADP solutions by breakdown products (ADP/AMP) was assessed by HPLC, the levels were too low to interfere with the binding assays described here (Matthew Sanders –Personal Communication).

NADH displacement data were analysed using non-linear least-squares fits to equation (6) with the K_d for NADH binding fixed at the value determined in the direct titration (65μM). Although this approach ignores any contribution from the binding of AXPs to the weaker of the two sites the dissociation constant determined for binding of AXP to the stronger of the two sites is in good agreement with that determined using competition with the C-AXPs.

Analysis of the displacement of C-ATPs by AXPs is a more complicated because of the multiplicity of species formed. The displacement of C-ATP by ATP clearly occurs in two phases and experiments performed at different starting ratios of C-ATP to AMPK indicated that the C-ATP displaced by low concentrations of added AXP was from the stronger of the two sites (i.e. the strong C-AXP site is also the strong AXP site). Approximate values for the

AXP binding constants were estimated by treating the two parts of the curve separately and using equation (6). We then developed a method which permitted analysis of the whole curve. For any mixture of P (AMPK), L (C-AXP) and X (AXP) the observed fluorescence signal (F_{OBS}) is given by:

$$F_{OBS} = F_L[L] + F_{PL_I}[PL_I] + F_{PL_{II}}[PL_{II}] + F_{PL_IL_{II}}[PL_IL_{II}] + F_{PL_I}[PL_IX_{II}] + F_{PL_{II}}[PX_IL_{II}]$$

Equation 9

Note: Because the AMPK and AXP have no fluorescence contribution we were able to set $F_P = F_{PX_I} = F_{PX_{II}} = F_{PX_IX_{II}} = 0$ and we also included the assumptions that $F_{PL_IX_{II}} = F_{PL_I}$ and $F_{PX_IL_{II}} = F_{PL_{II}}$. The displacement data were then analysed using non-linear least-squares fits to equation (9) with the K_ds for C-ATP binding fixed at the values determined in the direct titrations (see Section 3.4.3.1). Although it would in principle be possible to calculate equilibrium concentrations though the approaches described above it was simpler in this case to calculate them using the method developed by Storer and Cornish-Bowden (described in Section 4.2.5)(*250*).

3.3.2 Circular Dichroism

CD measurements were performed using a Jasco J-715 spectropolarimeter. Far-UV spectra were recorded at 20°C, over a range of λ 195-260nm, using 1mm fused silica cuvettes (Hellma) with a protein concentration of 0.15mg/ml diluted in dH_20. Near-UV spectra were recorded using 10mm fused silica cuvettes (Hellma) with a protein concentration which produced an absorbance in the range of 1-1.5 (~1mg/ml). The CD signal:noise ratio is proportional to the square root of the number of scans and to the square root of the time constant; therefore 30-40scans were recorded with a time constant of 0.25sec, scanning speed 200nm/min and a spectral bandwidth of 1nm, averaged and the baseline subtracted.

CD intensities were converted from millidegrees and presented as molar CD extinction coefficient ($\Delta\varepsilon_M$) for near-UV data or the mean residue CD extinction coefficient ($\Delta\varepsilon_{MRW}$) for far-UV data. Calculated as either:

$$\Delta\varepsilon_M = \frac{S}{32980 \times C_M \times L}$$

Equation 10

$$\Delta\varepsilon_{MRW} = \frac{S \times MRW}{32980 \times C_{mg/ml} \times L}$$

Equation 11

Where:

L= pathlength (cm); C_M = concentration (M); $C_{mg/ml}$ = concentration (mg/ml); S = CD signal (millidegrees); MRW = Mean Residue Weight (Da).

MRW is calculated as MW/N, where MW is the molecular weight and N is the appropriate number of peptide bonds.

Secondary structure content was determined from far-UV spectra using in-house software written by Dr Stephen Martin (NIMR). These programs use a database of reference spectra of proteins with known secondary structure content to iteratively solve a series of simultaneous equations (one for each λ) by a least squares method. This allows the determination of the fraction of α-helix, β–sheet, random coil and β-turn described by the experimental sample.

Thermal denaturation experiments were performed at a fixed λ = 222nm in a 2mm fused silica cuvette (Hellma) with a protein sample of 0.3mg/ml. The temperature ranged from 5-95^{o}C and was controlled by a Jasco PTC-348WI Peltier system. Data were converted to $\Delta\varepsilon_{MRW}$ as before. T_m values were calculated from the first derivative of the unfolding curve.

3.3.3 Multi-Angle Laser Light Scattering (MALLS)

A Superdex S200 size-exclusion column (volume 24ml) was equilibrated with 50mM Tris.HCl pH 8.0, 300mM NaCl, 3mM Sodium Azide, 1mM TCEP at a flow rate of 0.5ml/min. 100μl protein samples, concentration 2mg/ml, were injected onto the column using a syringe at ambient temperature. The scattered light intensity and protein concentration of the column eluate were recorded using a DAWN-HELEOS laser photometer and an OPTILAB-rEX differential refractometer (dRI) (d*n*/d*c* = 0.186), respectively. The weight-averaged molecular mass of material contained in chromatographic peaks was determined from the combined data from both detectors using the ASTRA software version 5.1 (Wyatt Technology).

3.4 Results and Discussion

3.4.1 Expression of recombinant AMPK complexes

A $\alpha 1\beta 1\gamma 1$ construct was used throughout these studies. Expression of recombinant AMPK is well characterised. The subunits were co-expressed on a tricistronic vector and transformed into a competent *E.coli* cell line. Protein was affinity purified via the N-Terminal $\alpha 1$ polyhis-tag and further purified by size-exclusion chromatography (see Chapter 2). The complex was phosphorylated *in vitro* with CaMKKβ, as described in Section 2.2.4.

Figure 14 shows the purified product of AMPK expression and purification resolved by SDS-PAGE. The β-subunit has an anomalous electrophoretic mobility, as commented on in Neumann *et al* (2003) (*245*). This makes resolution of the β and the γ-subunit difficult despite their different molecular weights (30kDa and 37kDa respectively).

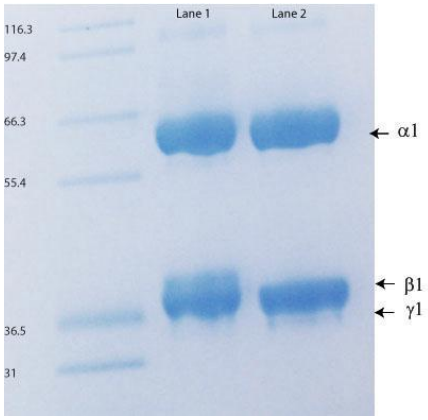

Figure 14: Expression and purification of recombinant α1β1γ1.

Lane 1; phosphorylated AMPK, Lane 2; unphosphorylated AMPK. The purified protein was resolved on a 10% SDS-PAGE Novex gel and stained with InstantBlue stain. The molecular weight markers are indicated on the left (kDa) and the identity of the bands is indicated on the right.

3.4.2 Binding of Staurosporine to AMPK

Staurosporine (Figure 15b) is a potent inhibitor of both tyrosine and serine/threonine protein kinases. Staurosporine acts by blocking ATP binding to the α-kinase domain, as confirmed in the crystal structure of AMPK and other kinases (*1, 251*). The ATP binding site is conserved between kinases; one of the challenges in developing specific inhibitors as drug candidates is being able to achieve acceptable selectivity (*252*). Mg.ATP binds in a conserved pocket between the two kinase lobes of the α-subunit; staurosporine is a non-selective kinase inhibitor which binds competitively at this site. The binding of the inhibitor staurosporine to full-length AMPK was monitored with a view to studying the binding of ADP/ATP via competition experiments.

Excitation of staurosporine at 296nm results in emission bands at 378nm and 396nm, upon binding to many protein kinases the fluorescence signal is enhanced. A competitive displacement assay for evaluating the binding affinity of small molecules to protein kinases using staurosporine has previously been described (*253*).

Although the binding of staurosporine to AMPK does not produce a large change in fluorescence intensity it was possible to determine equilibrium dissociation constants by monitoring changes in the intensity ratio for the two major emission peaks at 378 and 396nm (Figure 15a). As expected, staurosporine was found to bind to full length AMPK with high affinity and 1:1 stoichiometry (Figure 16). Although analysis of such high affinity interactions can be difficult it was possible to determine equilibrium dissociation constants of 1.68 ± 0.47nM for phosphorylated AMPK and 5.63 ± 2.88nM for the unphosphorylated form.

There are six hydrogen-bonds formed between staurosporine and AMPK (PDB ID: 2Y94). There are also substantial Van der Waal and hydrophobic interactions which contribute to the high affinity binding.

Previously Engh *et al* correlated the buried surface area of a kinase inhibitor to its inhibition i.e. the larger the interaction surface the more potent the inhibitor (*254*). The buried surface area of the staurosporine: AMPK interaction is around 320Å (as calculated from PDB: 2Y94), and this is amongst the largest of the reported interfaces (*254*). AMPK is inhibited by staurosporine with commercially reported IC_{50} values of between 14.2nM and 67nM (*255, 256*). These IC_{50} values and the low nanomolar K_d values reported here fit the model proposed by Engh *et al* (2002) (*254*).

Binding of staurosporine was also monitored in the presence of 0.5mM ADP, ATP and Mg.ATP (Figure 16). No significant competition with nucleotides was observed, suggesting that binding of nucleotide at the α-kinase ATP binding pocket is relatively weak. It is not surprising that Mg.ATP binding to kinases is relatively weak, especially for the inactive kinase (discussed further in Chapter 5) (*257*). The Mg.ATP binding site buries all but the terminal γ-phosphate which is transferred to the substrate during catalysis. The lack of accessibility to the site contributes to the low binding affinities of Mg.ATP and slow dissociation of ADP (*257*).

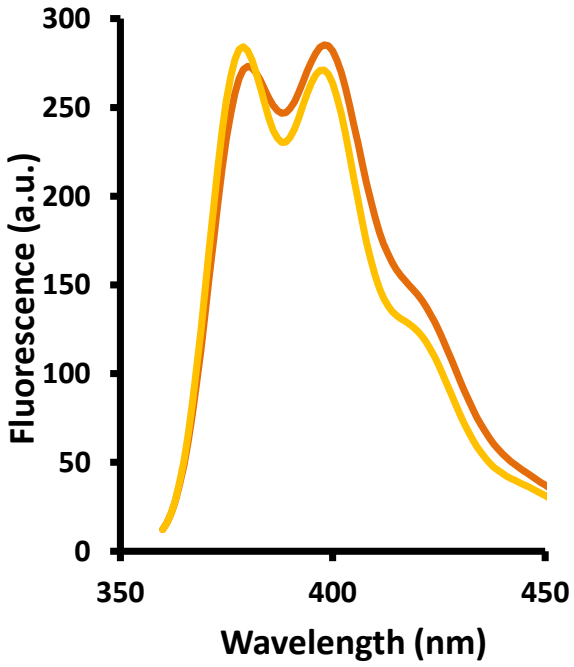

A

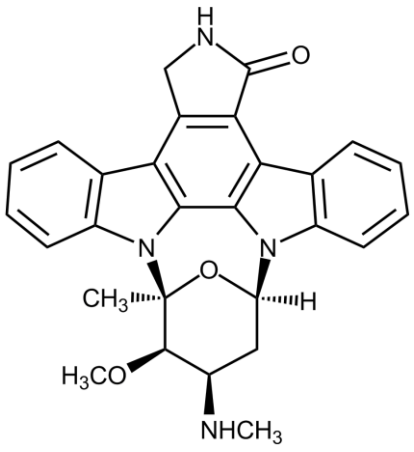

B

Figure 15: A) Emission spectra of staurosporine in the presence and absence of phosphorylated AMPK.

Yellow) On excitation at 335nm, the emission spectrum of 0.06µM staurosporine shows two bands centred at 378 and 396nm. Orange) Addition of 0.37µM phosphorylated AMPK produces a change in the intensity ratio for these two peaks.

B) Staurosporine.

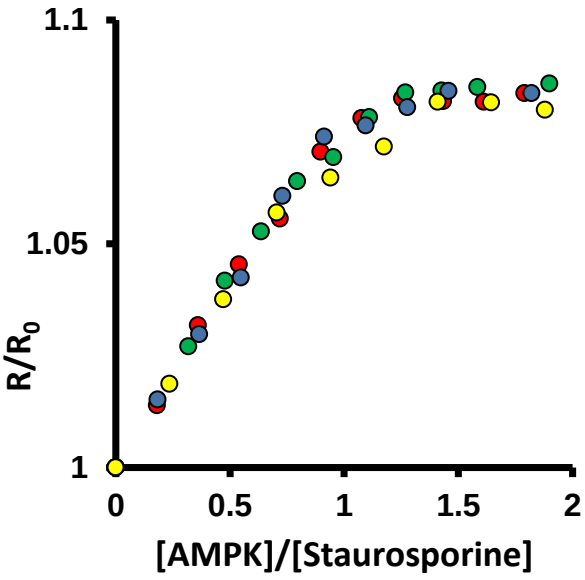

A

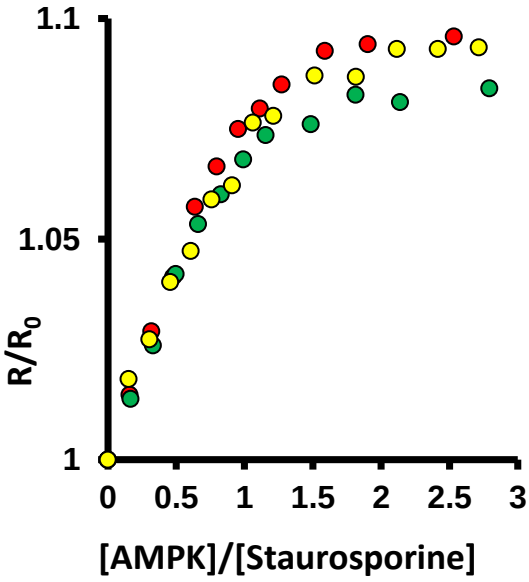

B

Figure 16: Determination of the equilibrium dissociation constant for the binding of staurosporine to A) phosphorylated and B) unphosphorylated AMPK.

Titration of staurosporine with AMPK in the presence of no nucleotide (red), 0.5mM ATP (green), 0.5mM ADP (yellow) and 0.5mM ATP/1.9mM $MgCl_2$ (>95% Mg.ATP) (blue). The change in the ratio of emission peak intensities (where R and R_0 are the intensity ratios λ 396:378nm in the presence/absence of AMPK) is plotted as a function of [AMPK]/[Staurosporine]. No significant differences in curve shape or signal intensity were observed in the different nucleotide conditions, and 1:1 stoichiometry was observed throughout.

3.4.3 Binding of nucleotides to AMPK

3.4.3.1 Direct coumarin excitation experiments

Coumarin labelled analogues of ADP and ATP were used as probes to monitor nucleotide binding to AMPK (Figure 13D; Section 3.2.3). Initial experiments suggested C-AXP's bound AMPK tighter than the mant-AXP's previously used by the Gamblin group (*87*). The higher affinity interaction facilitates analysis of subsequent competition experiments.

Only binding of AXP to γ1 containing heterotrimers was considered; upon expression bacterial, recombinant AMPK complexes which contain γ2 or γ3 isoforms are found to degrade from the N-terminus to produce a stable 'γ1-like' truncate (Personal Communication – Matthew Sanders). The significance of this instability *in vivo* is unknown.

A stoichiometry of 2:1 for C-ADP and C-ATP binding to phosphorylated and unphosphorylated full length AMPK and to the truncated crystallisation construct (Chapter 5), was demonstrated by performing titrations at low temperature in the absence of salt (Figure 17). Equilibrium dissociation constants at 20^{o}C in the presence of 100mM salt were then determined as described in the Section 3.3 (Figure 18 inset).

Reducing temperature decreases the kinetic energy of the system and therefore tends to increases the affinity of protein:ligand interactions. Decreasing the temperature also reduces the energy lost via non-radiative relaxation from the excited to ground state, increasing the fluorescence signal. Many binding interfaces are reliant on electrostatic interactions, therefore decreasing the buffer salt concentration reduces 'masking' of the

charged residues and increases the binding affinity. Experimental conditions of 7°C and 0mM NaCl are far from physiological. 20°C, 100mM NaCl offers a compromise on sensitivity versus relevant biological conditions.

To confirm that C-AXP's do not bind the α-kinase domain a number of control titrations with full length and truncated crystallisation constructs were performed in an isopropanol containing buffer with and without staurosporine (Table 4). The isopropanol is necessary to ensure staurosporine remains soluble throughout the experiments. The addition of isopropanol to the buffer weakened binding of C-AXPS to AMPK slightly, but no significant differences were observed in the presence/absence of the inhibitor, or between the truncated and full-length protein samples. It is therefore concluded that C-AXP's do not bind to the α-kinase domain and that staurosporine is not needed in subsequent titrations (Table 4, Table 5 and Table 6). C-AXP's have previously been demonstrated to be better substrates for ATPases than for kinases. This is because the kinase ATP binding pocket has a high specificity with respect to ribose modifications, and in this case the coumarin fluorophore is conjugated to a hydroxyl of the ribose (Figure 13D) (*248*). Therefore it is unlikely that C-AXP's are capable of binding to the α-kinase domain.

Equilibrium dissociation constants for AXP binding to phosphorylated, unphosphorylated and truncated AMPK were determined through displacement of C-ATP from the AMPK:$(C\text{-}ATP)_2$ complex (Figure 18). Fluorescence emission was monitored at 470nm, experiments were performed at 20°C in the presence of 100mM salt. AXP's bound with a stoichiometry of 2:1 and K_d values were determined as described in Section 3.3 (Table 7 and Table 8).

The presence of $MgCl_2$ in the buffers reduced the fluorescence signal upon C-AXP binding to AMPK to about 1/5 of that in its absence (Figure 19). Mg.C-AXP binding to AMPK was weakened at both exchangeable AXP sites by between five- and fifteen-fold compared to free C-AXP. The effect appeared to saturate at $[Mg^{2+}] > 0.5$mM for C-ATP and at $[Mg^{2+}]$ between 2 and 5mM for C-ADP, consistent with the fact that Mg^{2+} binds significantly more strongly to ATP than ADP (Table 4 and Table 5).

Through displacement of C-ATP it was determined that phosphorylated AMPK binds Mg.ATP 32-fold weaker at the tighter AXP binding site, and 3.5-fold weaker at the second site compared to free ATP (Table 7). This highlights the sensitivity of the AMPK AXP binding sites for the Mg^{2+} bound state of nucleotides.

Previous studies indicated that Mg^{2+} has no effect on the binding of ATP to AMPK; in both cases truncated protein constructs were used suggesting that perhaps the effect is only apparent in the complete heterotrimer (described in Section 3.2.1) (*86, 87*). Sensitivity to Mg^{2+} bound versus free ATP contrasts AMPK with other proteins, such as kinases and GTPases whose affinity for nucleotide is strongly and positively dependent on the presence of Mg^{2+} (*258*).

My studies show that Mg.ATP binds 3-30 fold weaker than ADP to AMPK. Physiologically the majority of ATP exists as Mg.ATP (3-8mM) whilst most ADP is free (50-200μM), therefore the weaker affinity of Mg.ATP for AMPK should facilitate ADP to compete for binding to the heterotrimer *in vivo* and to regulate activity, despite its significantly lower cellular concentration. This idea is explored in much greater detail in Chapter 4.

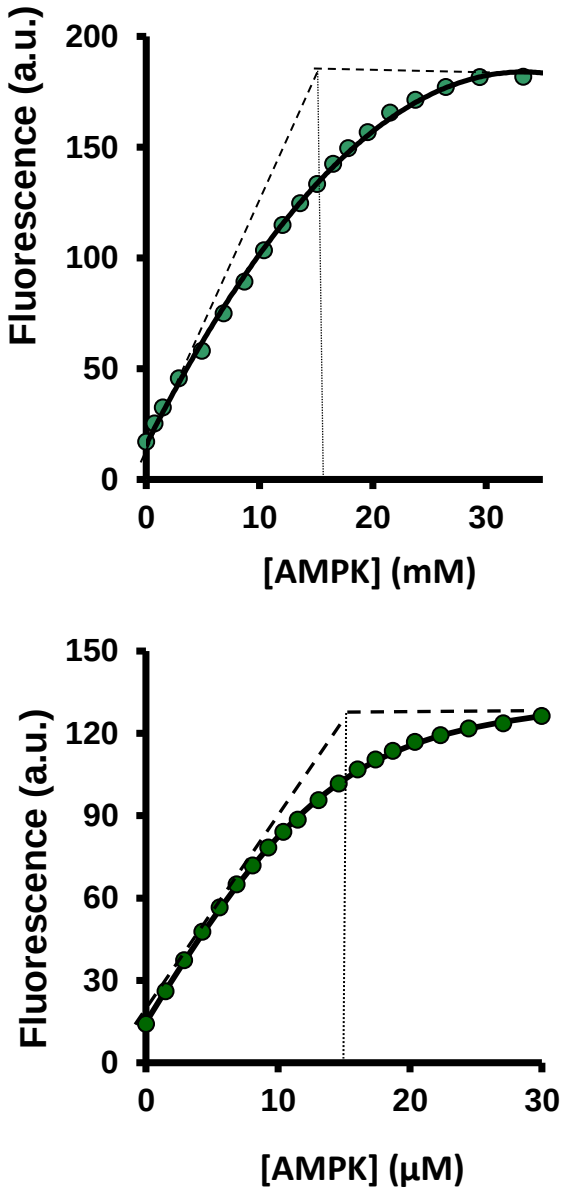

Figure 17: (A) Determination of stoichiometry for C-ATP binding to AMPK.

Titration of 24.6µM C-ATP with phosphorylated AMPK.

(B) Determination of stoichiometry for C-ADP binding to AMPK; Titration of 25.2µM C-ADP with phosphorylated AMPK. In each case the change in emission intensity at 470nm, on excitation at 430nm, is plotted as a function of the [AMPK]. Hashed lines indicate the stoichiometric point; the intensity plateaus when the protein concentration is half that of the coumarin ligand, indicating 2:1 binding. Measurements were performed at 7^{o}C in 25mM Tris, 1mM TCEP (pH 8).

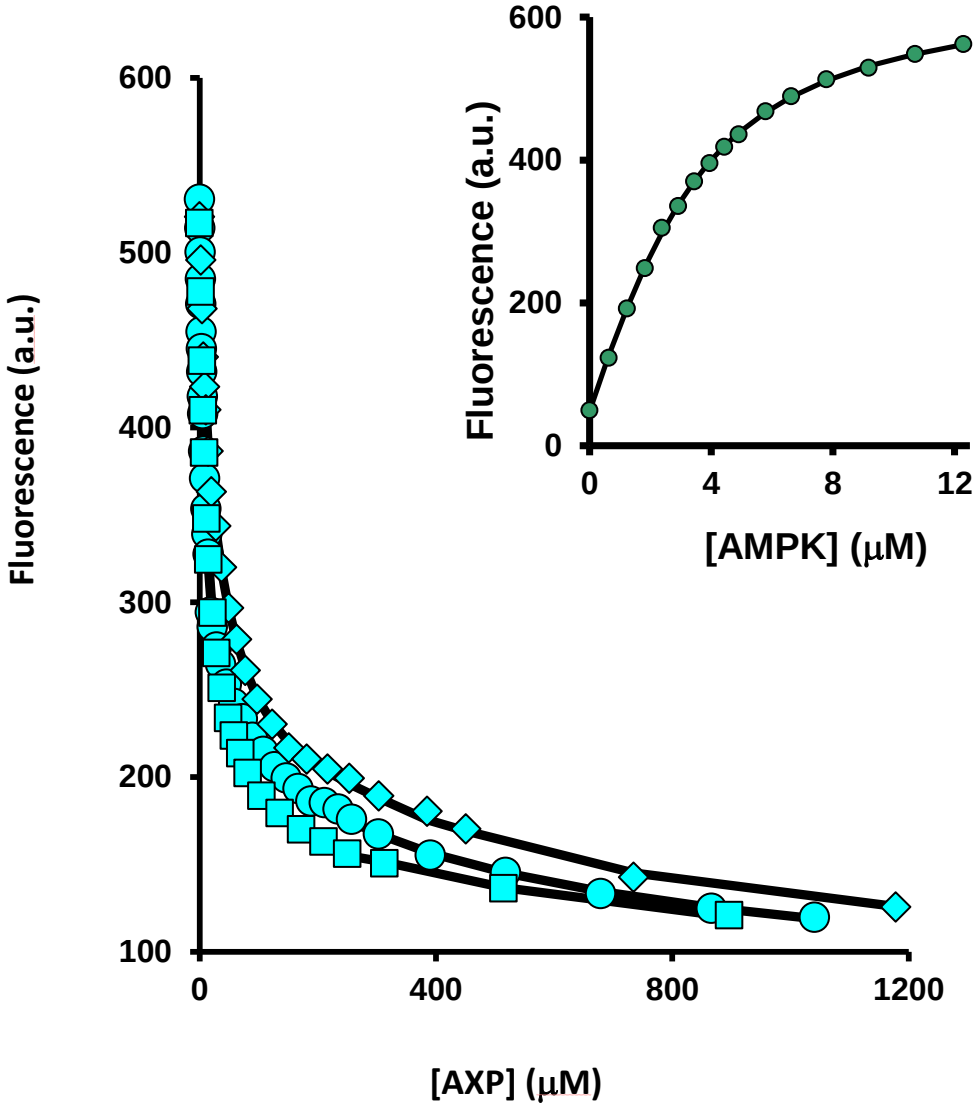

Figure 18: Measurement of equilibrium dissociation constants for the binding of AXPs to phosphorylated AMPK.

Displacement of C-ATP from the AMPK:$(C\text{-}ATP)_2$ complex by ATP (square), ADP (circle) and AMP (diamond) monitored using the change in fluorescence at 470nm (Excitation at 430nm). The solid lines are the computed best fits with $K_{d,I}$ and $K_{d,II}$ for C-ATP binding to AMPK fixed at 1.1 and 4.2 μM respectively in the analysis. Inset: Fluorescence titration of C-ATP with AMPK. All measurements were performed at 20°C in 25mM Tris, 1mM TCEP, 100mM NaCl (pH 8).

Phosphorylated-AMPK	**C-ADP**		**C-ATP**	
Buffer condition	**K_{dI} (μM)**	**K_{dII} (μM)**	**K_{dI} (μM)**	**K_{dII} (μM)**
	0.85 (0.11)	4.89 (1.27)	1.25 (0.14)	5.9 (2.03)
1mM $MgCl_2$	1.83 (0.35)	13.51 (5.39)	8.5 (3.2)	18.6 (6.2)
5mM $MgCl_2$	6.22 (1.58)	18.8 (1.1)	nd	nd
20% isopropanol	3.62 (1.29)	20.95 (7.05)	1.89 (0.68)	18.57 (6.42)
20% isopropanol & 17μM Staurosporine	2.31 (1.08)	14.76 (6.76)	2.13 (0.54)	13.79 (2.61)

Table 4: Equilibrium dissociation constants for the binding of C-AXPs to phosphorylated AMPK.

Dissociation constants were determined at 20°C by fluorescence titrations of C-ATP with AMPK in 25mM Tris, 1mM TCEP, 100mM NaCl (pH 8) with and without 1mM/5mM $MgCl_2$, 20% isopropanol and 17μM staurosporine (as indicated in the table). The K_d values are reported as the mean (± SD) determined from at least three independent measurements. nd: Not determined.

Unphosphorylated-AMPK	**C-ADP**		**C-ATP**	
Buffer condition	**K_{dI} (μM)**	**K_{dII} (μM)**	**K_{dI} (μM)**	**K_{dII} (μM)**
	0.45 (0.03)	3.14 (0.75)	0.24 (0.07)	5.37 (2.00)
1mM $MgCl_2$	1.47 (0.39)	9.24 (3.45)	4.33 (1.04)	25.5 (1.53)
5mM $MgCl_2$	6.54 (1.47)	26.5 (2.3)	nd	nd
20% isopropanol	1.93 (1.27)	11.0 (3.33)	0.72 (0.4)	10.12 (4.02)
20% isopropanol & 17μM Staurosporine	1.64 (1.09)	18.5 (4.08)	1.46 (0.65)	7.45 (3.05)

Table 5: Equilibrium dissociation constants for the binding of C-AXPs to unphosphorylated AMPK.

Dissociation constants were determined at 20°C by fluorescence titrations of C-ATP with AMPK in 25mM Tris, 1mM TCEP, 100mM NaCl (pH 8) with and without 1mM/5mM $MgCl_2$, 20% isopropanol and 17μM staurosporine (as indicated in the table). The K_d values are reported as the mean (± SD) determined from at least three independent measurements. nd: Not determined.

Truncated-AMPK	**C-ADP**		**C-ATP**	
Buffer condition	**K_{dI} (μM)**	**K_{dII} (μM)**	**K_{dI} (μM)**	**K_{dII} (μM)**
	1.07 (0.23)	5.94 (1.40)	0.81 (0.08)	9.59 (2.16)
20% isopropanol	3.61 (1.02)	14.6 (6.72)	1.87 (0.58)	16.71 (4.78)
20% isopropanol & 17μM Staurosporine	4.98 (1.46)	15.12 (7.04)	2.55 (1.05)	18.8 (5.83)

Table 6: Equilibrium dissociation constants for the binding of C-AXPs to truncated AMPK.

Truncated AMPK refers to the crystallisation construct, (rat $\alpha1_{396\text{-}548}$ human $\beta2_{187\text{-}272}$ rat $\gamma1_{1\text{-}330}$). Dissociation constants were determined at 20°C by fluorescence titrations of C-ATP with AMPK in 25mM Tris, 1mM TCEP, 100mM NaCl (pH 8), 20% isopropanol and 17μM staurosporine (as indicated in the table). The K_d values are reported as the mean (± SD) determined from at least three independent measurements.

Phosphorylated	K_{dI} (μM)	K_{dI} (μM)	K_{dII} (μM)
Ligand	***vs* NADH**	***vs* C-ATP**	
AMP	1.6 (0.5)	2.5 (0.6)	80 (25)
ADP	1.3 (0.5)	1.5 (0.4)	50 (15)
ATP	0.9 (0.3)	1.7 (0.5)	65 (15)
Mg.ATP	32 (12)	55 (8)	230 (80)
Mg.ADP	nd	21 (9)	85 (35)

Table 7: Equilibrium dissociation constants for the binding of AXPs to phosphorylated AMPK. Dissociation constants were determined at 20°C by competition against NADH or C-ATP in 25mM Tris, 1mM TCEP, 100mM NaCl (pH 8) with and without 5mM $MgCl_2$ (as indicated in the table). The K_d values are reported as the mean (± SD) determined from at least three independent measurements**.** nd: Not determined.

Unphosphorylated	K_{dI} (μM)	K_{dII} (μM)
Ligand	***vs* C-ATP**	
AMP	2.13 (0.75)	78 (24)
ADP	0.86 (0.31)	63 (19)
ATP	0.51 (0.13)	61 (18)

Table 8: Equilibrium dissociation constants for the binding of AXPs to unphosphorylated AMPK. Dissociation constants were determined by displacement of C-ATP. Experimental conditions as described in Table 7.

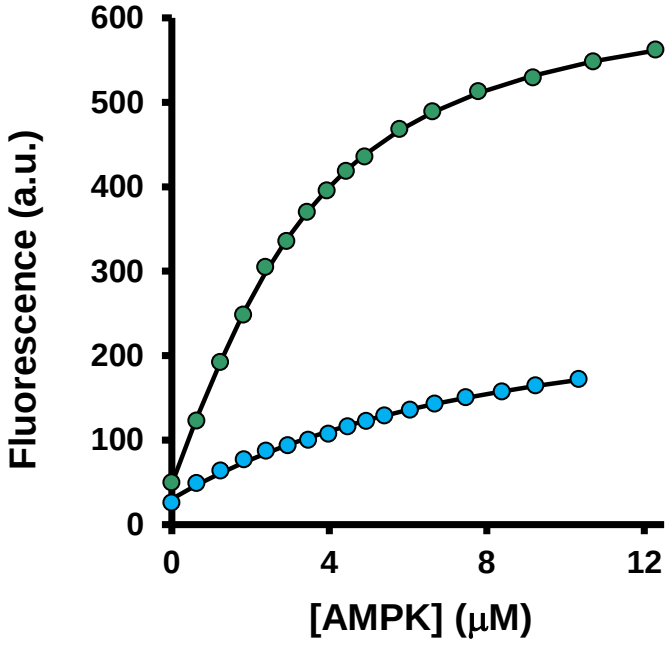

Figure 19: Measurement of equilibrium dissociation constants for the binding of C-ATP to phosphorylated AMPK in the presence of Mg^{2+}.

The change in fluorescence at 470nm (Excitation at 430nm) was monitored in the presence (blue) and absence (green) of 1mM $MgCl_2$. The solid lines are the computed best fits. All measurements were performed at 20°C in 25mM Tris, 1mM TCEP, 100mM NaCl (pH 8).

3.4.3.2 Cooperativity

Systems involving multiple binding sites can show co-operative binding behaviour, that is, the affinity of ligand binding at one site may depend on whether or not another site is occupied. In general, it is easiest to assume that a binding event is non-cooperative, both energetically (i.e. α = 1) and spectroscopically (the optical properties of the ligand in one site are not affected by occupancy of the other). The classic example of positive cooperativity is oxygen binding to the $(\alpha\beta)_2$ globin chains of haemoglobin.

There are two common ways to represent cooperativity in a system;

1) Through use of the Hill equation, which assumes that only the unbound and fully bound complexes exist, therefore in systems where a single site may be bound and another remain empty, i.e. those which are not strongly positively cooperative, these approximations are problematic (*259*).
2) Via a co-cooperativity factor, α. If $\alpha < 1$ binding is positively cooperative, if $\alpha > 1$ then binding is negatively cooperative, and α = 1 there is no cooperativity (where we are dealing with dissociation constants). α can only be properly determined if the binding sites are identical. In the case of multiple ligands binding to a single protein the reaction scheme is often defined as;

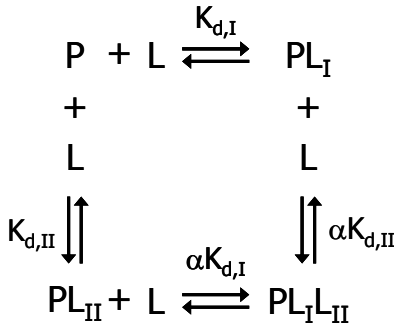

Cooperativity can only be properly determined in a binding assay where the degree of saturation ([bound ligand]/[total protein]) can be determined as a function of free ligand concentration. This can be done with techniques such as equilibrium dialysis (which requires high [protein]) and through the use of radioactive-labelled nucleotides in a filter based binding assay (access to which was not available). It is not generally possible using optical methods as the free ligand concentration is not measured directly.

In their 2004 study, Scott *et al,* studied isolated AMPK γ-subunit CBS domains. They fitted their binding data to the Hill equation and determined a Hill coefficient of ~2, suggesting binding is positively co-operative (*86*). The 2007 Xiao *et al* study, and subsequent work of Peter Saiu (PhD Thesis) assumed binding was independent at the two sites, both spectroscopically and energetically (*87*).

In the work presented here the sites were assumed to be energetically and spectroscopically non-cooperative (α = 1), although the contributions to the fluorescence signal from the C-AXP binding at the two sites was thought to be different. A number of fits were performed with positive and negative cooperativity factors included in the fitting equations used in the analysis of the C-AXP binding curves. The effect of $\alpha > 1$, $\alpha < 1$ on the resultant K_d and statistical values was recorded (Table 9). If there is negative cooperativity (α>1) then the K_d for the weaker site would be lower when the strong site was unoccupied (and vice versa). Although the intrinsic K_d for the weaker site could therefore be lower than I report the only experimental observable is binding to this site when the other site is occupied.

α	K_{dI} (μM)	K_{dII} (μM)	χ^2
1	0.30	8.40	1.15
0.2	0.29	43.00	1.15
2	0.31	4.00	1.15

Table 9: Effect of α on K_d.

Fitting of a single titration of phosphorylated AMPK with C-ADP, the α parameter was varied as indicated and the outputted K_d and χ^2 values recorded. Equivalent to the data displayed in Table 4.

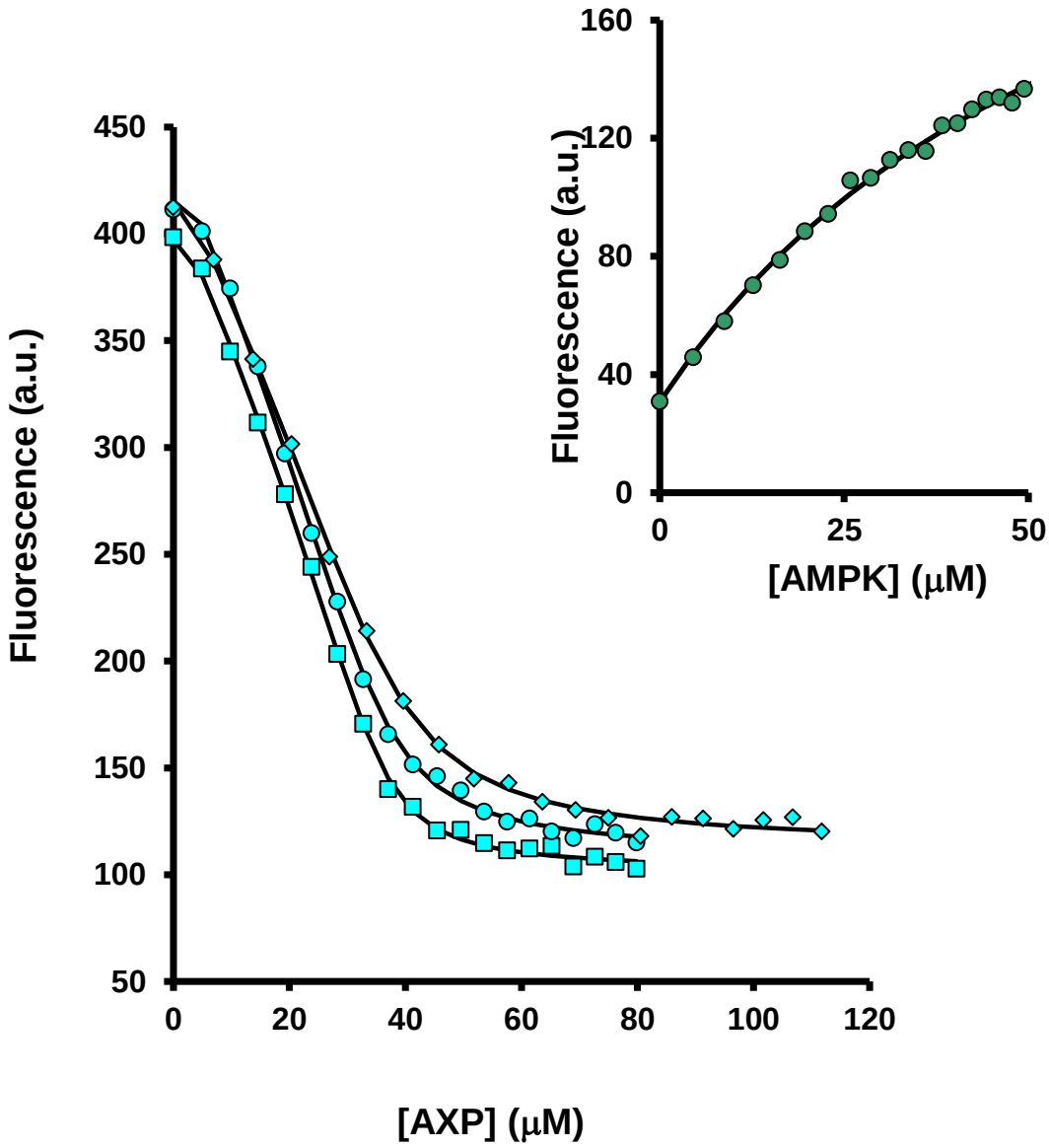

Figure 20: Measurement of equilibrium dissociation constants for the binding of AXPs to phosphorylated AMPK.

Displacement of NADH from the AMPK:NADH complex by AXPs monitored using the change in fluorescence at 435nm (Excitation at 340nm). The solid lines are the computed best fits with the K_d for NADH fixed at 65 μM in the analysis. Inset: Fluorescence titration of NADH with AMPK. All measurements were performed at 20^{o}C in 25mM Tris, 1mM TCEP, 100mM NaCl (pH 8).

3.4.3.3 NADH experiments

In order to complement the coumarin titrations, the binding of NADH to AMPK was quantified. Previously K_d values of 18.3μM and 156μM were reported for NADH and NAD^+ binding to the truncated crystallisation construct (Peter Saiu – PhD Thesis).

NADH binds weakly to full-length AMPK even at low temperature in the absence of added salt but analysis of these binding curves using a 1:1 model was significantly better than a 2:1 model. Two additional pieces of evidence suggest a 1:1 model for the binding of NADH is appropriate. Firstly the experiments in which NADH is displaced by AXP's show that when a mixture of AMPK (32μM) and NADH (15μM) is titrated with AXPs almost complete displacement of NADH is observed when just over one equivalent of AXP is added. Secondly, the C-AXPs which bind to two sites on AMPK cannot be completely displaced by NADH.

In the absence of salt and at 7°C a K_d of around 22μM is estimated for NADH binding AMPK and at 20°C, 100mM salt the binding is significantly weaker, around 65μM. Equilibrium dissociation constants for AXP binding to phosphorylated, unphosphorylated and truncated AMPK were determined through displacement of NADH from the AMPK:NADH complex (Table 7, Table 8 and Figure 20). Emission was monitored at 435nm, experiments were performed at 20°C in the presence of 100mM NaCl, K_d values were determined as described in the Section 3.3. NADH binding was not affected by the presence of Mg^{2+}, as NADH binds magnesium very weakly. Importantly, the AXP K_d values determined through displacement of NADH corresponded well to the 'tight' C-AXP binding site.

The cellular concentrations of NAD^+/NADH are estimated at 0.1-0.4mM with the oxidised form greatly in excess (*260, 261*). With such weak binding affinities, it is unlikely that much, if any, AMPK is bound by these co-factors in a cellular environment.

Whilst the binding of NADH does not directly regulate AMPK, it can compete *in vitro* for binding at one of the regulatory sites. Importantly NADH competes with allosteric activation by AMP, but not the protection against dephosphorylation by AMP/ADP. This suggests that the two exchangeable sites have different regulatory roles and is considered in Chapter 4.

3.4.3.4 FRET-based binding experiments

A complementary FRET-based approach was also used to study the binding of nucleotides to AMPK (see Section 3.2.4). Usefully, this methodology requires significantly less protein than the direct coumarin excitation experiments previously described.

C-ADP and C-ATP bound AMPK complexes have different intensity emission spectra in both direct excitation (430nm) and FRET (290nm) experiments. The C-ADP bound complex has a consistently lower fluorescence signal when compared to the C-ATP bound complex. The signal intensity also varies between unphosphorylated and phosphorylated samples (Figure 21). This is not surprising since the fluorescence signal can be strongly affected by small changes in the environment of the fluorophore.

Titrations of both unphosphorylated and phosphorylated AMPK with C-AXP were performed. Tryptophan residues were excited at 290nm and C-AXP emission monitored at λ 450-550nm. Emission and excitation spectra of the relevant fluorophores are shown in Figure 22, the overlap between AMPK emission and C-ATP excitation is highlighted. Experiments were performed at 20^{o}C in the presence of 100mM NaCl (Figure 23, Figure 24).

These titrations did not permit the stoichiometry of the AMPK:C-AXP complex to be ambiguously determined, although the χ^2 values were generally improved (on average, 1.6-fold) when fitting to a two-site rather than a one-site model.

Analysis of the FRET-binding curves gave equilibrium dissociation constants for C-AXP binding in reasonable agreement with those determined for the tighter AXP binding site using direct excitation (Table 10). The second dissociation constant was generally poorly defined and, in some cases, there was little evidence for any contribution from binding at the second site. This suggests that a large proportion of the observed FRET signal derives from binding at the tighter site only.

There are several potential reasons for this; the binding of a second C-AXP may not be accompanied by a significant fluorescence change or that the efficiency of transfer to the second site is lower. It is also conceivable that binding at the second site has some unexpected effect on the fluorescence properties of the system, for example if a tryptophan is able to transfer energy to both coumarins then binding of the second will reduce transfer to the first. There is the further possibility of fluorescence homotransfer between the two coumarin molecules when the second binds.

In hindsight, the presence of multiple donor tryptophan residues and two acceptor coumarin fluorophores makes analysis of these experiments challenging.

Owing to the uncertainty with the C-AXP:AMPK K_d values and stoichiometries determined by the FRET method only single repeats of AXP dissociation titrations were performed (Figure 23 and Figure 24). This binding data was not analysed further and therefore no K_d values for AXP:AMPK binding were determined by this method. Nevertheless, the form of these curves is consistent with the results obtained in the direct coumarin titrations (Section 3.4.3.1).

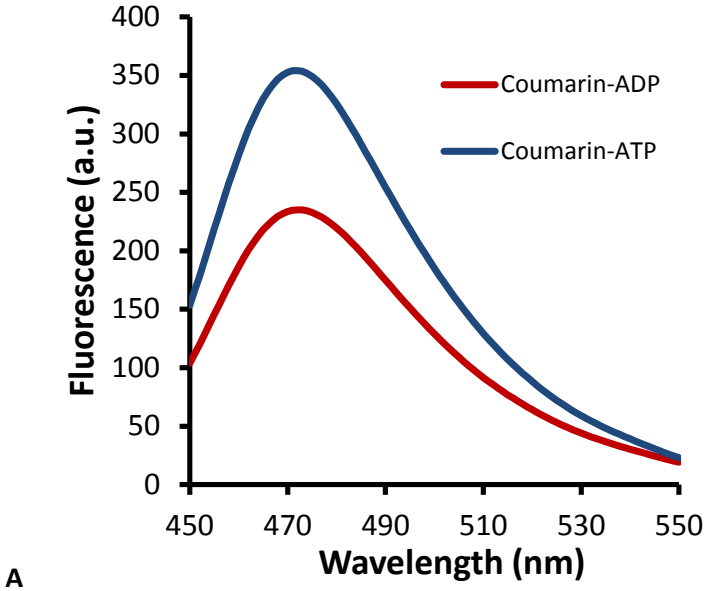

A

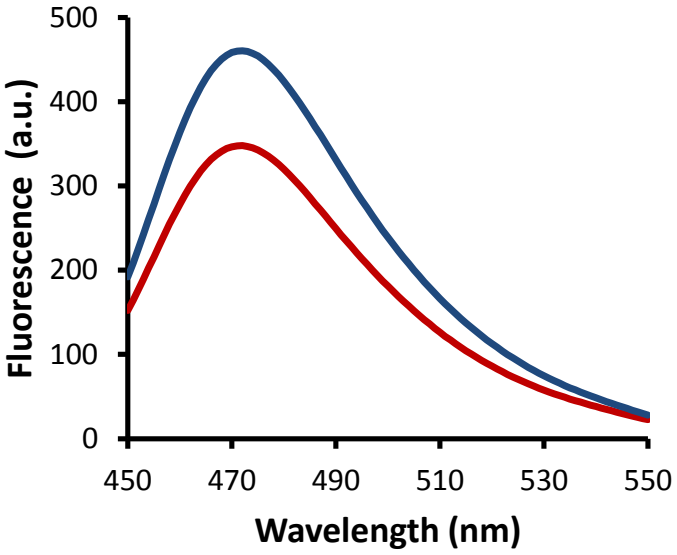

B

Figure 21: **A) Emission spectra C-AXP complexed to phosphorylated AMPK.**

5.6μM C-ADP (red) and C-ATP (blue) in complex with 2.1μM AMPK.

B) Emission spectra C-AXP complexed to unphosphorylated AMPK; 5μM C-ATP (red) and C-ADP (blue) complex with 2.1μM AMPK. All spectra were recorded at 20°C in 25mM Tris, 1mM TCEP, 100mM NaCl (pH 8). Excitation at 290nm. Nb. the C-AXP sites are not completely saturated under these conditions.

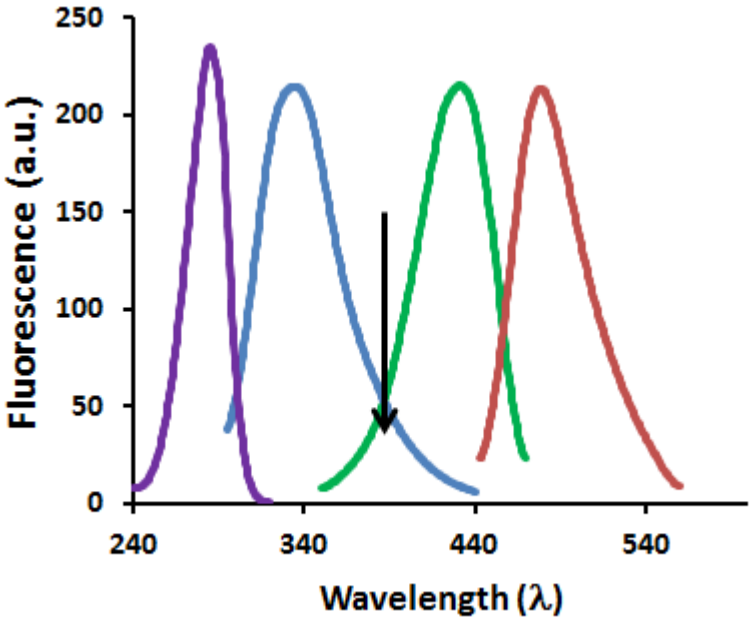

Figure 22: Emission and excitation spectra or AMPK and C-ATP.

Purple) Excitation spectrum of 6.2μM phosphorylated AMPK, λ_{em} 335nm. Blue) Emission spectrum of 6.2μM phosphorylated AMPK, λ_{ex} 290nm. Green) Excitation spectrum of 5μM C-ATP, λ_{em} 480nm. Red) Emission spectrum of 5μM C-ATP, λ_{ex} 430nm.

Arrow indicates the overlap between AMPK intrinsic fluorescence and C-ATP excitation which is required for FRET. All spectra measured at 20°C, medium sensitivity, in 25mM Tris, 1mM TCEP, 100mM NaCl (pH 8).

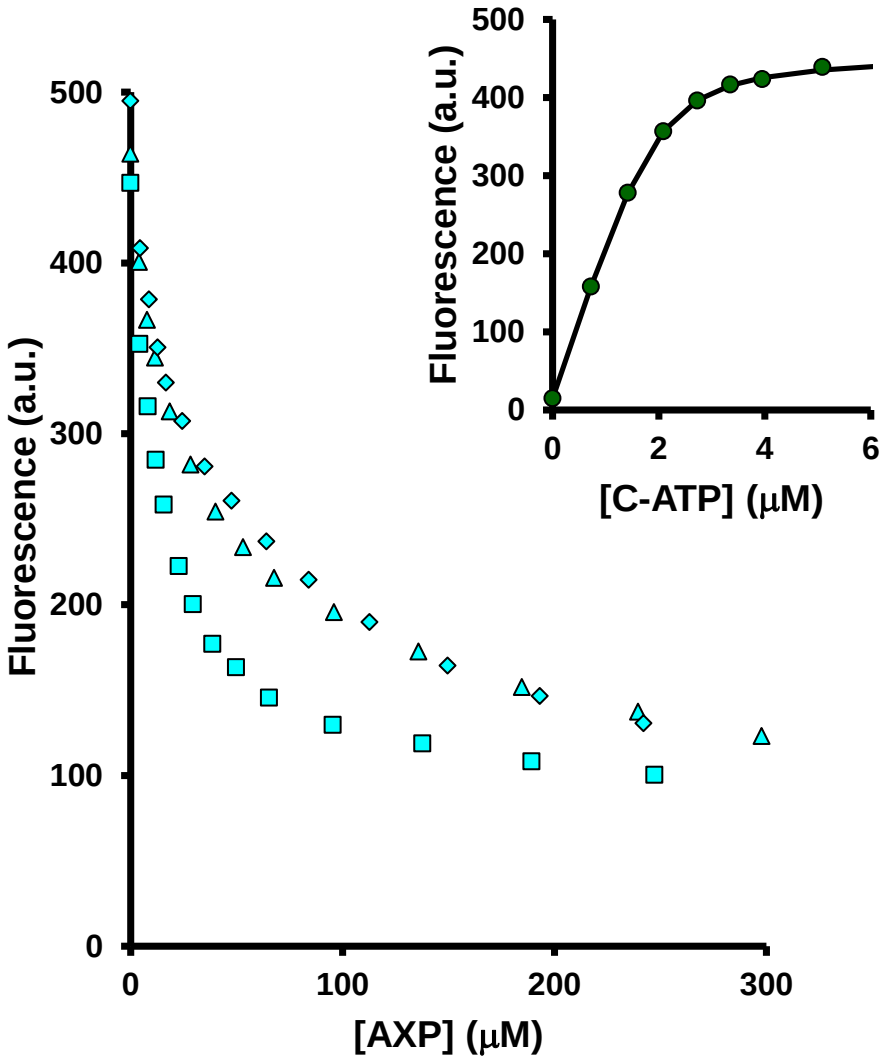

Figure 23 : Measurement of equilibrium dissociation constants for the binding of AXPs to unphosphorylated AMPK.

Displacement of C-ATP from the AMPK:$(C\text{-}ATP)_2$ complex by ATP (square), ADP (circle) and AMP (diamond) monitored using the change in fluorescence at 470nm (Excitation at 290nm). Inset: Fluorescence titration of C-ATP with 2μM AMPK. All measurements were performed at 20°C in 25mM Tris, 1mM TCEP, 100mM NaCl (pH 8).

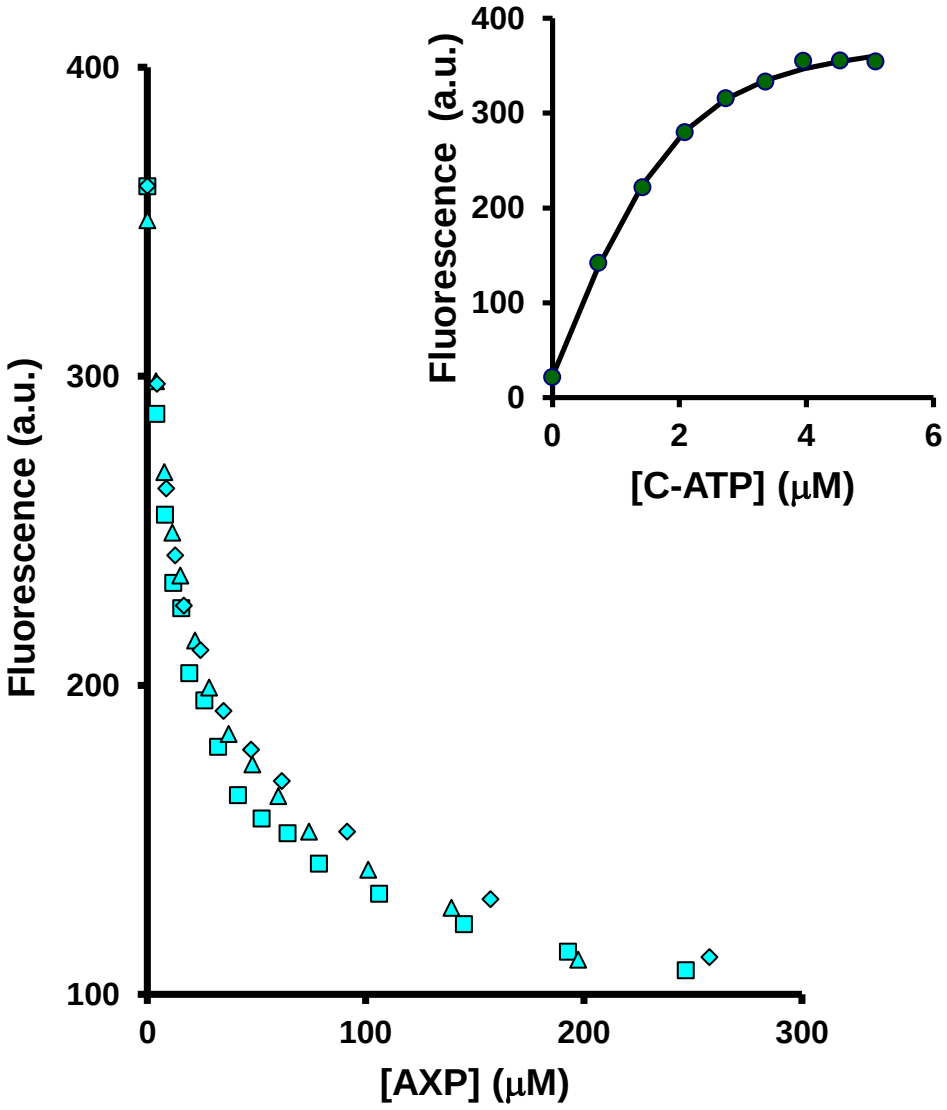

Figure 24: Measurement of equilibrium dissociation constants for the binding of AXPs to phosphorylated AMPK.

Displacement of C-ATP from the AMPK:$(C\text{-}ATP)_2$ complex by ATP (square), ADP (circle) and AMP (diamond) monitored using the change in fluorescence at 470nm (Excitation at 290nm). Inset: Fluorescence titration of C-ATP with 2μM AMPK. All measurements were performed at 20°C in 25mM Tris, 1mM TCEP, 100mM NaCl (pH 8).

Protein	K_{dI} (μM) C-ADP	K_{dI} (μM) C-ATP
Phosphorylated AMPK	0.75 (0.24)	0.78 (0.21)
Unphosphorylated AMPK	0.53 (0.16)	0.14 (0.05)

Table 10: Equilibrium dissociation constants for the binding of C-AXPs to AMPK.

Dissociation constants were determined at 20^{o}C by fluorescence titrations of C-ATP with AMPK in 25mM Tris, 1mM TCEP, 100mM NaCl (pH 8). The K_d values are reported as the mean (± SD) determined from at least three independent measurements.

3.4.3.5 AMPK mutants

It was observed that NADH competed with only the allosteric regulation by AMP and not protection against dephosphorylation conferred by both AMP and ADP suggesting that the two exchangeable AXP binding sites mediate different regulatory effects (discussed further in Chapter 4). In order to further explore this, a series of point mutants were designed, cloned and purified with the intention of specifically eliminating nucleotide binding at each of the exchangeable binding sites (Site-1 or Site-3).

In 2007 Xiao *et al* highlighted that in mammalian AMPK each AXP binding pocket has an aspartate residue which forms a bi-dentate interaction with the 2' and 3' hydroxyl groups of the ribose (D244 in Site-3, D89 in Site-1 and D316 in Site-4). In the fourth potential binding site (Site-2) this aspartate is replaced with an arginine. They suggested that this might be the reason AXP does not bind to Site-2 in mammalian AMPK.

D→A point mutants were generated in Site-1, Site-4 and Site-3 with the aim of eliminating AXP binding (*177*). Interestingly, the α-kinase regulation of these three mutants by AXP was impaired, with the D244A (Site-3) mutant having the most severe effect on allosteric activation and protection against dephosphorylation by AMP (Faith Mayer – PhD Thesis). However none of the D→A mutants ablated C-ADP binding. For the three D→A mutants a two-site binding model improved χ^2 values between 2 and 10-fold compared to a one-site model, suggesting a stoichiometry of 2:1 was maintained (C-ADP:AMPK). The equilibrium dissociation constants are given in Table 11.

The binding of NADH/AXP to full-length, phosphorylated D89A (Site-1) AMPK was also not disrupted (Table 12). It is perhaps superficially surprising that the nucleotide regulation of AMPK activity was perturbed in these mutants whereas the binding of AXP remained largely unaffected. Presumably, it is not the binding itself which is disrupted in these

mutants but instead the transduction of the AMP/ADP binding event to the α-kinase, or the stability/conformation of the complex. I can conclude that mutation of these conserved asparate residues does not abolish binding at each site, and therefore these mutants should not be employed in this role as has been previously reported (*177*).

A further mutagenesis strategy to delineate the separate effects of the two AXP binding sites was to introduce residues with large side chains, such as tryptophan, at positions which might be expected to block the nucleotide binding pocket, or to introduce negatively charged residues in positions which might make unfavourable interactions with the nucleotide phosphate groups. In conjunction with Matthew Sanders (NIMR) the binding of NADH and AMP (through competition with NADH) to full-length AMPK K169E, K242E, T86D, T86W, and T88D was characterised (Table 13). None of the γ-subunit mutants abolished AMP binding. Two-site binding models are consistent with the data and improve χ^2 values by at least 2-fold, in some cases modest increases in equilibrium dissociation constants were determined compared to wild-type but all the mutants maintained regulation by AMP/ADP (Faith Mayer – PhD Thesis).

Modelling of these mutations onto the γ-subunit crystal structure demonstrates that the relevant residues can adopt alternate rotamers which do not disrupt the AXP binding pockets in the anticipated manner, perhaps explaining the regulatory/binding phenotypes.

Recently, Chen *et al* (*144*) described a number of point mutants which reduced allosteric activation of AMPK. Only mutants directed at Site-3 and Site-4 produced this phenotype. However, no measurement of the binding affinity or stoichiometry of nucleotide interactions was described. It is feasible that mutation of Site-3 and Site-4 resulted in a

change of nucleotide binding affinity at Site-1, or that the mutations affected the stability or conformation of the complex.

Further mutational analysis was conducted on the CBS domains of SNF1 and is described in Appendix 1.2.2.1. Similarly, these mutants showed no distinctive effects on nucleotide binding.

The γ-subunit is described as a 'flattened disc', of ~60Å across and 30Å deep. CBS 1 + 2 and CBS 3 + 4 form two Bateman domains; the AXP binding sites are located between pairs of adjacent helix-loop strands from the tandem CBS motifs. The four CBS motifs contribute varying numbers of basic residues for interaction with the nucleotide phosphates (e.g. CBS2 contributes H151, R152 and K170 whilst CBS3 contributes none); there is therefore a high degree of connectivity between the sites. Such interdependence means that introducing a mutation directed at a single site has implications for the structure of the other sites which make up the γ-subunit. It therefore proved problematic to design further mutants with which to 'knock out' binding at a single site without affecting the properties of a second.

	C-ADP	
Protein	**K_{dI} (μM)**	**K_{dII} (μM)**
Wild-type	1.1 (0.02)	2 (0.5)
D89A (Site-1)	0.7 (0.1)	1.5 (0.3)
D244A (Site-3)	3.5 (1.2)	4 (1.0)
D316A (Site-4)	1.0 (0.1)	1.8 (0.4)

Table 11: Equilibrium dissociation constants for the binding of C-ADP to AMPK DA mutants.
Wild-type and mutant proteins (as indicated in the table) were IMAC purified and unphosphorylated. Dissociation constants were determined at 20°C by fluorescence titrations of C-ADP with AMPK in 25mM Tris, 1mM TCEP, 100mM NaCl (pH 8). The K_d values are reported as the mean (± SD) determined from at least two independent measurements.

Ligand	**K_{dI} (μM)**	**K_{dI} (μM)**
	Wild type	**D89A**
	***vs* NADH**	
AMP	1.6 (0.5)	0.95 (0.25)
ADP	1.3 (0.5)	1.25 (0.25)
ATP	0.9 (0.3)	1.40 (0.40)

Table 12: Equilibrium dissociation constants for the binding of AXP to AMPK γD89A.
Wild-type and D89A mutant proteins (as indicated in the table) were fully-purified and phosphorylated. Dissociation constants were determined at 20°C by fluorescence displacement titrations of NADH with AXP in 25mM Tris, 1mM TCEP, 100mM NaCl (pH 8). The K_d values are reported as the mean (± SD) determined from at least two independent measurements.

	NADH	AMP (*vs NADH)*
Protein	**K_{dI} (μM)**	**K_{dI} (μM)**
Wild-type	11.0 (4.5)	2.5 (0.5)
K169E (Site-3)	9.5 (2.7)	1.6 (0.1)
K242E (Site-1)	5.7 (0.1)	2.8 (1.2)
T86D (Site-1)	7.5 (1.5)	1.2 (0.2)
T86W (Site-1)	9.6 (0.8)	13.2 (1.4)
T88D (Site-1)	7.1 (0.4)	1.5 (0.3)

Table 13: Equilibrium dissociation constants for the binding of NADH and AMP to AMPK γ mutants.

Wild-type and mutant proteins (as indicated in the table) were phosphorylated. NADH: Dissociation constants were determined by fluorescence titrations of NADH with AMPK. AMP: Dissociation constants were determined by displacement of NADH by AMP. Experiments were performed in 25mM Tris, 1mM TCEP, (pH 8) at 7^{o}C. The K_d values are reported as the mean (± SD) determined from at least two independent measurements.

3.4.4 Biophysical sample characterisation

A number of techniques were employed to try and identify characteristic differences between phosphorylated and unphosphorylated protein samples, and also to establish that the samples were of a high quality.

3.4.4.1 Circular Dichroism (CD)

CD is a method used to study the conformation of proteins in solution. CD is the differential absorption of left- and right- handed circularly polarised light. In order to be visible in a CD spectrum a chromophore must be inherently chiral or located in an asymmetric environment. In the near-UV spectral region (310-255nm) relevant chromophores are the side chains of tryptophan, tyrosine, phenylalanine and the disulphide bond. In the far-UV region (below 250nm) it is the peptide bond which dominates the signal producing bands at ~220nm and ~190nm. Tyrosine, tryptophan, and phenylalanine can also make significant contributions in this region.

Although it provides only low resolution structural information CD does have major advantages over other techniques; it can be sensitive to changes in protein conformation, a wide range of solvent conditions can be used with relatively little sample required and the spectra are reasonably quick to acquire.

Analysis of far-UV spectra provides information about the secondary structure content of a protein sample and can be used to monitor protein unfolding. Near-UV CD offers information about the tertiary structure of a protein. Both can be used to detect conformational changes in proteins in response to a pH, temperature, etc.

Far-UV CD spectra of both phosphorylated and unphosphorylated AMPK were collected (Figure 25). All the spectra collected are dominated by the α-helical signals at 222, 208 and 190-195nm, as is often the case for α/β containing proteins. Estimation of their secondary structure content highlighted no significant differences between the two AMPK species (Table 14). At 70^{o}C no dramatic loss of phosphorylated AMPK secondary structure was observed, although some α-helical content was lost and β-sheet gained (Table 14). Addition of 20% isopropanol to the buffers, as described in Section 3.4.2 for staurosporine titrations (Table 4, Table 5 and Table 6), results in an increase of helical content by around 10% and reduction of β-sheet, turn and unordered content for both phosphorylated and unphosphorylated AMPK (Table 14). The secondary structure of both species can be stable in buffer conditions and at temperatures well-above those used in the fluorescence assays performed as part of this work.

Near-UV spectra of phosphorylated and unphosphorylated AMPK were collected (Figure 26). The spectra of both AMPK species are dominated by the tyrosine signal (band maxima at 275-282nm), although contributions from phenylalanine are also observed in the region 255-270nm. No significant signal from tryptophan residues is observed (fine structure above 280nm); the observed bands are the sum of all contributions, both positive and negative, for this reason no tryptophan signal is observed despite AMPK containing many such residues. The most striking feature of the near-UV spectra is the differences between the phosphorylated and unphosphorylated samples. This difference reflects local changes in the tertiary structure surrounding one or more tyrosine residues, because AMPK (human $\alpha1\beta1\gamma1$) contains 43 tyrosine residues it is difficult to interpret the spatial focus of this change in structure.

Thermal unfolding of phosphorylated and unphosphorylated AMPK was monitored (Figure 27). Tris.HCl, present in the standard buffer, has a high thermal coefficient, therefore protein samples were diluted in water to minimise change in pH as the temperature was increased. The unphosphorylated sample unfolds with a T_m = 75^{o}C. Phosphorylated AMPK failed to unfold, instead a drop in signal at around 60^{o}C was observed, this is indicative of fibril formation/increased β-content. It is unclear what the relevance, if any, this has in a cellular context.

Differences in the secondary structure and stability of phosphorylated and unphosphorylated AMPK samples are to be expected. Obviously the two species represent different functional states (active/inactive) and bind nucleotide/staurosporine with different affinities. That the differences appear quite pronounced, particularly in the case of the thermal unfolding data, may suggest significant changes in the overall architecture of the two AMPK states.

In the α1β2(ΔGBD)γ1 phosphorylated structure (shown in Figure 5) the α-kinase adopts a conformation in which the T-loop forms an interface with the β-subunit thus protecting αT172 from dephosphorylation by phosphatases. It is unlikely that this state is adopted in the unphosphorylated protein, as the T-loop only adopts a conformation compatible with this interface when it is phosphorylated. It is suggested that the preceding linker region is increasingly mobile in the inactive state, causing the α-kinase to be flexibly tethered to the rest of the heterotrimer. Therefore significant differences between the overall architecture, and biophysical properties of the phosphorylated and unphosphorylated protein samples are at least consistent with the available crystal structures.

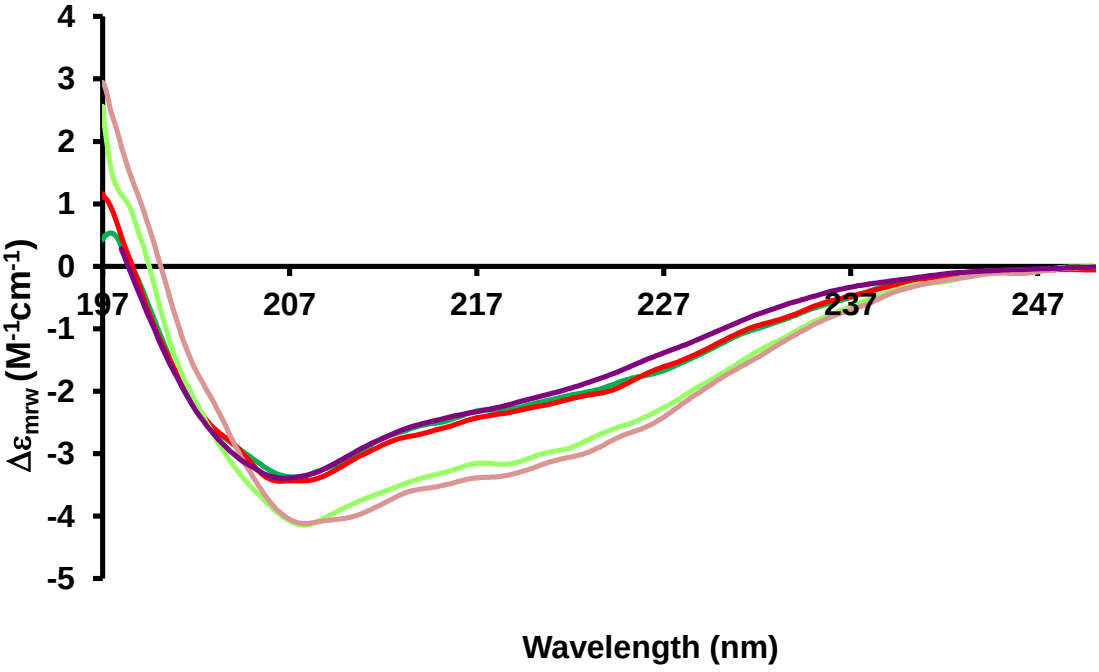

Figure 25: Far-UV CD spectra (AMPK).

Green) Phosphorylated AMPK (aq); Red) Unphosphorylated AMPK (aq); pale Green) Phosphorylated AMPK (20% iso); Pink) Unphosphorylated AMPK (20% iso); Purple) Truncated AMPK (aq). Where (aq) refers to 25mM Tris, 1mM TCEP, 100mM NaCl (pH 8), and (20% iso) refers to (aq) with 20% isopropanol. All spectra were collected at 20^{o}C.

Protein	%			
	α-helix	β-sheet	Turns	Unordered
Unphosphorylated AMPK (aq)	23.4	21.4	19.7	35.5
Unphosphorylated AMPK (20% iso)	34.4	17.5	18.8	29.4
Phosphorylated AMPK (aq)	23.7	20.9	19.5	35.9
Phosphorylated AMPK (20% iso)	32.9	17.2	19.4	30.5
Phosphorylated AMPK (aq) 70°C	20.1	24.8	21.0	34.1
Truncated AMPK (aq)	22.6	21.0	20.0	36.5

Table 14: Secondary structure content predictions.

Where (aq) refers to 25mM Tris, 1mM TCEP, 100mM NaCl (pH 8), and (20% iso) refers to (aq) with 20% isopropanol, all spectra were collected at 20^{o}C unless otherwise specified.

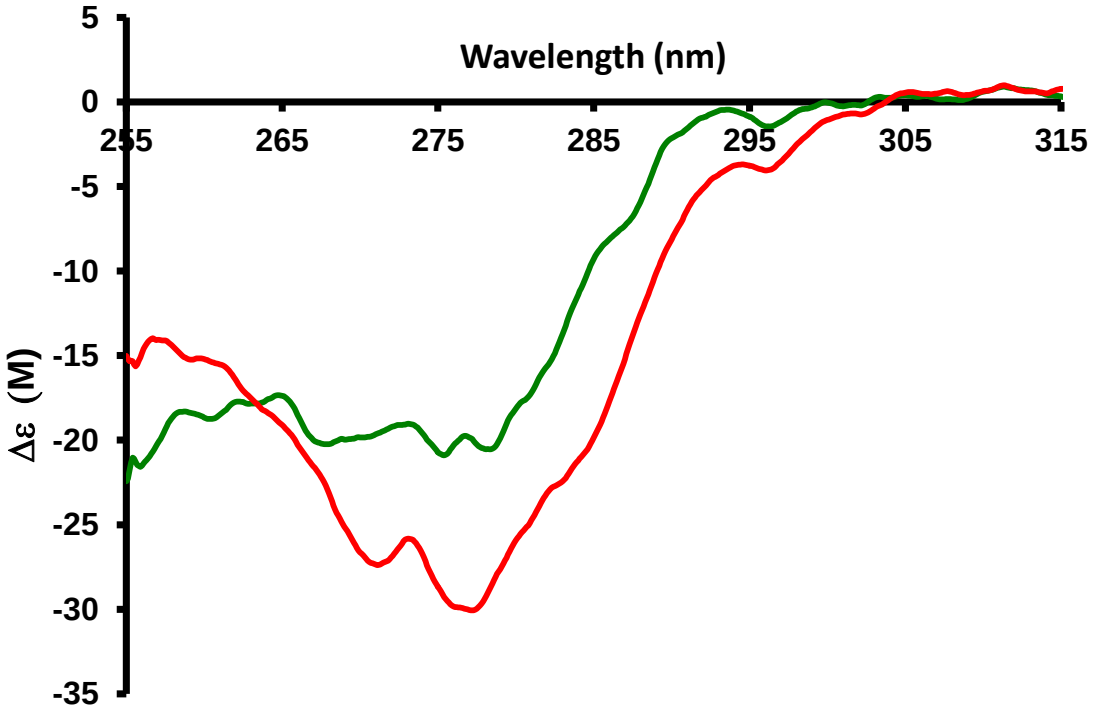

Figure 26: Near-UV CD spectra (AMPK).

Green) Phosphorylated AMPK; Red) Unphosphorylated AMPK. Spectra recorded in 25mM Tris, 1mM TCEP, 100mM NaCl (pH 8) at 20^{o}C.

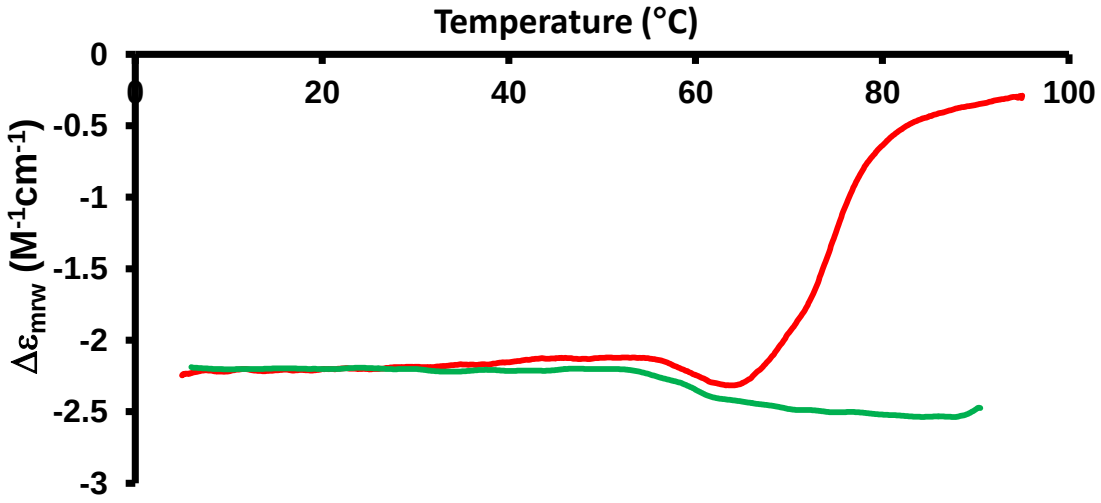

Figure 27: Thermal denaturation (AMPK).

Phosphorylated (green) and unphosphorylated (red) AMPK. Protein samples were diluted in water.

3.4.4.2 Multi-Angle Laser Light Scattering (MALLS)

A protein sample in solution will scatter light dependent on the number and molecular weight of the macromolecular particles in contains. SEC-MALLS uses chromatography to initially separate particles based on their size, then measures the light scattering at multiple angles together with the protein concentration of the eluent using a differential refractometer. These data when combined are used to independently determine absolute molecular weight of the protein, assess the degree of aggregation and heterogeneity of a sample, and determine the oligomer state. For large proteins (>200kDa) information about the shape of the molecule can also be inferred.

SEC-MALLS was employed to determine the absolute molar mass of full-length phosphorylated and unphosphorylated AMPK. Both samples elute as single peaks from the size exclusion column with no indication of higher molecular weight or aggregated species (Figure 28). Absolute molecular weight values of between 136-141kDa were determined, comparing well to the calculated molecular weight of 132kDa. These data show that protein samples used for *in vitro* binding experiments described in this Thesis are homogenous and of a high-quality. However, examination of the elution profile of phosphorylated AMPK compared to unphosphorylated reveals a shift to an earlier retention time suggesting that upon phosphorylation AMPK becomes less compact or interacts differently with the column. Although these differences might be expected as the two protein species represent different functional states, in order to understand the differences at a molecular level, it may be of interest in the future to conduct further sedimentation velocity experiments.

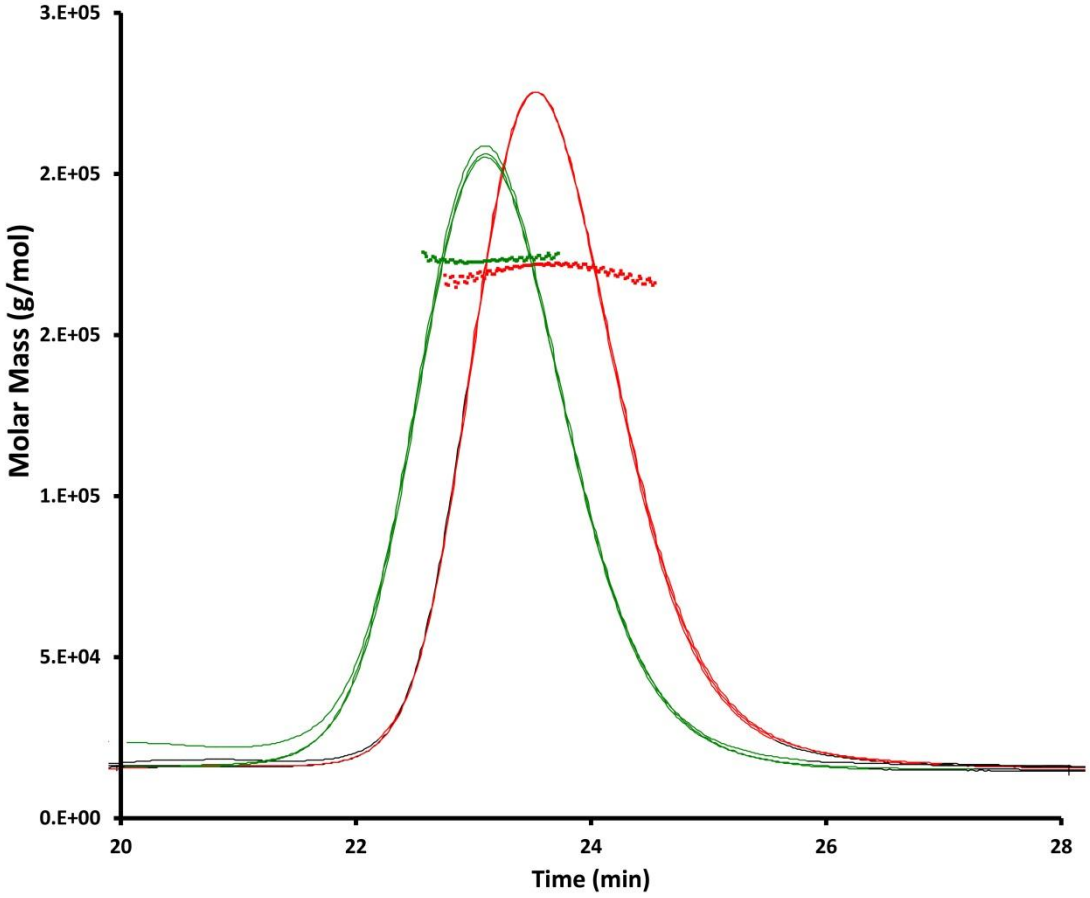

Figure 28: SEC-MALLS spectra (AMPK).

Continuous lines represent; molar mass distribution of phosphorylated (green) and unphosphorylated (red) full-length AMPK samples, 2) Squares represent the UV absorption at 280nm of the samples. Spectra recorded in, 50mM Tris (pH 8), 100mM NaCl, 3mM Sodium Azide, 1mM TCEP at ambient temperature.

3.5 Conclusion

Using a combination of direct C-AXP excitation, FRET and NADH fluorescence experiments this Chapter demonstrated that regulatory nucleotides bind exchangeably at two sites to full-length phosphorylated and unphosphorylated AMPK. One site bound free AXP with significantly higher affinity (~2μM) than the other (~65μM). Only small differences in binding between the active and inactive AMPK species were observed. Mg.ATP similarly binds competitively but with a weaker affinity than regulatory nucleotides (55μM at the tighter site, 230μM at the weaker site).

It is suggested that the weaker binding of Mg.ATP is critical in the competition for binding by regulatory nucleotides, given cellular conditions, in which Mg.ATP concentrations are significantly higher than those of AMP/ADP. This idea is explored in greater detail in the following Chapter.

In an attempt to specifically ablate AXP binding at the two exchangeable sites a number of point mutants in the γ-subunit were generated but failed to knock-out binding of AXP to AMPK in the manner intended.

The nanomolar affinity interaction between the α-kinase ATP binding pocket and staurosporine, a kinase inhibitor, was also characterised.

The CD and MALLS spectra of phosphorylated and unphosphorylated AMPK were compared confirming that the samples were homogenous and well-folded. These studies did highlight some differences in the biophysical characteristics of the two species, particularly in terms of their thermostability and overall architecture. It is interesting that structural differences between the active and inactive AMPK samples are detectable in this way.

Chapter 4: AMPK Kinetics and Modelling

4.1 Abstract

A spectrophotometric coupled assay was used to monitor AMPK kinetics and its regulation by nucleotides. NADH binds at Site-1, the tighter of the two AXP sites, and competes with allosteric activation of AMPK by AMP but not with the protective effect of AMP/ADP against dephosphorylation. Therefore AMP binding at Site-1 mediates allostery, and AMP/ADP binding at Site-3 mediates protection against dephosphorylation.

In order to expand upon this conclusion, the AXP binding constants determined in Chapter 3 were used to model binding site occupancies over the concentration ranges used in the *in vitro* assays. The modelling demonstrates that Site-1 and Site-3 become occupied by AMP in a manner consistent with the dose response of their proposed regulatory properties (allostery and protection against dephosphorylation, respectively).

Estimations of *in vivo* intracellular AXP concentrations were used to model Site-1/Site-3 AXP occupation in a cellular context, in which Mg.ATP concentrations are significantly higher than those of AMP/ADP. The model utilises the K_d values determined in the previous chapter (AXP binding to AMPK) to demonstrate that;

1) Allosteric activation by AMP is, perhaps, unlikely to be an important regulatory factor *in vivo* under normal conditions.
2) ADP can effectively compete with Mg.ATP for binding at the regulatory binding site (Site-3) despite the high concentrations of antagonistic Mg.ATP.

4.2 Introduction

4.2.1 Kinase cascades

The reversible phosphorylation of proteins features prominently in cellular signal transduction. Serine, threonine, tyrosine and histidine residues are phosphorylated by kinases and dephosphorylated by phosphatases. The human genome encodes roughly 500 protein kinases and about a third as many protein phosphatases. Because aberrant phosphorylation is the cause of many human diseases these enzymes receive significant attention as potential drug targets (*262*).

Phosphorylation of a target can bring about a range of effects; targeting for degradation or relocalisation, activation or inactivation, and enabling interactions with binding partners (*262*). For example, in the MAPK kinase pathway, multiple kinases are phosphorylated in sequence and this has the result of amplifying a small external signal to produce a large downstream response (*263*). Cascade systems also allow for feedback networks which can modify the activity of upstream kinases.

AMPK is phosphorylated on αT172 by upstream kinases and exerts its effects through phosphorylation of many downstream targets. It is therefore at the heart of an enzymatic cascade which senses intracellular signals (Ca^{2+}, AMP/ADP, glycogen) and extracellular signals (adiponectin, leptin etc.) and transduces them through the cell resulting in transcriptional changes and altered cellular metabolism.

Although it is convenient to think of discrete cascades, in reality signal transduction comprises wide networks of interacting proteins, which when stimulated, produce broad, far reaching effects.

4.2.2 AMPK Kinetics

AMPK is a group transfer enzyme, catalysing the covalent attachment of a phosphate (from ATP) to an acceptor serine or threonine present on a substrate. Group transfer reactions can be either compulsory-order (one substrate must bind first) or random-order. Kinases require an essential divalent metal ion, usually Mg^{2+} to facilitate the phosphoryl transfer reaction and assist in ATP binding (*264*). Although the kinetics of group transfer enzymes generally obey the simple Michaelis-Menten equation the expressions for the substrate K_m values and the catalytic rate are invariably complex, mechanism-dependent, combinations of rate constants (see Section 4.4.1.5).

AMPK is itself a substrate for phosphatases and upstream kinases (see Section 1.5.1). LKB1 has been shown to have a K_m for AMPK of 5.4 ± 1.4nM, and PP2Cα a K_m of 160 ± 20nM (*265*). Given a cellular AMPK concentration of around 150nM, these data suggest that LKB1 operates under zero-order conditions ([AMPK] >> K_m of LKB1 for AMPK), a fact that may be integral in explaining AMPK activation (see Section 4.4.2.5) (*265*).

4.2.3 SAMS peptide

Experimentally, AMPK activity is often measured by monitoring the phosphorylation of a small peptide known as SAMS (HMR**SAMS**GLHLVKRR). This sequence is based on the target motif of the AMPK substrate, ACC (*266*). In general, the amino acids four residues or less from the phosphorylation site are the most significant for directing phosphoryl transfer (*264*). A consensus motif was defined requiring a hydrophobic side chain at P-5 and P+4, and basic residues at P-4 or P-3, additional basic residues at P-6 or P+3 increase substrate specificity (*126, 267*). The presence of a amphipathic helix extending from P-5 to P-16 may also contribute to substrate affinity (*268*). These basic residues are positioned to interact with an acidic patch present on the α catalytic domain, and the P-5 residue anchors itself in a hydrophobic pocket on the surface of the kinase structure (*126*).

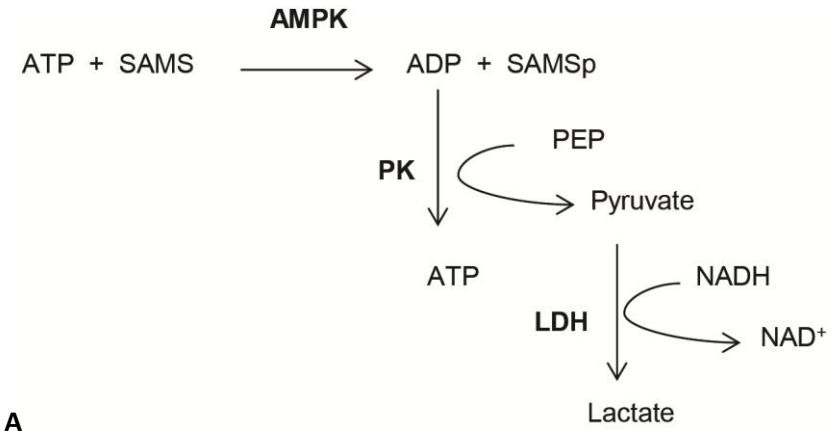

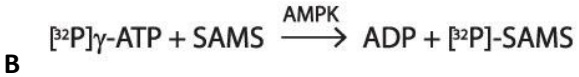

Figure 29: A) NADH coupled assay.

AMPK kinetics were monitored using a continuous spectrophotometric assay. The decrease in absorbance at 340nm is monitored as NADH is converted into NAD^+, this is related with a 1:1 stoichiometry to phosphorylation of a small substrate peptide by AMPK. PK; Pyruvate kinase, PEP; Phosphoenol Pyruvate, LDH; Lactate Dehydrogenase.

B) [P^{32}]γ-ATP peptide assay. AMPK phosphorylation activity is monitored through incorporation of radioactive [^{32}P] into the SAMS peptide substrate (*266*).

4.2.4 Coupled Assays

It is not possible to follow AMPK phosphorylation reactions directly using a spectrophotometer because the phospho-peptide product has no suitable optical signal and ADP has the same extinction coefficient as ATP. There are numerous applications in which a reaction may be monitored by linking it to a second process that provides the appropriate spectroscopic signal. The essential requirement is, of course, that the linked process is very much faster than the one being studied, so that it does not affect the rate of the process being investigated. The release of ADP when SAMS is phosphorylated can be monitored by linking it to the PK and LDH system in which the conversion of NADH to NAD^+ provides the optical signal (either fluorescence or absorbance). All kinase activity measurements with the SAMS peptide were therefore made using the continuous spectrophotometric coupled enzyme assay based on one initially described by Cook *et al* (Figure 29a) (*269*). The classic radioactivity assay that is also often used to monitor AMPK kinetics is shown in Figure 29b.

4.2.5 The Cornish-Bowden method

In order to simulate the regulation of AMPK by AXPs one needs to be able to calculate binding site occupancy under different starting conditions. The complexity of the AMPK system means that it is not possible to derive an analytical solution for calculating the concentrations of the different species present at equilibrium. There are, however, several simple iterative methods for calculating equilibrium concentrations in complex systems and one of these, the Cornish-Bowden method, is described here and is the basis for the work described in Section 4.4.2 (*250*). The method will be illustrated for the following reaction scheme:

$$P + L \overset{K_{a,L}}{\leftrightarrow} PL \qquad\qquad P + N \overset{K_{a,N}}{\leftrightarrow} PN$$

The association constants (units: M^{-1}) are defined as:

$$K_{a,L} = \frac{[PL]}{[P][L]} \qquad K_{a,N} = \frac{[PN]}{[P][N]}$$

The total concentrations of the protein and the ligands (P_0, L_0, and N_0) are given by:

$$P_0 = [P] + [PL] + [PN]$$

$$L_0 = [L] + [PL]$$

$$N_0 = [N] + [PN]$$

The concentrations of the species present in complex systems can always be expressed in terms of the concentrations of the individual components and the association constants characterising the system. In this case, the concentrations of the two complexes (PL and PN) can be expressed in terms of the concentrations of the individual components (P, L, and N) as follows:

$$P_0 = [P] + K_{a,L}[P][L] + K_{a,N}[P][N] \qquad \textbf{Equation 12}$$

$$L_0 = [L] + K_{a,L}[P][L] \qquad \textbf{Equation 13}$$

$$N_0 = [N] + K_{a,N}[P][N] \qquad \textbf{Equation 14}$$

Rearranging these equations gives:

$$[P] = \frac{P_0}{1+K_{a,L}[L]+K_{a,N}[N]} \qquad \textbf{Equation 15}$$

$$[L] = \frac{L_0}{1+K_{a,L}[P]} \qquad \textbf{Equation 16}$$

$$[N] = \frac{N_0}{1+K_{a,N}[P]} \qquad \textbf{Equation 17}$$

The procedure for obtaining the equilibrium concentrations is then as follow. Each free concentration is initially set to the corresponding total concentration (i.e., [P] = P_0 etc.) and an improved estimate of [P] (called [P1]) is obtained from Equation 15 as:

$$[\mathrm{P1}] = \frac{\mathrm{P_0}}{1 + \mathrm{K_{a,L}L_0} + \mathrm{K_{a,N}N_0}}$$

This improved estimate of [P] is then used along with the remaining original estimates (L_0 and N_0) to calculate improved estimates of [L] and [N] (called [L1] and [N1]) as follows:

$$[\mathrm{L1}] = \frac{\mathrm{L_0}}{1 + \mathrm{K_{a,L}}[\mathrm{P1}]}$$

$$[\mathrm{N1}] = \frac{\mathrm{N_0}}{1 + \mathrm{K_{a,N}}[\mathrm{P1}]}$$

This procedure is then repeated to get a new estimate of [P] (called [P2]) calculated as:

$$[\mathrm{P2}] = \frac{\mathrm{P_0}}{1 + \mathrm{K_{a,L}}[\mathrm{L1}] + \mathrm{K_{a,N}}[\mathrm{N1}]}$$

and further estimates of [L] and [N] are obtained in a similar way.

$$[\mathrm{L2}] = \frac{\mathrm{L_0}}{1 + \mathrm{K_{a,L}}[\mathrm{P2}]}$$

$$[\mathrm{N2}] = \frac{\mathrm{N_0}}{1 + \mathrm{K_{a,N}}[\mathrm{P2}]}$$

The iterations are continued until the new estimates no longer change. Provided that the procedure converges to a solution that satisfies Equations 12 to 14 simultaneously, the solution must describe the equilibrium state of the system, because a given set of equilibrium constants defines a unique state. Once [P], [L], and [N] are known the

concentrations of the complexes may be calculated from the expressions for the association constants. Note: The order in which the new estimates are calculated is unimportant.

The following table shows how quickly the procedure converges. The calculation was performed with the following association constants and total concentrations.

$K_{a,L} = 1 \times 10^5\ M^{-1}$ $K_{a,N} = 2 \times 10^5\ M^{-1}$

$P_0 = 10\ \mu M$ $L_0 = 50\ \mu M$ $N_0 = 20\ \mu M$

Iteration	[P] (μM)	[L] (μM)	[N] (μM)
Start	10	50	20
1	1	45.455	16.667
2	1.1263	44.939	16.323
3	1.1417	44.876	16.282
4	1.1436	44.869	16.277
5	1.1439	44.868	16.276
6	1.1439	44.868	16.276

4.2.6 Measurement of intracellular nucleotide concentrations

In order to simulate the occupancy of AMPK binding sites by AXP it is necessary to have estimates of the intracellular nucleotide concentrations. Many of the techniques used to determine intracellular AXP concentrations have low temporal resolution; the primary methods being;

1) High Performance Liquid Chromatography (HPLC) – nucleotides are extracted, often via perchloric acid treatment, and their relative concentrations determined through HPLC separation and comparison to known standards (*270*).
2) NMR – ^{31}P-NMR can be used to determine the concentration of ATP, phosphocreatine (PCr) and phosphate (*271*).

3) Biosensors - For example, protein or RNA based ADP/ATP intracellular biosensors (*272, 273*).

Free AMP/ADP concentrations are often estimated from measurements of the PCr, creatine (Cr), ATP and AXP (AMP_0 + ADP_0 + AMP_0) concentrations, based on the near-equilibrium nature of the adenylate kinase (discussed in more detail in Section 4.2.7) and creatine kinase reactions (*274*). It is important to consider the short-term impact of PCr on ATP concentrations; for example in the skeletal muscle PCr acts as an energy (ATP) reserve during periods of intense exercise.

Depending on the species, cell-type, extraction protocol, and measurement technique concentrations ranging from 2-20mM ATP (*270, 275*), 0.009-3mM ADP(*271, 275*) and 1-350μM AMP (*276, 277*) have been reported. With such variation present in the literature, averages are often quoted as 3-8mM ATP, 50-200μM ADP and 1-5μM AMP (*1*).

4.2.7 Adenylate Kinase

Adenylate kinase catalyses the conversion of two molecules of ADP into one of ATP and one of AMP. It operates at near-equilibrium, responding rapidly to changes in cellular nucleotide concentrations. The AMP:ATP ratio in cells varies with the square of the ADP:ATP ratio making AMP a sensitive indicator of the energy status of the cell. For many years AMP was therefore assumed to be the major regulator of AMPK activity.

The concentrations of AMP and ADP can be calculated as follows, given total AXP and ATP concentrations:

$$2\mathrm{ADP} \overset{\mathrm{k}}{\leftrightarrow} \mathrm{ATP} + \mathrm{AMP}$$

Where the equilibrium constant is given by Equation 18:

$$K = \frac{[ATP][AMP]}{[ADP]^2}$$ **Equation 18**

The total concentration of adenine nucleotides, N_0 is given by:

$$N_0 = [ATP] + [ADP] + [AMP]$$

Substituting in Equation 18 gives

$$K = \frac{[ATP](N_0 - [ATP] - [ADP])}{ADP^2}$$

$$K[ADP]^2 = [ATP](N_0 - [ATP] - [ADP]) = [ATP]N_0 - [ATP]^2 - [ATP][ADP]$$

$$K[ADP]^2 + [ATP][ADP] + [ATP]^2 - [ATP]N_0 = 0$$

For any given ATP concentration and total adenine nucleotide concentration the concentration of ADP is given as the solution of the quadratic equation:

$$[ADP] = \frac{-b + \sqrt{b^2 - 4ac}}{2a}$$

Where: $a = K$; $b = [ATP]$; $c = [ATP]^2 - [ATP]N_0$

The concentration of AMP is then given by:

$$[AMP] = N_0 - [ATP] - [ADP]$$

4.3 Methods

4.3.1 Kinetics

4.3.1.1 General

Assays contained the following components in a total volume of 0.5ml: 50mM Hepes (pH 7.5), 10mM $MgCl_2$, 0.2mM TCEP, 100mM NaCl, 12 units of pig heart LDH, 8 units of rabbit muscle PK, 1mM PEP, 150µM NADH, plus ATP and SAMS peptide at appropriate concentrations. Reactions were initiated by the addition of phosphorylated AMPK to a final concentration of ~3nM (unless otherwise specified), and initial rates (at 25^{o}C) were obtained by recording absorbance changes at 340nm. The assays were performed in a temperature controlled Jasco V-550 UV/Vis spectrophotometer, using quartz micro-cuvettes with 10mm pathlength (Hellma).

Doubling the concentrations of the coupling enzymes had no effect on the recorded velocities; therefore these enzymes are operating fast enough for the measured rates to be a true reflection of AMPK kinetics. The measured rates were also shown to be directly proportional to the concentration of phosphorylated AMPK.

4.3.1.2 K_m determination

The K_m for the SAMS peptide was determined by measuring initial rates at different SAMS concentrations with a fixed ATP concentration of 200µM. The K_m for ATP was determined by measuring initial rates at different ATP concentrations with a fixed SAMS peptide concentration of 90µM. K_m and V_{max} values were determined by non-linear least-squares regression to the Michaelis-Menten equation:

$$V_0 = \frac{V_{max}[S]}{K_m + [S]}$$

4.3.1.3 ATPase activity

The ATPase activity was monitored as described in Section 4.3.1.1, excluding SAMS peptide from the reaction mix, and using a higher AMPK concentration (1μM).

4.3.1.4 Staurosporine Inhibition

Staurosporine inhibition was monitored using the assay described in Section 4.3.1.1. All reaction components, excluding SAMS peptide, were preincubated with 10nM AMPK and 8nM staurosporine for 3 minutes. The reaction was initiated through addition of the substrate.

4.3.1.5 Allosteric activation

Allosteric activation of AMPK by AMP was studied by measuring the initial rate at increasing AMP concentrations using the assay described in Section 4.3.1.1. Effects of NADH on the allosteric activation by AMP were investigated at two concentrations of AMP (18 and 88μM) by measuring the initial rate at different concentrations of NADH. The SAMS peptide and ATP concentrations were 90μM and 200μM respectively.

4.3.1.6 Dephosphorylation assays

Phosphorylated AMPK was incubated with 0.5mM AMP or ADP ('incubation mix'). An aliquot of AMPK was diluted to approximately 0.5μM in kinase assay buffer at each timepoint (50mM Hepes (pH 7.5), 2mM $MgCl_2$, 0.2mM TCEP, 100mM NaCl). 5μl of this diluted solution was added to 500μl of standard assay mixture (with [SAMS peptide] = 100μM and [ATP] = 250μM). PP2Cα was then added to the remaining solution, which was incubated at 25^{o}C, and further initial rate measurements were taken at defined time intervals. The concentration dependence of AMP/ADP protection were examined by including the relevant nucleotide at different concentrations in the starting incubation mix,

and monitoring the reduction in active (phosphorylated) AMPK at a fixed time point compared to 0min.

The coupled assay monitors ADP release as SAMS is phosphorylated. It was important to ensure that carryover of ADP from the incubation mix was kept to a minimum, and did not interfere with recording of the initial rate. This was achieved through dilution of the incubation mix by greater than 100-fold into kinase assay buffer, before addition of an aliquot to the assay mix.

Small differences in the concentrations and activities of the phosphatase and kinase, and contamination of nucleotides by their breakdown products may affect the observed rates. Every effort was taken to keep concentrations constant, use the same batches of enzyme within similar time frames, and to use fresh AXP preparations. Temperature control was also very important to maintain consistency.

4.3.1.7 Materials

LDH/PK, ATP, ADP, AMP, NADH and PEP were purchased from Sigma. The peptide was synthesised by Dr Graham Bloomberg at The University of Bristol and dissolved in water.

Recombinant human PP2Cα was a kind gift from Prof David Carling (CSC Hammersmith).

4.4 Results and Discussion

4.4.1 AMPK Kinetics

AMPK kinetics are generally assayed by monitoring the phosphorylation of the SAMS peptide in the presence of γ-^{32}P ATP (Figure 29b) (*1, 266*). The complementary use of the NADH coupled assay (Figure 29a) to monitor AMPK activity is beneficial because it is much quicker than the established method, allowing mutant or truncated protein preparations to be rapidly tested for activity without the use of radioactivity.

4.4.1.1 ATPase

It is not uncommon for kinases to have an intrinsic ATPase activity. Phosphate and phosphorylated peptide are unique products of the ATPase and kinase reactions respectively. ADP on the other hand is a common product of both reactions. Therefore although continuous spectrophotometric assays based on the detection of ADP production have been successfully employed in the study of kinases they are not generally used if the kinase has significant ATPase activity.

It was found that AMPK does indeed have an intrinsic ATPase activity (Figure 30), the reaction has a K_m of 24.2μM, similar to that of the phosphorylation reaction. However the V_{max} is very low, 4.87nM.S^{-1}. This corresponds to a catalytic rate of 0.005S^{-1}, which is very much lower (2000-fold) than the catalytic rate of the phosphorylation reaction (calculated in Section 4.4.1.2).

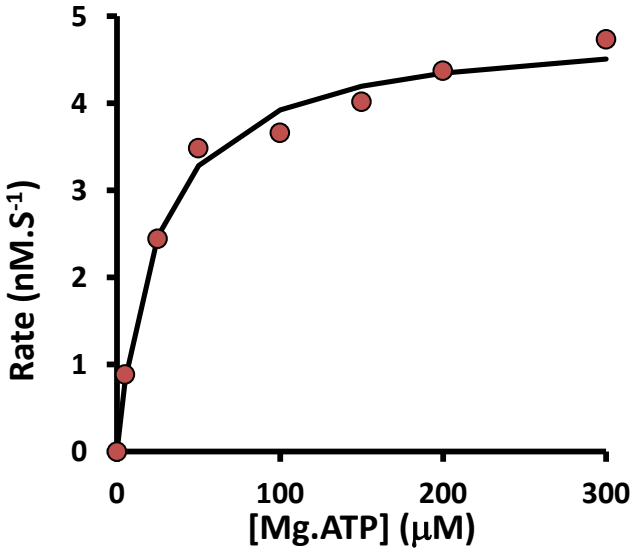

Figure 30: AMPK's intrinsic ATPase activity.

The production of ADP was monitored as a function of [Mg.ATP]. Results are an average of at least 3 repeats. The solid line is the computed best fit.

4.4.1.2 K_m determination

Since the continuous spectrophotometric assay has not previously been used with AMPK it was first necessary to demonstrate its validity and robustness. The K_m values determined for the SAMS peptide (53.6 ± 1.9µM - Figure 31) and Mg.ATP (24.4 ± 0.93µM - Figure 31) were in good agreement with previously published values (53, 54). The apparent V_{max} values calculated as 34.7 and 24nM.S^{-1} at these SAMS and Mg.ATP concentrations respectively are also in good agreement. The catalytic rate is therefore greater than 12S^{-1}.

4.4.1.3 Allosteric activation by AMP

The assay was then used to study allosteric activation by AMP. Figure 32 shows that concentrations of AMP greater than 20µM can produce approximately two-fold activation of the enzyme in the presence of 200µM ATP. Allosteric activation by AMP was demonstrated to be around 2.7 fold at concentrations between 50-120µM AMP. This compares with previously published results where AMPK (γ1) was activated 3.5-fold by 50µM AMP (34).

AMP allosteric activation was inhibited by high concentrations of NADH (Figure 33), demonstrating the competitive nature of their binding. There was, however, no effect of NADH on AMP/ADP protection against dephosphorylation by phosphatases (*1*). Since NADH is thought to bind at Site-1 it is hypothesised that AMP binding at this site is responsible for allosteric activation (discussed further in Section 4.4.2.1). A structure of AMPK complexed with NADH would greatly support this assignment of function.

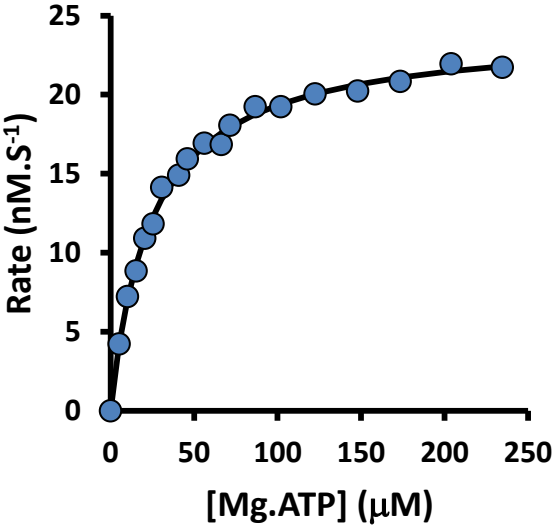

A

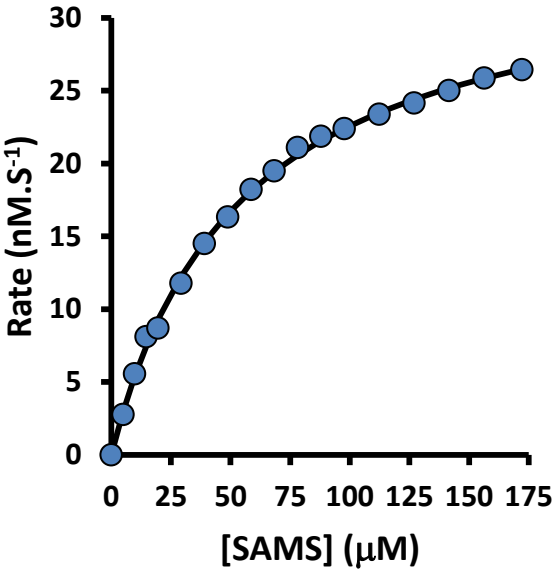

B

Figure 31: Determination of K_m values (AMPK).

K_m with respect to (A) ATP (SAMS = 90μM) and (B) SAMS peptide (Mg.ATP = 200μM); Recombinant AMPK complex ($\alpha 1\beta 1\gamma 1$) was phosphorylated with CaMKKβ and its activity measured at a range of substrate concentrations. Activity of AMPK is plotted as a function of substrate concentration. The solid lines are the computed best fits.

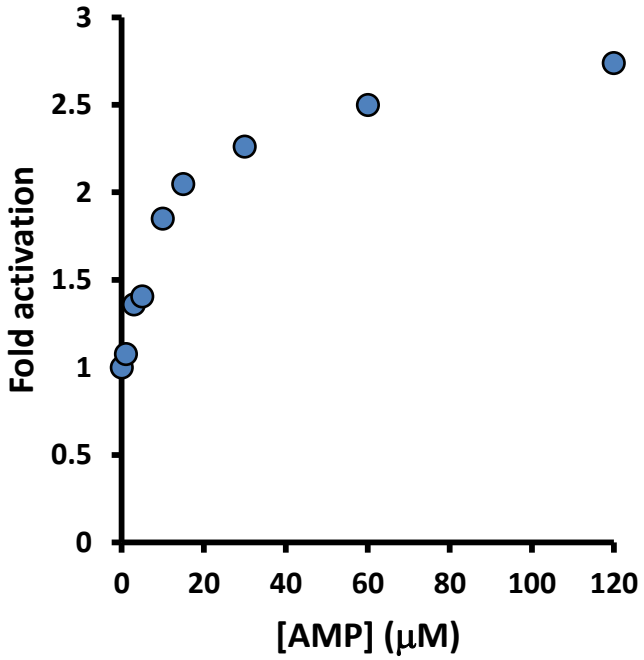

Figure 32: Allosteric activation (AMPK).

AMPK activity was measured in the presence or absence of varying concentrations of AMP with constant level of NADH (150μM), ATP (200μM) and Mg^{2+} (10mM). Results are displayed as fold-increase compared to no AMP condition.

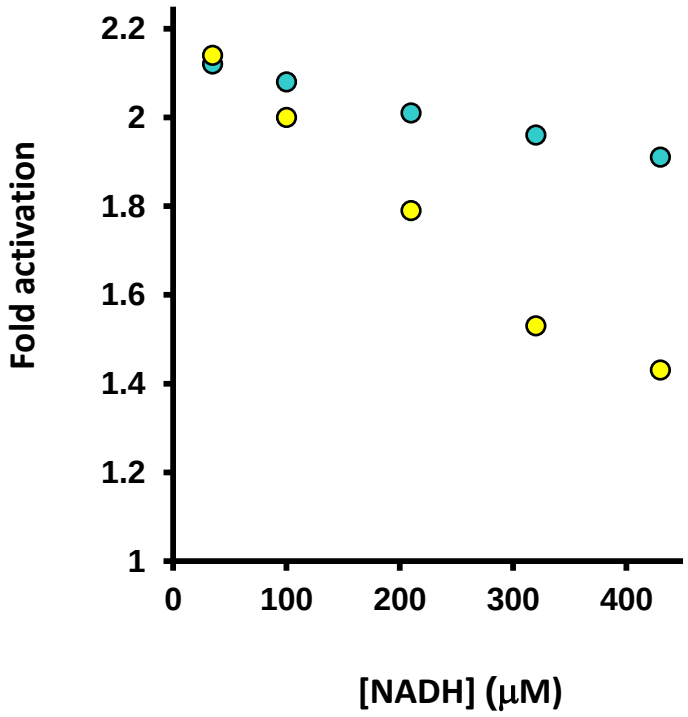

Figure 33: NADH competition with allosteric activation (AMPK).

Allosteric activation of AMPK by 18μM (yellow) and 88μM (blue) AMP in the presence of increasing NADH concentrations. Results are displayed as fold-increase compared to no AMP condition, the mean ± SEM (n>3).

4.4.1.4 Protection against dephosphorylation

In vivo, the rate of αT172 dephosphorylation by phosphatases is critical in determining the equilibrium between active and inactive AMPK. Therefore, the protective effect of AMP/ADP against dephosphorylation of αT172 by PP2Cα was studied. Figure 34 shows time courses for dephosphorylation reactions carried out in the presence and absence of 500μM AMP and ADP confirming that both provide protection. Over the time course there appears to be a greater protective effect of ADP than AMP. This was not observed in the original report of ADP protection, however in that case only protection at a fixed time point (20min) was determined (*1*). As shown in Figure 34, at the 20 minute time point the difference between the AMP and ADP effects is not yet particularly apparent and this is probably why this effect was previously overlooked. Interestingly, greater protection by ADP was also described by Oakhill *et al* (2011) (*177*). Taken together this suggests that ADP may be a more potent activator than was initially thought.

The concentration dependence of the protecting effect of AMP was studied by incubating phosphorylated AMPK with PP2C in the presence of different concentrations of AMP and determining the percentage of phosphorylated αT172 remaining after 25 minutes (Figure 35). The concentration dependence of ADP protection was also monitored, because it appeared to protect more effectively than AMP, a 45minute time point was used in this case (Figure 36). Both AMP and ADP protection against αT172 dephosphorylation appear to saturate at around 0.2mM AXP, consistent with the values reported here and by Xiao *et al* (2011)(*1*).

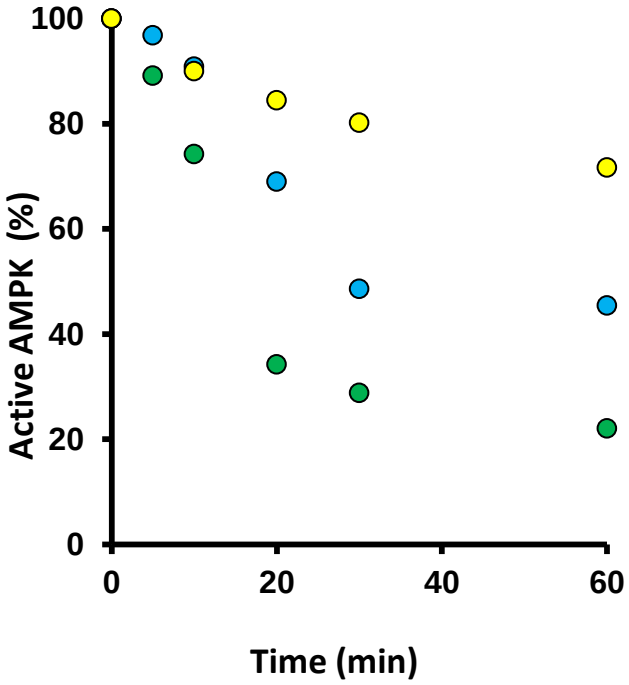

Figure 34: Protection against dephosphorylation by AMP (AMPK).

Phosphorylated AMPK was incubated in the presence of PP2C (green) and 500μM AMP/ADP (Blue/Yellow). At a number of time points AMPK activity was measured. Results are displayed as percentage of phosphorylated αT172 remaining compared to 0min (100%).

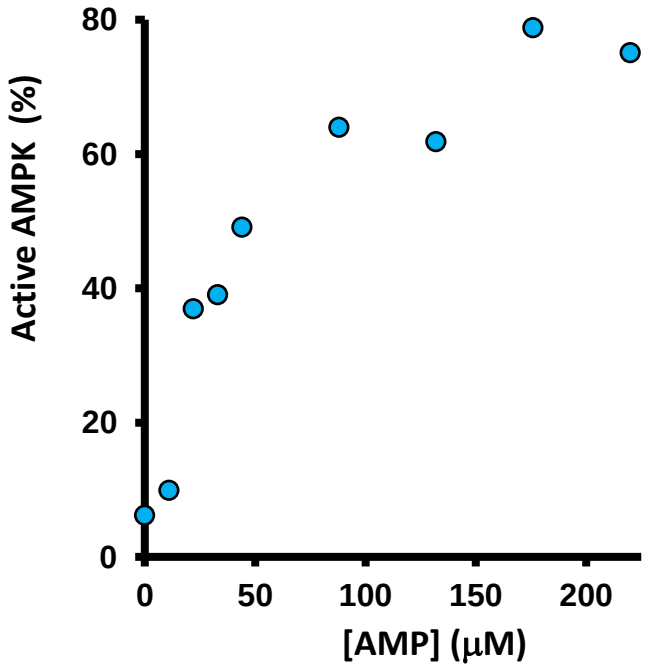

Figure 35: **Protection against dephosphorylation by AMP (AMPK).**

Phosphorylated AMPK was incubated in the presence or absence of PP2C, and in the presence of increasing AMP concentrations. After 25minutes AMPK activity was measured. Results are displayed as percentage of phosphorylated αT172 remaining. All phosphatase assays were performed at 25°C. The concentration of AMP carried over to the activity assay from 220μM AMP was 4.3μM. This was kept constant in all other assays. The SAMS and ATP concentrations were 100 and 250μM respectively.

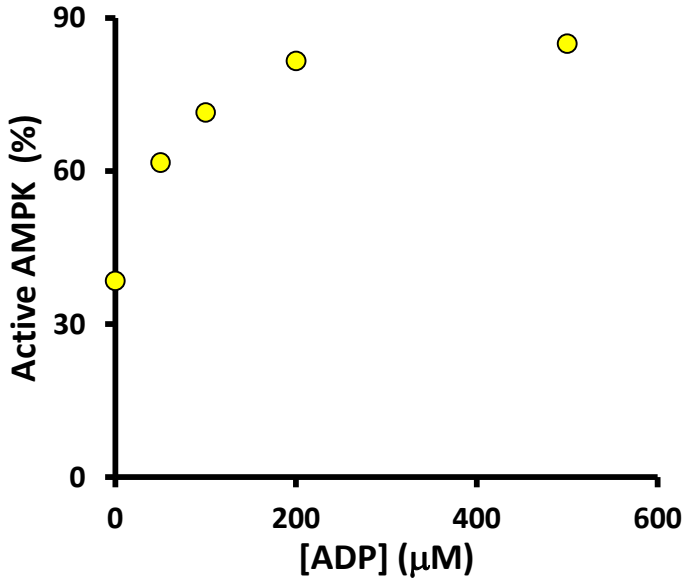

Figure 36: Protection against dephosphorylation by ADP (AMPK).

Phosphorylated AMPK was incubated in the presence or absence of PP2C, and in the presence of increasing AMP concentrations. After 45minutes AMPK activity was measured. Results are displayed as percentage of phosphorylated αT172 remaining. All phosphatase assays were performed at 25°C. The SAMS and ATP concentrations were 100 and 250μM respectively.

4.4.1.5 Mg.ATP affinity for the α-kinase

In Chapter 3, the binding constants for AXPs to the γ-subunit were determined, it was demonstrated that C-AXP's do not bind measurably to the catalytic nucleotide binding pocket in the α-subunit. Mg.ATP is the preferred ligand for this site and is assumed that it binds with higher affinity than free ATP. Following the observations in Section 3.4.2 (Figure 16), in which Mg.ATP did not compete with staurosporine binding, it was assumed that Mg.ATP bound the α-kinase domain significantly weaker than the very tight binding of the inhibitor.

Further evidence of a weak interaction was obtained through competition of increasing Mg.ATP with staurosporine inhibition of AMPK activity (Figure 37a). Only an estimation of the K_d (>0.5mM) was determined. Using the methods described in Section 3.3.1 it is possible to calculate that the percentage inhibition of AMPK by staurosporine (compared to the absence of inhibitor), given 5mM Mg.ATP (physiological), would be 93%, 75% and 58% given Mg.ATP K_d values of 25μM, 150μM or 0.5mM. Given the experimentally determined value is around 60%, it is clear that the Mg.ATP:kinase interaction is weak.

Given that cellular Mg.ATP is in the millimolar range, a low affinity (0.5mM for example) would mean that α-kinase ATP-binding site would still be occupied in the majority of AMPK heterotrimers (Figure 37b).

The question then is why is the apparent K_d for Mg.ATP significantly higher than the K_m for Mg.ATP (~ 0.5mM and 24.4μM respectively).

In the simplest case the K_m is equal to or greater than the K_d:

$$E + S \underset{k_{-1}}{\overset{k_1}{\leftrightarrow}} ES \xrightarrow{k_2} E + P$$

Where the expressions for K_m and K_d are:

$$K_d = \frac{k_{-1}}{k_1} \qquad\qquad K_m = \frac{k_{-1} + k_2}{k_1}$$

In this case if k_2 is significantly smaller than k_{-1} then the K_m is approximately equal to the K_d. However as the complexity of the reaction schemes increases so do the number of terms which define the K_m, therefore the relationship between K_m and K_d is more complicated.

For example, in the case of a bi-substrate, compulsory order reaction:

$$E + A \underset{k_{-1}}{\overset{k_1}{\leftrightarrow}} EA + S \underset{k_{-2}}{\overset{k_2}{\leftrightarrow}} EAS \xrightarrow{k_3} EDP \xrightarrow{k_4} E + D + P$$

The expressions for K_m and K_d are:

$$K_d(EA) = \frac{k_{-1}}{k_1} \qquad K_m(S) = \frac{k_4}{k_2}\left(\frac{k_{-2} + k_3}{k_3 + k_4}\right) \qquad K_m(A) = \frac{k_3 k_4}{k_1(k_3 + k_4)}$$

Although the mechanism of AMPK catalysis is unknown (be it compulsory or random order), this demonstrates how a K_d value is not restrained to be equal to or greater than the K_m in a complex catalytic reaction such as that of AMPK phosphorylation (*257*).

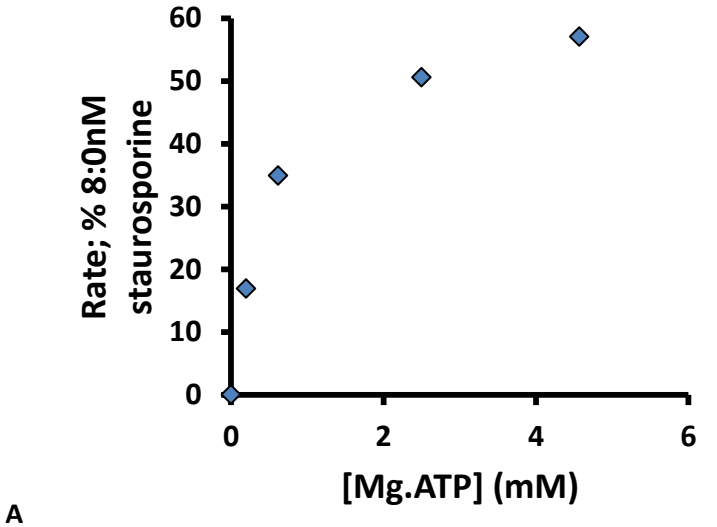

A

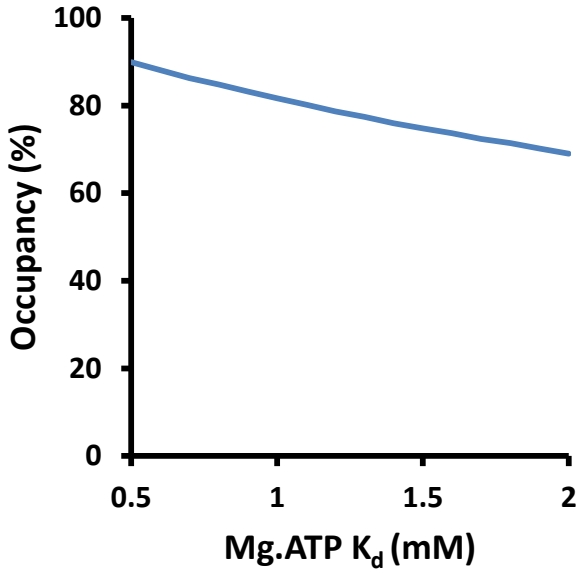

B

Figure 37: A) Mg.ATP competition with Staurosporine inhibition.

Samples taken from a preincubated solution containing 10nM AMPK, 8nM staurosporine and a range of Mg.ATP concentration were assayed. Data is plotted as % inhibition compared to no staurosporine rates. In addition to the standard buffer conditions, 20% isopropanol was used throughout.

B) Simulation of the % occupancy of the α-kinase ATP-binding site.

Experimental data defined a K_d of greater than 0.5mM. Over this range, the occupancy of the ATP-binding site ranges from 70-90% as a function of the Mg.ATP K_d. Given a fixed ATP concentration of 5mM and free Mg^{2+} concentration of 0.5mM**.**

4.4.2 Modelling of AMPK kinetics

4.4.2.1 The regulatory roles of Site-1 and Site-3

Two regulatory sites on the γ-subunit bind nucleotides exchangeably. Binding of AMP at Site-1 is thought to be responsible for allosteric activation and binding of AMP/ADP at Site-3 is thought to be responsible for protection of αT172 against dephosphorylation by phosphatases (*1*).

NADH binds AMPK with a 1:1 stoichiometry (Section 3.4.3.3). Site-1 is thought to be the tighter, NADH, binding site because this site is fully occupied in electron density maps of crystals soaked with a 1:1 molar ratio of AXP (Personal Communication - Bing Xiao). Increasing concentrations of NADH compete with the allosteric activation of AMPK by AMP, suggesting that Site-1 mediates this regulatory effect.

Site-3 is the second, weaker, nucleotide binding site. The observation that NADH does not compete with the protective effect of AMP/ADP against αT172 dephosphorylation, suggests that it is Site-3 which mediates this regulatory effect.

Interestingly, in the structure of active AMPK determined within the Gamblin laboratory, a loop (the α–hook) extends from the α-subunit and forms a lid over Site-3 (Figure 5). It is suggested that the α-hook binds in this way in the presence of AMP/ADP and acts to restrict the flexibility of the preceding α-linker region and in doing so promotes the interaction of the α-kinase with the regulatory subunit and thus stabilisation of the activation loop (Figure 38). This interaction in turn protects αT172 from dephosphorylation. Mutation of the α-hook (R375Q/T377A/D379A/E380A) results in a loss of AMP/ADP protection but not of allosteric activation (*1*). Modelling of Mg.ATP into this site in the active complex suggests that the γ-phosphate prevents binding of the α-hook and thus the stabilisation. In this way AMPK is able to differentiate between AMP/ADP and Mg.ATP binding at Site-3.

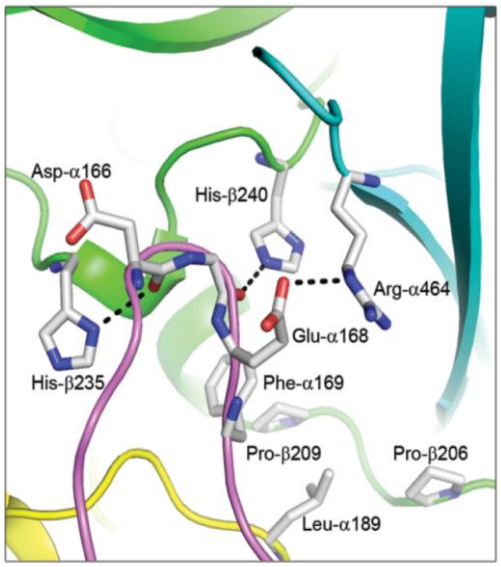

Figure 38: The interface between the activation loop and the regulatory fragment.

The interface is shown in more detail in a similar orientation as in Figure 5. Potential electrostatic interactions are indicated by dashed lines. Taken from (*1*).

4.4.2.2 The program

Using the K_d values determined in Section 3.4.3.1 the occupancy of Site-1 and Site-3 by regulatory nucleotides under the *in vitro* assay conditions, used to monitor allostery and protection against dephosphorylation was modelled.

The program was written in Visual Basic Version 6.0 and based on the Cornish-Bowden method (previously discussed in Section 4.2.5).

A number of parameters, for example nucleotide and cation concentrations, must be supplied by the user (Figure 39a). The program calculates the concentrations of all nucleotide species, based on published binding constants for the interactions between AXP and cations/protons etc. and the K_d values of the AXP:AMPK interactions (Figure 39b and Figure 40)(*278*). Of course the *in vitro* assays were all carried out using phosphorylated (active) AMPK, therefore equilibrium binding constants for AXP binding to AMPK were taken from Table 7.

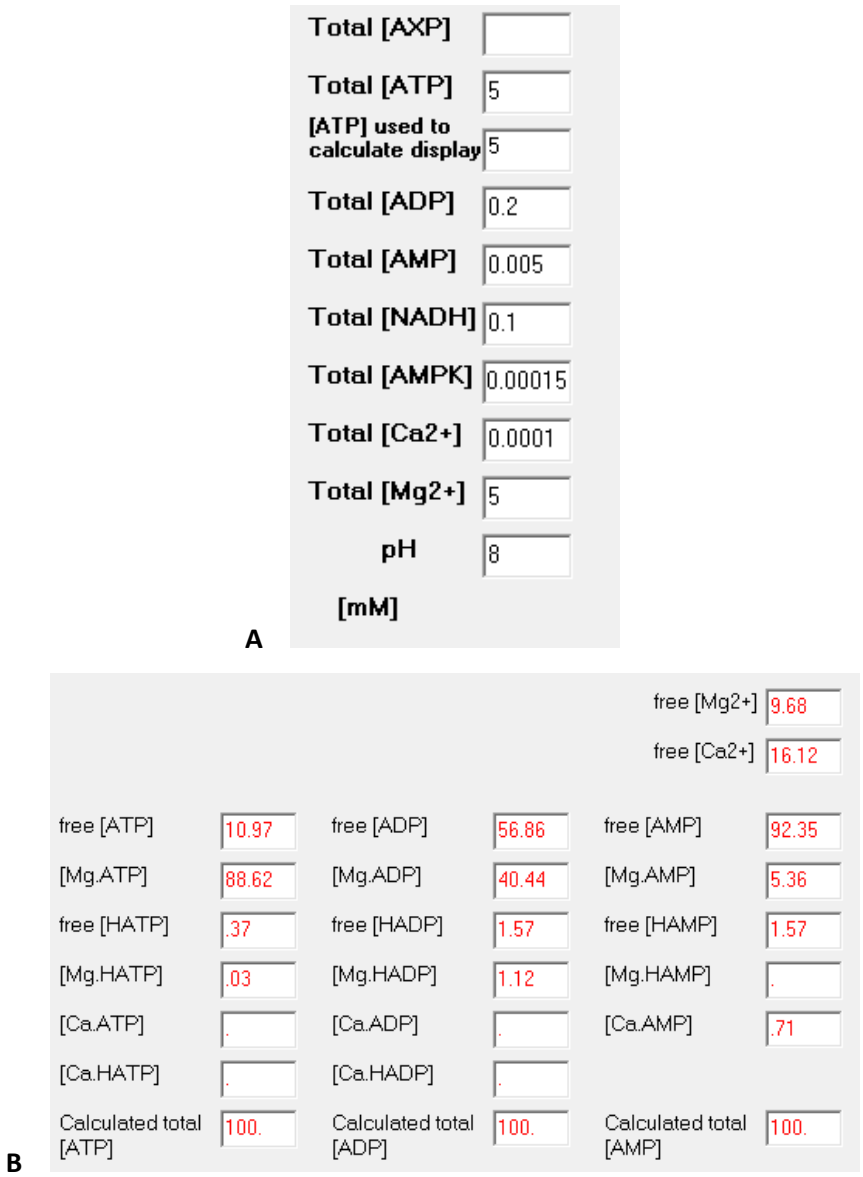

Figure 39: Screenshot of the user interface.

A) Inputs. B) Calculation of the concentrations of AXP species: Displayed as percentages of the total concentration.

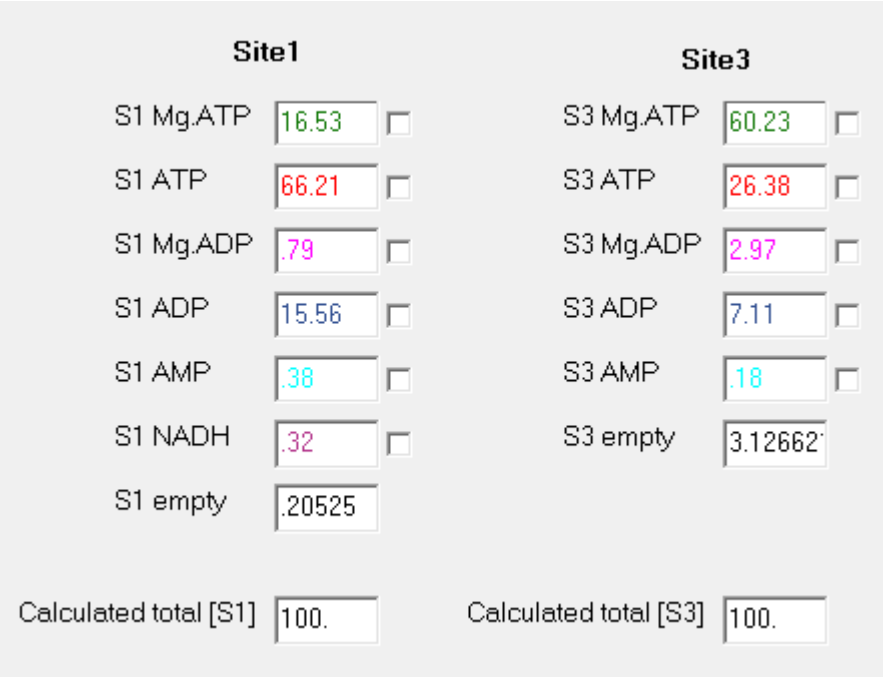

Figure 40: Screenshot of the user interface.

Occupancy of Site-1 and Site-3 by nucleotides: Displayed as percentages of the total concentration.

4.4.2.3 *In vitro* occupancy results

Figure 41 shows the percentage occupancy of Sites-1 and 3 calculated under the conditions of the 'allosteric activation experiment' shown in Figure 32 (10mM Mg^{2+}, 0mM Ca^{2+}, 10nM AMPK, 200μM ATP, 0mM ADP, 150μM NADH, pH 8.0 and variable AMP) compared with the measured fold-activation (scaled with the assumption that fold-activation is proportional to percentage occupancy). At maximal fold-activation (AMP ~100μM) Site-1 is 80-90% occupied by AMP, whilst Site-3 is only ~50% occupied. Although the agreement is only approximate it is clear that occupancy of Site-1 correlates better with the observed effect. Given that the dissociation constants measured in Chapter 4 are, in some cases, relatively poorly defined the agreement is not unreasonable.

Figure 42 shows the percentage occupancy of Sites-1 and 3 calculated under the conditions of the 'protection against αT172 dephosphorylation' experiment shown in Figure 35 (10mM Mg^{2+}, 0mM Ca^{2+}, 0.01mM AMPK, 0mM NADH, 0mM ATP, 0mM ADP and variable AMP) compared with the amount of phosphorylated AMPK remaining after 25 minutes. In this case it is clear that protection against dephosphorylation correlates much better with occupancy of Site-3. Under these conditions Site-1 is almost completely saturated at 25μM AMP, whilst the regulatory effect saturates at concentrations greater than 200μM (at which point Site-3 is >70% occupied).

Taken together, this work provides further evidence for the assignment of AMP binding at the tighter site (Site-1) being the mediator of allosteric activation and binding of AMP/ADP at the weaker site (Site-3) being responsible for protection against dephosphorylation of αT172.

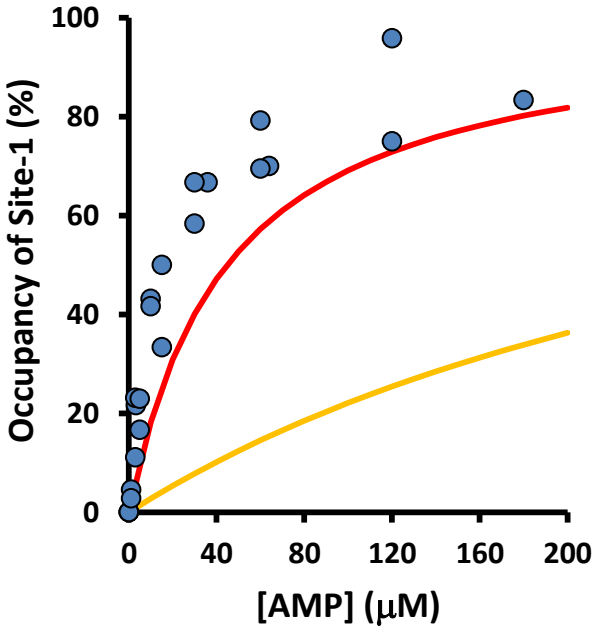

Figure 41: Modelling of allostery (AMPK).

Blue: Allosteric fold activation shown as % site occupancy, corresponds to Figure 32 (assuming that at full activation, the relevant binding site is 100% occupied). Red: % occupancy of Site-1. Yellow: % occupancy of Site-3 by AMP.

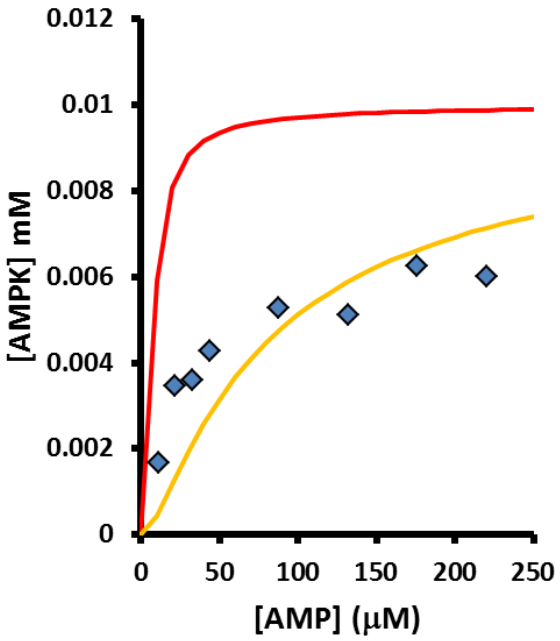

Figure 42: Modelling of protection against dephosphorylation by AMP (AMPK).

Blue active AMPK after 25min (corresponds to Figure 35). Red: occupancy of Site-1 by AMP. Yellow: occupancy of Site-3 by AMP. Displayed as AMPK concentration plotted against AMP concentration. The total AMPK concentration used in the *in vitro* assays was 0.01mM.

4.4.2.4 Modelling of '*in vivo*' AMPK occupancy

Whilst the modelling of *in vitro* assay conditions ties the work from Chapter 4 to that in Section 3.4.3, and is a useful test of the model, the ultimate aim is to comment on how nucleotides are responsible for AMPK activation in an '*in vivo*' situation.

For this purpose it is assumed that 'a signal' results in increased AMP/ADP and decreased Mg.ATP concentrations, altering the binding site occupancy of AMPK, and translating to increased activity. I aimed to test three important points:

1) That occupation of Site-1 by AMP when '*in vivo*' nucleotide concentrations are used in the program is negligible, and therefore that allosteric activation is unlikely to be an important factor under 'normal' *in vivo* conditions.
2) That occupancy of Site-3 by ADP can be significant compared to that of Mg.ATP and therefore that ADP can successfully compete for binding and protect αT172 from dephosphorylation by phosphatases in an '*in vivo'* setting.
3) That there is a significant increase of regulatory nucleotide occupancy of Site-3 when 'stressed' nucleotide concentrations are used in the calculation.

First it was necessary to define the AXP and ion concentrations which represent 'basal' and 'stressed' cellular states. The ranges of cellular nucleotides which are often quoted are [ATP] = ~5mM, [ADP] 50-200μM and [AMP] 1-5μM, and a free Mg^{2+} concentration of 0.5mM (*1, 275, 279-281*). The low end of these AMP/ADP estimates corresponds to a basal situation and the top end to a stressed situation. The ATP concentration is decreased by the increases in the AMP and ADP concentrations.

Despite the relative increase in AMP concentration (from 1 to 5μM) being a little greater than that of ADP (50 to 200μM) it is the absolute concentrations that determines the

occupancy of the binding sites. As such the potential occupancy of ADP is much greater than that of AMP.

The calculations show that the occupation of Site-1 by AMP, i.e. the increase in AMPK which is allosterically activated, is from 0.09% to 0.39% (at 1μM and 5μM AMP respectively). A drop in ATP/Mg.ATP occupancy of Site-1 is observed (from 94.9% to 82.3%), but it is ADP which increases significantly in occupancy (and, of course, ADP does not allosterically activate AMPK). Given the very low basal level and small increase in occupancy it is unlikely that AMP binding at Site-1, and therefore allostery itself, is an important regulatory effect *in vivo*. Perhaps this regulation only comes into play as a 'last ditch' attempt to rescue the cell from death when AMP concentrations become very high.

The cellular concentrations of ATP are significantly higher than those of the regulatory nucleotides (AMP and ADP) so it has always been a challenge to envisage how AMP/ADP could regulate the enzyme. In Chapter 3 it was suggested that the weaker binding of Mg.ATP (the predominant cellular species - Figure 43), relative to free AXP, was sufficient to allow ADP to compete effectively for binding to the γ-subunit. The concentrations of AMP appear too low for it to significantly occupy either Site-1 or Site-3, as demonstrated above in relation to allosteric activation. However, the change in occupancy of Site-3 by ADP, which protects against dephosphorylation of αT172, could be 4-fold, increasing from 2.68% to 10.14% (50μM and 200μM ADP respectively).

It is encouraging that the model can predict an increase in occupancy of the regulatory site by ADP given basal and elevated cellular AXP concentrations. This effectively demonstrates that ADP can compete with the high ATP/Mg.ATP concentrations for binding and therefore be capable of regulating AMPK.

The mitochrondrial uncoupler, 2,4-dinitrophenol (DNP) in conjunction with sorbitol, rapidly alters the cellular ADP:ATP ratio and thus potently activate AMPK. Together these compounds activated AMPK 12-fold relative to untreated cultured muscle cells (*282*). It seems reasonable to assume that this represents maximal activation of AMPK (i.e. 100%), and therefore that up to 8% of AMPK is active under basal conditions. This value is perhaps a little higher than the 2.5 to 10% ADP-bound fraction under basal and 'activated' conditions predicted by the model, but is certainly within an acceptable range.

The phosphatase reaction is thought to be important in determining the proportions of phosphorylated and unphosphorylated AMPK (since LKB1 is constitutively active). It is therefore likely that ADP is the universal activator of AMPK, operating in all cell types and in response to a multitude of stress/signals through modulation of the susceptibility of AMPK to phosphatase activity.

4.4.2.4.1 Adenylate Kinase

Adenylate kinase catalyses the conversion of two molecules of ADP into one of ATP and AMP. It has often been suggested that because the AMP:ATP ratio increases as the square of the ADP:ATP ratio, that AMP is a more sensitive indicator of the cellular energy status. Simulations show that over the cellular AXP concentrations used in the *in vivo* modelling (Section 4.4.2.4) AMP concentrations do change by a slightly larger proportion that ADP but that the highest concentration reached is insufficient for AMPK regulatory sites to be significantly occupied (Figure 44). Under these conditions, the absolute increase in ADP concentration is larger than that of AMP, and therefore is the more effective monitor of cellular energy status.

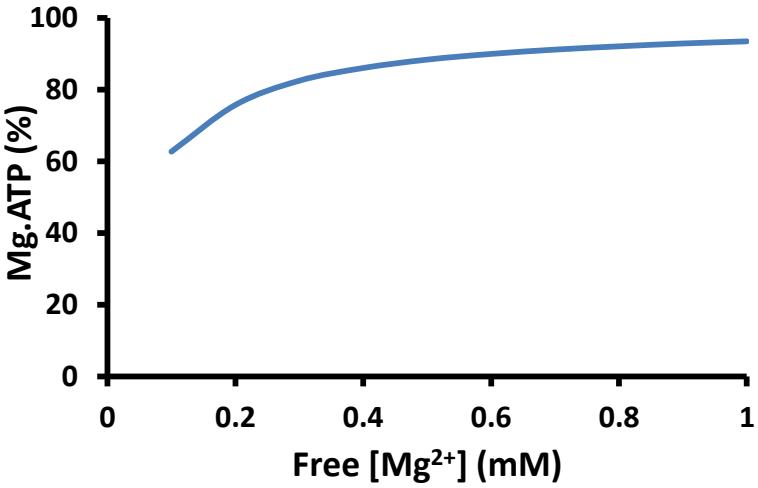

Figure 43: % Mg.ATP over the physiological range of free Mg^{2+} concentration (AMPK).

Given starting nucleotide concentrations of 5mM ATP, 50μM ADP and 1μM AMP, 150nM AMPK, pH 8.0.

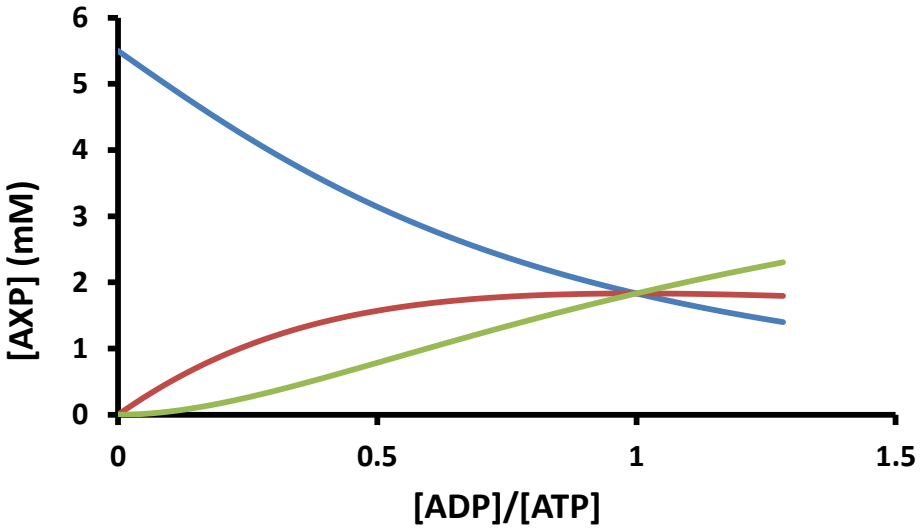

Figure 44: Changes in nucleotide concentration.

ATP (blue), ADP (red) and AMP (green) plotted against [ADP]/[ATP]. Fluctuations in the cellular nucleotide concentrations rarely decrease the ATP concentration this dramatically; in fact increases in AMP/ADP of only fractions of a millimolar are to be expected.

If the ATP concentration decreases by less than 10% then there is a significant increase in the ADP concentration but a very small increase in the AMP concentration.

Calculated based on the adenylate kinase reaction, with a fixed total AXP concentration of 5.5mM and K= 1, (method described in Section 4.2.7).

4.4.2.4.2 Limitations of the model

Whilst modelling of AMPK binding site occupancies by AXP can be considered a success there are a number of additional factors which should be considered:

1) The standard deviations associated with the AMPK:AXP K_d values are unavoidably large and these errors can have a significant effect on calculations of the % occupancy.
2) The *in vivo* nucleotide and cation concentrations used in modelling occupancy are not well determined. Often the techniques used place the cells under some stress so concentrations may not be accurate. Additionally, nucleotide and cation concentrations vary with tissue-type and with cellular localisation/compartment.
3) Different AMPK γ isoforms may be bound by AXP with different affinities (this work described only AXP binding to γ1), different heterotrimeric complexes may also be regulated to differing extents by ADP (this work described only regulation of α1).
4) It is unknown what proportion of AMPK must be bound by ADP in order for sufficient activation of the kinase to occur. Perhaps there is a large AMPK pool, of which only a small percentage must be ADP-bound/activated in order to achieve the relevant downstream effects.

4.4.2.4.3 Linking Site-3 occupancy to AMPK activation

Having calculated the proportions of AMPK regulatory sites bound by nucleotide, it is important to link this to changes in αT172 phosphorylation and therefore activation (Figure 45).

In terms of the allosteric effect this is straightforward; we know that AMPK bound at Site-1 by AMP is ~2-fold more active than unbound AMPK. However as was already established, this may not be an important point of regulation *in vivo*.

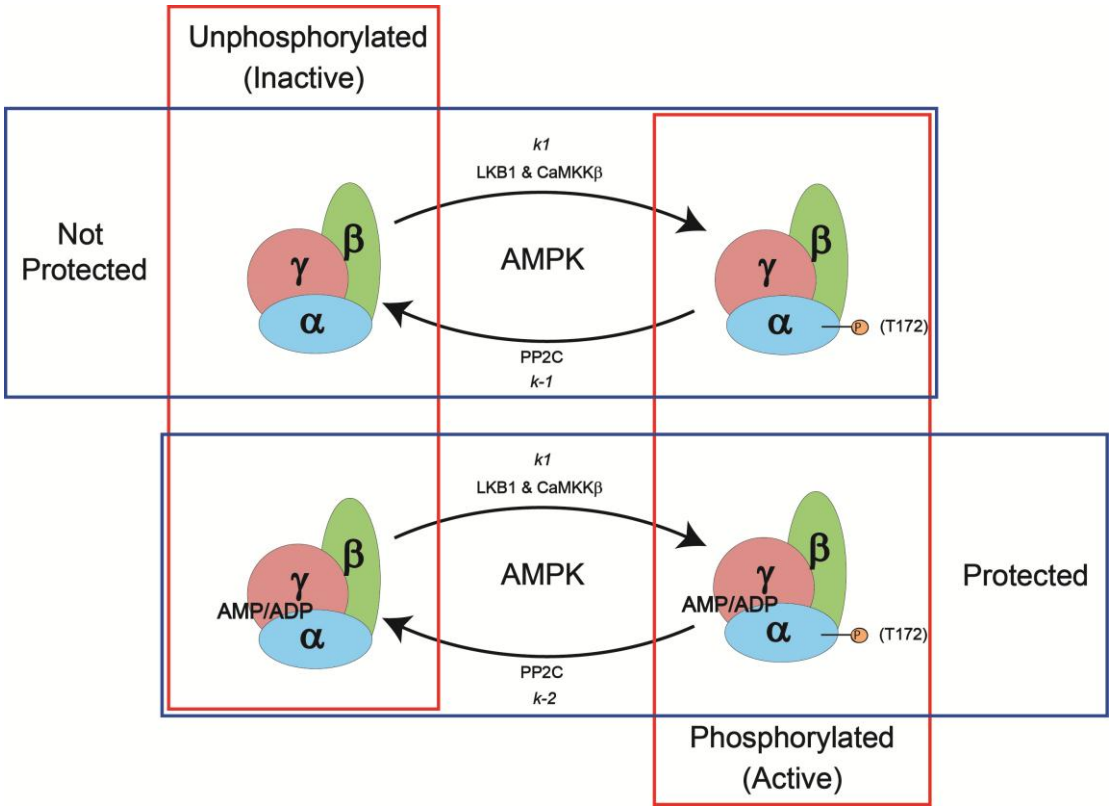

Figure 45: AMPK species.

There are at least four major AMPK states, unphosphorylated and therefore inactive, or phosphorylated and therefore active. Either of these states may be bound by AMP/ADP and therefore protected against dephosphorylation. The concentrations of the two AMPK species are defined by the rates of the kinases and phosphatases, and the nucleotide concentrations and their binding affinities.

It is more challenging to define the effect of AMP/ADP binding at Site-3 on protection against dephosphorylation. This depends upon the relative rates of the phosphatase when AMPK is bound by regulatory nucleotide and by non-regulatory nucleotide. The identity of the *in vivo* AMPK phosphatase(s), and therefore detailed information about its activity is unavailable.

We have proposed that αT172 is protected from dephosphorylation when the T-loop/α-kinase interacts with the regulatory subunit (Figure 38) such that two species exist, kinase-regulatory fragment bound and kinase flexibly linked. ADP/AMP binding to the γ-subunit shifts the equilibrium from the free to the bound form. In terms of regulation the important, but unanswerable, question is to what extent does AMP/ADP binding alter the k_{on} and k_{off} of this equilibrium.

It is clear that ADP binding does not cause a complete shift to a bound-kinase form as one would then expect to see little or no dephosphorylation at saturating [ADP], even at long time points. A partial shift in the equilibrium towards a completely protected bound form could explain the results in terms of a reduction in the effective substrate concentration. Ultimately the question is what are the changes in k_{on}/k_{off} rates of the kinase interaction with the regulatory subunit, given occupancy of Site-3 by ADP rather than to Mg.ATP?

Even when we have kinetically defined the effect of ADP binding on phosphatase activity, there are a number of factors in addition to those listed in Section 4.4.2.4.2, which may result in an underestimation of cellular AMPK activation;

1) It is unknown what the basal level of AMPK activity is, although a low (<8%) basal level of AMPK activity can be inferred from the mitochondrial uncoupling. It is also necessary to define what fold-increase in activity is required for activation of downstream targets,

again work with mitochondrial uncouplers provides information about maximal levels of AMPK activation (*282*).

2) ADP binding may also increase the rates of the upstream kinases.
3) The role of the proposed AID on activation and nucleotide binding is unknown.
4) Myristoylation, acetylation, ubiquitination, glycogen and endocrinological signals also modulate the equilibrium between phosphorylated and unphosphorylated AMPK in a cell-type, localisation and signal dependent manner. These factors are hard to introduce to the model of AMPK activation since their roles are varied and not completely understood.

I do conclude that it is ADP binding to the γ-subunit which acts as a universal activator of AMPK. It is simplistic to model AMPK activation 'as a function of ADP binding', since a multitude of other signals influence the amount of αT172 which is phosphorylated in vivo, therefore a more sophisticated model of AMPK regulation in the future may reveal more complexity than demonstrated here. Further information about the rates of the kinase/phosphatase activity, other regulatory signals and the mechanism through which αT172 is protected against dephosphorylation is required in order for such a model to be produced.

4.4.2.5 Ultrasensitivity

In some cases biological systems are activated with a sensitivity of more, or less, than would be predicted by standard Michealis-Menten approximations. Ultrasensitivity is defined as a response where an increase from 10% to 90% of maximal requires a change in the initial signal of less than 81-fold (*283*). AMPK activation in INS-1 cells has been shown to be ultrasensitive in response to AICAR treatment (*265*).

There are three ways, which may act in concert, that ultrasensitivity can be achieved;

1) Positive Cooperativity – where the binding of a ligand/activator increases the affinity of a second. There is no evidence for this in the AMPK system.
2) Multistep Ultrasensitivity – A single activator acts at multiple stages of a cascade, with rate constants of the effectors within a narrow range (*284*).
3) Zero-order Ultrasensitivity – One or more enzymes are operating under zero-order conditions, that is, the substrate concentration is significantly higher than the K_m therefore the enzyme operates at V_{max}. If a single enzyme in a futile cycle (e.g. a phosphorylation-dephosphorylation cycle) operates under zero-order and the second under first-order conditions a lag at the top or the bottom of the curve is observed (*284*).

Previously the multistep activation of AMPK by AMP was considered as the source of ultrasensitivity (*265*), however it is likely that ADP binding is the key regulator of AMPK activity, as is demonstrated throughout this Chapter. Therefore multistep ultrasensitivity (by AMP) is no longer a viable explanation for the *in vivo* observation that AMPK is activated in an ultrasensitive manner (*1, 177*). Suggesting, perhaps, that AMPK activation operates mainly through zero-order effects.

The equilibrium between phosphorylated and unphosphorylated AMPK is maintained through activity of the kinase and phosphatase. An increase in ADP shifts the equilibrium

from favouring the phosphatase reaction to the kinase reaction, which is both constitutively active and operating under zero-order conditions. This switch relies upon carefully balanced reaction rates, which are therefore sensitive to changes in ADP concentration over a narrow range and results in rapid activation/inactivation of AMPK.

Whilst ultrasensitivity is not considered further in this thesis, it is an interesting mechanism through which high sensitivity may be introduced into the regulation of AMPK, and should be considered in the future modelling studies on the activation of AMPK *in vivo.*

4.5 Conclusion

In this Chapter I demonstrated that a coupled spectrophotometric assay can be used to effectively monitor AMPK catalysis and a number of kinetic parameters were determined. Binding of AMP at Site-1 mediates allosteric activation *in vitro* and binding of AMP/ADP at Site-3 mediates protection of αT172 against dephosphorylation by phosphatases (*1*). This was demonstrated experimentally through competition of NADH with these regulatory effects and through simulation of the *in vitro* assays.

Simulation of AMPK binding site occupancies, given estimations of intracellular AXP concentrations, suggest that 1) allosteric activation by AMP may not be an important regulatory point *in vivo,* 2) ADP can effectively compete with Mg.ATP for binding at the regulatory binding site, and 3) this occupancy increases 4-fold when 'stressed' AXP concentrations are used.

Chapter 5: Structure of a truncated AMPK complex

5.1 Abstract

In this Chapter X-ray crystallography was used to determine the structure of a truncated AMPK complex with C-ADP. The AMPK structure is compared to an unlabelled ADP-bound form. This study verified that C-ADP bound in a homologous fashion to ADP, specifically in the same exchangeable binding pockets, and revealed the additional contacts made between the fluorescent adduct and AMPK.

5.2 Introduction – X-ray Crystallography

5.2.1 Overview

X-ray crystallography, Nuclear Magnetic Resonance (NMR) and cryo-Electron Microscopy (EM) are the three most widely used techniques to investigate the macromolecular structure of proteins. Each has a number of benefits and limitations which make their use complementary in the study of different biological questions. NMR is often used as a solution state technique and provides information about the kinetics and dynamics of a protein; however its use in structure determination is generally limited to proteins with a molecular weight of under 50kDa (*285*). Single particle cryo-EM can produce low resolution (>5Å) structures of asymmetric protein complexes with molecular weight between 0.1-0.5MDa (*286*). X-ray crystallography has no size limitations per se and it offers the highest atomic resolution, however it requires that the protein molecules are amenable to crystallisation. Over 80% of the protein structures present in the PDB were determined by X-ray crystallography.

X-ray crystallography proceeds through four major steps: 1) protein purification; 2) crystallisation; 3) data collection; 4) data processing. A fifth may be added if a homologous structure is not available for molecular replacement, in this case the 'phase problem' must be overcome.

This introduction was compiled from a number of sources:

Notes from the BCA Protein Crystallography Summer School 2010; 'Protein Crystallography with Coffee' - Airlie McCoy (*287*); 'Crystals, X-rays and Proteins' – D. Sherwood and J. Cooper (*288*); Personal Communications - Bing Xiao and Steven Gamblin (NIMR).

5.2.2 Crystallography

Crystal Packing and Symmetry

A crystal is a solid in which the molecules are arranged in a lattice constructed of identical unit cells, described by three dimensions *a, b* and *c*, and three inter-axial angles α, β and γ. Each unit cell has the same environment as every other one. The simplest lattice arrangement is termed primitive (P). The lattice may also be arranged as body centred (I centred), centred on all faces (F centred) or centred on a single face (A, B, or C centred).

Crystal symmetry is defined as the set of operations, the application of which superimposes the asymmetric unit on itself. There are three types of crystallographic symmetry; rotation, reflection and inversion. Since proteins exist in a single chiral form the latter two symmetry types are not present in their crystals. 2-fold, 3-fold, 4-fold and 6-fold rotational symmetry are allowed in a protein crystal; their presence places restrictions on the unit cell parameters of the lattice. There are seven 'crystal systems' which conform to the definition of a unit cell and to the possible symmetry operations; triclinic, monoclinic, orthorhombic, tetragonal, trigonal, hexagonal and cubic. When combined with the possible centring operations they give rise to 14 distinct lattice types.

Further lattice complexity is added by the presence of screw axes. Screw rotations are described as the order of the rotation (2, 3, 4 or 6) followed by a subscript indicating the fraction of the unit cell of the translation. There are 11 crystallographically allowed screw rotations. Combining all the point groups and lattice types gives a total of 65 unique space group symmetries possible for protein crystals. Some are particularly favourable for packing of globular molecules; over a quarter of the structures in the PDB belong to the space group $P2_12_12_1$.

The unit cell dimensions determine the spacing and arrangement of the reciprocal space lattice. The symmetry relationships between the intensities of reflections, and the patterns

of systematically absent reflections, arises from the crystallographic symmetry operators that apply to each crystal.

The asymmetric unit is the smallest unit of structure that can generate the whole crystal after application of the crystal symmetry. There can be any number of molecules in the asymmetric unit, the occurrence of more than one copy gives rise to the phenomenon of non-crystallographic symmetry. Knowing the space group, the unit cell, and the contents of the asymmetric unit defines the positions of all atoms in the crystal.

Braggs Law

X-rays have a wavelength on the order of 0.1nm (1Å) which is comparable to the spacing between atoms in a protein. The crystal lattice acts as a diffraction grating allowing the underlying molecular transform to be sampled in a discrete fashion. When the diffracted waves constructively interfere an interference (or diffraction) pattern is produced. The arrangement of unit cells, according to the unit cell parameters and space group, determines the spacing and symmetry of the reciprocal lattice, whilst the arrangement of atoms within the asymmetric unit defines the underlying molecular transform and thus the intensity of each reflection.

Diffraction is described by Braggs law, which relates the distance between the layers of atoms in the crystalline lattice (*d*), the wavelength of the X-rays (λ), the angle of incidence of the X-ray beam (θ) and the order of the reflection (*n*).

$$2d\ sin(\theta) = n\lambda$$

Reciprocal Space versus Real Space

Within a crystal the position of atoms are described in terms of real space co-ordinates. Reflections arising from diffraction are described in terms of their position in reciprocal space (constructed based on 1/*d*). Thus, a large unit cell dimension results in reflections which are close together in reciprocal space.

The axes in reciprocal space are termed a*, b* and c* (a* being perpendicular to b, c, b* to a, c, and c* to a, b), and the angles between them $\alpha*$, $\beta*$, and $\gamma*$.

The miller indices describe the position of reflections within reciprocal space. Each reflection is assigned a Miller index, that is a set of the three integers (*h, k, l*). The spacing *d* in Bragg's Law is given by the Miller indices, which denote the plane in the crystal for which Bragg's Law is satisfied for that reflection.

Friedals Law states that the intensity of any given reflection (*h, k, l*) is equal to the intensity of the reflection (*-h, -k, -l*), thus the diffraction pattern has a centre of symmetry.

The intensities (F) of each reflections are determined by the position of atoms within the asymmetric unit. Every atom makes a contribution (positive, negative or zero) to the intensity of each reflection.

Structure factor *(F)* determination

The structure factor equation relates how intensities (*F*) of reflections arises from the position of each atom, and follows the general form:

$$F(hkl) = \sum_{n=1}^{N} f_n e^{2\pi i(hx_n + ky_n + lz_n)}$$

But is perhaps expressed more helpfully as:

$$A(hkl) = \sum_{n=1}^{N} f_n \cos 2\pi(hx + ky + lz)$$

$$B(hkl) = \sum_{n=1}^{N} f_n \sin 2\pi(hx + ky + lz)$$

Where: $A = F\cos\emptyset$ $B = F\sin\emptyset$ and thus $F = \sqrt{A^2 + B^2}$ $\emptyset = \tan\frac{B}{A}$

So structure factors can be calculated from a given model (F_{calc}) but only structure amplitudes can be directly measured for a crystal (F_{obs}). Ultimately refinement aims to minimise the differences between these F_{obs} and F_{calc} values.

Electron density *(ρ)* determination

A Fourier transform is used to convert a given set of amplitudes (F) and phases (φ) to an electron density map. Electron density at a given point in real space, is given by:

$$\rho(x, y, z) = \frac{1}{V}\sum_h \sum_k \sum_l |F|(h, k, l)e^{[-2\pi i(hx+ky+lz)+\varphi(h,k,l)}$$

Molecular replacement

Full information about the phases of the diffracted waves cannot be extracted from protein crystal diffraction. 'The phase problem' can be solved directly, in the case of small molecules, or experimentally using isomorphous replacement or anomalous scattering methods. These techniques rely on changes in reflection intensities when a reference wave of known phase interferes with a diffracted wave of unknown phase. In the first the reference wave comes from heavy atoms and in the latter from, for example, selenomethionine.

Another approach to phasing is molecular replacement, which takes initial estimates of the phases from a model and iteratively improves them. This relies on the existence of a structure with reasonable similarity (often associated with at least 20% sequence identity) to the target structure.

The model and target structures must be computationally aligned; this is achieved traditionally through the use of Patterson functions. The Patterson function is a Fourier transform calculated from intensities alone; setting all the phase values to zero. It produces an interatomic vector map containing both intramolecular and intermolecular information. The Patterson functions calculated from the model and experimental data are compared; first the model structure data must be correctly rotated/orientated (based upon self-vectors) then translated to the correct position (based upon cross-vectors). Maximum-likelihood methods play an increasing role in the computation of rotation and translation operations used in molecular replacement.

Refinement and Model Building

The electron density is displayed as a contour map with peaks at the atomic positions. F_o-F_c maps reveal positive and negative electron density arising from differences between the calculated and observed intensities. The amino-acid chain and ligands are modelled into the map. Manual and automated refinement of the structure aims to make the model fit the experimental data as closely as possible, minimising differences in the F_o-F_c map. The process is interactive and iterative. Higher resolution maps allow the model to be built more easily and often largely automatically.

The crystallographic R-factor is monitored to follow the progress of refinement. Values of around $1/10^{th}$ of the resolution limit are considered acceptable, thus reflecting the fact that high resolution refinement results in much more accurate coordinates. During the process of refining and building the model it is important to avoid over fitting of the data and model bias. This occurs because of the relatively low observation:parameter ratio. In order to avoid this problem a number of reflections are left out of the refinement, the R_{free} is independent of the refinement process and should improve with the R-factor.

A number of geometrical factors contribute to the model refinement process; the lengths of the bonds and angles between atoms, the conformations of secondary structure elements e.g. α-helices and β-sheets and restrictions on the conformation of the peptide backbone. Adding these parameters as restraints in refinement acts to improve the observation:parameter ratio. This is important because at about 2-5Å resolution most crystals only provide one observation (reflection) per refined parameter (4 per atom; x, y, z and B-factor).

Rigid body refinement refines the position of protein domains, therefore the number of parameters being fitted is greatly decreased. Translation-libration-screw (TLS) refinement also treats groups of atoms as single units, refining the B-factors as a function of their translation and libration (oscillations). These 'bulk' corrections can thus be refined with a high observation:parameter ratio even with low resolution data. Non-crystallographic symmetry i.e. if you have more than one protein molecule in the asymmetric unit, can be used to improve the electron density maps by real space averaging, as can solvent flattening techniques. There are many methods employed in the process of model- building and refinement, only the key techniques have been touched upon.

5.2.3 Crystallography Work-flow

Protein purification

Generally, protein crystallisation is highly dependent on the homogenity and monodispersity of the sample. Generation of recombinant proteins in a stable, soluble and concentrated form for X-ray crystallography often proves to be a major bottleneck in the process (*289*). In many cases large numbers of constructs are screened before a protein sufficiently fulfils these criteria. Constructs can be designed to reduce the number of domains present and decrease flexible linkers or N/C terminal regions. Many constructs are designed around the products of limited proteolysis experiments.

Protein solubility can be improved in a number of ways; attachment of solubilising fusion tags, mutations of surface hydrophobic residues or oligomerisation interfaces and use of orthologous proteins from alternative organisms (*289*).

Protein stability can be improved through use of thermostable homologous proteins from bacterial species, co-expression of chaperones or binding partners, and expression in mammal cell lines to increase post-translational modifications.

The ability to achieve high levels of protein concentration can be improved through introduction of ligands, binding partners, mutation of oligomerisation interfaces and optimisation of salt concentrations and pH.

Crystallisation

The second bottleneck in the process is the production of protein crystals. Crystallisation has a reputation for being a 'black art' because of the difficulty in predicting the conditions which will lead to crystal formation.

Crystallisation occurs when the concentration of the protein in solution is greater than its limit of solubility. In many cases the sample will precipitate, however, through screening of many buffer conditions (varying pH, salts, additives, organic solvents, polymers etc.) it is possible to produce protein crystals. The process of crystallisation proceeds through a number of stages, first the protein becomes supersaturated, next an energy barrier must be overcome in order for nuclei to form from which the crystal lattice grows. If the sample is impure contaminants are incorporated into the lattice blocking further growth. Ideally the buffer conditions result in a small number of nucleations that grow into crystals greater than 100μm in size. This process depends on both the starting precipitants concentrations and how they vary over time.

Using vapour diffusion experiments the precipitant concentration can be altered over the early course of the crystallisation. Precipitant and protein are mixed in a small drop either suspended over a larger volume of precipitant (hanging drop) or sitting in a well surrounded by a precipitant reservoir (sitting drop), these sealed wells are generally incubated at a constant temperature (often 18^{o}C). Through evaporation of water molecules and other volatile species the two liquids equilibrate over time.

The introduction of crystallisation robots has significantly increased the number of precipitant conditions which can be screened, and decreased the amount of protein required per condition as they can accurately pipette nanolitre sample volumes. Additionally the availability of commercial screening kits makes large numbers of buffers readily accessible.

The resolution to which a crystal diffracts is a function of both its size and the order of the lattice:

- Size is important because the number of unit cells in the crystal is proportional to its volume, and the strength of the X-ray scattering is proportional to the number of unit cells. Therefore a larger crystal, provided it is well ordered, will usually produce diffraction data with a better signal:noise ratio.
- The crystalline order also affects the strength of the scattering; it is usually inversely correlated to solvent content (high solvent content correlating with looser packing – most crystals are 50-60% solvent).
- Conformational heterogeneity of the sample can also contributes to disorder within the crystal lattice.
- Crystal mosaicity is a function of the order of the microdomains within the crystals. The mosaicity associated with a given reflection relates to the 'sharpness' of the reflection with respect to the angular rotation range. Highly mosaic crystals (>0.75^{o}) have a lower signal:noise than low mosaicity crystals (<0.5^{o}) and thus diffract to lower resolution.

Crystal handling

During exposure to X-rays crystals suffer from radiation damage, resulting in a breakdown of crystalline order. In order to minimise this radiation damage diffraction data is collected at liquid N_2 (temperature; ~100K). For the solvent within the crystal to produce amorphous,

rather than crystalline, ice most crystals require a cryo-protectent to be added to the mother liquid. Many crystallisation conditions require the addition of cryo-protectant, this subjects the crystal to changes in osmotic pressure which can result in cracking or loss of order. If the solvent is not sufficiently cryo-protected ice crystals will form damaging the lattice and producing a strong diffraction pattern which interferes with the diffraction of the protein. Glycerol, 2-methyl-2,4-pentanediol (MPD) and low molecular weight polyethylene glycol (PEG) are often used as cryo-protectants.

The process of 'fishing' for crystals, mounting them in a loop and flash freezing them can put a lot of physical stress on the crystal which may also result in cracking or a loss of order.

Data collection

There are two major X-ray sources commonly available to structural biologists; home sources which are typically Cu/W rotating anode generators and synchrotron sources. The latter offers high brightness, high intensity, higher energy, tuneable, monochromatic X-rays which often greatly improve the quality of the data and rate of data collection.

Typically crystals mounted in cryo-loops are placed on a goniometer and maintained within a nitrogen cryo stream. The crystal is rotated around a fixed axis perpendicular to the beam path. Diffraction patterns are collected at regular oscillations (0.1-2^{o}) such that a complete data set is acquired (i.e. have sampled the whole of reciprocal space). The unit cell and space group of the crystal are often determined prior to data collection so that an optimal collection strategy can be produced. For example, an orthorhombic space group requires only 90^{o} of data to be collected for all the unique reflections to be measured.

The diffracted X-ray's are detected on a charge-coupled device (CCD), the distance of the detector from the crystal determines the maximum resolution of the data-set.

Auto-indexing, Integration and Scaling

The basic problem encountered with the interpretation of diffraction patterns is the fact that they are a series of 2D planes sampling the 3D reciprocal lattice.

The first step of data processing (autoindexing) determines the unit cell, lattice type, mosaicity and orientation of the unit cell with respect to the instrument.

The data from each diffraction pattern is integrated and scaled into a single dataset, characterised by Miller indexes, intensities and associated errors for each reflection. The scaling together of diffraction images must be refined to account for fluctuations in the beam strength, radiation damage, the crystal volume in the beam path, and differences in the background signal across the detector. Ideally the dataset has high signal-noise, high redundancy and high completeness.

Molecular replacement, Model Building, Refinement and Structure Validation

The starting point is a set of coordinates for a model structure. Once this model can be positioned appropriately, model phases can be calculated for the new (experimental) structure. The process of improving an electron density maps through refinement of the atomic positions and temperature factors, and the process of building a model into the density, are increasingly combined into single automated programmes (as described in Section 5.2.2).

Before a structure can be deposited in the PDB it must be validated in a number of ways. This is to ensure that at an atomic and secondary structure level it conforms to stereochemical and geometrical parameters, e.g. planarity, bond angles/lengths, hydrogen bonding distances, torsion angles etc. Robust validation helps to eliminate incorrect structures.

5.3 Methods

5.3.1 Crystallisation of AMPK with C-ADP

Crystals of AMPK, rat $\alpha1_{396-548}$ human $\beta2_{187-272}$rat $\gamma1_{1-330}$, were grown by vapour diffusion at 18^{o}C in sitting drop trays of 24 wells. The reservoir volume was 500µl. AMP was present at two times the protein concentration (9mg/ml). Drops were prepared by mixing equal volumes of AMPK-AMP with well solution (7% PEG-3350, 0.1mM 2-(*N*-morpholino)ethanesulfonic acid (MES) pH 5.5) in a 2µl drop. Crystals appeared in two days and grew to a maximal size over 7 days. Crystals that reached at least 50µM in width were deemed suitable for soaking with C-ADP solution (starting concentration 2mM). Crystals were harvested with a loop and transferred into a drop of reservoir solution containing 10% ethylene glycol, and subsequently into a second drop containing 25% ethylene glycol before being plunged into liquid nitrogen (100K). Frozen crystals were stored in liquid nitrogen until data collection.

Crystals were screened for diffraction in-house on a MicroMax 007HF rotating anode coupled to a RaxisIV^{++} detector. Crystals were maintained at 100K and were exposed for 2 minutes at 0.5^{o} oscillation at 1.54λ in two orientations 90^{o}C apart. For those crystals which diffracted during screening a full data set was collected by the oscillation method (0.5^{o}/frame, 2 seconds/frame, 0.97λ) at the Diamond Synchrotron Light Source (UK). A single crystal was used to collect the data set, which was processed as described in Section 5.4.

5.3.2 Materials

24-well plates from Hampton Research. MES, ethylene glycol and PEG 3350 from Sigma.

5.4 Results and Discussion

The truncated AMPK complex crystallised here (rat $\alpha1_{396-548}$human $\beta2_{187-272}$rat $\gamma1_{1-330}$ - Figure 46) was designed from the results of limited proteolysis and sequence analysis. Recombinant protein was overexpressed in a BL21 *E.coli* cell line, following lysis protein was purified through Ni^{2+}-affinity and gel filtration steps (described in Chapter 2). Purity was assessed by SDS-PAGE (Figure 47) and DLS.

The AMPK truncate has previously been crystallised by members of the Gamblin laboratory in complex with AMP/ADP/ATP/mant-AXP/ZMP, some structures of which are described in Xiao at el (2007) (*87*). Use of similar crystallisation conditions (7% PEG-3350, 0.1mM MES pH 5.5) yielded a number of crystals which stained yellow (the colour of the coumarin chromophores) upon soaking with 0.5mM C-ADP. Crystals typically belong to the orthorhombic space group $P2_12_12_1$.

Diffraction data extending to 2.5Å Bragg spacing were measured and processed using Denzo and Scalepack (*290*). The structure was solved by molecular replacement with 2V8Q as a model using Phaser (*291*). All three nucleotides, as well as water molecules were omitted from the molecular replacement and initial phase calculations. Crystallographic refinement was carried out using the rigid body, simulated annealing and TLS protocol program package Phenix (*292*) and additionally Refmac5 (*293*). Models were manually adjusted and water molecules added using Coot (*294*). Figures were created with pymol (http://pymol.sourceforge.net/). Crystallographic statistics are shown in Table 15.

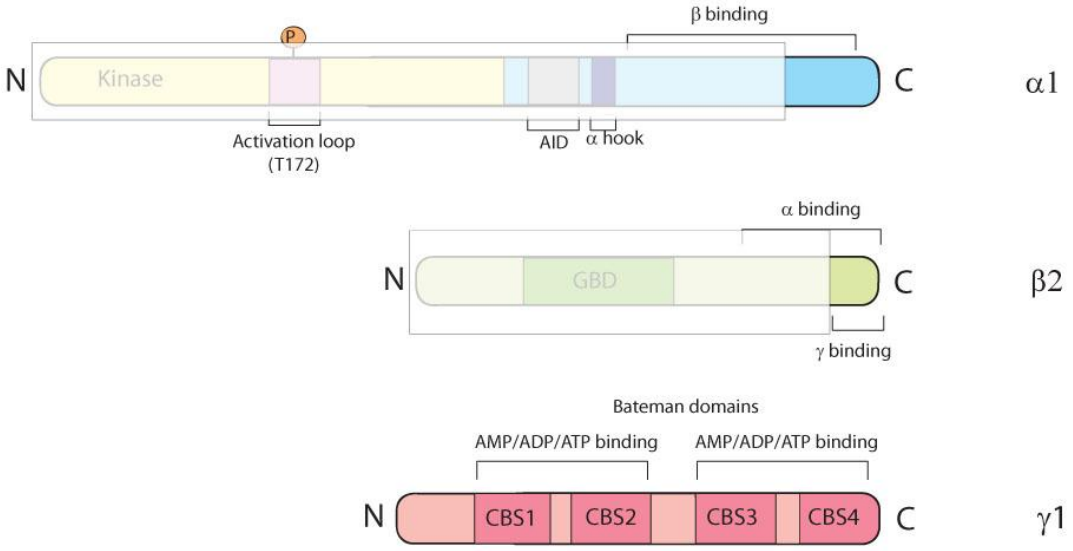

Figure 46: Domain schematic of AMPK crystallisation construct.

The shaded areas are not present in the truncated crystal structure. Abbreviations: AID: autoinhibitory domain, GBD: glycogen binding domain (also referred to as the carbohydrate binding module), CBS: cystathionine β-synthase.

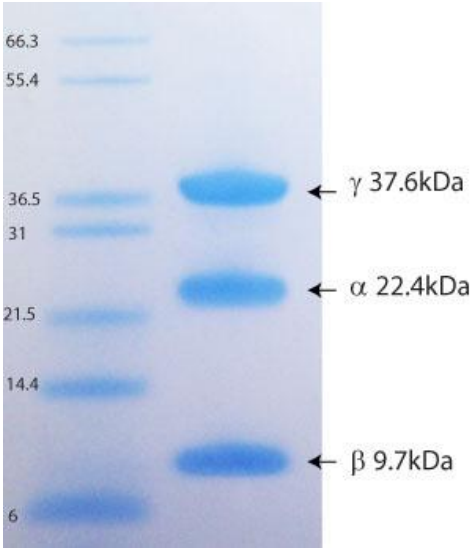

Figure 47: Purified recombinant rat $\alpha1_{396-548}$human $\beta2_{187-272}$rat $\gamma1_{1-330}$.

The purified protein was resolved on a 12-14% SDS-PAGE Novex gel and stained with InstantBlue. The molecular weight markers are indicated on the left (kDa) and the identity of the bands and their molecular weights on the right.

	C-ADP/AMPK complex
Data Collection	
Space group	$p2_12_12_1$
Unit cell (Å)	c=125.3 a=48.9, b=124.0,
Resolution (Å) (high res)	30-2.5 Å (2.6-2.5Å)
Rsym %	6.3 (25.6)
Completeness	99.2 (99.9)
Redundancy	3.6 (3.7)
Refinement	
Numer of reflections (work/free)	25630/1386
R_{fac} % (work/free)	23.3/27.7
Rms bonds (Å)/angles(^{o})	0.008/1.30

Table 15: Crystallographic statistics.

The overall structure of the crystallised construct has been discussed by Xiao *et al* (*87*) and is shown in Figure 48 and Figure 49. Each of the three nucleotides sit in a partially basic pocket formed at the interface between a pair of CBS motifs. In my maps electron density corresponding to the non-exchangeable AMP (Site-4) and two C-ADP molecules bound in the exchangeable γ-domain Sites 1 and 3 was observed (Figure 49, Figure 50 and Figure 51).

Coumarin

In Site-1 residues 119-126 adopt altered conformations in order to accommodate the coumarin adduct. Most significant is that of Tyr-120 which forms a hydrophobic interaction with the coumarin ring (Figure 52a). The terminal NH_2 atoms of Lys-126 shift 8Å compared to their position in the ADP-bound structure and form a hydrogen bond with the coumarin group. Additionally the side chain of Asn-92 interacts with the coumarin moiety.

In Site-3 the loop formed by residues 265-271 moves in order to accommodate the coumarin-adduct (Figure 52b). The non-fluorescent moiety of the nucleotide occupies the same volume of space as in the ADP-bound structure. The only interaction between the coumarin and the protein is a hydrophobic stacking of the coumarin ring with Phe-243, this residue moves 3.6Å from its position in the ADP-bound structure (Figure 52b).

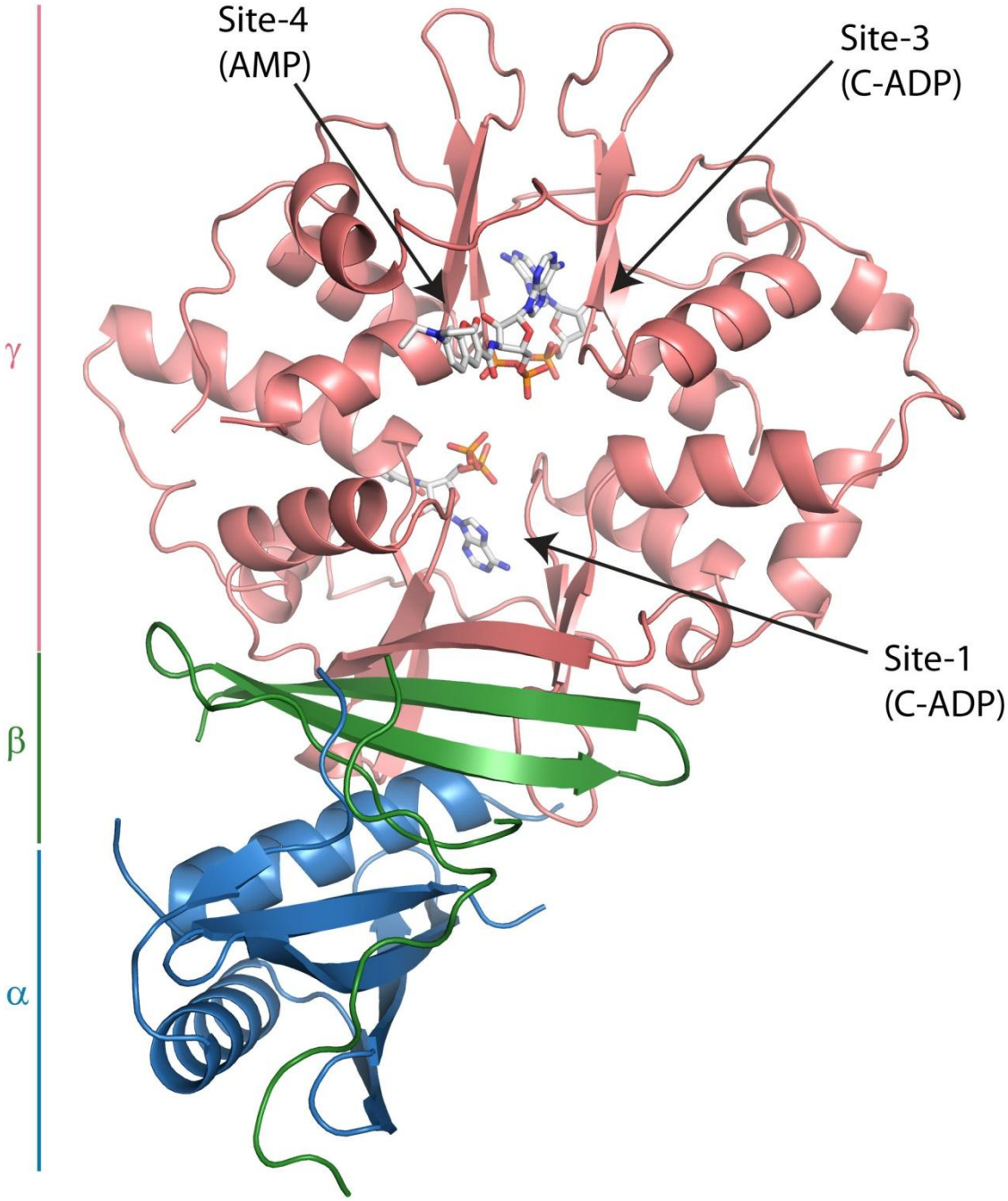

Figure 48: The C-ADP/AMPK complex.

Ribbons representation of the structure of the regulatory fragment of AMPK complexed with one AMP and two C-ADP molecules (AXP shown as white sticks and labelled). The subunits are indicated and coloured as follows γ; pink, β; green, α; blue. PDB ID: 2YA3.

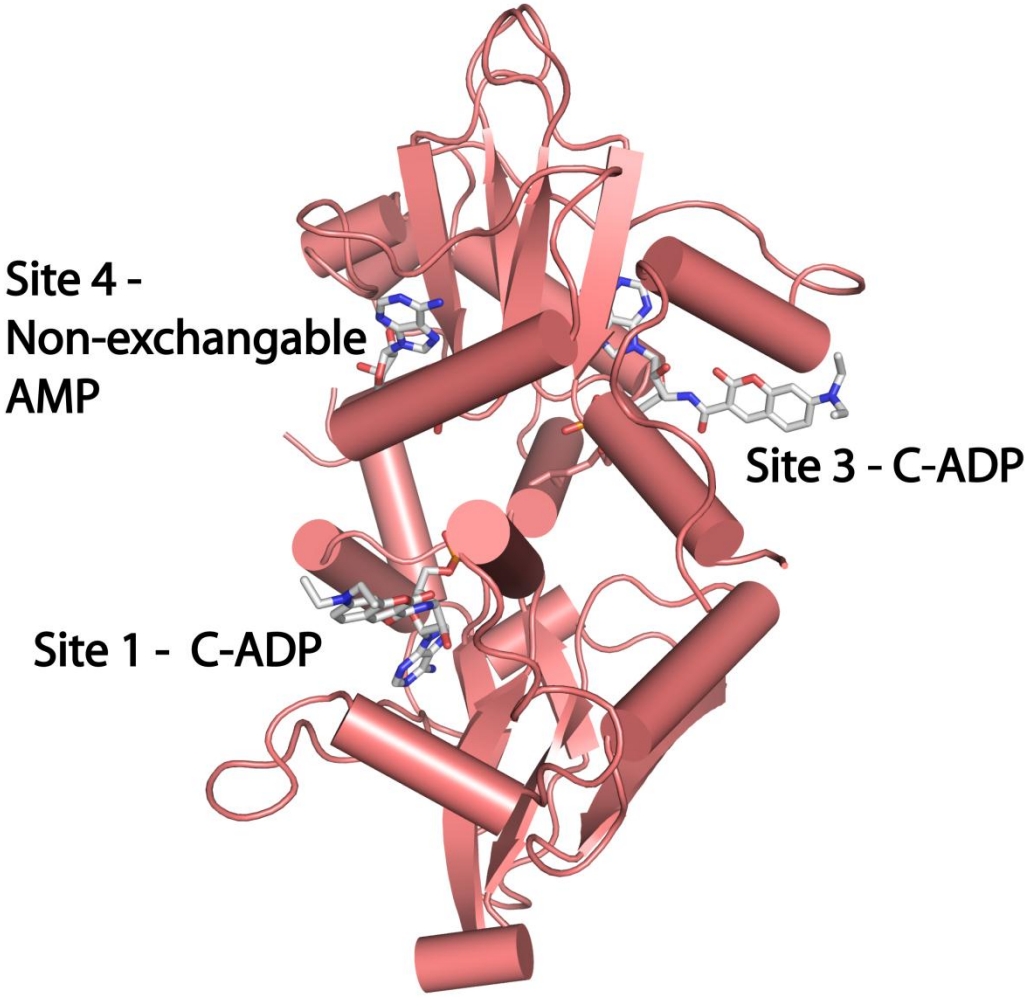

Figure 49: The γ-subunit from an orthogonal view to Figure 48.

Cartoon representation of the γ-subunit in pink; the positions of the bound AMP/C-ADP are shown in stick representation and labelled. PDB ID: 2YA3.

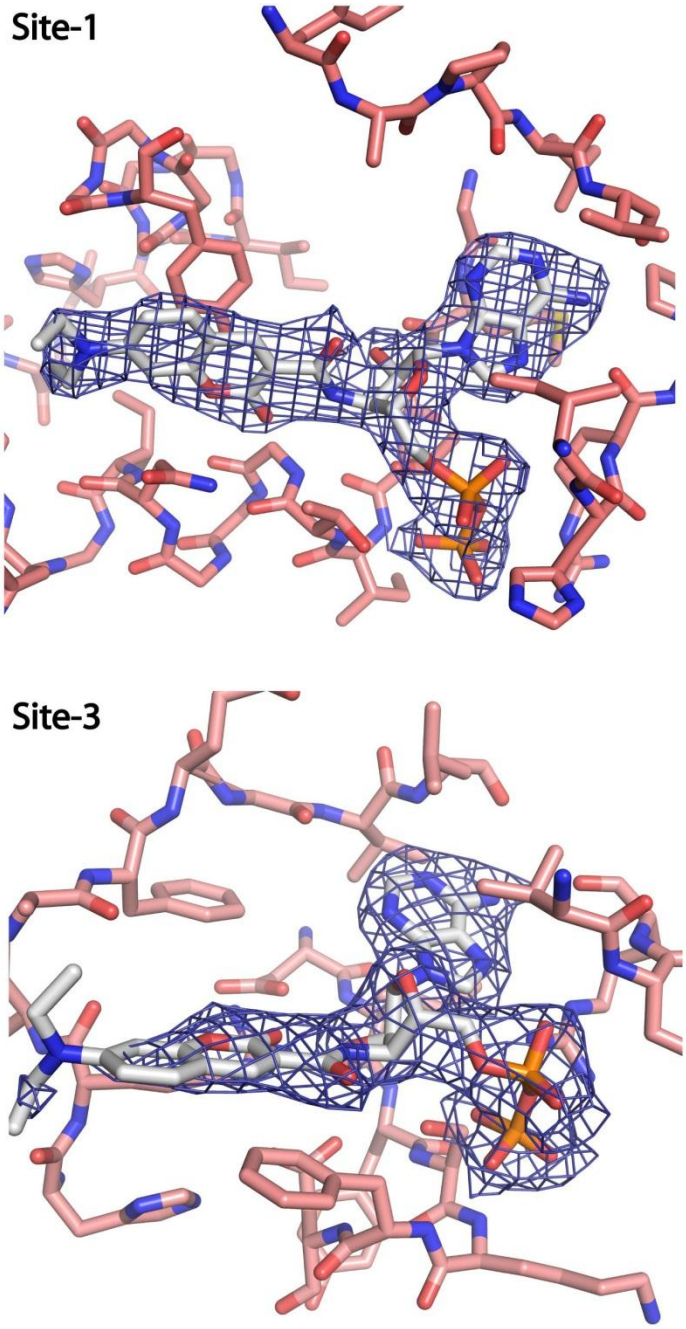

Figure 50: Expanded views of the C-ADP binding sites.

Electron density is from an F_o-F_c omit map where the nucleotide have been removed from the coordinate model, contoured at 1.0σ. PDB ID: 2YA3.

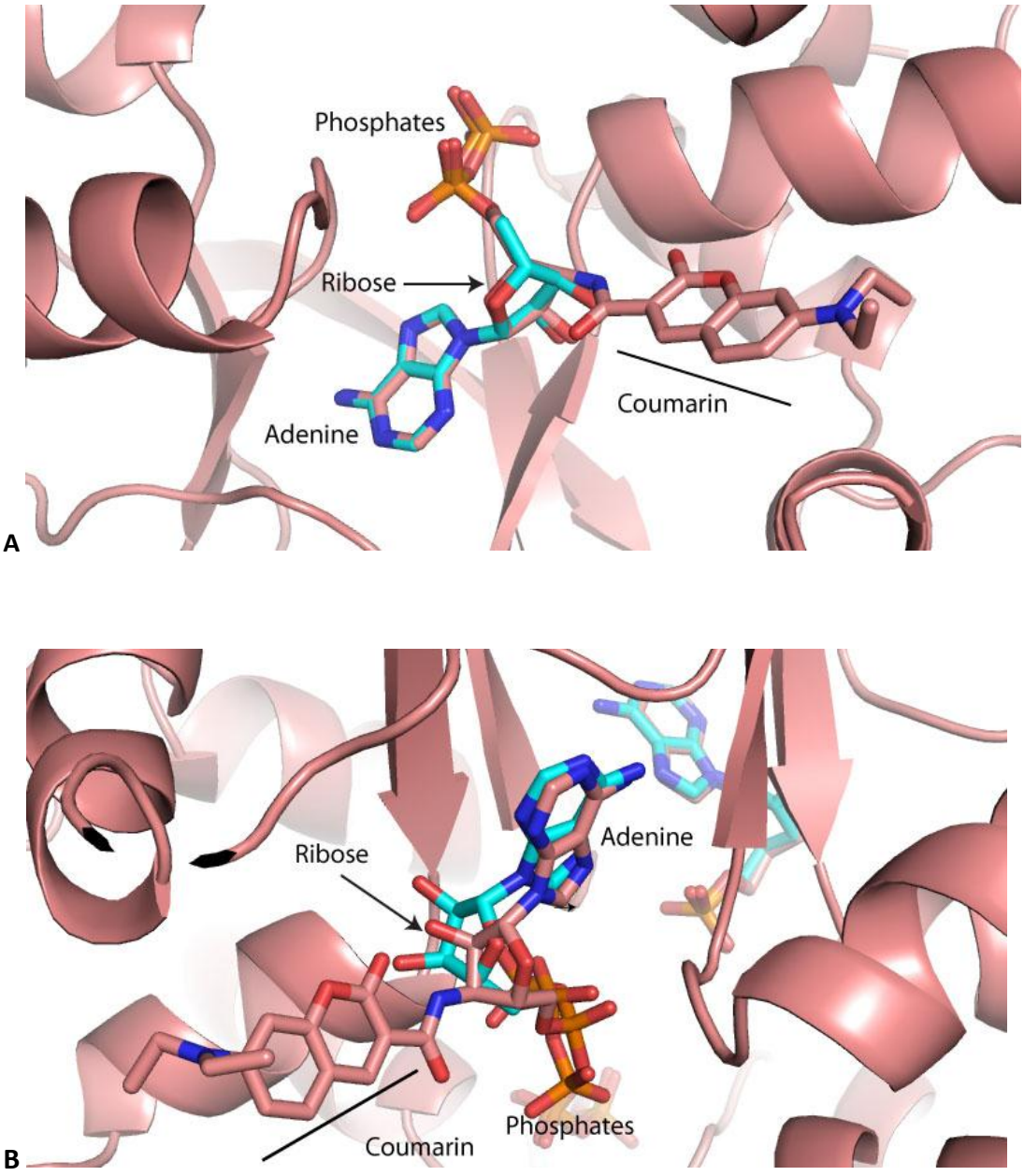

Figure 51: C-ADP and ADP bound to the γ-subunit.

Overlay of ADP (blue) and C-ADP (pink) bound structures at (A) Site-1, and (B) Site-3. The coumarin (labelled) fluorophore is conjugated to ribose and protrudes from the AXP binding site. PDB ID: 2YA3.

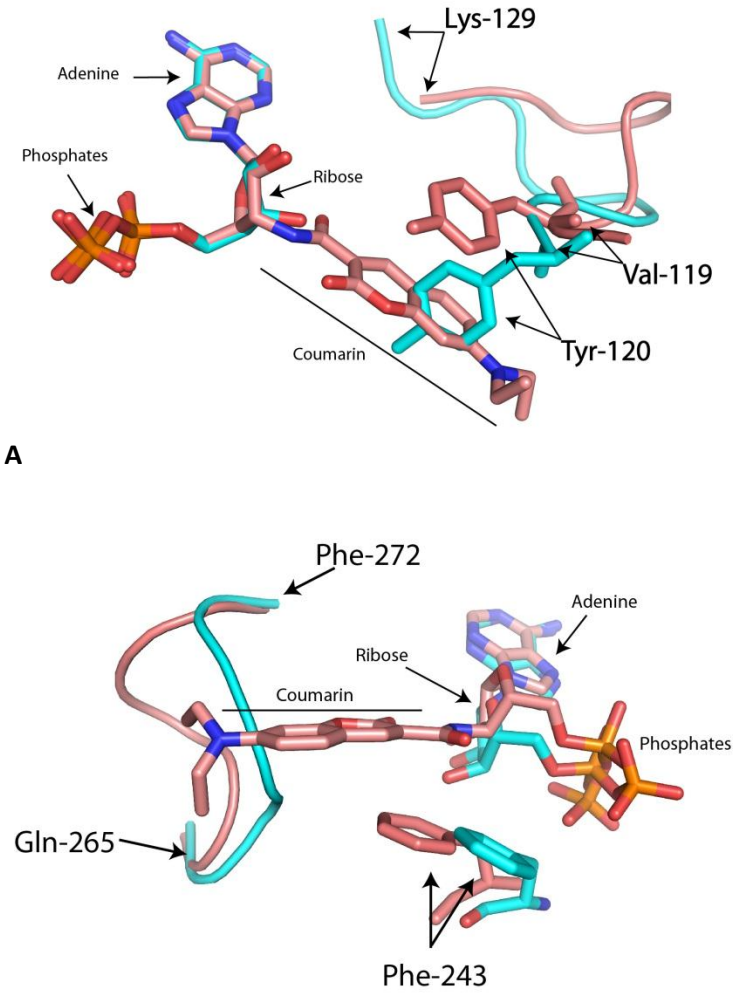

Figure 52: (A) Interactions of coumarin with Site-1.

Overlay of ADP-bound (blue) and C-ADP bound (pink) structures. Nucleotides are shown in stick representation. Tyr-120 is shifted to accommodate the coumarin fluorophore and forms a hydrophobic interaction with it. The loop extending from residue 119-126 adopts an altered conformation in the C-ADP bound structure.

(B) Interactions of coumarin with Site-3.

Overlay of ADP-bound (blue) and C-ADP bound (pink) structures. Phe-243 is shifted to form a hydrophobic interaction with the coumarin moiety. The loop extending from residue 265-272 is also labelled, and adopts an altered conformation in the C-ADP bound AMPK structure.

Adenine

In both sites the amino group at the N6 position of the adenine moiety forms two hydrogen bonds with the carbonyl groups of main chain residues (Val-129 and Arg-151 in Site-1; and Ala-204 and Ala-226 in Site-3). The N1 group is involved in a single hydrogen bond with a main chain amino group (Figure 53a) (Val-129 and Leu-276 in Site-1 and Site-3 respectively). In Site-3 the N7 amino group of adenosine interacts with the side chain of Arg-298. Additional hydrophobic interactions, such as those of Met-83 and Leu-128 with the adenosine ring in Site-1 also contribute to binding.

Ribose

One of the key features of the nucleotide binding site is the hydrogen bonding between the two ribose hydroxyl groups with the side chain of an aspartate residue (Asp-89 in Site 1, Asp-244 in Site 3 and Asp-316 in Site-4). Since the coumarin adduct is linked to the ribose group a number of these interactions are lost, although the C-AXP still bind tighter than their unlabelled equivalents (Section 3.4.3.1). The C-ADP in Site-3 is bound in a somewhat different conformation to ADP. The 2'-hydroxyl group of the ribose ring is shifted 1.8Å compared with the ADP structure. This is a result of small shifts in the orientation of D244 and its neighbours in order to accommodate changes in the main chain conformation following the movement of a nearby loop described earlier. In place of the hydrogen bonding between the 2' OH and Asp-244 there is an interaction with a water molecule not normally present in the site. Normal interactions with Arg-268 are also lost in the C-ADP structure (Figure 53b).

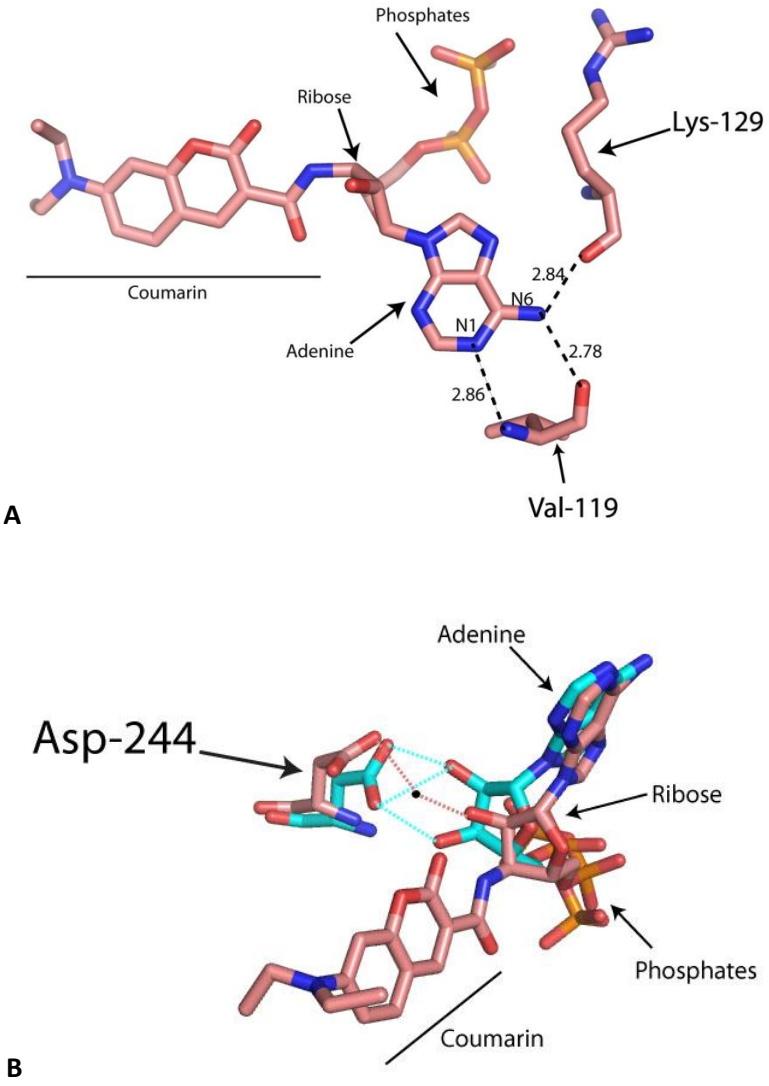

Figure 53: (A) Interactions of C-ADP adenosine ring with Site-1 residues.

A number of hydrogen bonds between the adenine ring and main chain carbonyl and amino groups are formed. Similar interactions are seen in all AXP:AMPK structures.

(B) Interactions of C-ADP ribose with Site-3 residues.

Asp-244 forms hydrogen bonds with the ADP (blue) ribose. In the C-ADP bound structure (pink), the nucleotide is shifted such that the 2' OH group interacts with a water molecule (shown as a blue sphere) rather than Asp-244.

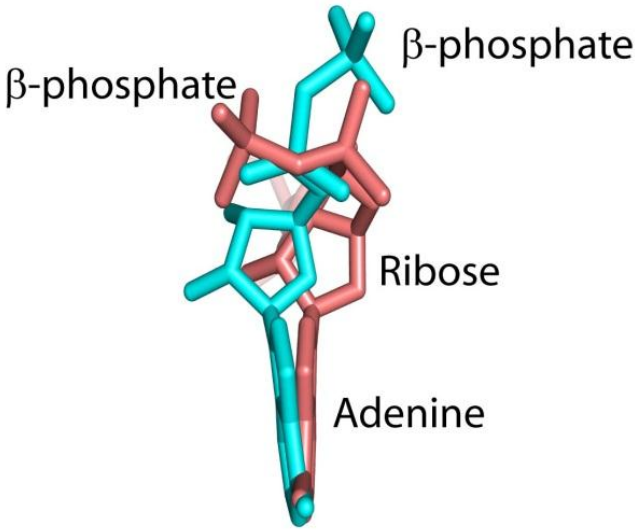

Figure 54: Interactions of C-ADP with Site-3.

Although the ADP (blue) and C-ADP (pink) nucleotides occupy the same volume of space, the α and β phosphates adopt different conformations.

Phosphates

The phosphate groups form a network of hydrogen bonds with the hydroxyl groups of a number of serine and threonine residues; Thr-86, Thr-88 with Site-1, and with the positively charged side-chains of a number of residues within the pocket; Arg-151, His-150 and Lys-242 with Site-1. In Site-3 the phosphates are present in a somewhat different conformation than observed in other structures, the α-phosphate forms hydrogen bonds with His-297, Ser-241 and Arg-298, whilst the β-phosphate interacts with Arg-69, Phe-243 and Arg-298 (Figure 54). However, despite this altered conformation the phosphates occupy the same volume of space within the binding pocket.

Discussion

The use of fluorescently-labelled nucleotides is undoubtedly a useful way to measure the binding of unlabelled AXP to proteins. However the presence of relatively large and hydrophobic fluorescent groups conjugated to the AXP may introduce additional, non-specific or non-competitive interactions between the ligand and the protein. This is not unprecedented particularly with large adducts such as julolidine derivatives of AXP (*247*). This can be controlled for in two ways; firstly by performing titrations in the presence of large concentrations of the native ligand and ensuring no signal change is observed, and secondly through crystallisation of the ligand:protein complex.

I verified that the coumarin nucleotide derivatives bound to the same sites as the unlabelled species by determining the crystal structure of the regulatory fragment in complex with C-ADP for comparison with an ADP bound structure. The 2:1 stoichiometry conforms with the conclusions drawn from the C-AXP fluorescence titrations (Section 3.4.3.1). No density corresponding to non–specific binding was observed, although this doesn't preclude weaker binding at sites blocked by crystal packing.

The structure presented here shows that the labelled ADP in Site-1 makes similar interactions as the unlabelled ADP. The C-ADP bound at Site-3 adopts a slightly different conformation to that in the ADP-bound structure; however the same volume of space is occupied and the stability of the protein is unaffected. In both sites additional contacts between the protein and the coumarin moiety were present: this is important because the coumarin group is attached to the ADP through the ribose group. Such contacts are necessary since they form the basis of the signal change upon C-AXP binding to the protein. It was long suspected that the fluorescence contribution of C-AXP's bound at the two sites was not equal. The coumarin moiety of the C-ADP bound at Site-3 is non-planar likely resulting in decreased fluorescence emission from this site (*295*).

Only two tryptophan residues are present in the γ-subunit. W116 is positioned close to the coumarin group of the ADP bound to Site-1 (the tighter site), it is likely FRET from this site is responsible for much of the signal observed in Section 3.4.3.4.

5.5 Conclusion

X-ray crystallography is a powerful technique for structure determination and as a tool to validate protein:ligand interactions and stoichiometries. The availability of a readily purifiable and crystallisable protein within the Gamblin laboratory allowed me to validate a number of conclusions drawn from the fluorimetry work presented in Chapter 3. Here I showed that an AMPK truncate bound to C-ADP with a stoichiometry of 2:1 and at the same sites as unlabelled ADP. No non-specific binding was observed nor any significant changes to the proteins structure or stability.

Chapter 6: SNF1 Summary

SNF1 is the *S.cerevisiae* AMPK ortholog, similar to AMPK it plays a role in managing cellular energy homeostasis (Appendix 1.1.2). SNF1 is a heterotrimer comprising α-like (Snf1), β-like (Gal 83, Sip1, and Sip2) and γ-like (Snf4) subunits (Appendix 1.1.3 and Figure 59). Unlike AMPK, SNF1 is not regulated by AMP but recently the Carling laboratory demonstrated ADP protection of T210 (equivalent to αT172 in AMPK) from dephosphorylation by phosphatases (Appendix 1.1.4) (*2*).

In parallel to the work studying AMPK, I characterised the binding of nucleotides to SNF1 and the enzymes regulation by ADP using the techniques described in Chapters 3 and 4. Due to space constraints the major conclusions of this work are described here and summarised in Figure 55, while the methods and results are given in Appendix 1.2.

Similar to AMPK, SNF1 binds two exchangeable nucleotides, however the yeast enzyme binds AXP much more weakly than AMPK (Appendix 1.2.2). K_d values of around 80μM and 1150μM (dependent on phosphorylation state of the sample) were determined for the tighter and weaker sites respectively (Table 17 and Table 18). The tighter site also binds NADH with an affinity of ~7μM, a crystal structure of SNF1 confirms that this is Site-4 of the Snf4-subunit (Figure 65)(*2*).

Unfortunately, the identity of the weaker site could not be determined via crystallography, likely due to the weak nature of the AXP:SNF1 interaction (2). Attempts to mutate AXP binding sites, with the aim of specifically ablating AXP binding at a single site and thus determining which is the second exchangeable site, were not successful (Appendix 1.2.2.1).

CD of wild-type and mutant proteins confirmed that the samples had similar secondary structure content (Appendix 1.2.3). It is thought that the inability to knock-out binding at each site is a homologous phenomenon to that described in relation to the AMPK mutants (see Section 1.2.2.1).

In Chapter 3 weaker binding of Mg.ATP relative to Mg^{2+}-free AXPs to AMPK was described. SNF1 was also found to bind Mg.ATP more weakly than AXPs (Appendix 1.2.2). In fact Mg.ATP probably binds SNF1 too weakly, particularly at the second site, for this to be physiologically relevant. This raises the interesting possibility that SNF1 acts directly as an ADP sensor.

Protection against T210 dephosphorylation by ADP was demonstrated using the NADH coupled spectrophotometric assay described in Section 4.2.4 (shown in Appendix 1.2.4). As NADH binds at the tighter site (Site-4) and does not compete with this regulatory effect, it seems that the weaker, but as yet unidentified, binding site mediates regulation of kinase activity (*2*).

ADP occupancy of the regulatory site over the concentration range used in the *in vitro* coupled assay was modelled. Occupancy of the weaker second site correlated with the dose-dependence of ADP protection against dephosphorylation, supporting the assignment of regulatory function to ADP binding at the weaker AXP site (Appendix 1.2.5).

No extensive attempts to model regulatory site occupancy given *S.cerevisiae* intracellular nucleotide (mM) and Mg^{2+} concentrations were undertaken, some simulations were performed to demonstrate that SNF1, most probably, acts directly as an ADP sensor as the weaker site is never completely saturated by nucleotide (Appendix 1.2.5).

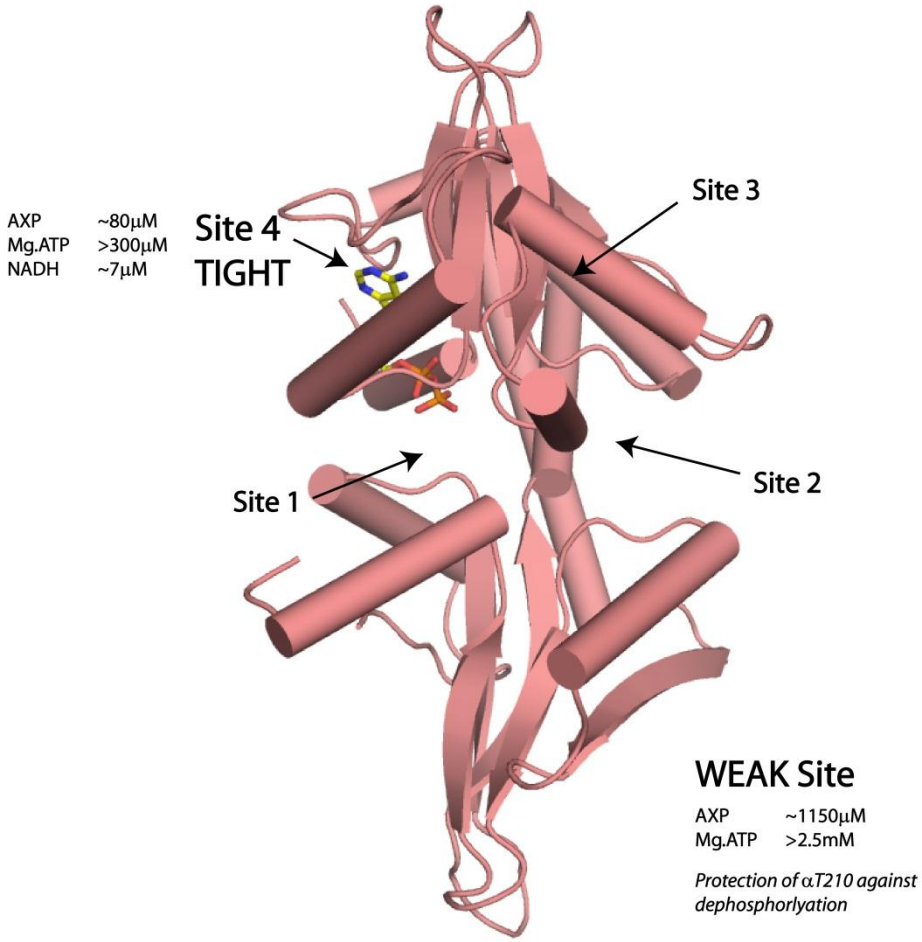

Figure 55: Summary of the AXP binding affinities and their regulatory roles in SNF1.

Ribbons representation of the SNF1 Snf4 subunit with one bound ADP molecule (PDB ID: 3T4N). The four potential AXP binding sites are labelled. The average K_d values for AXP and Mg.ATP interaction at the tighter exchangeable Site-4 and the weaker second site (as determined by C-ADP displacement – Table 17), are indicated. The location of the weaker AXP binding site is unknown, but binding of ADP at this second site is thought to mediate protection against T210 dephosphorylation.

Chapter 7: Discussion

AMPK has emerged as an integral regulator of cellular and whole body metabolism. By reacting to multiple stimuli AMPK is an important point of signal integration; sensing changes in cellular metabolism and coordinating a plethora of downstream responses. Upon activation, AMPK acts to minimise energy expenditure (by inhibiting processes such as protein synthesis, cell proliferation, fatty acid and glycogen synthesis) and maximise energy production (through increasing the supply of, and consumption of, lipids and carbohydrates). Thus, AMPK activates enzymes involved in the uptake and oxidation of fatty acids and glucose.

Regulation by ADP

AMPK was named on the basis that AMP regulates the activity of the kinase. Subsequently, ATP was shown to inhibit this activation and it was therefore proposed that AMPK responds to increases in the AMP:ATP ratio during periods of cellular energetic stress. In 1995 Davies *et al* showed that in addition to allosterically activating AMPK, AMP also protected αT172 (the residue critical in activation) against dephosphorylation by phosphatases (*164*).

For a number of years the role of ADP in the regulation of AMPK was largely ignored. Recently, the Carling laboratory re-examined the role of ADP and consistent with previous studies found that ADP did not allosterically activate the enzyme. However, ADP was shown to protect AMPK αT172 from dephosphorylation by phosphatases, in a manner similar to AMP. In parallel, they were also able to demonstrate that ADP protected the *S.cerevisiae* homologue of AMPK, SNF1, from dephosphorylation of T210 (equivalent to αT172 in AMPK).

ADP is present in the cell at a higher concentration (100-200μM) than AMP but lower than ATP (3-8mM) (*1, 275, 279-281*). It has always been difficult to understand how low (1-5μM) cellular concentrations of AMP could compete with ATP (3-8mM) for binding to the same sites on AMPK. Given that the cellular concentration ADP is around 10^2 greater than AMP, it is a more feasible candidate to compete with high concentrations of Mg.ATP. I argue that ADP is likely to be the key regulator of AMPK *in vivo* where modulation of the rate of dephosphorylation is critical in determining the fraction of AMPK which is activated (as the major upstream kinase, LKB1, is constitutively active).

In order to complement the observation that ADP regulates both AMPK and SNF1, and to address the issue of ADP competition with ATP, this project aimed to characterise the interactions of AXPs with both enzymes; determining the stoichiometry of those interactions and the associated equilibrium dissociation constants.

Through displacement of fluorescently labelled nucleotides, affinities for AXP (± Mg^{2+}) were determined. Binding of C-ADP to Site-1 and Site-3 of a truncated AMPK complex was confirmed through crystallography (Chapter 5). For both AMPK and SNF1 it was found that C-AXPs and AXPs bind exchangeably at two sites but each with significantly different affinities. Mg.ATP binds more weakly than free ATP to both enzymes (as summarised in Figure 56 and Figure 55). This relatively low affinity for Mg.ATP is important in explaining the competitive binding of regulatory nucleotides *in vivo* where Mg.ATP concentrations are very much greater than those of AMP/ADP (Chapter 3).

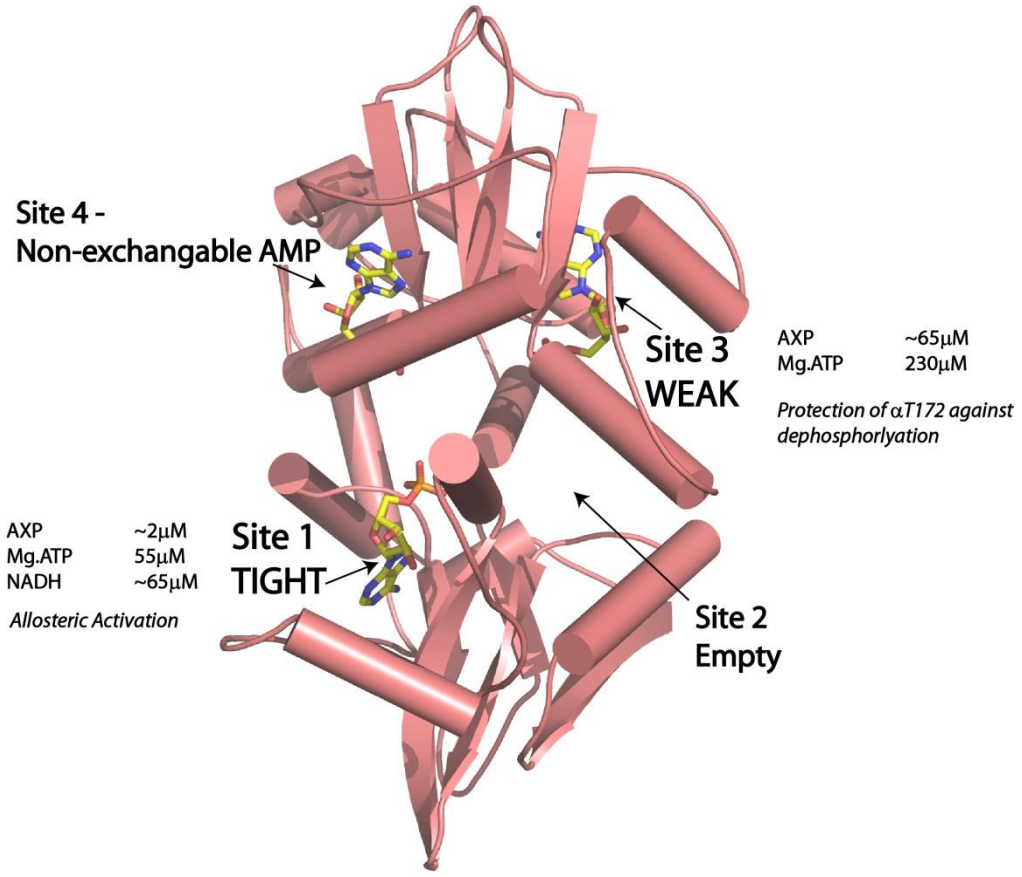

Figure 56: Summary of the AXP binding affinities and their regulatory roles in AMPK.

Ribbons representation of the mammalian γ-subunit with three bound AMP molecules (PDB ID: 2V8Q). The four potential AXP binding sites are labelled. The average K_d values for AXP and Mg.ATP interactions at the exchangeable sites (as determined by C-ATP displacement -Table 7) and the proposed regulatory roles, are indicated.

In addition to the use of fluorescently labelled nucleotides, displacement of NADH was used to study AXP interactions with AMPK. NADH binds at the tighter nucleotide binding site, Site-1. This is thought to be in the tighter site because 1:1 molar equivalent soaks of AMPK crystals consistently produce electron density maps with occupancy of Site-1 and not Site-3. Using a coupled spectrophotometric assay NADH was shown to compete with the allosteric activation of AMPK by AMP, but not with AMP/ADP protection against αT172 dephosphorylation. My conclusion, therefore, is that binding of AMP at Site-1 mediates allosteric activation, whilst binding of AMP/ADP at Site-3 mediates protection of αT172 against dephosphorylation (indicated in Figure 56) (Chapter 4).

Attempts were made to mutate Site-1 and Site-3 of AMPK (Chapter 3) in order to eliminate AXP binding at single sites and thus confirm assignment of distinct regulatory roles to the relevant sites. A number of point mutants were tested but in no case was specific AXP binding abolished. Significantly, mutants in which a conserved Asp residue, known to coordinate the ribose hydroxyls, was mutated to Ala, did not abolish AXP binding. The fact that these mutations do not eliminate binding in the expected manner, suggests that the aspartate:ribose interactions are not critical for AXP binding. In other studies these mutants have been assumed (without being tested) to specifically 'knock-out' binding at each site (*177*), an assumption which may not be valid.

It is clear that residues from more than one CBS provide contacts to a single AXP. I suggest that because the γ-subunit is a flat disc-shaped structure and that networks of residues within the 'core' interact with AXP bound at sites other than that to which they are nominally assigned, it is unsurprising that a particular mutant has effects beyond the site of mutation.

Recently, Chen *et al* described a number of γ-subunit point mutants which reduced allosteric activation of AMPK. Only mutants directed at Site-3 and Site-4 produced this phenotype, suggesting that it is not Site-1 which mediates allostery, as proposed in this thesis and elsewhere *(1, 144)*. However, Chen *et al* (2012) described no measurement of the binding affinity or stoichiometry of nucleotide interactions, nor was the effect of mutation on protection against dephosphorylation reported. It is more than possible that mutation of Site-3 and Site-4 resulted in reduced nucleotide binding at Site-1; as demonstrated in Section 3.4.3.5, and described in the previous paragraph. It is difficult to design 'AXP site-specific' mutants.

A program was designed to model occupancy at the two exchangeable nucleotide sites based upon the K_d values determined experimentally. Firstly, aiming to simulate the *in vitro* activity assays and regulation by nucleotide, and secondly to demonstrate whether likely physiological concentrations of AMP and ADP would be capable of competing with Mg.ATP.

First, the equilibrium dissociation constants determined in this study were used to calculate occupancy of AMPK binding sites under the conditions of the *in vitro* assays employed in studying allosteric activation and protection against dephosphorylation (where concentrations of the AXPs are, of course, known). Occupancy of AMPK Site-1 by AMP correlated with the concentration dependence of allosteric activation, whilst occupancy of Site-3 by AMP correlated with the dose dependence of protection of αT172 against dephosphorylation. Therefore, the modelling and experimentally determined K_d values support the assignment of the regulatory functions of the two AXP binding sites (Chapters 3 and 4).

Further modelling studies were performed in which site occupancy was determined from plausible estimates for intracellular nucleotide and magnesium concentrations (outlined in Chapter 4). Despite the relative increase in AMP concentration (1 to 5μM) being greater than that of ADP (50 to 200μM), it is the absolute concentrations that determines the occupancy of the binding sites. As such the potential occupancy of ADP is much greater than that of AMP.

The occupancy of both Site-1 and Site-3 by AMP was minimal (less than 0.4%). This suggests that perhaps AMP regulation, is not an important mechanism of AMPK activation in a cellular setting. However, as both AMP and A-769662 allosterically activate and glycogen allosterically inhibits AMPK, this phenomenon is hardly likely to be an artefact; but the mechanisms by which it works remain, for the moment, obscure.

Occupancy of Site-3 by ADP was found to be more significant (2.68%) despite competition for binding by Mg.ATP. Furthermore, ADP occupancy of this site was increased 4-fold when 'stressed' AXP concentrations were used in the modelling (to 10.14%). This modelling, based upon the K_d values measured in Chapter 3, clearly demonstrates that ADP has the potential to bind to, and regulate, a proportion of cellular AMPK in response to changes in cellular nucleotide ratios.

The mitochrondrial uncoupler, DNP in conjunction with sorbitol, rapidly alter the cellular ADP:ATP ratio and thus potently activate AMPK. Together these compounds activated AMPK 12-fold relative to untreated cultured muscle cells. This suggests that roughly 8% of AMPK might be active under normal conditions. This figure is in the same range (2.5-10%) estimated in my studies.

The modelling does, of course, have a number of limitations, not least the uncertainty surrounding the cellular AXP/Mg^{2+} concentrations which are cell-type dependent. It is also

unclear how to couple binding site occupancy to kinase activation, without first knowing the relative rates of phosphatase activity with respect to the ADP-bound and unbound AMPK(αT172). Furthermore, for modelling of the system, it will be necessary to know what the basal level of cellular AMPK activity is and what increase in active AMPK is required for downstream responses to occur. And, of course, these values may differ in a tissue, stimulus and isoform dependent manner.

In parallel to these studies, the Gamblin laboratory determined the structure of an active mammalian AMPK complex (α1β2(ΔGBD)γ1), which suggested a potential mechanism through which αT172 could be protected against dephosphorylation (summarised in Figure 57). The phosphorylated T-loop, ordered in this structure, interacts with the β-subunit and forms a number of contacts which stabilise the loop. In this conformation, access to the phosphorylated residue by phosphatases is blocked. The idea is that this protected state is promoted by AMP/ADP binding and results in protection against αT172 dephosphorylation. It is suggested that in the Mg.ATP bound form the T-loop is not stabilised through interaction with the β-subunit and is therefore more accessible to phosphatases/inactivation.

A second interesting feature of this crystal structure was the presence of a loop (known as the α-hook), situated in the linker joining the N-terminal kinase domain with the C-terminal scaffold domain. The α-hook interacts with the γ-subunit, forming a partial lid over the Site-3 AXP binding site. It is thought that the binding of regulatory AMP/ADP to Site-3 facilitates binding of the α-hook. Interaction of the α-hook with the γ-subunit is thought to restrict the flexibility of the preceding α-linker region and, in doing so, promote binding of the kinase domain to the regulatory subunit and therefore protect αT172 from

dephosphorylation. Upon occupancy of Site-3 by Mg.ATP, the α-hook is unable to bind to the γ-subunit owing to steric clashes between the γ-phosphate and the α-hook. It is proposed that dissociation of the hook, increases flexibility of the α-linker, destabilising the T-loop/β-subunit interface and ultimately resulting in the kinase domain becoming flexibly tethered to the rest of the heterotrimer (summarised in Figure 57). It will be interesting in the future to determine the on/off rates which describe the interchange between the bound/unbound (active/inactive) state of the α-kinase, and how they differ in the presence of regulatory nucleotides. It is probable that the variation in thermostability, tertiary structure and mobility observed via CD and MALLS were due to differences in the overall architecture of the bound/unbound kinase AMPK structures.

It is unclear how the AID, crystallised in an isolated kinase structure but not featuring clearly in the α1β2(ΔGBD)γ1 structure, fits into this model of AMPK regulation. Perhaps the autoinhibited kinase structure exists when the α-kinase is flexibly tethered to the rest of the heterotrimer offering an extra level of AMPK regulation.

An important question that remains from these studies is how AMPK is allosterically activated by AMP binding at Site-1 but not by ADP/ATP. From an energetic consideration only a small change in the structure might be required to mediate this activatory effect, perhaps as little as the introduction of an additional hydrogen bond.

SNF1

Displacement of fluorescently labelled nucleotides (C-ATP) and NADH was also used to determine equilibrium dissociation constants for the interaction between SNF1 and AXP. SNF1 was found to bind two AXP's exchangeably, with one site having significantly higher affinity than the other (Appendix 1).

NADH binds SNF1 at Site-4 (verified in a crystal structure (*2*)), the tighter of the two AXP binding sites. Similarly to AMPK, NADH does not compete with the protective effect of ADP against dephosphorylation, suggesting that it is the second, weaker, nucleotide binding site which mediates this effect in SNF1 (indicated in Figure 55) (Appendix 1). Probably owing to the very weak AXP binding at the second site (>1mM), crystallographic studies were unable to reveal its identity.

The interaction between Mg.ATP and SNF1 at the weaker site could not be determined in these studies (>1mM), and is perhaps too weak to be physiologically relevant, given intracellular Mg.ATP concentrations in the millimolar range. This suggests that SNF1 acts directly as an ADP sensor (Appendix 1).

AMPK Regulation

The present study was undertaken to determine the relationship between AMPK activity and regulation by nucleotides. However, in a cellular context the system is more complex. Glycogen, for example, is an allosteric inhibitor of AMPK activity perhaps acting by reducing access of substrates to the α-kinase. It would be interesting to determine what affect, if any, glycogen and the other ligands have on nucleotide binding and on the bound/unbound conformation of the α-kinase.

Changes in Ca^{2+} concentration also influence AMPK regulation, independent of AXP concentrations, through regulation of its upstream kinase, CaMKKβ. Whilst some stimuli may only influence Ca^{2+} or nucleotide levels, most stresses, e.g. exercise, are likely to cause simultaneous activation of AMPK through both pathways. In many instances there is a close relationship between changes in Ca^{2+} and nucleotide levels, providing complementary pathways to activate AMPK.

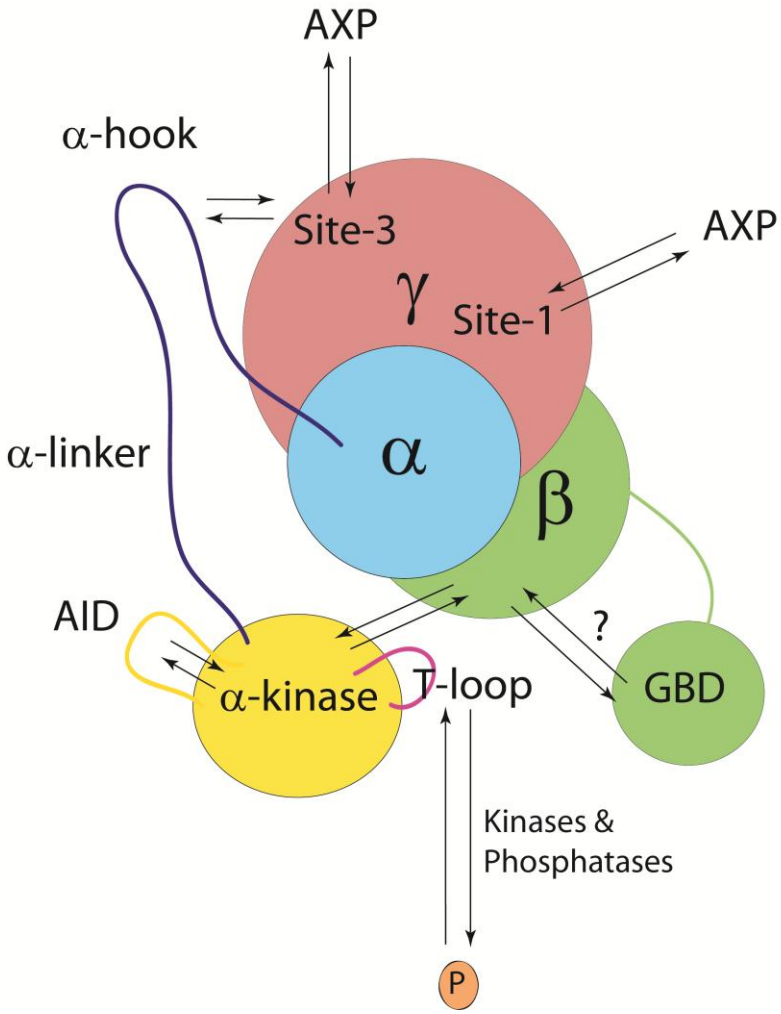

Figure 57: Model of AMPK regulation.

It is suggested that interactions of the α-hook (dark blue) with Site-3 restricts the flexibility of the α-linker (dark blue) promoting interaction of the α-kinase (yellow) with the β-subunit (green). In this bound conformation the T-loop (pink loop) is stabilised and αT172 protected from dephosphorylation. The T-loop is phosphorylated at αT172 by upstream kinases and dephosphorylated by phosphatases, the rates of these reactions is as yet undetermined and depends on the bound/unbound conformation of the α-kinase. Nucleotide binding to the γ-subunit affects the proportion of bound/unbound α-hook, and therefore bound/unbound α-kinase domain.

Additionally the GBD is flexibly tethered to the rest of the heterotrimer, and interacts with the rest of the heterotrimer, an interface overlapping the α-kinase:β-subunit binding surface. The AID (yellow loop) is also thought to interact with and inhibit the α-kinase domain.

In addition to the ligands which regulate AMPK there are several post translational modifications which may alter the enzyme's activity. The role of these modifications is still relatively poorly understood. For example, in the case of autophosphorylation βS108A mutants have altered AMP regulation and decreased basal activity. Although some differences between AXP affinities for phosphorylated versus unphosphorylated AMPK were observed in Chapter 3 (in general tighter binding to the unphosphorylated form), no binding studies were performed with specific autophosphorylation mutants. Myristoylation of the β-subunit has been reported to cause AMP/ADP to promote phosphorylation of AMPK. It would be interesting to determine whether these effects are the result of weaker nucleotide binding to AMPK, and if so which site mediates these effects. Or, alternatively, due to disruption of the mechanism through which AMP binding is transduced to the α-kinase via the α-hook.

It is probably the case that the complex interplay between acetylation, myristoylation, ubiquitination, and phosphorylation/dephosphorylation of AMPK modulates its activation state.

The different characteristics of subunit isoforms, splice variants etc. also affect AMPK regulation. γ-subunit isoforms and splice variants are most likely to affect the affinity of the heterotrimer for AXPs, potentially shifting the point at which AMPK becomes significantly ADP-bound and therefore activated. There are studies which show key differences in the AMP regulation of these isoforms, e.g. allosteric activation of γ2-containing complexes is around 3.7-fold compared to 1.7-fold in γ1-containing complexes (*138*). Due to the poor expression of the γ2 and γ3 isoforms, the binding of AXP to these isoforms has not been examined. It would be interesting to undertake biophysical and structural studies on these isoforms to see if they reveal anything about the differences in nucleotide binding and regulation.

β-subunit isoforms regulate the localisation of the heterotrimer be it to cellular membranes or to glycogen, and mediate regulation by sugars and myristoylation. The β-subunit also plays an important role in mediating the activatory effect of A-769662 and perhaps other pharmaceutical agents. Therefore, the different β-isoforms present an important opportunity for targeted drug design.

The α-subunit isoforms may perhaps have altered enzymatic properties and different preferences with regards to their upstream kinases and phosphatases; they also have varied substrate specificities and different regulatory mechanisms mediated through phosphorylation of their C-terminal tails. Interestingly, α2-containing complexes extracted from cells display higher fold allosteric activation compared to α1-containing heterotrimers, although they seem to have similar dose-response curves (*138*). In the future it would be interesting to examine α2-containing complexes to see if they display any differences in nucleotide binding affinities, and to determine if α1/α2 containing heterotrimers are protected against dephosphorylation by AMP/ADP with similar concentration dependence. As the model in Figure 57 demonstrates, there could be a complex interplay between binding of AXP, interactions of the α-hook/linker and the autoinhibited state, which determines the bound/unbound state of the α-kinase. Isoform specific differences in the on/off rates which describe the interchange between these conformations may have a significant impact on the proportion of active/inactive (bound/unbound) AMPK.

AMPK Activation and Effects

Owing to the complex nature of the regulation of AMPK heterotrimers the conditions under which the enzyme becomes activated are unlikely to be the same in different cell-types. Although zero-order ultrasensitivity models, discussed in Section 4.4.2.5, predict what is essentially step-like activation it seems probable that the AMPK response need not be 'all or nothing'. It is possible that regulation operates along a concentration gradient; at low levels of AMPK activation certain targets are phosphorylated, and as activated AMPK levels rise other substrates become important. Such a process may be based upon diffusion, localisation or substrate availability.

With so many downstream targets, affecting a wide range of fundamental cellular processes, it would seem important that small fluctuations in ATP concentrations are not 'overreacted to' by binary AMPK activation, and that those processes which can most quickly to restore ATP levels are prioritised over other options which may be used as a long-term effect.

It seems paradoxical that AMPK appears to either activate or inhibit a particular process dependent on the cell-type being studied. This is evident in the case of apoptosis, where activation of AMPK can either promote or inhibit cell death. One can only speculate as to what may underpin these observations; is it a property of the AMPK heterotrimers present in different tissues (i.e. differences between the subunit isoforms)? Or perhaps it is due to some fundamental property of the different cell-types, such as expression/localisation of substrates, concentrations of regulators or exposure to stresses?

Concluding Remarks

The two major conclusions drawn from this work, published in Xiao *et al* (2011)(*1*) and Mayer *et al* (2011)(*2*), and summarised in Figure 55 and Figure 56, are;

1) In the mammalian AMPK system, AMP binding at Site-1 mediates allosteric activation and AMP/ADP binding at the weaker Site-3 mediates protection against αT172 dephosphorylation. In the yeast SNF1 system ADP binding at the weaker of the two sites mediates protection of T210 against dephosphorylation.
2) The somewhat weaker binding of Mg.ATP compared to ADP in both AMPK and SNF1 systems, allows ADP to compete effectively with the high intracellular concentrations of Mg.ATP, thus allowing ADP to regulate both enzymes *in vivo*.

Despite being the subject of many years of intensive study there remains a great deal which is unknown about AMPK, its regulation, and its cellular role. ADP certainly appears to be an important regulator of AMPK, and is perhaps one of the few 'universal' signals which activate AMPK.

Understanding the complex interplay between the regulators of AMPK and the downstream effects of activation (or inhibition) on cellular activity will ultimately require a much more sophisticated modelling study than that possible in this Thesis (Chapter 4). However, it seems probable that integration of the wealth of information available about AMPK, particularly its regulation and activation, into a single model will be important in understanding the threshold at which AMPK is activated in a cellular environment. Coupling such a model of AMPK regulation to modelling of stimulation/inhibition of the multiple downstream effectors will potentially reveal how crosstalk between AMPK-regulated pathways controls so many central cellular processes.

Appendix 1: Nucleotide binding to SNF1

1.1 Introduction

1.1.1 Overview

In 1981, SNF1 serine/threonine protein kinase was genetically identified in a screen of *S.cerevisiae* strains unable to utilise sucrose as a carbon source (*snf, s*ucrose-*n*on*f*ermenting). Mutants had defects in the expression of the *SUC2* gene which encodes the sucrose degrading enzyme, invertase (*6*). Although AMPK was named in 1988, its orthology to SNF1 was not apparent until cDNA encoding an AMPK α domain was cloned in 1994. The convergence of the yeast and mammalian studies marked the creation of the AMPK family (*6*). SNF1 is activated by phosphorylation of T210 and inactivated by dephosphorylation of this residue (summarised in Figure 58).

1.1.2 SNF1 cellular targets/activity

SNF1 kinase activity focuses on adaption to glucose limitation and the response to cellular stresses. It also has roles in nutrient responsive developmental processes (e.g. meiosis and sporulation), ageing and haploid invasive growth (*296*). These actions are carried out through transcriptional regulation and direct activation of effector molecules.

Yeast cells principally metabolise glucose and other sugars as their energy source. However they are capable of adapting to changes in the available carbon-sources in the environment. Nutrient-induced signalling networks allow rapid adaption to changes in conditions and derepression of these processes is crucial for adaption and survival. Glucose is known to repress genes involved in the metabolism of non-preferred carbon sources and to induce those involved with its usage, for example glycolytic enzymes. The SNF1 pathway is one of three glucose sensing systems, the others operating through Snf3/Rgt2 and cyclic AMP.

The SNF1 heterotrimer is involved in the transcriptional activation of glucose-repressed and inhibition of glucose-induced gene sets, through the phosphorylation of transcriptional activators and repressors e.g. Sip4, Cat8 and Mig1, or by stimulating the transcriptional machinery directly. For example, in Snf1 mutants Mig1 remains in the nucleus rather than translocating to the cytoplasm upon glucose depletion, thereby the glucose-repressed state of numerous genes is maintained (*297*). Significant glucose repression is still observed in *snf1 mig1* double knockout cell lines, demonstrating the functional redundancy of multiple pathways in glucose inhibition (*298*).

Additionally, SNF1 kinase regulates a number of metabolic pathways during nutrient limitation. Nutrient limitation leads to an increase in glycogen synthesis brought about through dephosphorylation and thereby activation of glycogen synthase (GS) (the enzyme responsible for 1→ 4 glycogen chain extension) by the GAC1/Glc7 phosphatase complex. SNF-mediated phosphorylation of this phosphatase is key in its activation. SNF1 also phosphorylates and inhibits GS kinase Pho8, an enzyme which inactivates GS (*299*). Both SNF1 and its substrates are localised to glycogen during nutrient limitation.

SNF1 has also been shown to inhibit anabolic pathways such as lipid biosynthesis during periods of nutrient limitation, an activity which is homologous to the mammalian AMPK. SNF1 negatively regulates acetyl-coA carboxylase, the first enzyme of the fatty acid synthesis pathway (*300*). SNF1 is also responsible for upregulation of the *INO1,* the gene-product of which is required in a rate limiting step of inositol-containing phospholipid biosynthesis; as a consequence *snf1Δ* mutants are auxotrophs for inositol (*301*).

In yeast cells stress factors influence a wide range of cellular functions in a 'general stress response'. These stress factors regulate the co-ordinated induction of many stress genes through the presence of a conserved *cis*-element in their promoters, namely the *St*ress *R*esponse *E*lement (STRE). Two factors, Msn2 and Msn4 regulate this element. Mutant cell lines deficient in negative regulators of SNF1 (e.g. *reg1Δ*) have abnormally active SNF1, and during periods of carbon starvation this activity inhibits the nuclear import of Msn2, reducing the cellular stress response. However osmotic and heat-shock induced Msn2 import is not affected ,suggesting stress-dependent differences in the processes regulating Msn2 translocation (*302*).

Snf1Δ mutants show severe growth defects when grown in the presence of 1.2M NaCl or 0.3M LiCl, demonstrating a link between SNF1 activity and salt stress (*299*). It is thought that SNF1 is involved in the regulation of *ENA1* expression, the gene-product of which is a P-type ATPase involved in the extrusion of Na^+ from the cytosol (*303*).

It is clear that the SNF1 enzyme has a central role in maintaining the viability of yeast cells, particularly in the response to changes in the extracellular environment, particularly nutrient availability.

1.1.3 SNF1 subunits

Similar to the mammalian AMPK enzyme, SNF1 is a complex formed of three subunits the equivalent of the AMPK αβγ subunits, arranged with 1:1:1 stoichiometry (summarised in Figure 59). Formation of the heterotrimer is independent of glucose availability (*304*). All three subunits are required for activity (*305*).

The α subunit

The Snf1 (α) catalytic subunit is constitutively expressed from the *SNF1* gene (Figure 59) (*306*). The N-terminal catalytic domain has a classic bi-lobal kinase fold as described elsewhere (Appendix 1.4.2) (*129, 307*).

A C-terminal regulatory domain mediates interaction with the kinase domain, the Snf4 (γ) and β subunits, and with the Glc7-Reg1 phosphatase complex. There is also a short unconserved sequence N-terminal to the kinase domain containing a stretch of 13 histidines which do not appear to be essential for function (*304*). An AID has been defined through mutational analysis. This sequence lies between residues 381 to 414 in the central portion of the protein. Residues in this region have also been implicated in the αγ reversible interaction, which is thought to regulate the kinase's catalytic activity (*308*). Deletion of the AID increases kinase activity (*308*) and relieves the requirement for Snf4 to activate Snf1 (*309*). The extreme C-terminal region (515-633) of Snf1 is required for interaction with β subunits (*308*).

Activation of the Snf1 kinase requires phosphorylation of T210 by upstream kinases, its mutation to alanine results in a phenotype similar to that of the *SNF1*Δ mutant (*310*). Furthermore, complex formation with the β and γ subunits is essential for kinase activity even when T210 is phosphorylated (*305*).

SNF1 has been shown to phosphorylate the SAMS peptide *in vitro (300).* SNF1 and AMPK are thought to have similar but distinguishable substrate recognition motifs. If anything SNF1 has a more stringent substrate specificity than AMPK defined as n-X-R-X-X-S-X-X-X-n (n = hydrophobic residue, X = any residue). (*267, 311*).

The β subunits

The *S. cerevisiae* genome encodes 3 β-subunits; Sip1, Sip2 and Gal3 (Figure 59). The relative abundance of the β-subunits is regulated by glucose availability with Gal83 being the major isoform, Sip2 expression increasing during growth on non-fermentable carbon sources, and Sip1 concentrations remaining comparatively low throughout (*312*).

The isoforms have different preferences for phosphorylation by Sak1, Tos3 and Elm1 upstream kinases (discussed in Appendix 1.1.4). The β-subunit is key in the association of the heterotrimeric complex (*305*). In the absence of a β-subunit, Snf4 is unable to associate with Snf1, although similarly in the absence of Snf4 only trace amounts of β-subunit interact with Snf1 (*305*).

SNF1 has been shown to localise to glycogen via its β-subunit GBD motif and through association with Reg1, a regulatory subunit of the Glc7 phosphatase which is also localised to glycogen, and which is thought to dephosphorylate SNF1. The isoforms have different affinities for glycogen binding with Gal83 binding strongly *in vitro* and Sip2 very weakly (*296*). Mutations in the GBD result in disregulation of the kinase, relieving glucose inhibition of SNF1 and therefore upregulating SNF1 dependent processes such as glycogen accumulation and expression of GS and Sip4 activation (*161, 313, 314*).

The N-terminal sequences are divergent and confer subcellular localisation patterns of the SNF1 heterotrimer. In glucose loaded systems all three isoforms are cytoplasmic, upon glucose depletion Sip1 localises to the vacuolar membrane (requiring N-terminal myristoylation), Gal83 to the nucleus and Sip2 remains cytoplasmic (*312*).

Both Sip1 And Sip2 are thought to be N-terminally myristoylated (*296*). The β-subunits are both also auto-phosphorylated by Snf1 and phosphorylated by other kinases (for example Casein Kinase II) although it remains unclear what role this plays in regulating the complex (*315*). Sip2 is also thought to be acetylated in an age-dependent manner (*316*).

The γ subunit

Snf4 is homologous to the AMPK γ-domain. It is a constitutively expressed protein of 331 residues that is capable of binding to the Snf1 and β-subunits as previously discussed (Figure 59) (*317*). It is required for catalytic activity of the heterotrimeric kinase complex both *in vivo* and *in vitro (300). Snf4Δ* cells exhibit a similar phenotype to that of *Snf1Δ* cells (*318*).

Snf4 consists of four CBS domains forming two Bateman domains, which are capable of adenine nucleotide binding (*319*). Both the S.*cerevisiae* and *S.pombe* Snf4 subunits have been crystallised and show extensive structural homology with the mammalian γ subunit (described in Appendix 1.4.4)(*2, 143, 188, 189*). Similar to AMPK four presumptive nucleotide binding sites exist, however in Snf4 only two are thought to bind nucleotides. Binding of nucleotides at the weaker site regulates the kinase as described in Appendix 1.1.4.

1.1.4 Regulation of SNF1

SNF1 is rapidly activated by phosphorylation of T210 on the activation loop of the Snf1 kinase domain in response to glucose limitation (*296*). This activation is transient, that is, after adaptation minimal SNF1 activity is required for continued growth in the glucose limited environment (*320*). Phosphatase mediated dephosphorylation is responsible for inactivation of the kinase (summarised in Figure 58).

The upstream kinases and phosphatases of SNF1 and AMPK retain cross-species activity indicating some structural and functional conservation between the mammalian and fungal pathways (*321*).

Upstream kinases

Three upstream kinases were identified through a combination of genetics screens and mass spectrometry of affinity purified protein complexes (*147, 322, 323*). Snf1 T210 is phosphorylated by three related upstream kinases; Snf1 activating kinase-1 (Sak1), Elm1 and Tos3 (*296*). These kinases are highly similar and functionally redundant; only triple mutant cell lines share a phenotype with *Snf1Δ*. These enzymes are not thought to be glucose regulated but seem to be differentially active dependent on carbon-source availability. Sak1 is the major activating kinase, it forms a stable complex with the SNF1 kinase (*324*). Elm1 and Tos3 form more transient interactions with SNF1 (*325*).

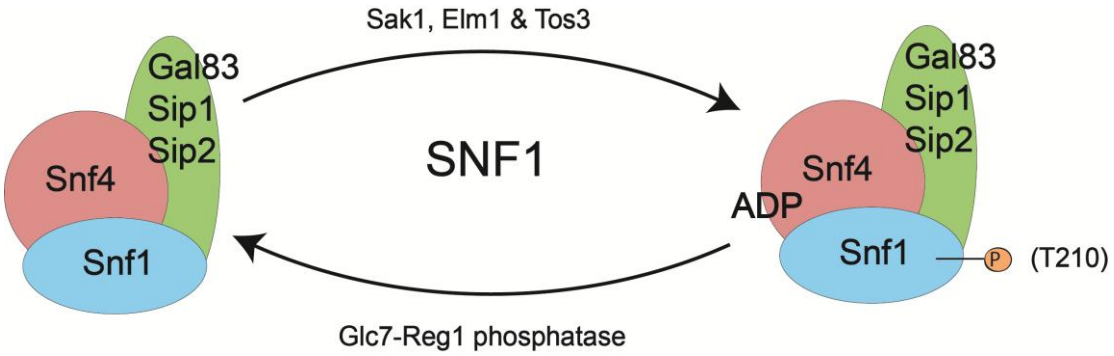

Figure 58: SNF1 kinase cycle.

Phosphorylation of SNF1 by upstream kinases results in a fully active kinase complex. Dephosphorylation by the relevant phosphatases returns the protein to an inactive state. ADP binding to Snf4 protects T210 from dephosphorylation by phosphatases.

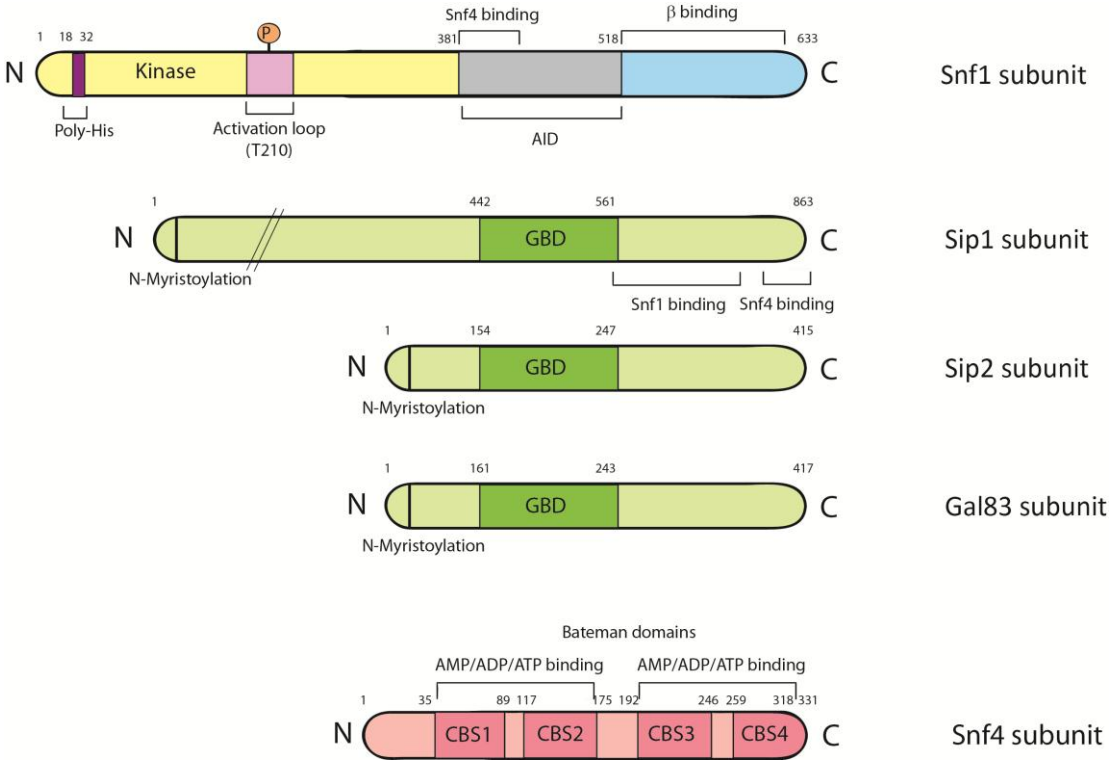

Figure 59: Domain schematic of SNF1 subunits.

Abbreviations: AID: autoinhibitory domain, GBD: Glycogen Binding Domain (also referred to as the carbohydrate binding module), CBS: Cystathionine β-synthase.

SNF1 Phosphatases

Dephosphorylation of T210 is catalysed by the PP1 family phosphatase Glc7, complexed with a regulatory subunit; Reg1. Multiple regulatory subunits are known to bind Glc7 and mediate its roles in numerous pathways. T210 is dephosphorylated in glucose-rich conditions by Glc7 (*326*), and in *Reg1Δ* mutant cell lines this effect is lost (*321*). In fact in *Reg1Δ* and *Glc7Δ* cell lines SNF1 is constitutively active (*327*).

A number of yeast two-hybrid and co-immunoprecipitation studies have shown phosphorylated T210 dependent binding between Reg1 and Snf1 (*327, 328*). Reg1 is cytoplasmically localised in both glucose-rich and glucose-limited conditions (*329*). In the original model it was suggested that the SNF1:Reg1 interaction targets the kinase to glycogen particles where the Glc7 phosphatase is localised. Upon SNF1 dephosphorylation Reg1 dissociates and inactive SNF1 is released to the cytosol (*327*). Reg1 is phosphorylated in a SNF1-dependent manner allowing dissociation of the Glc7:Reg1 complex and perhaps stimulating Glc7 phosphatase activity (*330*). More recent data suggests that the Reg1:SNF1 and Reg1:Glc7 interactions require the same binding surface, and that the interactions between Reg1, Glc7 and SNF1 must be more dynamic than originally thought (*331*).

There is substantial evidence that the Glc7:Reg1 complex dephosphorylates SNF1 *in vivo,* however recently a second phosphatase has been implicated in SNF1 regulation. Sit4, a PP2A-like phosphatase was more recently implicated in T210 dephosphorylation (*332*). SNF1 and Sit4 were shown to co-purify, and T210 phosphorylation increase in *Sit4Δ* mutants. PP2A family members have previously been shown to inactivate AMPK and SNF1 *in vitro* (*300*).

Regulation by nucleotide

Regulation of SNF1 by AMP, either allosteric or through protection against dephosphorylation, has not been reported previously even at high AMP concentrations (*2, 179, 300*). However SNF1 activity has been shown to correlate with the cellular AMP:ATP ratio and mutations throughout the CBS domains disrupt activity (*161, 333*). For many years it remained a mystery as to why there was an apparent lack of nucleotide regulation of SNF1. Recently, it was shown by members of the Gamblin/Carling laboratories that ADP binding to Snf4 activates the SNF1 kinase through protecting T210 from dephosphorylation (*2*). This nucleotide protects T210 against dephosphorylation by a wide-range of phosphatases

both *in vitro* and *in vivo,* although it remains unclear which nucleotide binding site is responsible for this regulation (*2*). A simple model for Snf4 regulation of Snf1 kinase would be that ADP binding prevents the AID binding to the kinase domain, a conformational change regulated in some way by glucose availability (*328*).

Although no direct measurements of interactions between nucleotides and SNF1 have previously been reported crystal structures of the Snf4 subunit are bound by AXP's (Table 2, Figure 60). The *S.pombe* Snf4 subunit binds to two nucleotides at Site-2 and 4. This work demonstrated that AMP and ATP competitively bind at the same site, and that whilst Snf4 does not bind GMP it does bind cAMP (*142, 188*). No biochemical information about the AXP regulation of this homolog is available; it is therefore unclear what the relevance of this binding is physiologically. In crystal structures the *S.cerevisiae* Snf4 subunit binds nucleotide at a single site, Site 4. As both the mammalian and the *S.pombe* analogues are known to bind at least two nucleotides it is possible that the crystallisation conditions, truncated construct or low affinities precluded nucleotide occupancy of a second site.

1.2 Results and Discussion

1.2.1 Expression of recombinant SNF1 complexes

A $Snf1_{(50-633),}$ $Sip2_{(101-415)}$Snf4 construct was used throughout these studies. The Sip2 isoform was used in preference to Gal83 in order to complement the *S. cerevisiae* crystal structure determined within the Gamblin Laboratory (*2*).

Expression of recombinant AMPK is a well characterised system. The SNF1 subunits were co-expressed as described in Chapter 2 and transformed into a competent *E.coli* cell line. Recombinant SNF1 protein was affinity purified via the N-Terminal Snf1 polyhis-tag and further purified by size-exclusion chromatography (see Chapter 2). Figure 61 shows the product of SNF1 expression, purification and phosphorylation resolved by SDS-PAGE.

The complex was phosphorylated *in vitro* with CaMKKβ, as described for mammalian AMPK in Section 2.2.4. Although this is the mammalian upstream kinase it has previously been demonstrated to effectively phosphorylate the critical T210 residue positioned on the kinase activation loop (*179*).

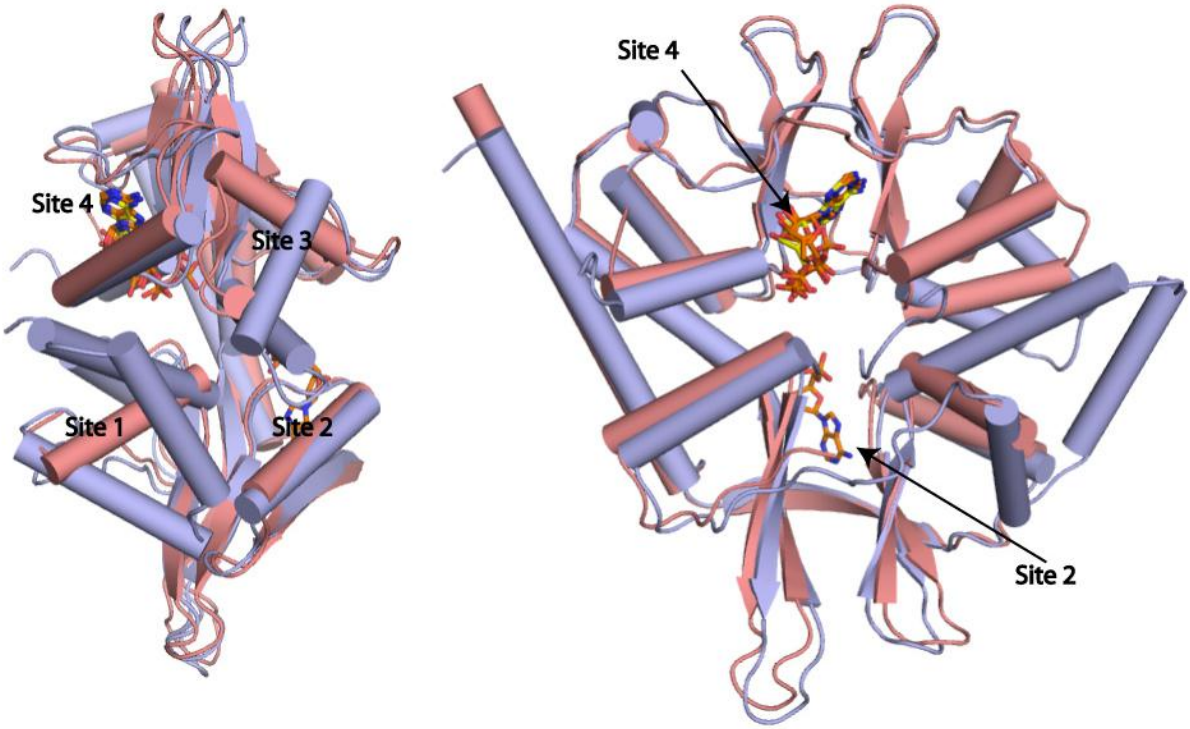

Figure 60: Overlay of *S.cerevisiae* and *S.pombe* Snf4 subunits from two angles.

Cartoon representations of *S.cerevisiae* Snf4 (pink) complexed with ADP (yellow sticks) (PDB ID: 3T4N) and *S.pombe* SNF4 (blue sticks) complexed with ADP and ATP (orange) (PDB ID: 2QRD). Sites are as numbered.

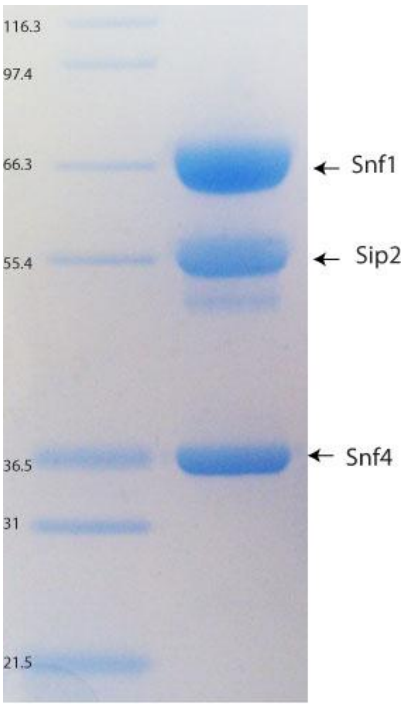

Figure 61: Purified, phosphorylated recombinant SNF1 (Snf1$_{(50-633)}$, Sip2$_{(101-415)}$Snf4).

The purified protein was resolved on a 12-14% SDS-PAGE Novex gel and stained with InstantBlue. The molecular weight markers are indicated on the left (kDa) and the identity of the bands on the right.

1.2.2 Binding of nucleotides to SNF1

A similar approach to that described in Chapter 3 was taken to determine the binding constants of nucleotides interacting with the SNF1 heterotrimer.

Similar to AMPK the Snf1 subunit has an Mg.ATP binding pocket within its kinase domain. C-AXP's did not compete for binding with staurosporine to mammalian AMPK, and the literature suggests that ribose-modified nucleotides do not bind to kinase Mg.ATP-binding pockets. Therefore it was assumed that C-AXPs did not bind to the Snf1-subunit and no controls in the presence of staurosporine were performed.

C-ADP and C-ATP were used as probes to monitor nucleotide binding (Figure 13d). Upon binding SNF1 C-ATP undergoes a larger fluorescence change compared to C-ADP (Figure 62). In fact C-ATP produced a larger fluorescence enhancement upon protein binding than C-ADP in all the experiments described in this thesis.

It was possible to demonstrate a stoichiometry of at least 2:1 by performing titrations at low temperatures and in the absence of salt, χ^2 values improved between 10- and 25-fold when fitting to a two-site rather than a one-site model (Table 16). Binding of nucleotides to SNF1 is much weaker than to AMPK in general and it is impossible to rule out the possibility that K_{dII} represents the weak binding of nucleotide at more than one site. However due to the statistical improvement upon fitting to a two-site model, the predicted homology with *S.pombe* Snf4 and the AMPK γ-subunit which both bind two exchangeable nucleotides, and the regulatory data it was decided to assume nucleotide bound at two sites. Equilibrium dissociation constants at 20^{o}C in the presence of 100mM salt were determined as described in Section 3.3.1 (Figure 63). Unphosphorylated SNF1 bound C-AXP tighter than the phosphorylated form (Table 16). Displacement titrations with C-ADP were performed to define equilibrium dissociation constants for AXP binding (Table 17).

NADH also proved to be a useful reporter for AXP binding to SNF1. NADH binds to SNF1 with 1:1 stoichiometry with equilibrium dissociation constants in the low micromolar range (Table 16). The binding of NADH to SNF1 is significantly stronger than to AMPK. Displacement titrations produced dissociation constants for AXPs which were consistent with the tighter C-ADP site (Figure 64 and Table 18). Crystallographic studies suggest that

NADH binds in Site-4, and therefore that this is the 'tight' nucleotide binding site (Figure 65)(*2*). It is unclear to which site the second 'weak' nucleotide binds. NADH does not compete with ADP regulation of SNF1, therefore nucleotide binding to the second weaker site must be responsible for mediating this effect (*2*).

Under *S.cerevisiae* physiological conditions, most of the ATP, and some of the ADP, is complexed with magnesium. Therefore, the effects of magnesium on nucleotide binding were explored. Experiments with C-ADP and C-ATP binding to phosphorylated SNF1 demonstrated that magnesium does weaken binding since it 'flattens' the binding curve (Figure 66). Analysis of the curves is difficult but estimates of K_d values were obtained (Table 19 and Figure 66). Binding of C-ATP at the 'tight' site (Site-4) was weakened around 4-fold in the presence of 5mM $MgCl_2$, whilst a robust binding constant for Mg.C-ATP at the second site was undeterminable but is greater than 500μM (much weaker than free C-ATP). AXP binding to SNF1 is significantly weaker than for C-AXP's; AXP's bind SNF1 around 8-10 fold weaker at the tight site (Site-4), and 25-40 fold weaker at the second site compared with the corresponding C-AXP. These data suggest that the binding constant for Mg.ATP at the second, regulatory, site is too weak to be physiologically relevant (discussed further in Appendix 1.2.5).

Similar to the data presented here, in which *S.cerevisiae* binds Mg.AXP much weaker than free AXP, *S.pombe* Snf4 has previously been shown to bind AXP uncoordinated by cations preferentially. Townley *et al* (2007) demonstrated that *S.pombe* Snf4 crystals grown in the presence of Gd^{3+}lanthanide had no bound ions. This ion is known to substitute for Mg^{2+} cations in ATP substructures and provides a large anomalous signal for crystallographic studies (*188*). This observation suggests that unbound AXP are preferentially bound by Snf4, since the phosphate charge balance can be provided by the side chains of arginine residues rather than by bound cations.

1.2.2.1 Snf4 mutants

It is suggested that ADP binding at the second, weaker site is responsible for mediating protection of T210 against dephosphorylation for two reasons: 1) ADP protects SNF1 T210 from dephosphorylation by phosphatases with a half maximal effect of 500μM (*2*).

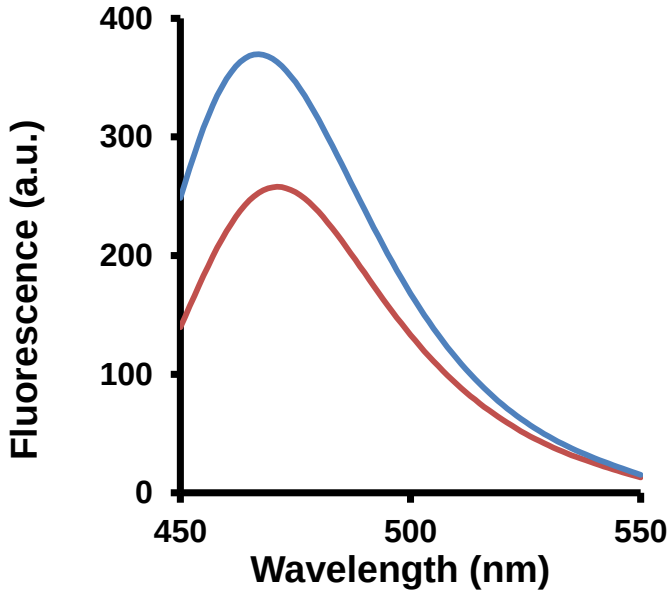

Figure 62: Emission spectra of SNF1/C-AXP complexes.

5μM C-ADP (red) and C-ATP (blue) in the presence of 21μM phosphorylated SNF1. C-AXPs were excited at 470nm and emission spectra recorded from 450 to 550nm at 20^{o}C in the presence of 25mM Tris, 1mM TCEP, and 100mM NaCl (pH 8.0).

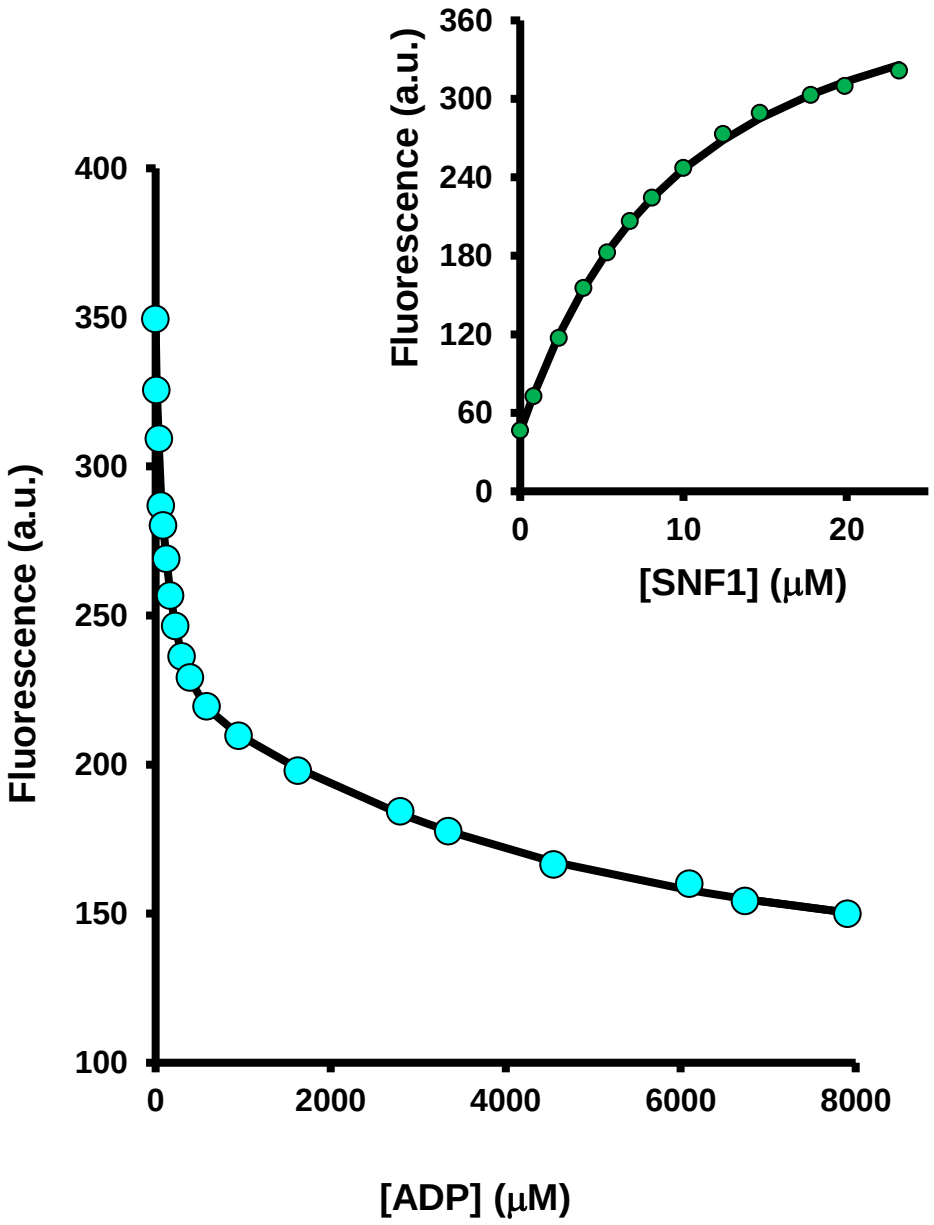

Figure 63: Measurement of equilibrium dissociation constants for the binding of AXPs to phosphorylated SNF1.

Displacement of C-ADP from the SNF1:$(C\text{-}ADP)_2$ complex by ADP monitored using the change in fluorescence at 470nm (excitation at 430nm). The solid lines are the computed best fits with $K_{d,I}$ and $K_{d,II}$ for C-ADP binding fixed at 9 and 27μM respectively. Inset: Titration of C-ADP with SNF1 plotted as change in fluorescence intensity as a function of SNF1 concentration. All measurements were carried out at 20°C in 50mM Tris, pH8, 100mM NaCl, 1mM TCEP (pH 8.0).

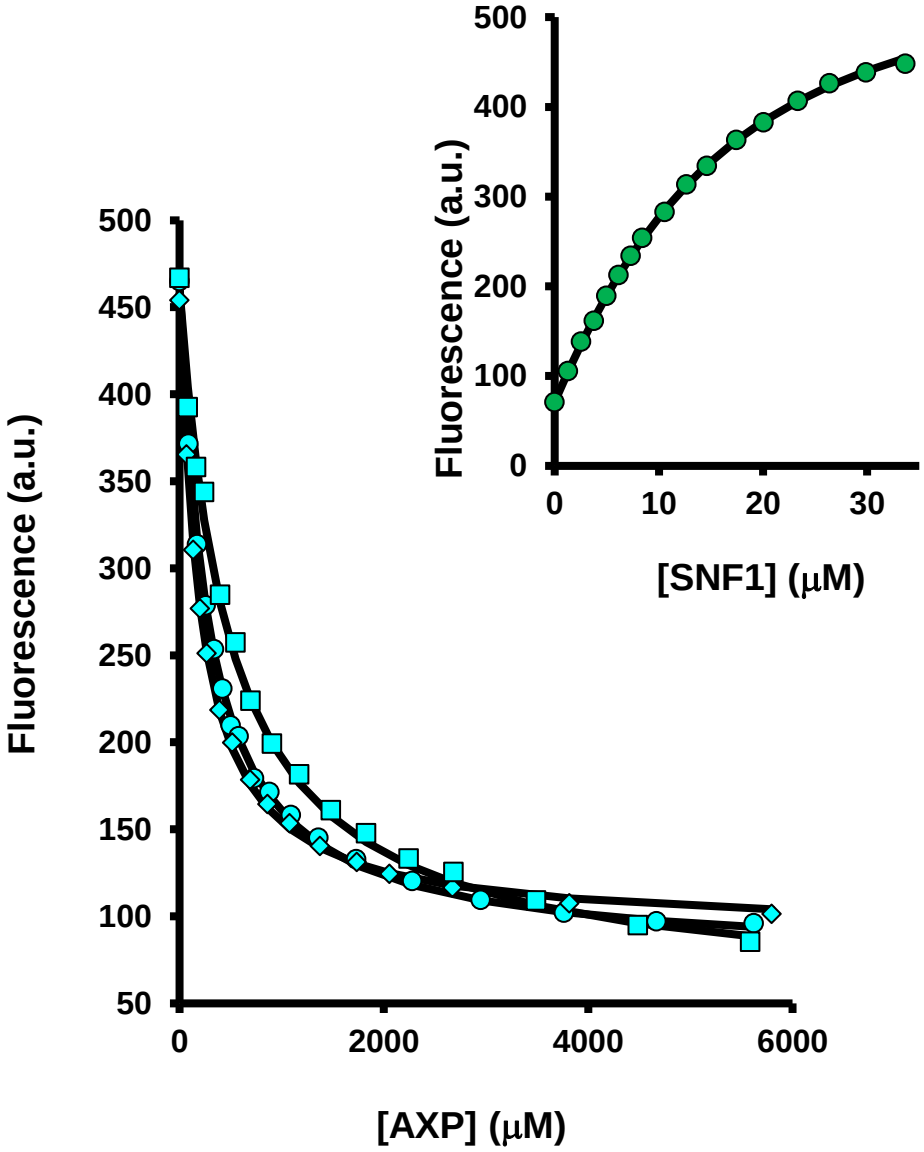

Figure 64: Measurement of equilibrium dissociation constants for the binding of AXPs to phosphorylated SNF1.

Displacement of NADH from the SNF1:NADH complex by AXPs monitored using the change in fluorescence at 435nm (excitation at 340nm). The solid lines are the computed best fits with the K_d for NADH fixed at 12.3μM Inset: Titration of NADH with SNF1 plotted as change in fluorescence intensity as a function of SNF1 concentration. All measurements were carried out at 20°C in 50mM Tris, pH8, 100mM NaCl, 1mM TCEP (pH 8.0).

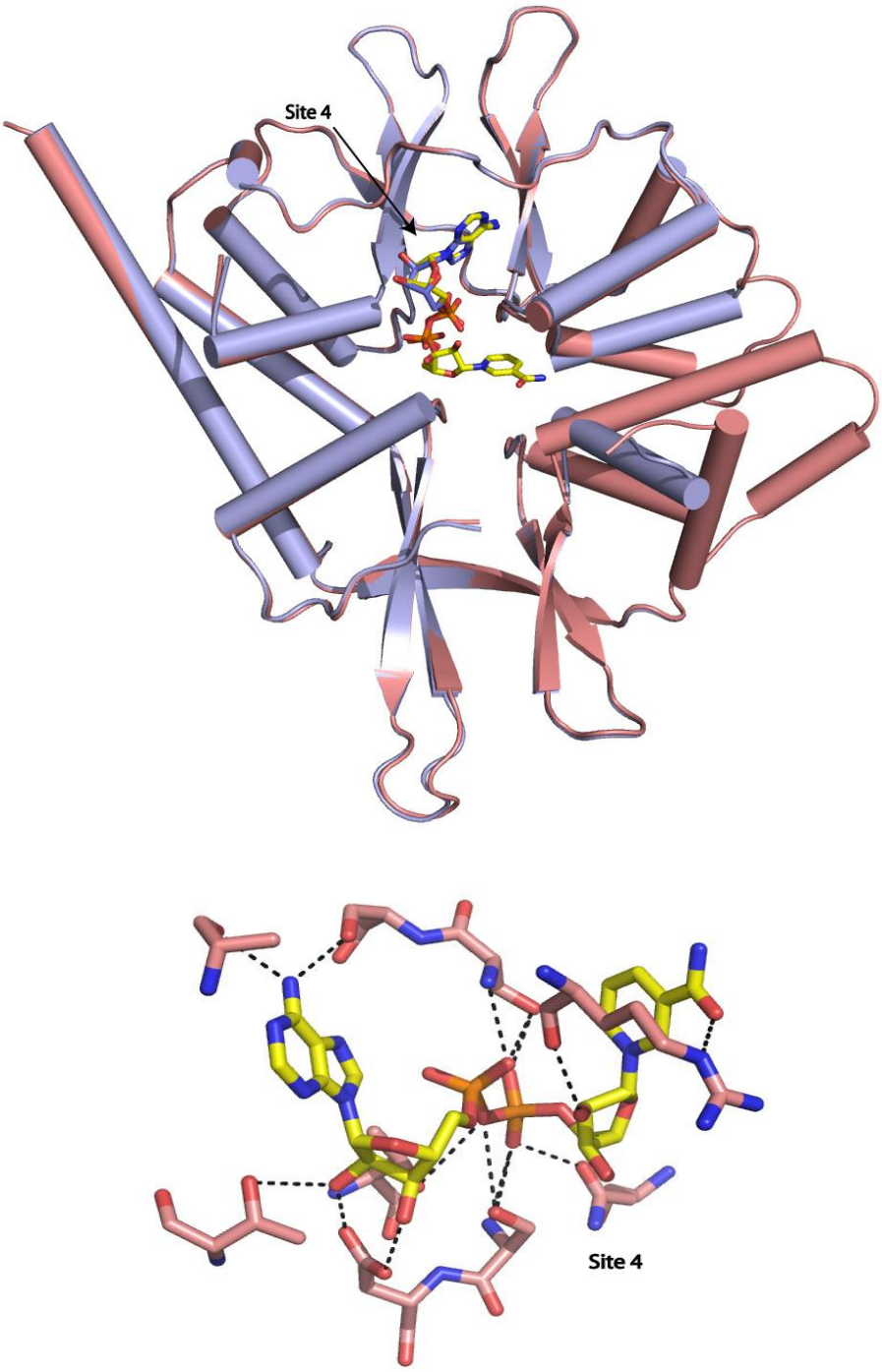

Figure 65: NADH binding to Site-4 (SNF1).

A) Overlay of the crystal structures of NADH (Pink, yellow sticks) and ADP (purple, blue sticks) bound to the *S.cerevisiae* Snf4 subunit. Both ligands bind at Site-4 (PDB ID: 3TE5, 3T4N). B) NADH makes similar contacts with Snf4 side chains as AXP. There are a number of additional interactions with the ribose and nicotinamide groups.

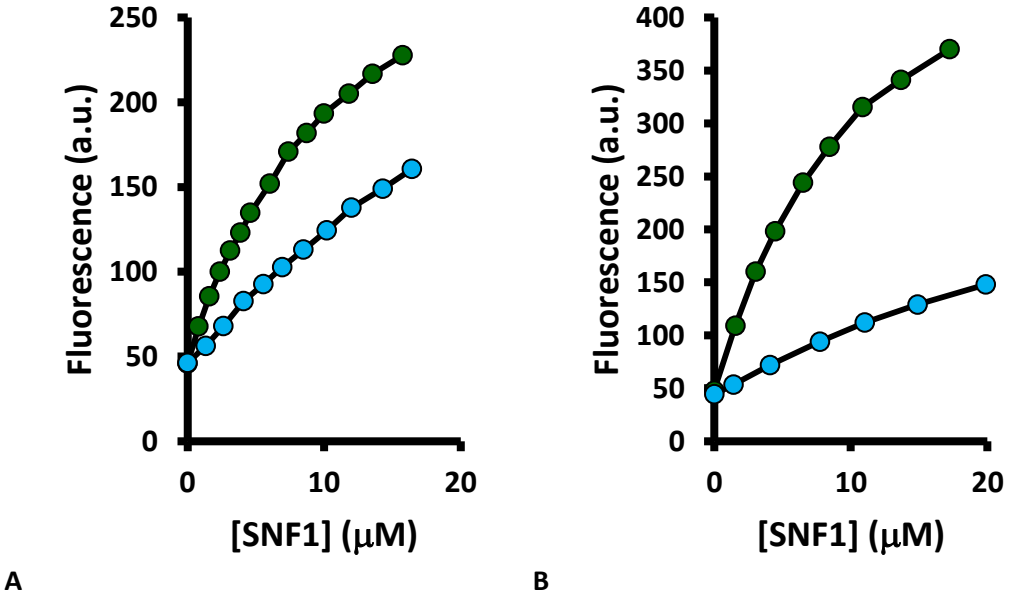

Figure 66: Measurement of equilibrium dissociation constants for the binding of AXPs to phosphorylated SNF1.

A) Titration of C-ADP with SNF1. **(B)** Titration of C-ATP with SNF1. All measurements were carried out at 20°C in 50mM Tris, pH8, 100mM NaCl, 1mM TCEP (pH 8.0) plus (blue) or minus (green) 5mM $MgCl_2$.

		NADH	C-ADP		C-ATP	
SNF1	**Temp, Salt**	**K_d (μM)**	**K_{dI} (μM)**	**K_{dII} (μM)**	**K_{dI} (μM)**	**K_{dII} (μM)**
Phosphorylated	7°C	0.42 (0.19)	3.6 (1.5)	14.5 (3.1)	5.7 (3.1)	15.5 (5.4)
Unphosphorylated	0mM NaCl	0.65 (0.14)	2.6 (1.3)	9.9 (3.5)	1.9 (0.9)	12.3 (4.1)
Phosphorylated	20°C	12.3 (3.4)	9.1 (3.1)	30.7 (7.3)	11.8 (5.3)	27.1 (9.3)
Unphosphorylated	100mM NaCl	4.7 (1.5)	7.5 (3.4)	22.5 (8.5)	9.9 (4.3)	21.0 (7.3)

Table 16: Equilibrium dissociation constants for the binding of NADH and C-AXPs (SNF1).
Dissociation constants were determined at 7/20°C by fluorescence titrations of C-AXP with SNF1 in 25mM Tris, 1mM TCEP (pH 8.0), with or without NaCl. The K_d values are reported as the mean (± SD) determined from at least two independent measurements.

Ligand	K_{dI} (μM)	K_{dII} (μM)
	***vs* C-ADP**	
AMP	65 (15)	1450 (350)
ADP	91 (25)	760 (200)
ATP	85 (22)	1200 (300)

Table 17: Equilibrium dissociation constants for the binding of AXPs to phosphorylated SNF1.
Dissociation constants were determined at 20°C by competition against C-ADP. The K_d values shown are the mean (±SD) determined from at least two independent measurements. All measurements were carried out at 20°C in 50mM Tris, pH8, 100mM NaCl, 1mM TCEP (pH 8.0).

	Phosphorylated	Unphosphorylated
	vs NADH	
Ligand	**K_d (μM)**	**K_d (μM)**
AMP	55 (12)	13.2 (1.7)
ADP	72 (14)	33.6 (1.7)
ATP	120 (25)	38.3 (13.4)

Table 18: Equilibrium dissociation constants for the binding of AXPs to phosphorylated and unphosphorylated SNF1.

Dissociation constants were determined at 20°C by competition against NADH. The K_d values shown are the mean (±SD) determined from at least 3 independent measurements. All measurements were carried out at 20°C in 50mM Tris, pH8, 100mM NaCl, 1mM TCEP (pH 8.0).

	K_{dI} (μM)	K_{dII} (μM)
Mg.C-ADP	45.1 (16.8)	95.9 (32.6)
Mg.C-ATP	41.6 (3.6)	nd

Table 19: Equilibrium dissociation constants for the binding of Mg.C-AXPs (SNF1).

Dissociation constants were determined at 20^{o}C by fluorescence titrations of C-AXP with phosphorylated SNF1 in 25mM Tris, 1mM TCEP, 100mM NaCl, 5mM $MgCl_2$ (pH 8.0). The K_d values are reported as the mean (± SD) determined from at least two independent measurements. nd: Not determined.

The ADP binding constant for the second site is similar to this value suggesting that it is binding of ADP at this site which is responsible for regulation of the complex. 2) NADH binds at the tighter Site-4 and does not compete with regulation by ADP. Unfortunately the identity of the second site was not determined via X-ray crystallography due to the weak binding of AXP. Attempts were made to specifically ablate AXP binding at each site and confirm the identity of the weaker binding site via mutagenesis.

As described in Section 3.4.3.5 D→A mutants have been widely used in the AMPK field to 'knock out' binding and specific AXP binding sites, through interruption of the ribose interaction with the protein. This key aspartate residue is conserved in Site-1, 3 and 4 of SNF1, and these residues were mutated to alanine. Equilibrium dissociation constants of C-ADP and NADH binding to these mutants were determined (Table 20). Although effects on binding were observed, none of the mutants specifically or completely ablated binding of these ligands. For example, despite crystallographic evidence that NADH binds in Site-4 the D83A mutation in Site-1 weakens NADH binding around 4-fold whilst the Site-4 D312A mutation only has a 2.5-fold effect.

In the typical AXP binding site a number of branched-chain residues, often valine, co-ordinate the adenine moiety. Several mutants were designed to disrupt these interactions and preclude AXP binding. Again, equilibrium dissociation constants of C-ADP and NADH binding were determined (Table 21). In all cases binding of C-ADP was weakened at both sites compared to wild-type SNF1. NADH binding was also weakened in all cases, except the S144W (Site-1) mutant which appeared to bind with a slightly tighter affinity. However none of the mutants completely abolished AXP binding, therefore the identity of the second site remains elusive.

S.pombe SNF1 binds AXP at Site-2 and 4 which are situated on diagonally opposed sides of the Snf1 subunit (Figure 60). In fact Site-2 is thought to be an ADP specific binding site (*142*). Additionally mammalian AMPK exchangeably binds two AXP's at sites in the same diagonal arrangement (*87*). In *S.cerevisiae* it is Site-2 which lies diagonally opposite the known tight Site-4, if we assume that this arrangement is conserved perhaps it would have been sensible to further explore the effect of mutations on AXP binding to Site-2. However homologous tryptophan mutations in Site-2 did not have any effect on ADP regulation, suggesting that the binding was unaffected (*2*).

	NADH	C-ADP	
Snf4 protein	**K_d (μM)**	**$K_{d,I}$ (μM)**	**$K_{d,II}$ (μM)**
Wild-type	18.7 (3.8)	4.2 (0.4)	14.7 (4.9)
D83A (Site-1)	75.7 (29.9)	1.8 (0.7)	24.9 (4.9)
D240A (Site-3)	14.3 (3.7)	2.6 (1)	45.3 (19)
D312A (Site-4)	45 (4.2)	8.4 (4.1)	38.9 (5.6)

Table 20: Equilibrium dissociation constants for binding of NADH and C-ADP to wild-type and mutant SNF1.

The K_d values shown are the mean (±SD) from 3 (NADH) or 2 (C-ADP) independent experiments All measurements were carried out using unphosphorylated truncated SNF1 ($Snf1_{398-633}$ $Sip2_{154-415}$ Snf4) complexes at 20°C in 50mM Tris (pH 8.0), 150mM NaCl, 1mM TCEP (NADH) and 7°C in 50mM Tris, pH 8, 1mM TCEP (C-ADP).

	NADH	C-ADP	
Snf4 protein	**K_d (μM)**	**$K_{d,I}$ (μM)**	**$K_{d,II}$ (μM)**
Wild-type	12.3 (3.4)	3.6 (1.5)	14.5 (3.1)
L78W (Site-1)	13.9 (3.6)	10.5 (2.1)	27 (11)
S144W (Site-1)	7.8 (0.7)	8.1 (2.2)	36 (10.5)
V220W (Site-4)	15.1 (4.1)	6.9 (1.8)	23.5 (6.9)
V307W (Site-4)	12.2 (5.0)	8.7 (1.2)	35 (8.5)

Table 21: Equilibrium dissociation constants for binding of NADH and C-ADP to wild-type and mutant SNF1.

The K_d values shown are the mean (±SD) from 2 independent experiments. All measurements were carried out using phosphorylated full-length Snf1 $Gal83_{154-415}$ Snf4 complexes at 20°C in 50mM Tris, 150mM NaCl, 1mM TCEP (pH 8.0).

1.2.3 Circular Dichroism

The use of far-UV CD for studying the secondary structure content of protein samples in solution was described in Section 3.3.2. Spectra of both phosphorylated and unphosphorylated SNF1 were collected at 20^{o}C (Figure 67). Estimation of their secondary structure content highlighted no significant differences between the two AMPK species (Table 22). Thermal unfolding of the two protein samples suggested that neither was classically denatured, instead a drop in signal at ~55^{o}C was observed indicating the formation of β-fibrils (Figure 68). This is analogous of the denaturation of phosphorylated AMPK described earlier in Section 3.4.4.1. Far-UV spectra collected at 80^{o}C and analysed for their secondary structure content confirm this increase in β-content (Table 22 and Figure 67).

Near-UV CD offers information about the tertiary structure of a protein, spectra of phosphorylated and unphosphorylated SNF1 were collected (Figure 69). The observed spectral bands are the sum of all absorptions, both positive and negative, for this reason the signals may be small despite the large numbers of tryptophan, phenylalanine and tyrosine residues present in SNF1. The spectra of both SNF1 species contain a negative tyrosine band with a maximum between 255-270nm, a positive tryptophan band at ~290nm and positive phenylalanine signal between 255-270nm. In both cases the phosphorylated sample produces higher intensity bands than unphosphorylated SNF1 suggesting some local differences in the environment of a number of aromatic amino acids in the two species.

The binding of AXP to a number of Snf4 point mutants was described in Appendix 1.2.2.1. The far-UV CD spectra of these proteins were recorded and compared with the relevant wild-type SNF1 as indicated in the figure legends (Figure 70 and Figure 71). No significant differences between the secondary structure content of these mutants and wild-type SNf1 were observed, suggesting that these point mutations have little effect on the overall heterotrimeric structure or stability (Table 23).

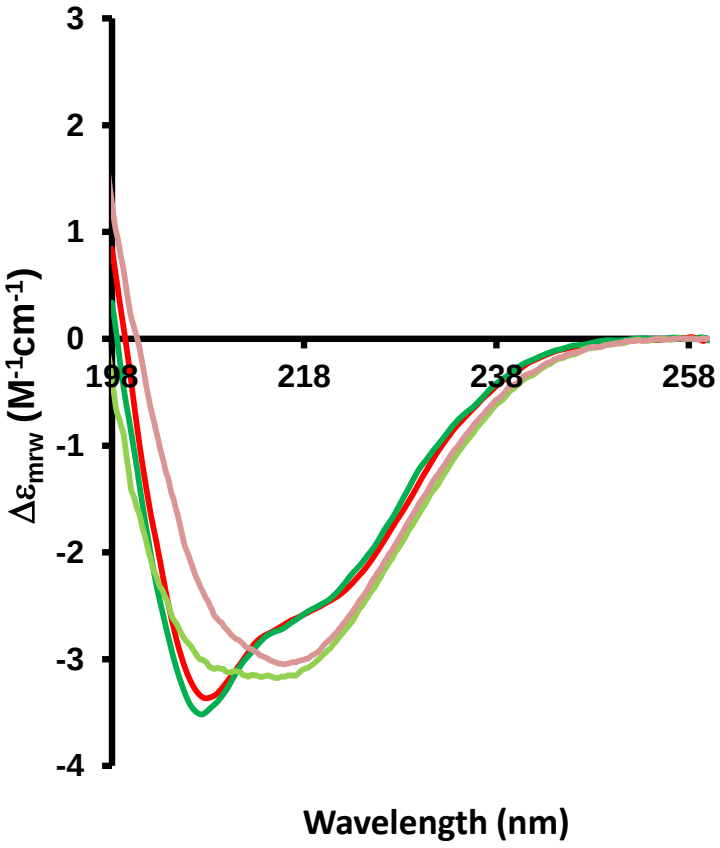

Figure 67: Far-UV CD spectra (SNF1).

Phosphorylated (green) and unphosphorylated (red) SNF1 far-UV CD spectra were recorded at 20°C. Phosphorylated (pale green) and unphosphorylated (pink) SNF1 far-UV CD spectra were recorded at 80°C. Samples were diluted in water.

	%			
SNF1	**α**	**β**	**Turns**	**Unordered**
Unphosphorylated (20°C)	25.2	21.5	19.7	33.5
Phosphorylated (20°C)	23.7	22.2	19.9	34.6
Unphosphorylated (80°C)	20.6	26.7	22.6	31.3
Phosphorylated (80°C)	20.3	22.1	20.3	38.7
Truncated wild-type	18.5	26.7	20.9	33.2

Table 22: Secondary structure content predictions (SNF1).

Truncated ($Snf4_{(1-322)}Sip2_{(304-415)}$His-$Snf1_{(457-633)}$), phosphorylated and unphosphorylated ($Snf1_{(50-633),}$ $Sip2_{(101-415)}Snf4$) SNF1 far-UV CD spectra were recorded at the indicated temperatures and secondary structure content predicted as described Chapter 3.

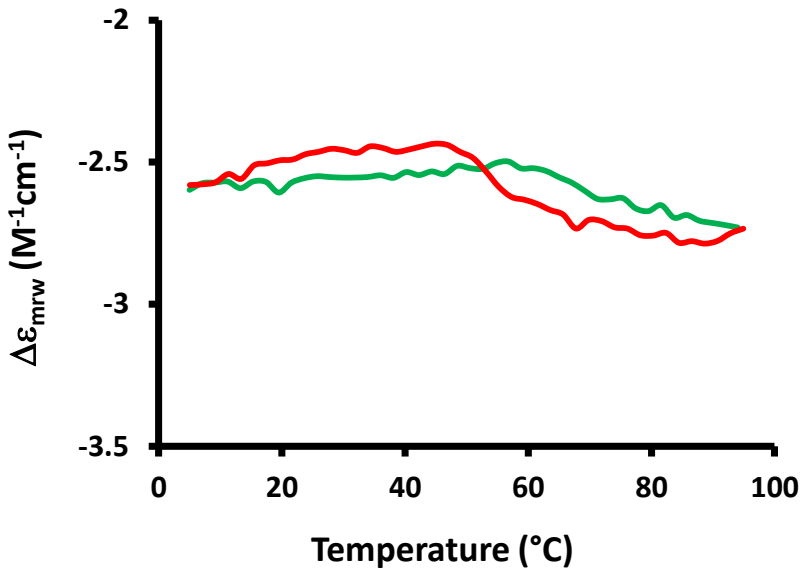

Figure 68: Thermal denaturation (SNF1).

Phosphorylated (green) and unphosphorylated (red) SNF1. Protein samples diluted in water.

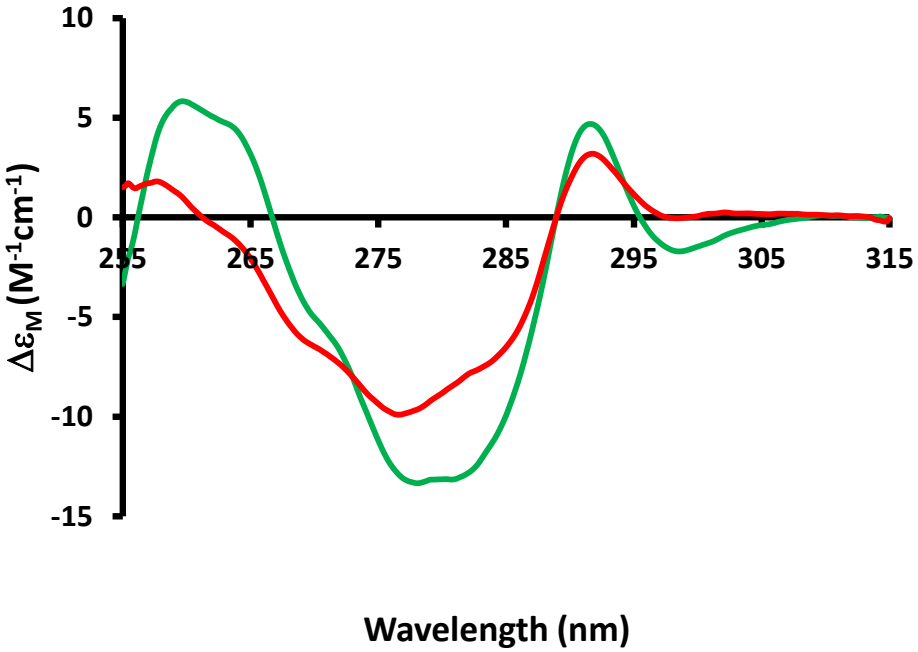

Figure 69: Near-UV CD spectra (SNF1).

Phosphorylated (green) and unphosphorylated (red) SNF1. Protein samples diluted in water.

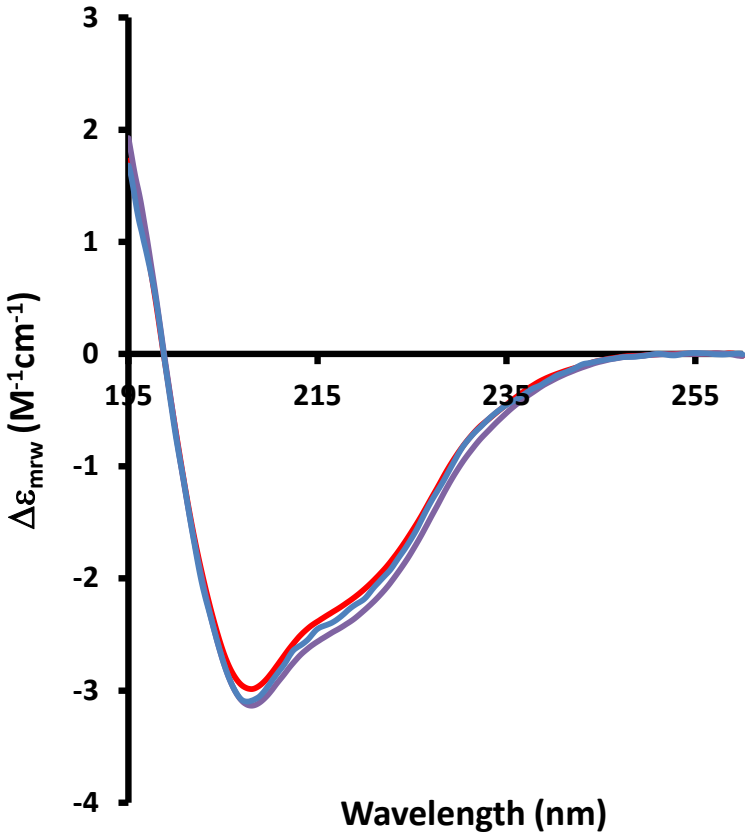

Figure 70: Far-UV CD spectra (SNF1).

Wild-type truncated ($Snf1_{398-633}$ $Sip2_{154-415}$ Snf4) SNF1 (red), D312A mutant (blue) and D240A mutant (purple). Samples were diluted in water and recorded at 20^{o}C.

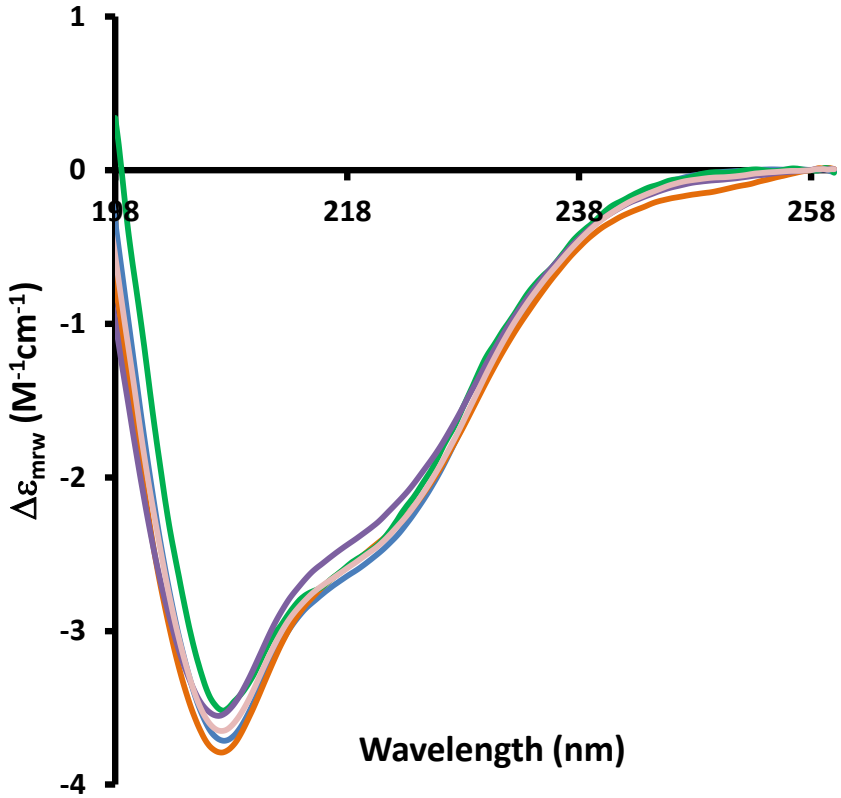

Figure 71: Far-UV CD spectra (SNF1).

Phosphorylated wild-type SNF1 (green), L78W (orange), V220W (blue), V307A (purple) and S144W (pink). Samples were diluted in water and recorded at 20°C.

	%			
Snf4 mutant	**α**	**β**	**Turns**	**Unordered**
D240A (Site-3)	20.4	25.4	21.2	32.6
D312A (Site-4)	18.9	26.4	21.1	33.0
Phosphorylated L78W (Site-1)	23.4	18.0	17.8	40.8
Phosphorylated S144W (Site-1)	21.4	18.5	17.8	42.3
Phosphorylated V220W (Site-4)	23.7	19.2	19.0	38.5
Phosphorylated V307W (Site-4)	23.4	19.1	18.6	39.2

Table 23: Secondary structure content predictions.

Far-UV CD spectra of Snf4 point mutants were recorded and secondary structure content predicted as described in the Section 3.3.2. Truncated ($Snf4_{(1-322)}Sip2_{(304-415)}$His-$Snf1_{(457-633)}$) and phosphorylated (Snf1, $Gal83_{(101-415)}$ Snf4) SNF1 backgrounds were used in these experiments.

1.2.4 Kinetics

The NADH-coupled spectrophotometric assay has not previously been used to study SNF1 kinetics/activity. Initially I determined the K_m values with respect to the SAMS peptide (18.8μM, Figure 72b) and ATP (157.1μM, Figure 72a). The V_{max} values calculated as 19.2nM/Sec and 17.0nM/Sec at saturating ATP and SAMS concentrations respectively.

Although there are many examples of the classic SAMS peptide assay being used to monitor SNF1 activity, there are almost no reports of the K_m/V_{max} with respect to SNF1's substrates (*2, 147, 300*). A single example suggested a K_m of 108μM with respect to SAMS. In their study SNF1 was purified from yeast cells, unlike the bacterially expressed recombinant SNF1 used in this work, perhaps this explains the differences in the calculated and published K_m value (*267*).

It has previously been reported that SNF1 is neither allosterically activated nor protected from dephosphorylation by AMP. However, ADP was recently shown to protect T210 from dephosphorylation by phosphatases. The time course and concentration dependence of this effect were demonstrated using the NADH-coupled assay (Figure 73). The effect saturates at around 1.5mM ADP, with half maximal activation at around 500μM, in line with the previous report of this regulation (*2*).

The Snf1 kinase Mg.ATP binding pocket binds Mg.ADP (the product of the phosphorylation reaction). It must also be considered that high Mg.ADP concentrations may inhibit the kinase reaction in some way. This is unlikely for two reasons; 1) the affinity of ADP and ATP for the kinase is very low, for AMPK Mg.ATP binds with an affinity of greater than 0.5mM, 2) although the incubation contains high concentrations of ADP the aliquot transferred to the kinase reaction is very low (~1μM) and is immediately converted to ATP by the coupled assay enzymes. Only if the k_{off} for Mg.ADP were very slow could this inhibit SNF1 phosphorylation.

NADH binds in Site-4 (as observed in the crystal structure of a SNF1 truncate (*2*)) with a K_d of 12.3μM (Table 16). It was demonstrated in Mayer *et al* (2001) using the standard SAMS assay (Figure 29b) that when NADH is included in the incubation mix at increasing concentrations no competition with the protective effect of ADP is observed. Therefore, I can conclude that binding of ADP at Site-4 is not responsible for the protection against dephosphorylation (*2*).

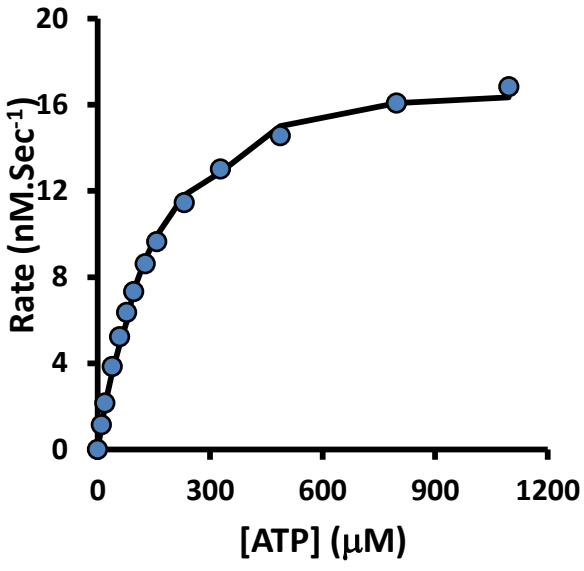

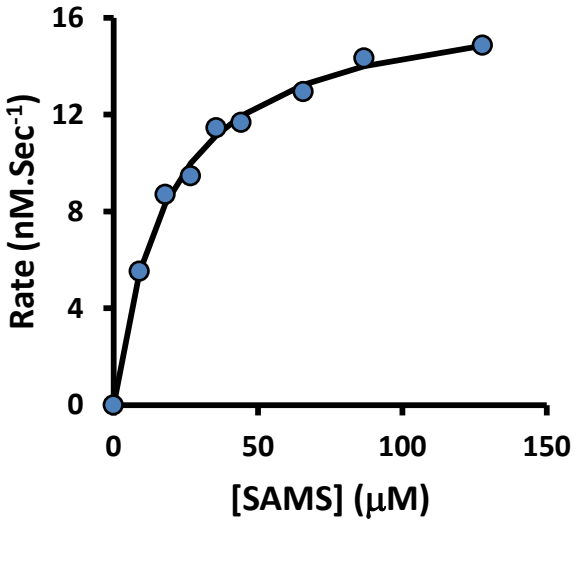

Figure 72: Determination of K_m values (SNF1).

With respect to (A) ATP (SAMS = 130μM) and (B) SAMS peptide (ATP = 500μM). SNF1 was phosphorylated *in vitro* and its activity measured at a range of substrate concentrations. Activity of SNF1 is plotted as a function of substrate concentration. Solid lines depict the velocity of the reactions measured by the NADH coupled assay.

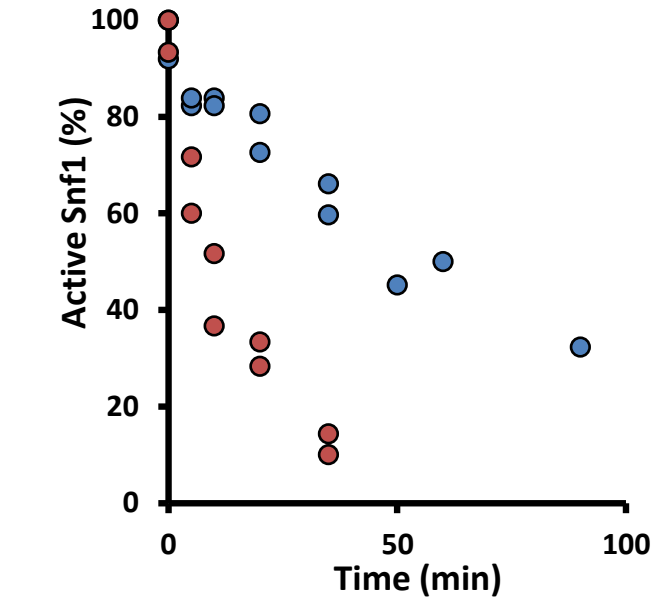

A

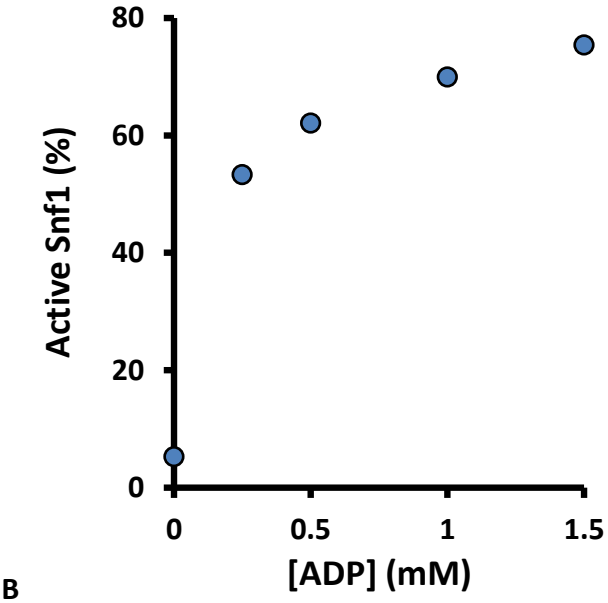

B

Figure 73: Phosphatase assays (SNF1).

(A) 8.5μM phosphorylated SNF1 was incubated in the presence of PP2C, with (blue) and without 1mM ADP (red). At a number of time points AMPK activity was measured. **(B)** Phosphorylated SNF1 was incubated in the presence of PP2C and increasing ADP concentrations. After 40 minutes, SNF1 activity was measured, results are displayed as percentage of phosphorylated T172 remaining. All phosphatase assays were performed at 25^{o}C. SAMS and ATP concentrations were 100μM and 500μM respectively.

1.2.5 Modelling

A modified version of the program outlined in Section 4.4.2.2 was produced to allow calculation of the occupancy of the two SNF1 nucleotide binding sites. The results presented in Mayer *et al* (2011) demonstrate, through competition with NADH, that binding of ADP at Site-4 cannot be responsible for the protection against dephosphorylation (*2*). The first aim of the modelling was therefore to demonstrate that the second weaker nucleotide binding site would become occupied by ADP over a concentration range which is consistent with the observed concentration dependence of the ADP protecting effect (Figure 73).

The second more ambitious aim was to demonstrate that physiologically realistic variations in AXP concentrations could bring about significant increases in ADP-bound SNF1 species, and therefore active phosphorylated SNF1. Yeast cells are able to survive much greater decreases in ATP concentration and increases in AMP/ADP concentrations than mammalian cells. It is not therefore unreasonable that the protecting effect of ADP on dephosphorylation in SNF1 is seen over a higher concentration range than with AMPK. This would also be consistent with the observation that SNF1 has evolved to function with significantly weaker binding constants for AXPs.

In vitro occupancy of Snf4 binding sites

Modelling the occupancy of SNF1 nucleotide binding sites was more problematic than modelling the mammalian system, particularly because there are unavoidably large errors associated with some SNF1:AXP K_d values described in Appendix 1.2.2, especially those for the weaker of the two sites.

Calculation of AXP species concentrations (H.AXP, Mg.AXP, Ca.AXP etc) was performed as described in Section 4.2.5 via the Cornish-Bowden method. The *in vitro* assays were all carried out using phosphorylated (active) SNF1. Equilibrium binding constants for AXP binding to Site-4 and the second site were taken from Table 17.

Good estimates of K_d values for the binding of Mg.AXP species to SNF1 were not determined using the fluorescence techniques described in Appendix 1.2.2 owing to the weakness of the interactions. K_d values for Mg.C-ATP/Mg.C-ADP binding at Site 4 (the tighter, NADH binding site) and Mg.C-ADP binding to the second weaker site were compared to those for these nucleotides uncoordinated by Mg^{2+}. The extent to which the presence of Mg^{2+} would reduce

the strength of the interaction with AXPs was assumed to be the same as for C-AXPs (Table 19) and binding constants estimated in this way are given in Table 24. There are, of course, very substantial errors associated with these estimations. For example, in the case of ADP binding at the weaker site (30.7 ± 7.3μM for C-ADP 95.9 ± 32.6μM for Mg.C-ADP, and 760 ± 200μM for ADP) the fold reduction for C-ADP is 3.1 ±1.3μM and the estimated K_d for Mg.ADP is then 2350 ±1150μM.

The concentration dependence of the protective effect of ADP on T210 dephosphorylation determined using the SAMS assay (Figure 17) is similar to that observed using different methods (*2*).

The pre-incubated phosphatase reaction contained only 10mM Mg and ADP in addition to SNF1 and the phosphatase. Therefore the only nucleotide species present (and therefore able to occupy the sites) are Mg.ADP and ADP. The modelling (Figure 74) shows occupancy of the weak site as a function of the total ADP concentration. Although substantial occupancy of the regulatory site is seen over this ADP concentration range the shape of the curve is not precisely the same as that observed experimentally (Figure 73). There may, of course, be many reasons for this discrepancy:

- The binding constant for Mg.ADP is very poorly defined (2350 ±1150μM – see above) and Figure 74 shows the substantial effect of varying the K_d in this range.
- The ADP is around 85% Mg^{2+}-bound in the presence of 10mM magnesium over the range of ADP concentrations used. It is assumed that both species protect against dephosphorylation and this may not be the case.
- The occupancy of Site-4 also varies over this ADP concentration range and it may be that occupancy of this site could modulate the effect of ADP/Mg.ADP bound in the regulatory site.
- Since dissociation constants for the SNF1 system are poorly determined one cannot exclude the possibility that occupancy of Site-4 could have some cooperative effect on occupancy of the regulatory site (described in relation to AMPK in Section 3.4.3.2).

If we assume that the SNF1 activation loop is protected in the same way as in the AMPK system (i.e. packing of the phosphorylated T210 residue against the regulatory domain) then

two species exist: kinase-bound and kinase-free. ADP binding to Snf4 is then assumed to shift the equilibrium from the free to the bound form. In terms of regulation the important, but unanswerable, question is to what extent does ADP binding shift this equilibrium.

***In vivo* occupancy of Snf4 binding sites**

Any truly successful model of SNF1 requires one to answer (at least) the following questions; What are the nucleotide (AXP) levels in yeast and how much do they change under stress conditions? What is the intracellular free Mg^{2+} concentration? What is the concentration of phosphorylated SNF1 under 'resting conditions' and how much must it be elevated to generate the required response? What are the enzymatic characteristics (particularly the K_m values) of the kinases and phosphatases that regulate the phosphorylation-dephosphorylation cycle in SNF1? How precisely does the protecting effect of ADP/Mg.ADP work and does it provide complete or only partial protection? What is the role of the AID?

Most of these questions cannot be answered easily, but it is of interest to consider what the binding constants determined in this work, in concert with plausible estimates of AXP and Mg^{2+} concentrations, can tell us about regulation of SNF1 by ADP *in vivo.*

A number of methods to monitor intracellular nucleotide concentrations have been developed, the primary methods are described in Section 4.2.6. Literature estimates of adenine nucleotide concentrations in *S.cerevisiae* are often highly variable, for example, ATP 2-8mM and ADP 1.1-4mM (*273, 334, 335*). It seems that yeast are more tolerant of large fluctuations in nucleotide levels than mammalian cells.

Intracellular Mg^{2+} concentrations affect the percentage of ADP present as Mg.ADP (Figure 75), and therefore the extent to which the regulatory site is occupied (as Mg.ADP binds SNF1 more weakly than ADP). The free Mg^{2+} concentration is unknown but is thought to be between 0.1mM and 1mM in eukaryotic cells and is not thought to fluctuate with environmental Mg^{2+} concentrations (*281*). Given these concentrations the ratio of ADP:Mg.ADP would change from 1:0.15 at 0.1mM free Mg^{2+} to 1:1.5 at 1mM (Figure 75); this is therefore a very important factor in SNF1 regulation.

Even total concentrations of adenine nucleotides in *S.cerevisiae* are not high enough to completely saturate the regulatory site. Mg.ATP (present at mM concentrations) binds SNF1 very weakly (K_d >2.5mM) at the regulatory site and most (>95% for a free Mg^{2+} concentration of 1mM) of the cellular ATP will be present as this species. As noted above,

the concentrations of ADP/Mg.ADP will depend on the free Mg^{2+} concentration but even at low [Mg^{2+}] the ADP concentration (in which case most ADP is free and this form binds more tightly) would not be high enough to saturate the regulatory site.
It therefore seems that SNF1 may simply act as a direct sensor of ADP/Mg.ADP concentrations, and that the binding of ATP is not physiologically relevant.

In the majority of documented cases of ATP depletion the ADP concentrations actually fluctuate around a rather narrow range, and any increases are transient. Perhaps the sensitivity of SNF1 activation is such that these small ADP concentrations are sufficient to stimulate the relevant downstream pathways, microenvironmental ADP concentrations play a role or perhaps the methods used to determine cellular nucleotide concentrations are an inaccurate representation of the real cellular state.

Nonetheless it is clear that ADP is a key activator of SNF1. Of course, SNF1 activation is mediated by numerous factors in addition to ADP increases, such as cellular localisation of SNF1, β-subunit isoform, availability of substrates, and post-translational modifications (phosphorylation, myristoylation and acetylation). The kinetics of the upstream kinases and phosphatase(s), their localisation and concentration are also integral to controlling the extent of SNF1 activation.

	Kd_I (μM)	**Kd_{II} (μM)**	**Kd_I (μM)**
C-AXP	9.1 (C-ADP)	30.7 (C-ADP)	11.8 (C-ATP)
C-AXP 5mM $MgCl_2$	45.1 (C-ADP)	95.9 (C-ADP)	41.6 (C-ATP)
Ratio	*5-fold*	*3-fold*	*3.5-fold*
AXP	91 (ADP)	760 (ADP)	85 (ATP)
AXP (5mM $MgCl_2$)	*451 (ADP)*	*2374 (ADP)*	*299 (ATP)*

Table 24: Estimation of Mg.AXP K_d values.

Equilibrium binding constants were determined as described in Appendix 1.2.2 and displayed in Table 16 (row 2), Table 19 (row 3) and Table 17 (row 5). The fold decrease in affinity of C-AXP compared to Mg.C-AXP affinity and the estimated binding constants for Mg.AXP species are italicised.

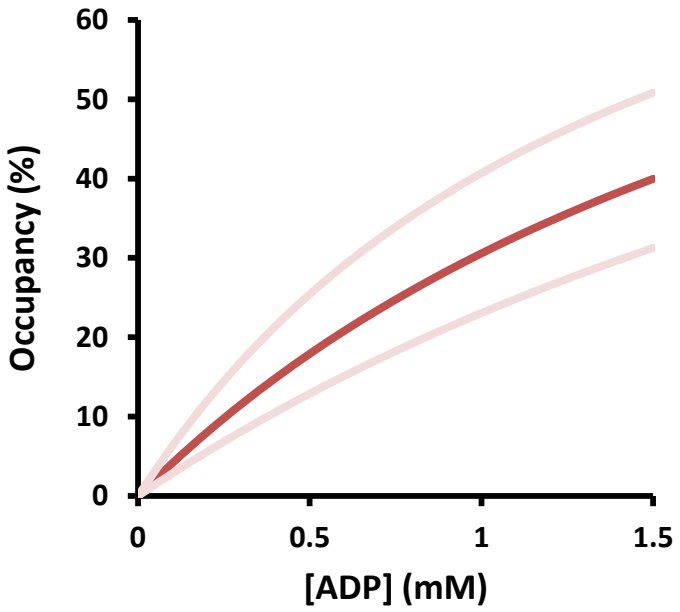

Figure 74: % occupancy of SNF1 nucleotide binding sites.

% occupancy of the second, weaker, site by Mg.ADP/ADP (red), calculated from K_d values in Table 24. **±** experimentally determined error measurements (light red) (Table 16 and Table 17).

Input: 0mM NADH, 0mM AMP, 0mM ATP, 0.00825mM SNF1, 10mM $MgCl_2$, 0mM $CaCl_2$, pH 7.5.

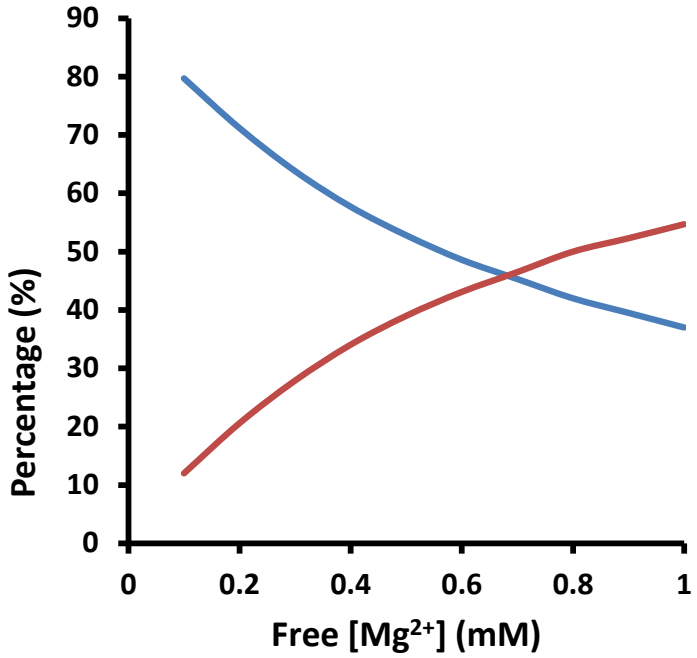

Figure 75: ADP and Mg.ADP species.

% free ADP (blue) and % Mg.ADP (red) species over the excepted eukaryotic range of free Mg^{2+} concentrations. Starting AXP values taken from (*336*), wild-type *S.cerevisiae* cells grown on Trehalose media (1.06mM AMP, 2.5mM ADP, 4mM ATP).

References

1. Xiao, B., Sanders, M. J., Underwood, E., Heath, R., Mayer, F. V., Carmena, D., Jing, C., Walker, P. A., Eccleston, J. F., Haire, L. F., Saiu, P., Howell, S. A., Aasland, R., Martin, S. R., Carling, D., and Gamblin, S. J. (2011) Structure of mammalian AMPK and its regulation by ADP, *Nature 472*, 230-233.
2. Mayer, F. V., Heath, R., Underwood, E., Sanders, M. J., Carmena, D., McCartney, R. R., Leiper, F. C., Xiao, B., Jing, C., Walker, P. A., Haire, L. F., Ogrodowicz, R., Martin, S. R., Schmidt, M. C., Gamblin, S. J., and Carling, D. (2011) ADP regulates SNF1, the Saccharomyces cerevisiae homolog of AMP-activated protein kinase, *Cell Metab 14*, 707-714.
3. Kahn, B. B., Alquier, T., Carling, D., and Hardie, D. G. (2005) AMP-activated protein kinase: Ancient energy gauge provides clues to modern understanding of metabolism, *Cell Metabolism 1*, 15-25.
4. Zhang, B. B., Zhou, G., and Li, C. (2009) AMPK: An Emerging Drug Target for Diabetes and the Metabolic Syndrome, *Cell Metabolism 9*, 407-416.
5. Hardie, D. G., and Carling, D. (1997) The AMP-activated protein kinase - Fuel gauge of the mammalian cell?, *European Journal of Biochemistry 246*, 259-273.
6. Carlson, M., Osmond, B. C., and Botstein, D. (1981) Mutants of yeast defective in sucrose utilization, *Genetics 98*, 25-40.
7. Hardie, D. G. (2008) AMPK: a key regulator of energy balance in the single cell and the whole organism, *International Journal of Obesity 32*, S7-S12.
8. Hardie, D. G., Scott, J. W., Pan, D. A., and Hudson, E. R. (2003) Management of cellular energy by the AMP-activated protein kinase system, *FEBS Letters 546*, 113-120.
9. Huang, S., and Czech, M. P. (2007) The GLUT4 glucose transporter, *Cell Metab 5*, 237-252.
10. Kurth-Kraczek, E. J., Hirshman, M. F., Goodyear, L. J., and Winder, W. W. (1999) 5' AMP-activated protein kinase activation causes GLUT4 translocation in skeletal muscle, *Diabetes 48*, 1667-1671.
11. Ojuka, E. O., Nolte, L. A., and Holloszy, J. O. (2000) Increased expression of GLUT-4 and hexokinase in rat epitrochlearis muscles exposed to AICAR in vitro, *J Appl Physiol 88*, 1072-1075.
12. Russell, R. R., 3rd, Bergeron, R., Shulman, G. I., and Young, L. H. (1999) Translocation of myocardial GLUT-4 and increased glucose uptake through activation of AMPK by AICAR, *Am J Physiol 277*, H643-649.
13. Barnes, K., Ingram, J. C., Porras, O. H., Barros, L. F., Hudson, E. R., Fryer, L. G. D., Foufelle, F., Carling, D., Hardie, D. G., and Baldwin, S. A. (2002) Activation of GLUT1 by metabolic and osmotic stress: potential involvement of AMP-activated protein kinase (AMPK), *Journal of Cell Science 115*, 2433-2442.
14. Mu, J., Brozinick, J. T., Jr., Valladares, O., Bucan, M., and Birnbaum, M. J. (2001) A role for AMP-activated protein kinase in contraction- and hypoxia-regulated glucose transport in skeletal muscle, *Mol Cell 7*, 1085-1094.
15. Sakamoto, K., and Holman, G. D. (2008) Emerging role for AS160/TBC1D4 and TBC1D1 in the regulation of GLUT4 traffic, *Am J Physiol Endocrinol Metab 295*, E29-37.
16. Zaid, H., Antonescu, C. N., Randhawa, V. K., and Klip, A. (2008) Insulin action on glucose transporters through molecular switches, tracks and tethers, *Biochem J 413*, 201-215.

17. Jakobsen, S. N., Hardie, D. G., Morrice, N., and Tornqvist, H. E. (2001) 5'-AMP-activated protein kinase phosphorylates IRS-1 on Ser-789 in mouse C2C12 myotubes in response to 5-aminoimidazole-4-carboxamide riboside, *Journal of Biological Chemistry 276*, 46912-46916.
18. Wang, C., Mao, X., Wang, L., Liu, M., Wetzel, M. D., Guan, K. L., Dong, L. Q., and Liu, F. (2007) Adiponectin sensitizes insulin signaling by reducing p70 S6 kinase-mediated serine phosphorylation of IRS-1, *J Biol Chem 282*, 7991-7996.
19. Zheng, D., MacLean, P. S., Pohnert, S. C., Knight, J. B., Olson, A. L., Winder, W. W., and Dohm, G. L. (2001) Regulation of muscle GLUT-4 transcription by AMP-activated protein kinase, *J Appl Physiol 91*, 1073-1083.
20. McGee, S. L., and Hargreaves, M. AMPK-mediated regulation of transcription in skeletal muscle, *Clin Sci (Lond) 118*, 507-518.
21. Carling, D., and Hardie, D. G. (1989) The substrate and sequence specificity of the amp-activated protein-kinase - phosphorylation of glycogen-synthase and phosphorylase-kinase, *Biochimica et Biophysica Acta 1012*, 81-86.
22. Aschenbach, W. G., Hirshman, M. F., Fujii, N., Sakamoto, K., Howlett, K. F., and Goodyear, L. J. (2002) Effect of AICAR treatment on glycogen metabolism in skeletal muscle, *Diabetes 51*, 567-573.
23. Marsin, A. S., Bouzin, C., Bertrand, L., and Hue, L. (2002) The stimulation of glycolysis by hypoxia in activated monocytes is mediated by AMP-activated protein kinase and inducible 6-phosphofructo-2-kinase, *J Biol Chem 277*, 30778-30783.
24. Marsin, A. S., Bertrand, L., Rider, M. H., Deprez, J., Beauloye, C., Vincent, M. F., Van den Berghe, G., Carling, D., and Hue, L. (2000) Phosphorylation and activation of heart PFK-2 by AMPK has a role in the stimulation of glycolysis during ischaemia, *Curr Biol 10*, 1247-1255.
25. Tuerk, R. D., Thali, R. F., Auchli, Y., Rechsteiner, H., Brunisholz, R. A., Schlattner, U., Wallimann, T., and Neumann, D. (2007) New candidate targets of AMP-activated protein kinase in murine brain revealed by a novel multidimensional substrate-screen for protein kinases, *J Proteome Res 6*, 3266-3277.
26. Hong, Y. H., Varanasi, U. S., Yang, W., and Leff, T. (2003) AMP-activated protein kinase regulates HNF4alpha transcriptional activity by inhibiting dimer formation and decreasing protein stability, *J Biol Chem 278*, 27495-27501.
27. Kawaguchi, T., Osatomi, K., Yamashita, H., Kabashima, T., and Uyeda, K. (2002) Mechanism for fatty acid "sparing" effect on glucose-induced transcription: regulation of carbohydrate-responsive element-binding protein by AMP-activated protein kinase, *J Biol Chem 277*, 3829-3835.
28. Leclerc, I., Lenzner, C., Gourdon, L., Vaulont, S., Kahn, A., and Viollet, B. (2001) Hepatocyte nuclear factor-4alpha involved in type 1 maturity-onset diabetes of the young is a novel target of AMP-activated protein kinase, *Diabetes 50*, 1515-1521.
29. Koo, S. H., Flechner, L., Qi, L., Zhang, X., Screaton, R. A., Jeffries, S., Hedrick, S., Xu, W., Boussouar, F., Brindle, P., Takemori, H., and Montminy, M. (2005) The CREB coactivator TORC2 is a key regulator of fasting glucose metabolism, *Nature 437*, 1109-1111.
30. Screaton, R. A., Conkright, M. D., Katoh, Y., Best, J. L., Canettieri, G., Jeffries, S., Guzman, E., Niessen, S., Yates, J. R., 3rd, Takemori, H., Okamoto, M., and Montminy, M. (2004) The CREB coactivator TORC2 functions as a calcium- and cAMP-sensitive coincidence detector, *Cell 119*, 61-74.
31. Viollet, B., Andreelli, F., Jorgensen, S. B., Perrin, C., Flamez, D., Mu, J., Wojtaszewski, J. F., Schuit, F. C., Birnbaum, M., Richter, E., Burcelin, R., and Vaulont, S. (2003)

Physiological role of AMP-activated protein kinase (AMPK): insights from knockout mouse models, *Biochemical Society Transactions 31*, 216-219.

32. Long, Y. C., Barnes, B. R., Mahlapuu, M., Steiler, T. L., Martinsson, S., Leng, Y., Wallberg-Henriksson, H., Andersson, L., and Zierath, J. R. (2005) Role of AMP-activated protein kinase in the coordinated expression of genes controlling glucose and lipid metabolism in mouse white skeletal muscle, *Diabetologia 48*, 2354-2364.
33. Bonen, A., Han, X. X., Habets, D. D., Febbraio, M., Glatz, J. F., and Luiken, J. J. (2007) A null mutation in skeletal muscle FAT/CD36 reveals its essential role in insulin- and AICAR-stimulated fatty acid metabolism, *Am J Physiol Endocrinol Metab 292*, E1740-1749.
34. Carling, D., Clarke, P. R., Zammit, V. A., and Hardie, D. G. (1989) Purification and characterization of the AMP-activated protein kinase. Copurification of acetyl-CoA carboxylase kinase and 3-hydroxy-3-methylglutaryl-CoA reductase kinase activities, *European Journal of Biochemistry 186*, 129-136.
35. Hardie, D. G., and Pan, D. A. (2002) Regulation of fatty acid synthesis and oxidation by the AMP-activated protein kinase, *Biochem Soc Trans 30*, 1064-1070.
36. Saha, A. K., and Ruderman, N. B. (2003) Malonyl-CoA and AMP-activated protein kinase: an expanding partnership, *Mol Cell Biochem 253*, 65-70.
37. Foretz, M., Carling, D., Guichard, C., Ferre, P., and Foufelle, F. (1998) AMP-activated protein kinase inhibits the glucose-activated expression of fatty acid synthase gene in rat hepatocytes, *J Biol Chem 273*, 14767-14771.
38. Woods, A., Azzout-Marniche, D., Foretz, M., Stein, S. C., Lemarchand, P., Ferre, P., Foufelle, F., and Carling, D. (2000) Characterization of the role of AMP-activated protein kinase in the regulation of glucose-activated gene expression using constitutively active and dominant negative forms of the kinase, *Molecular and Cellular Biology 20*, 6704-6711.
39. Horton, J. D., Goldstein, J. L., and Brown, M. S. (2002) SREBPs: activators of the complete program of cholesterol and fatty acid synthesis in the liver, *J Clin Invest 109*, 1125-1131.
40. Park, K. G., Min, A. K., Koh, E. H., Kim, H. S., Kim, M. O., Park, H. S., Kim, Y. D., Yoon, T. S., Jang, B. K., Hwang, J. S., Kim, J. B., Choi, H. S., Park, J. Y., Lee, I. K., and Lee, K. U. (2008) Alpha-lipoic acid decreases hepatic lipogenesis through adenosine monophosphate-activated protein kinase (AMPK)-dependent and AMPK-independent pathways, *Hepatology 48*, 1477-1486.
41. An, Z., Wang, H., Song, P., Zhang, M., Geng, X., and Zou, M. H. (2007) Nicotine-induced activation of AMP-activated protein kinase inhibits fatty acid synthase in 3T3L1 adipocytes: a role for oxidant stress, *J Biol Chem 282*, 26793-26801.
42. Ren, J., Pulakat, L., Whaley-Connell, A., and Sowers, J. R. (2010) Mitochondrial biogenesis in the metabolic syndrome and cardiovascular disease, *J Mol Med (Berl) 88*, 993-1001.
43. Cool, B., Zinker, B., Chiou, W., Kifle, L., Cao, N., Perham, M., Dickinson, R., Adler, A., Gagne, G., Iyengar, R., Zhao, G., Marsh, K., Kym, P., Jung, P., Camp, H. S., and Frevert, E. (2006) Identification and characterization of a small molecule AMPK activator that treats key components of type 2 diabetes and the metabolic syndrome, *Cell Metab 3*, 403-416.
44. Steinberg, G. R., Michell, B. J., van Denderen, B. J., Watt, M. J., Carey, A. L., Fam, B. C., Andrikopoulos, S., Proietto, J., Gorgun, C. Z., Carling, D., Hotamisligil, G. S., Febbraio, M. A., Kay, T. W., and Kemp, B. E. (2006) Tumor necrosis factor alpha-induced skeletal muscle insulin resistance involves suppression of AMP-kinase signaling, *Cell Metab 4*, 465-474.

45. Carling, D., Zammit, V. A., and Hardie, D. G. (1987) A common bicyclic protein kinase cascade inactivates the regulatory enzymes of fatty acid and cholesterol biosynthesis, *FEBS Lett 223*, 217-222.
46. Steinberg, G. R., and Kemp, B. E. (2009) AMPK in Health and Disease, *Physiological Reviews 89*, 1025-1078.
47. Dowling, R. J., Topisirovic, I., Fonseca, B. D., and Sonenberg, N. (2010) Dissecting the role of mTOR: lessons from mTOR inhibitors, *Biochim Biophys Acta 1804*, 433-439.
48. Inoki, K., Li, Y., Xu, T., and Guan, K. L. (2003) Rheb GTPase is a direct target of TSC2 GAP activity and regulates mTOR signaling, *Genes Dev 17*, 1829-1834.
49. Gwinn, D. M., Shackelford, D. B., Egan, D. F., Mihaylova, M. M., Mery, A., Vasquez, D. S., Turk, B. E., and Shaw, R. J. (2008) AMPK phosphorylation of raptor mediates a metabolic checkpoint, *Molecular Cell 30*, 214-226.
50. Horman, S., Browne, G., Krause, U., Patel, J., Vertommen, D., Bertrand, L., Lavoinne, A., Hue, L., Proud, C., and Rider, M. (2002) Activation of AMP-activated protein kinase leads to the phosphorylation of elongation factor 2 and an inhibition of protein synthesis, *Curr Biol 12*, 1419-1423.
51. Hoppe, S., Bierhoff, H., Cado, I., Weber, A., Tiebe, M., Grummt, I., and Voit, R. (2009) AMP-activated protein kinase adapts rRNA synthesis to cellular energy supply, *Proc Natl Acad Sci U S A 106*, 17781-17786.
52. Weisova, P., Concannon, C. G., Devocelle, M., Prehn, J. H., and Ward, M. W. (2009) Regulation of glucose transporter 3 surface expression by the AMP-activated protein kinase mediates tolerance to glutamate excitation in neurons, *J Neurosci 29*, 2997-3008.
53. Concannon, C. G., Tuffy, L. P., Weisova, P., Bonner, H. P., Davila, D., Bonner, C., Devocelle, M. C., Strasser, A., Ward, M. W., and Prehn, J. H. (2010) AMP kinase-mediated activation of the BH3-only protein Bim couples energy depletion to stress-induced apoptosis, *J Cell Biol 189*, 83-94.
54. Imamura, K., Ogura, T., Kishimoto, A., Kaminishi, M., and Esumi, H. (2001) Cell cycle regulation via p53 phosphorylation by a 5'-AMP activated protein kinase activator, 5-aminoimidazole- 4-carboxamide-1-beta-D-ribofuranoside, in a human hepatocellular carcinoma cell line, *Biochem Biophys Res Commun 287*, 562-567.
55. Fullerton, M. D., Steinberg, G. R., and Schertzer, J. D. (2012) Immunometabolism of AMPK in insulin resistance and atherosclerosis, *Mol Cell Endocrinol*.
56. Jones, R. G., Plas, D. R., Kubek, S., Buzzai, M., Mu, J., Xu, Y., Birnbaum, M. J., and Thompson, C. B. (2005) AMP-activated protein kinase induces a p53-dependent metabolic checkpoint, *Mol Cell 18*, 283-293.
57. Lee, D. H., Lee, T. H., Jung, C. H., and Kim, Y. H. (2012) Wogonin induces apoptosis by activating the AMPK and p53 signaling pathways in human glioblastoma cells, *Cell Signal*.
58. Wang, W., Fan, J., Yang, X., Furer-Galban, S., de Silanes, I. L., von Kobbe, C., Guo, J., Georas, S. N., Foufelle, F., Hardie, D. G., Carling, D., and Gorospe, M. (2002) AMP-activated kinase regulates cytoplasmic HuR, *Molecular and Cellular Biology 22*, 3425-3436.
59. Findlay, G. M., Harrington, L. S., and Lamb, R. F. (2005) TSC1-2 tumour suppressor and regulation of mTOR signalling: linking cell growth and proliferation?, *Curr Opin Genet Dev 15*, 69-76.
60. Eckel, R. H., Grundy, S. M., and Zimmet, P. Z. (2005) The metabolic syndrome, *Lancet 365*, 1415-1428.

61. Azizi, F., Salehi, P., Etemadi, A., and Zahedi-Asl, S. (2003) Prevalence of metabolic syndrome in an urban population: Tehran Lipid and Glucose Study, *Diabetes Res Clin Pract 61*, 29-37.
62. Steinberg, G. R., Smith, A. C., Van Denderen, B. J., Chen, Z., Murthy, S., Campbell, D. J., Heigenhauser, G. J., Dyck, D. J., and Kemp, B. E. (2004) AMP-activated protein kinase is not down-regulated in human skeletal muscle of obese females, *J Clin Endocrinol Metab 89*, 4575-4580.
63. Minokoshi, Y., Alquier, T., Furukawa, N., Kim, Y. B., Lee, A., Xue, B., Mu, J., Foufelle, F., Ferre, P., Birnbaum, M. J., Stuck, B. J., and Kahn, B. B. (2004) AMP-kinase regulates food intake by responding to hormonal and nutrient signals in the hypothalamus, *Nature 428*, 569-574.
64. Blanco Martinez de Morentin, P., Gonzalez, C. R., Saha, A. K., Martins, L., Dieguez, C., Vidal-Puig, A., Tena-Sempere, M., and Lopez, M. (2011) Hypothalamic AMP-activated protein kinase as a mediator of whole body energy balance, *Rev Endocr Metab Disord 12*, 127-140.
65. Claret, M., Smith, M. A., Batterham, R. L., Selman, C., Choudhury, A. I., Fryer, L. G., Clements, M., Al-Qassab, H., Heffron, H., Xu, A. W., Speakman, J. R., Barsh, G. S., Viollet, B., Vaulont, S., Ashford, M. L., Carling, D., and Withers, D. J. (2007) AMPK is essential for energy homeostasis regulation and glucose sensing by POMC and AgRP neurons, *J Clin Invest 117*, 2325-2336.
66. Zhou, G., Myers, R., Li, Y., Chen, Y., Shen, X., Fenyk-Melody, J., Wu, M., Ventre, J., Doebber, T., Fujii, N., Musi, N., Hirshman, M. F., Goodyear, L. J., and Moller, D. E. (2001) Role of AMP-activated protein kinase in mechanism of metformin action, *J Clin Invest 108*, 1167-1174.
67. Fryer, L. G. D., Parbu-Patel, A., and Carling, D. (2002) The anti-diabetic drugs rosiglitazone and metformin stimulate AMP-activated protein kinase through distinct signaling pathways, *Journal of Biological Chemistry 277*, 25226-25232.
68. Halseth, A. E., Ensor, N. J., White, T. A., Ross, S. A., and Gulve, E. A. (2002) Acute and chronic treatment of ob/ob and db/db mice with AICAR decreases blood glucose concentrations, *Biochem Biophys Res Commun 294*, 798-805.
69. Fujii, N., Jessen, N., and Goodyear, L. J. (2006) AMP-activated protein kinase and the regulation of glucose transport, *Am J Physiol Endocrinol Metab 291*, E867-877.
70. Bergeron, R., Previs, S. F., Cline, G. W., Perret, P., Russell, R. R., 3rd, Young, L. H., and Shulman, G. I. (2001) Effect of 5-aminoimidazole-4-carboxamide-1-beta-D-ribofuranoside infusion on in vivo glucose and lipid metabolism in lean and obese Zucker rats, *Diabetes 50*, 1076-1082.
71. Evans, J. M., Donnelly, L. A., Emslie-Smith, A. M., Alessi, D. R., and Morris, A. D. (2005) Metformin and reduced risk of cancer in diabetic patients, *BMJ 330*, 1304-1305.
72. Hadad, S. M., Fleming, S., and Thompson, A. M. (2008) Targeting AMPK: a new therapeutic opportunity in breast cancer, *Crit Rev Oncol Hematol 67*, 1-7.
73. Zakikhani, M., Dowling, R., Fantus, I. G., Sonenberg, N., and Pollak, M. (2006) Metformin is an AMP kinase-dependent growth inhibitor for breast cancer cells, *Cancer Res 66*, 10269-10273.
74. Swinnen, J. V., Beckers, A., Brusselmans, K., Organe, S., Segers, J., Timmermans, L., Vanderhoydonc, F., Deboel, L., Derua, R., Waelkens, E., De Schrijver, E., Van de Sande, T., Noel, A., Foufelle, F., and Verhoeven, G. (2005) Mimicry of a cellular low energy status blocks tumor cell anabolism and suppresses the malignant phenotype, *Cancer Res 65*, 2441-2448.

75. Brown, K. A., Samarajeewa, N. U., and Simpson, E. R. (2012) Endocrine-related cancers and the role of AMPK, *Mol Cell Endocrinol*.
76. Hadad, S. M., Appleyard, V., and Thompson, A. M. (2009) Therapeutic metformin/AMPK activation promotes the angiogenic phenotype in the ERalpha negative MDA-MB-435 breast cancer model, *Breast Cancer Res Treat 114*, 391.
77. Hadad, S., Iwamoto, T., Jordan, L., Purdie, C., Bray, S., Baker, L., Jellema, G., Deharo, S., Hardie, D. G., Pusztai, L., Moulder-Thompson, S., Dewar, J. A., and Thompson, A. M. (2011) Evidence for biological effects of metformin in operable breast cancer: a pre-operative, window-of-opportunity, randomized trial, *Breast Cancer Res Treat 128*, 783-794.
78. Kato, K., Ogura, T., Kishimoto, A., Minegishi, Y., Nakajima, N., Miyazaki, M., and Esumi, H. (2002) Critical roles of AMP-activated protein kinase in constitutive tolerance of cancer cells to nutrient deprivation and tumor formation, *Oncogene 21*, 6082-6090.
79. Laderoute, K. R., Amin, K., Calaoagan, J. M., Knapp, M., Le, T., Orduna, J., Foretz, M., and Viollet, B. (2006) 5'-AMP-activated protein kinase (AMPK) is induced by low-oxygen and glucose deprivation conditions found in solid-tumor microenvironments, *Mol Cell Biol 26*, 5336-5347.
80. Jeon, S. M., Chandel, N. S., and Hay, N. (2012) AMPK regulates NADPH homeostasis to promote tumour cell survival during energy stress, *Nature 485*, 661-665.
81. Coven, D. L., Hu, X., Cong, L., Bergeron, R., Shulman, G. I., Hardie, D. G., and Young, L. H. (2003) Physiological role of AMP-activated protein kinase in the heart: graded activation during exercise, *Am J Physiol Endocrinol Metab 285*, E629-636.
82. Dyck, J. R., and Lopaschuk, G. D. (2006) AMPK alterations in cardiac physiology and pathology: enemy or ally?, *J Physiol 574*, 95-112.
83. Arad, M., Seidman, C. E., and Seidman, J. G. (2007) AMP-activated protein kinase in the heart: role during health and disease, *Circ Res 100*, 474-488.
84. Milan, D., Jeon, J. T., Looft, C., Amarger, V., Robic, A., Thelander, M., Rogel-Gaillard, C., Paul, S., Iannuccelli, N., Rask, L., Ronne, H., Lundstrom, K., Reinsch, N., Gellin, J., Kalm, E., Roy, P. L., Chardon, P., and Andersson, L. (2000) A mutation in PRKAG3 associated with excess glycogen content in pig skeletal muscle, *Science 288*, 1248-1251.
85. Daniel, T., and Carling, D. (2002) Functional analysis of mutations in the gamma 2 subunit of AMP-activated protein kinase associated with cardiac hypertrophy and Wolff-Parkinson-White syndrome, *Journal of Biological Chemistry 277*, 51017-51024.
86. Scott, J. W., Hawley, S. A., Green, K. A., Anis, M., Stewart, G., Scullion, G. A., Norman, D. G., and Hardie, D. G. (2004) CBS domains form energy-sensing modules whose binding of adenosine ligands is disrupted by disease mutations, *Journal of Clinical Investigation 113*, 274-284.
87. Xiao, B., Heath, R., Saiu, P., Leiper, F. C., Leone, P., Jing, C., Walker, P. A., Haire, L., Eccleston, J. F., Davis, C. T., Martin, S. R., Carling, D., and Gamblin, S. J. (2007) Structural basis for AMP binding to mammalian AMP-activated protein kinase, *Nature 449*, 496-U414.
88. Mosconi, L., Pupi, A., and De Leon, M. J. (2008) Brain glucose hypometabolism and oxidative stress in preclinical Alzheimer's disease, *Ann N Y Acad Sci 1147*, 180-195.
89. Ballard, C., Gauthier, S., Corbett, A., Brayne, C., Aarsland, D., and Jones, E. (2011) Alzheimer's disease, *Lancet 377*, 1019-1031.

90. Salminen, A., Kaarniranta, K., Haapasalo, A., Soininen, H., and Hiltunen, M. (2011) AMP-activated protein kinase: a potential player in Alzheimer's disease, *J Neurochem 118*, 460-474.
91. Liu, Y., Liu, F., Iqbal, K., Grundke-Iqbal, I., and Gong, C. X. (2008) Decreased glucose transporters correlate to abnormal hyperphosphorylation of tau in Alzheimer disease, *FEBS Lett 582*, 359-364.
92. Thornton, C., Bright, N. J., Sastre, M., Muckett, P. J., and Carling, D. (2011) AMP-activated protein kinase (AMPK) is a tau kinase, activated in response to amyloid beta-peptide exposure, *Biochem J 434*, 503-512.
93. Vingtdeux, V., Davies, P., Dickson, D. W., and Marambaud, P. (2011) AMPK is abnormally activated in tangle- and pre-tangle-bearing neurons in Alzheimer's disease and other tauopathies, *Acta Neuropathol 121*, 337-349.
94. Greco, S. J., Sarkar, S., Casadesus, G., Zhu, X., Smith, M. A., Ashford, J. W., Johnston, J. M., and Tezapsidis, N. (2009) Leptin inhibits glycogen synthase kinase-3beta to prevent tau phosphorylation in neuronal cells, *Neurosci Lett 455*, 191-194.
95. Greco, S. J., Sarkar, S., Johnston, J. M., and Tezapsidis, N. (2009) Leptin regulates tau phosphorylation and amyloid through AMPK in neuronal cells, *Biochem Biophys Res Commun 380*, 98-104.
96. Won, J. S., Im, Y. B., Kim, J., Singh, A. K., and Singh, I. (2010) Involvement of AMP-activated-protein-kinase (AMPK) in neuronal amyloidogenesis, *Biochem Biophys Res Commun 399*, 487-491.
97. Vingtdeux, V., Giliberto, L., Zhao, H., Chandakkar, P., Wu, Q., Simon, J. E., Janle, E. M., Lobo, J., Ferruzzi, M. G., Davies, P., and Marambaud, P. (2010) AMP-activated protein kinase signaling activation by resveratrol modulates amyloid-beta peptide metabolism, *J Biol Chem 285*, 9100-9113.
98. Donmez, G., Wang, D., Cohen, D. E., and Guarente, L. (2010) SIRT1 suppresses beta-amyloid production by activating the alpha-secretase gene ADAM10, *Cell 142*, 320-332.
99. Li, J., Zeng, Z., Viollet, B., Ronnett, G. V., and McCullough, L. D. (2007) Neuroprotective effects of adenosine monophosphate-activated protein kinase inhibition and gene deletion in stroke, *Stroke 38*, 2992-2999.
100. Reznick, R. M., Zong, H., Li, J., Morino, K., Moore, I. K., Yu, H. J., Liu, Z. X., Dong, J., Mustard, K. J., Hawley, S. A., Befroy, D., Pypaert, M., Hardie, D. G., Young, L. H., and Shulman, G. I. (2007) Aging-associated reductions in AMP-activated protein kinase activity and mitochondrial biogenesis, *Cell Metab 5*, 151-156.
101. Qiang, W., Weiqiang, K., Qing, Z., Pengju, Z., and Yi, L. (2007) Aging impairs insulin-stimulated glucose uptake in rat skeletal muscle via suppressing AMPKalpha, *Exp Mol Med 39*, 535-543.
102. Turdi, S., Fan, X., Li, J., Zhao, J., Huff, A. F., Du, M., and Ren, J. (2010) AMP-activated protein kinase deficiency exacerbates aging-induced myocardial contractile dysfunction, *Aging Cell 9*, 592-606.
103. Liu, F., Benashski, S. E., Persky, R., Xu, Y., Li, J., and McCullough, L. D. (2011) Age-related changes in AMP-activated protein kinase after stroke, *Age (Dordr)*.
104. Cutler, R. G., Kelly, J., Storie, K., Pedersen, W. A., Tammara, A., Hatanpaa, K., Troncoso, J. C., and Mattson, M. P. (2004) Involvement of oxidative stress-induced abnormalities in ceramide and cholesterol metabolism in brain aging and Alzheimer's disease, *Proc Natl Acad Sci U S A 101*, 2070-2075.
105. Haus, J. M., Kashyap, S. R., Kasumov, T., Zhang, R., Kelly, K. R., Defronzo, R. A., and Kirwan, J. P. (2009) Plasma ceramides are elevated in obese subjects with type 2 diabetes and correlate with the severity of insulin resistance, *Diabetes 58*, 337-343.

106. Palestini, P., Masserini, M., Fiorilli, A., Calappi, E., and Tettamanti, G. (1993) Age-related changes in the ceramide composition of the major gangliosides present in rat brain subcellular fractions enriched in plasma membranes of neuronal and myelin origin, *J Neurochem 61*, 955-960.
107. Lee, J. W., Park, S., Takahashi, Y., and Wang, H. G. (2010) The association of AMPK with ULK1 regulates autophagy, *PLoS One 5*, e15394.
108. Kim, J., Kundu, M., Viollet, B., and Guan, K. L. (2011) AMPK and mTOR regulate autophagy through direct phosphorylation of Ulk1, *Nat Cell Biol 13*, 132-141.
109. He, C., Bassik, M. C., Moresi, V., Sun, K., Wei, Y., Zou, Z., An, Z., Loh, J., Fisher, J., Sun, Q., Korsmeyer, S., Packer, M., May, H. I., Hill, J. A., Virgin, H. W., Gilpin, C., Xiao, G., Bassel-Duby, R., Scherer, P. E., and Levine, B. (2012) Exercise-induced BCL2-regulated autophagy is required for muscle glucose homeostasis, *Nature 481*, 511-515.
110. Greer, E. L., Dowlatshahi, D., Banko, M. R., Villen, J., Hoang, K., Blanchard, D., Gygi, S. P., and Brunet, A. (2007) An AMPK-FOXO pathway mediates longevity induced by a novel method of dietary restriction in C. elegans, *Curr Biol 17*, 1646-1656.
111. Hashimoto, Y., and Soderling, T. R. (1989) Regulation of calcineurin by phosphorylation. Identification of the regulatory site phosphorylated by Ca2+/calmodulin-dependent protein kinase II and protein kinase C, *J Biol Chem 264*, 16524-16529.
112. Altarejos, J. Y., and Montminy, M. (2011) CREB and the CRTC co-activators: sensors for hormonal and metabolic signals, *Nat Rev Mol Cell Biol 12*, 141-151.
113. Blagosklonny, M. V. (2009) Inhibition of S6K by resveratrol: in search of the purpose, *Aging (Albany NY) 1*, 511-514.
114. Selman, C., Tullet, J. M., Wieser, D., Irvine, E., Lingard, S. J., Choudhury, A. I., Claret, M., Al-Qassab, H., Carmignac, D., Ramadani, F., Woods, A., Robinson, I. C., Schuster, E., Batterham, R. L., Kozma, S. C., Thomas, G., Carling, D., Okkenhaug, K., Thornton, J. M., Partridge, L., Gems, D., and Withers, D. J. (2009) Ribosomal protein S6 kinase 1 signaling regulates mammalian life span, *Science 326*, 140-144.
115. Anisimov, V. N., Berstein, L. M., Egormin, P. A., Piskunova, T. S., Popovich, I. G., Zabezhinski, M. A., Tyndyk, M. L., Yurova, M. V., Kovalenko, I. G., Poroshina, T. E., and Semenchenko, A. V. (2008) Metformin slows down aging and extends life span of female SHR mice, *Cell Cycle 7*, 2769-2773.
116. Carling, D., Thornton, C., Woods, A., and Sanders, M. J. (2012) AMP-activated protein kinase: new regulation, new roles?, *Biochem J 445*, 11-27.
117. Stapleton, D., Woollatt, E., Mitchelhill, K. I., Nicholl, J. K., Fernandez, C. S., Michell, B. J., Witters, L. A., Power, D. A., Sutherland, G. R., and Kemp, B. E. (1997) AMP-activated protein kinase isoenzyme family: Subunit structure and chromosomal location, *FEBS Letters 409*, 452-456.
118. Wojtaszewski, J. F., Nielsen, P., Hansen, B. F., Richter, E. A., and Kiens, B. (2000) Isoform-specific and exercise intensity-dependent activation of 5'-AMP-activated protein kinase in human skeletal muscle, *Journal of Physiology-London 528 Pt 1*, 221-226.
119. Birk, J. B., and Wojtaszewski, J. F. (2006) Predominant alpha2/beta2/gamma3 AMPK activation during exercise in human skeletal muscle, *Journal of Physiology-London 577*, 1021-1032.
120. Stapleton, D., Mitchelhill, K. I., Gao, G., Widmer, J., Michell, B. J., Teh, T., House, C. M., Fernandez, C. S., Cox, T., Witters, L. A., and Kemp, B. E. (1996) Mammalian AMP-activated protein kinase subfamily, *Journal of Biological Chemistry 271*, 611-614.

121. Salt, I., Celler, J. W., Hawley, S. A., Prescott, A., Woods, A., Carling, D., and Hardie, D. G. (1998) AMP-activated protein kinase: greater AMP dependence, and preferential nuclear localization, of complexes containing the alpha2 isoform, *Biochem J 334 (Pt 1)*, 177-187.
122. Suzuki, A., Okamoto, S., Lee, S., Saito, K., Shiuchi, T., and Minokoshi, Y. (2007) Leptin stimulates fatty acid oxidation and peroxisome proliferator-activated receptor alpha gene expression in mouse C2C12 myoblasts by changing the subcellular localization of the alpha2 form of AMP-activated protein kinase, *Mol Cell Biol 27*, 4317-4327.
123. Kazgan, N., Williams, T., Forsberg, L. J., and Brenman, J. E. Identification of a Nuclear Export Signal in the Catalytic Subunit of AMP-activated Protein Kinase, *Molecular Biology of the Cell*.
124. da Silva Xavier, G., Leclerc, I., Salt, I. P., Doiron, B., Hardie, D. G., Kahn, A., and Rutter, G. A. (2000) Role of AMP-activated protein kinase in the regulation by glucose of islet beta cell gene expression, *Proc Natl Acad Sci U S A 97*, 4023-4028.
125. Nolen, B., Taylor, S., and Ghosh, G. (2004) Regulation of Protein Kinases: Controlling Activity through Activation Segment Conformation, *Molecular Cell 15*, 661-675.
126. Oakhill, J. S., Scott, J. W., and Kemp, B. E. (2009) Structure and function of AMP-activated protein kinase, *Acta Physiologica 196*, 3-14.
127. Soderling, T. R. (1993) Protein kinases and phosphatases: regulation by autoinhibitory domains, *Biotechnol Appl Biochem 18 (Pt 2)*, 185-200.
128. Chen, L., Jiao, Z. H., Zheng, L. S., Zhang, Y. Y., Xie, S. T., Wang, Z. X., and Wu, J. W. (2009) Structural insight into the autoinhibition mechanism of AMP-activated protein kinase, *Nature 459*, 1146-U1139.
129. Rudolph, M. J., Amodeo, G. A., and Tong, L. (2010) An inhibited conformation for the protein kinase domain of the Saccharomyces cerevisiae AMPK homolog Snf1, *Acta Crystallogr Sect F Struct Biol Cryst Commun 66*, 999-1002.
130. Chen, Z., Heierhorst, J., Mann, R. J., Mitchelhill, K. I., Michell, B. J., Witters, L. A., Lynch, G. S., Kemp, B. E., and Stapleton, D. (1999) Expression of the AMP-activated protein kinase beta1 and beta2 subunits in skeletal muscle, *FEBS Letters 460*, 343-348.
131. Thornton, C., Snowden, M. A., and Carling, D. (1998) Identification of a novel AMP-activated protein kinase beta subunit isoform that is highly expressed in skeletal muscle, *Journal of Biological Chemistry 273*, 12443-12450.
132. Mitchelhill, K. I., Michell, B. J., House, C. M., Stapleton, D., Dyck, J., Gamble, J., Ullrich, C., Witters, L. A., and Kemp, B. E. (1997) Posttranslational modifications of the 5'-AMP-activated protein kinase beta1 subunit, *Journal of Biological Chemistry 272*, 24475-24479.
133. Oakhill, J. S., Chen, Z. P., Scott, J. W., Steel, R., Castelli, L. A., Ling, N., Macaulay, S. L., and Kemp, B. E. (2010) {beta}-Subunit myristoylation is the gatekeeper for initiating metabolic stress sensing by AMP-activated protein kinase (AMPK), *Proc Natl Acad Sci U S A*.
134. McBride, A., Ghilagaber, S., Nikolaev, A., and Hardie, D. G. (2009) The glycogen-binding domain on the AMPK beta subunit allows the kinase to act as a glycogen sensor, *Cell Metab 9*, 23-34.
135. Derave, W., Ai, H., Ihlemann, J., Witters, L. A., Kristiansen, S., Richter, E. A., and Ploug, T. (2000) Dissociation of AMP-activated protein kinase activation and glucose transport in contracting slow-twitch muscle, *Diabetes 49*, 1281-1287.
136. Polekhina, G., Gupta, A., van Denderen, B. J. W., Fell, S. C., Kemp, B. E., Stapleton, D., and Parker, M. W. (2005) Structural basis for glycogen recognition by AMP-activated protein kinase, *Structure 13*, 1453-1462.

137. Koay, A., Rimmer, K. A., Mertens, H. D. T., Gooley, P. R., and Stapleton, D. (2007) Oligosaccharide recognition and binding to the carbohydrate binding module of AMP-activated protein kinase, *FEBS Letters 581*, 5055-5059.
138. Cheung, P. C. F., Salt, I. P., Davies, S. P., Hardie, D. G., and Carling, D. (2000) Characterization of AMP-activated protein kinase gamma-subunit isoforms and their role in AMP binding, *Biochemical Journal 346*, 659-669.
139. Lang, T., Yu, L., Tu, Q., Jiang, J., Chen, Z., Xin, Y., Liu, G., and Zhao, S. (2000) Molecular cloning, genomic organization, and mapping of PRKAG2, a heart abundant gamma2 subunit of 5'-AMP-activated protein kinase, to human chromosome 7q36, *Genomics 70*, 258-263.
140. Kemp, B. E. (2004) Bateman domains and adenosine derivatives form a binding contract, *Journal of Clinical Investigation 113*, 182-184.
141. Turnley, A. M., Stapleton, D., Mann, R. J., Witters, L. A., Kemp, B. E., and Bartlett, P. F. (1999) Cellular distribution and developmental expression of AMP-activated protein kinase isoforms in mouse central nervous system, *J Neurochem 72*, 1707-1716.
142. Jin, X. S., Townley, R., and Shapiro, L. (2007) Structural insight into AMPK regulation: ADP comes into play, *Structure 15*, 1285-1295.
143. Rudolph, M. J., Amodeo, G. A., Iram, S. H., Hong, S. P., Pirino, G., Carlson, M., and Tong, L. (2007) Structure of the Bateman2 domain of yeast Snf4: dimeric association and relevance for AMP binding, *Structure 15*, 65-74.
144. Chen, L., Wang, J., Zhang, Y. Y., Yan, S. F., Neumann, D., Schlattner, U., Wang, Z. X., and Wu, J. W. (2012) AMP-activated protein kinase undergoes nucleotide-dependent conformational changes, *Nat Struct Mol Biol*.
145. Bateman, A. (1997) The structure of a domain common to archaebacteria and the homocystinuria disease protein, *Trends in Biochemical Sciences 22*, 12-13.
146. Kemp, B. E., Oakhill, J. S., and Scott, J. W. (2007) AMPK structure and regulation from three angles, *Structure 15*, 1161-1163.
147. Hong, S. P., Leiper, F. C., Woods, A., Carling, D., and Carlson, M. (2003) Activation of yeast Snf1 and mammalian AMP-activated protein kinase by upstream kinases, *Proceedings of the National Academy of Sciences of the United States of America 100*, 8839-8843.
148. Woods, A., Johnstone, S. R., Dickerson, K., Leiper, F. C., Fryer, L. G. D., Neumann, D., Schlattner, U., Wallimann, T., Carlson, M., and Carling, D. (2003) LKB1 is the upstream kinase in the AMP-activated protein kinase cascade, *Current Biology 13*, 2004-2008.
149. Hawley, S. A., Boudeau, J., Reid, J. L., Mustard, K. J., Udd, L., Makela, T. P., Alessi, D. R., and Hardie, D. G. (2003) Complexes between the LKB1 tumor suppressor, STRAD alpha/beta and MO25 alpha/beta are upstream kinases in the AMP-activated protein kinase cascade, *J Biol 2*, 28.
150. Woods, A., Johnstone, S. R., Dickerson, K., Leiper, F. C., Fryer, L. G., Neumann, D., Schlattner, U., Wallimann, T., Carlson, M., and Carling, D. (2003) LKB1 is the upstream kinase in the AMP-activated protein kinase cascade, *Curr Biol 13*, 2004-2008.
151. Alessi, D. R., Sakamoto, K., and Bayascas, J. R. (2006) LKB1-dependent signaling pathways, *Annu Rev Biochem 75*, 137-163.
152. Bouquin, N., Barral, Y., Courbeyrette, R., Blondel, M., Snyder, M., and Mann, C. (2000) Regulation of cytokinesis by the Elm1 protein kinase in Saccharomyces cerevisiae, *J Cell Sci 113 (Pt 8)*, 1435-1445.

153. Breeding, C. S., Hudson, J., Balasubramanian, M. K., Hemmingsen, S. M., Young, P. G., and Gould, K. L. (1998) The cdr2(+) gene encodes a regulator of G2/M progression and cytokinesis in Schizosaccharomyces pombe, *Mol Biol Cell 9*, 3399-3415.
154. Lizcano, J. M., Goransson, O., Toth, R., Deak, M., Morrice, N. A., Boudeau, J., Hawley, S. A., Udd, L., Makela, T. P., Hardie, D. G., and Alessi, D. R. (2004) LKB1 is a master kinase that activates 13 kinases of the AMPK subfamily, including MARK/PAR-1, *EMBO J 23*, 833-843.
155. Sakamoto, K., McCarthy, A., Smith, D., Green, K. A., Grahame Hardie, D., Ashworth, A., and Alessi, D. R. (2005) Deficiency of LKB1 in skeletal muscle prevents AMPK activation and glucose uptake during contraction, *EMBO J 24*, 1810-1820.
156. Sakamoto, K., Zarrinpashneh, E., Budas, G. R., Pouleur, A. C., Dutta, A., Prescott, A. R., Vanoverschelde, J. L., Ashworth, A., Jovanovic, A., Alessi, D. R., and Bertrand, L. (2006) Deficiency of LKB1 in heart prevents ischemia-mediated activation of AMPKalpha2 but not AMPKalpha1, *Am J Physiol Endocrinol Metab 290*, E780-788.
157. Hawley, S. A., Selbert, M. A., Goldstein, E. G., Edelman, A. M., Carling, D., and Hardie, D. G. (1995) 5'-AMP activates the AMP-activated protein kinase cascade, and Ca2+/calmodulin activates the calmodulin-dependent protein kinase I cascade, via three independent mechanisms, *J Biol Chem 270*, 27186-27191.
158. Woods, A., Dickerson, K., Heath, R., Hong, S. P., Momcilovic, M., Johnstone, S. R., Carlson, M., and Carling, D. (2005) Ca2+/calmodulin-dependent protein kinase kinase-beta acts upstream of AMP-activated protein kinase in mammalian cells, *Cell Metabolism 2*, 21-33.
159. Hawley, S. A., Pan, D. A., Mustard, K. J., Ross, L., Bain, J., Edelman, A. M., Frenguelli, B. G., and Hardie, D. G. (2005) Calmodulin-dependent protein kinase kinase-beta is an alternative upstream kinase for AMP-activated protein kinase, *Cell Metab 2*, 9-19.
160. Patel, N., Khayat, Z. A., Ruderman, N. B., and Klip, A. (2001) Dissociation of 5' AMP-activated protein kinase activation and glucose uptake stimulation by mitochondrial uncoupling and hyperosmolar stress: differential sensitivities to intracellular Ca2+ and protein kinase C inhibition, *Biochem Biophys Res Commun 285*, 1066-1070.
161. Momcilovic, M., Iram, S. H., Liu, Y., and Carlson, M. (2008) Roles of the glycogen-binding domain and Snf4 in glucose inhibition of SNF1 protein kinase, *Journal of Biological Chemistry 283*, 19521-19529.
162. Xie, M., Zhang, D., Dyck, J. R., Li, Y., Zhang, H., Morishima, M., Mann, D. L., Taffet, G. E., Baldini, A., Khoury, D. S., and Schneider, M. D. (2006) A pivotal role for endogenous TGF-beta-activated kinase-1 in the LKB1/AMP-activated protein kinase energy-sensor pathway, *Proc Natl Acad Sci U S A 103*, 17378-17383.
163. Haystead, T. A., Sim, A. T., Carling, D., Honnor, R. C., Tsukitani, Y., Cohen, P., and Hardie, D. G. (1989) Effects of the tumour promoter okadaic acid on intracellular protein phosphorylation and metabolism, *Nature 337*, 78-81.
164. Davies, S. P., Helps, N. R., Cohen, P. T., and Hardie, D. G. (1995) 5'-AMP inhibits dephosphorylation, as well as promoting phosphorylation, of the AMP-activated protein kinase. Studies using bacterially expressed human protein phosphatase-2C alpha and native bovine protein phosphatase-2AC, *FEBS Letters 377*, 421-425.
165. Garcia-Haro, L., Garcia-Gimeno, M. A., Neumann, D., Beullens, M., Bollen, M., and Sanz, P. (2010) The PP1-R6 protein phosphatase holoenzyme is involved in the glucose-induced dephosphorylation and inactivation of AMP-activated protein kinase, a key regulator of insulin secretion, in MIN6 beta cells, *FASEB J 24*, 5080-5091.

166. Wu, Y., Song, P., Xu, J., Zhang, M., and Zou, M. H. (2007) Activation of protein phosphatase 2A by palmitate inhibits AMP-activated protein kinase, *J Biol Chem 282*, 9777-9788.
167. Ravnskjaer, K., Boergesen, M., Dalgaard, L. T., and Mandrup, S. (2006) Glucose-induced repression of PPARalpha gene expression in pancreatic beta-cells involves PP2A activation and AMPK inactivation, *J Mol Endocrinol 36*, 289-299.
168. Horman, S., Vertommen, D., Heath, R., Neumann, D., Mouton, V., Woods, A., Schlattner, U., Wallimann, T., Carling, D., Hue, L., and Rider, M. H. (2006) Insulin antagonizes ischemia-induced Thr172 phosphorylation of AMP-activated protein kinase alpha-subunits in heart via hierarchical phosphorylation of Ser485/491, *J Biol Chem 281*, 5335-5340.
169. Kovacic, S., Soltys, C. L., Barr, A. J., Shiojima, I., Walsh, K., and Dyck, J. R. (2003) Akt activity negatively regulates phosphorylation of AMP-activated protein kinase in the heart, *J Biol Chem 278*, 39422-39427.
170. Hurley, R. L., Barre, L. K., Wood, S. D., Anderson, K. A., Kemp, B. E., Means, A. R., and Witters, L. A. (2006) Regulation of AMP-activated protein kinase by multisite phosphorylation in response to agents that elevate cellular cAMP, *J Biol Chem 281*, 36662-36672.
171. Djouder, N., Tuerk, R. D., Suter, M., Salvioni, P., Thali, R. F., Scholz, R., Vaahtomeri, K., Auchli, Y., Rechsteiner, H., Brunisholz, R. A., Viollet, B., Makela, T. P., Wallimann, T., Neumann, D., and Krek, W. (2010) PKA phosphorylates and inactivates AMPKalpha to promote efficient lipolysis, *EMBO J 29*, 469-481.
172. Dagon, Y., Hur, E., Zheng, B., Wellenstein, K., Cantley, L. C., and Kahn, B. B. (2012) p70S6 Kinase Phosphorylates AMPK on Serine 491 to Mediate Leptin's Effect on Food Intake, *Cell Metab 16*, 104-112.
173. Sanders, M. J., Ali, Z. S., Hegarty, B. D., Heath, R., Snowden, M. A., and Carling, D. (2007) Defining the mechanism of activation of AMP-activated protein kinase by the small molecule A-769662, a member of the thienopyridone family, *Journal of Biological Chemistry 282*, 32539-32548.
174. Suter, M., Riek, U., Tuerk, R., Schlattner, U., Wallimann, T., and Neumann, D. (2006) Dissecting the role of 5 '-AMP for allosteric stimulation, activation, and deactivation of AMP-activated protein kinase, *Journal of Biological Chemistry 281*, 32207-32216.
175. Warden, S. M., Richardson, C., O'Donnell, J., Jr., Stapleton, D., Kemp, B. E., and Witters, L. A. (2001) Post-translational modifications of the beta-1 subunit of AMP-activated protein kinase affect enzyme activity and cellular localization, *Biochem J 354*, 275-283.
176. Resh, M. D. (1999) Fatty acylation of proteins: new insights into membrane targeting of myristoylated and palmitoylated proteins, *Biochim Biophys Acta 1451*, 1-16.
177. Oakhill, J. S., Steel, R., Chen, Z. P., Scott, J. W., Ling, N., Tam, S., and Kemp, B. E. (2011) AMPK is a direct adenylate charge-regulated protein kinase, *Science 332*, 1433-1435.
178. Oakhill, J. S., Scott, J. W., and Kemp, B. E. (2012) AMPK functions as an adenylate charge-regulated protein kinase, *Trends Endocrinol Metab*.
179. Sanders, M. J., Grondin, P. O., Hegarty, B. D., Snowden, M. A., and Carling, D. (2007) Investigating the mechanism for AMP activation of the AMP-activated protein kinase cascade, *Biochemical Journal 403*, 139-148.
180. Qi, J., Gong, J., Zhao, T., Zhao, J., Lam, P., Ye, J., Li, J. Z., Wu, J., Zhou, H. M., and Li, P. (2008) Downregulation of AMP-activated protein kinase by Cidea-mediated ubiquitination and degradation in brown adipose tissue, *EMBO J 27*, 1537-1548.

181. Al-Hakim, A. K., Zagorska, A., Chapman, L., Deak, M., Peggie, M., and Alessi, D. R. (2008) Control of AMPK-related kinases by USP9X and atypical Lys(29)/Lys(33)-linked polyubiquitin chains, *Biochem J 411*, 249-260.
182. Lin, Y. Y., Kiihl, S., Suhail, Y., Liu, S. Y., Chou, Y. H., Kuang, Z., Lu, J. Y., Khor, C. N., Lin, C. L., Bader, J. S., Irizarry, R., and Boeke, J. D. (2012) Functional dissection of lysine deacetylases reveals that HDAC1 and p300 regulate AMPK, *Nature 482*, 251-255.
183. Bendayan, M., Londono, I., Kemp, B. E., Hardie, G. D., Ruderman, N., and Prentki, M. (2009) Association of AMP-activated protein kinase subunits with glycogen particles as revealed in situ by immunoelectron microscopy, *Journal of Histochemistry and Cytochemistry 57*, 963-971.
184. Hudson, E. R., Pan, D. A., James, J., Lucocq, J. M., Hawley, S. A., Green, K. A., Baba, O., Terashima, T., and Hardie, D. G. (2003) A novel domain in AMP-activated protein kinase causes glycogen storage bodies similar to those seen in hereditary cardiac arrhythmias, *Curr Biol 13*, 861-866.
185. Polekhina, G., Gupta, A., Michell, B. J., van Denderen, B., Murthy, S., Feil, S. C., Jennings, I. G., Campbell, D. J., Witters, L. A., Parker, M. W., Kemp, B. E., and Stapleton, D. (2003) AMPK beta subunit targets metabolic stress sensing to glycogen, *Curr Biol 13*, 867-871.
186. Wojtaszewski, J. F., Jorgensen, S. B., Hellsten, Y., Hardie, D. G., and Richter, E. A. (2002) Glycogen-dependent effects of 5-aminoimidazole-4-carboxamide (AICA)-riboside on AMP-activated protein kinase and glycogen synthase activities in rat skeletal muscle, *Diabetes 51*, 284-292.
187. Wojtaszewski, J. F., Nielsen, J. N., Jorgensen, S. B., Frosig, C., Birk, J. B., and Richter, E. A. (2003) Transgenic models--a scientific tool to understand exercise-induced metabolism: the regulatory role of AMPK (5'-AMP-activated protein kinase) in glucose transport and glycogen synthase activity in skeletal muscle, *Biochem Soc Trans 31*, 1290-1294.
188. Townley, R., and Shapiro, L. (2007) Crystal structures of the adenylate sensor from fission yeast AMP-activated protein kinase, *Science 315*, 1726-1729.
189. Amodeo, G. A., Rudolph, M. J., and Tong, L. (2007) Crystal structure of the heterotrimer core of Saccharomyces cerevisiae AMPK homologue SNF1, *Nature 449*, 492-495.
190. Henin, N., Vincent, M. F., and Van den Berghe, G. (1996) Stimulation of rat liver AMP-activated protein kinase by AMP analogues, *Biochimica et Biophysica Acta 1290*, 197-203.
191. Corton, J. M., Gillespie, J. G., Hawley, S. A., and Hardie, D. G. (1995) 5-aminoimidazole-4-carboxamide ribonucleoside. A specific method for activating AMP-activated protein kinase in intact cells?, *Eur J Biochem 229*, 558-565.
192. Winder, W. W. (2000) AMP-activated protein kinase: possible target for treatment of type 2 diabetes, *Diabetes Technol Ther 2*, 441-448.
193. McCrimmon, R. J., Fan, X., Ding, Y., Zhu, W., Jacob, R. J., and Sherwin, R. S. (2004) Potential role for AMP-activated protein kinase in hypoglycemia sensing in the ventromedial hypothalamus, *Diabetes 53*, 1953-1958.
194. Vincent, M. F., Marangos, P. J., Gruber, H. E., and Van den Berghe, G. (1991) Inhibition by AICA riboside of gluconeogenesis in isolated rat hepatocytes, *Diabetes 40*, 1259-1266.
195. Young, M. E., Radda, G. K., and Leighton, B. (1996) Activation of glycogen phosphorylase and glycogenolysis in rat skeletal muscle by AICAR--an activator of AMP-activated protein kinase, *FEBS Lett 382*, 43-47.

196. Goransson, O., McBride, A., Hawley, S. A., Ross, F. A., Shpiro, N., Foretz, M., Viollet, B., Hardie, D. G., and Sakamoto, K. (2007) Mechanism of action of A-769662, a valuable tool for activation of AMP-activated protein kinase, *Journal of Biological Chemistry 282*, 32549-32560.
197. Scott, J. W., van Denderen, B. J., Jorgensen, S. B., Honeyman, J. E., Steinberg, G. R., Oakhill, J. S., Iseli, T. J., Koay, A., Gooley, P. R., Stapleton, D., and Kemp, B. E. (2008) Thienopyridone drugs are selective activators of AMP-activated protein kinase beta1-containing complexes, *Chem Biol 15*, 1220-1230.
198. Garcia-Garcia, C., Fumarola, C., Navaratnam, N., Carling, D., and Lopez-Rivas, A. (2010) AMPK-independent down-regulation of cFLIP and sensitization to TRAIL-induced apoptosis by AMPK activators, *Biochem Pharmacol 79*, 853-863.
199. Benziane, B., Bjornholm, M., Lantier, L., Viollet, B., Zierath, J. R., and Chibalin, A. V. (2009) AMP-activated protein kinase activator A-769662 is an inhibitor of the Na(+)-K(+)-ATPase, *Am J Physiol Cell Physiol 297*, C1554-1566.
200. Hawley, S. A., Fullerton, M. D., Ross, F. A., Schertzer, J. D., Chevtzoff, C., Walker, K. J., Peggie, M. W., Zibrova, D., Green, K. A., Mustard, K. J., Kemp, B. E., Sakamoto, K., Steinberg, G. R., and Hardie, D. G. (2012) The Ancient Drug Salicylate Directly Activates AMP-Activated Protein Kinase, *Science*.
201. Bain, J., Plater, L., Elliott, M., Shpiro, N., Hastie, C. J., McLauchlan, H., Klevernic, I., Arthur, J. S., Alessi, D. R., and Cohen, P. (2007) The selectivity of protein kinase inhibitors: a further update, *Biochem J 408*, 297-315.
202. Fryer, L. G., Parbu-Patel, A., and Carling, D. (2002) Protein kinase inhibitors block the stimulation of the AMP-activated protein kinase by 5-amino-4-imidazolecarboxamide riboside, *FEBS Lett 531*, 189-192.
203. Hawley, S. A., Ross, F. A., Chevtzoff, C., Green, K. A., Evans, A., Fogarty, S., Towler, M. C., Brown, L. J., Ogunbayo, O. A., Evans, A. M., and Hardie, D. G. (2010) Use of cells expressing gamma subunit variants to identify diverse mechanisms of AMPK activation, *Cell Metab 11*, 554-565.
204. Lu, J., Wu, D. M., Zheng, Y. L., Hu, B., Zhang, Z. F., Shan, Q., Zheng, Z. H., Liu, C. M., and Wang, Y. J. (2010) Quercetin activates AMP-activated protein kinase by reducing PP2C expression protecting old mouse brain against high cholesterol-induced neurotoxicity, *J Pathol 222*, 199-212.
205. Scott, J. W., Ross, F. A., Liu, J. K., and Hardie, D. G. (2007) Regulation of AMP-activated protein kinase by a pseudosubstrate sequence on the gamma subunit, *EMBO Journal 26*, 806-815.
206. Foretz, M., Hebrard, S., Leclerc, J., Zarrinpashneh, E., Soty, M., Mithieux, G., Sakamoto, K., Andreelli, F., and Viollet, B. (2010) Metformin inhibits hepatic gluconeogenesis in mice independently of the LKB1/AMPK pathway via a decrease in hepatic energy state, *J Clin Invest 120*, 2355-2369.
207. Hawley, S. A., Gadalla, A. E., Olsen, G. S., and Hardie, D. G. (2002) The antidiabetic drug metformin activates the AMP-activated protein kinase cascade via an adenine nucleotide-independent mechanism, *Diabetes 51*, 2420-2425.
208. Hevener, A. L., Reichart, D., Janez, A., and Olefsky, J. (2001) Thiazolidinedione treatment prevents free fatty acid-induced insulin resistance in male wistar rats, *Diabetes 50*, 2316-2322.
209. Lessard, S. J., Lo Giudice, S. L., Lau, W., Reid, J. J., Turner, N., Febbraio, M. A., Hawley, J. A., and Watt, M. J. (2004) Rosiglitazone enhances glucose tolerance by mechanisms other than reduction of fatty acid accumulation within skeletal muscle, *Endocrinology 145*, 5665-5670.

210. Wang, M. Y., and Unger, R. H. (2005) Role of PP2C in cardiac lipid accumulation in obese rodents and its prevention by troglitazone, *Am J Physiol Endocrinol Metab 288*, E216-221.
211. Winder, W. W., and Hardie, D. G. (1996) Inactivation of acetyl-CoA carboxylase and activation of AMP-activated protein kinase in muscle during exercise, *Am J Physiol 270*, E299-304.
212. Rasmussen, B. B., and Winder, W. W. (1997) Effect of exercise intensity on skeletal muscle malonyl-CoA and acetyl-CoA carboxylase, *J Appl Physiol 83*, 1104-1109.
213. Fujii, N., Hayashi, T., Hirshman, M. F., Smith, J. T., Habinowski, S. A., Kaijser, L., Mu, J., Ljungqvist, O., Birnbaum, M. J., Witters, L. A., Thorell, A., and Goodyear, L. J. (2000) Exercise induces isoform-specific increase in 5'AMP-activated protein kinase activity in human skeletal muscle, *Biochem Biophys Res Commun 273*, 1150-1155.
214. Towler, M. C., and Hardie, D. G. (2007) AMP-activated protein kinase in metabolic control and insulin signaling, *Circulation Research 100*, 328-341.
215. Lee, Y. K., Park, S. Y., Kim, Y. M., and Park, O. J. (2009) Regulatory effect of the AMPK-COX-2 signaling pathway in curcumin-induced apoptosis in HT-29 colon cancer cells, *Ann N Y Acad Sci 1171*, 489-494.
216. Hwang, J. T., Ha, J., and Park, O. J. (2005) Combination of 5-fluorouracil and genistein induces apoptosis synergistically in chemo-resistant cancer cells through the modulation of AMPK and COX-2 signaling pathways, *Biochem Biophys Res Commun 332*, 433-440.
217. Park, I. J., Lee, Y. K., Hwang, J. T., Kwon, D. Y., Ha, J., and Park, O. J. (2009) Green tea catechin controls apoptosis in colon cancer cells by attenuation of H2O2-stimulated COX-2 expression via the AMPK signaling pathway at low-dose H2O2, *Ann N Y Acad Sci 1171*, 538-544.
218. Hwang, J. T., Ha, J., Park, I. J., Lee, S. K., Baik, H. W., Kim, Y. M., and Park, O. J. (2007) Apoptotic effect of EGCG in HT-29 colon cancer cells via AMPK signal pathway, *Cancer Lett 247*, 115-121.
219. Kim, Y. M., Hwang, J. T., Kwak, D. W., Lee, Y. K., and Park, O. J. (2007) Involvement of AMPK signaling cascade in capsaicin-induced apoptosis of HT-29 colon cancer cells, *Ann N Y Acad Sci 1095*, 496-503.
220. Khanal, P., Oh, W. K., Yun, H. J., Namgoong, G. M., Ahn, S. G., Kwon, S. M., Choi, H. K., and Choi, H. S. (2011) p-HPEA-EDA, a phenolic compound of virgin olive oil, activates AMP-activated protein kinase to inhibit carcinogenesis, *Carcinogenesis 32*, 545-553.
221. Ahn, J., Lee, H., Kim, S., Park, J., and Ha, T. (2008) The anti-obesity effect of quercetin is mediated by the AMPK and MAPK signaling pathways, *Biochem Biophys Res Commun 373*, 545-549.
222. Hwang, J. T., Kwak, D. W., Lin, S. K., Kim, H. M., Kim, Y. M., and Park, O. J. (2007) Resveratrol induces apoptosis in chemoresistant cancer cells via modulation of AMPK signaling pathway, *Ann N Y Acad Sci 1095*, 441-448.
223. Li, Y., Wang, P., Zhuang, Y., Lin, H., Liu, L., Meng, Q., Cui, T., Liu, J., and Li, Z. (2011) Activation of AMPK by berberine promotes adiponectin multimerization in 3T3-L1 adipocytes, *FEBS Lett 585*, 1735-1740.
224. Nguyen, P. H., Le, T. V., Kang, H. W., Chae, J., Kim, S. K., Kwon, K. I., Seo, D. B., Lee, S. J., and Oh, W. K. AMP-activated protein kinase (AMPK) activators from Myristica fragrans (nutmeg) and their anti-obesity effect, *Bioorg Med Chem Lett*.
225. Hwang, J. T., Lee, M. S., Kim, H. J., Sung, M. J., Kim, H. Y., Kim, M. S., and Kwon, D. Y. (2009) Antiobesity effect of ginsenoside Rg3 involves the AMPK and PPAR-gamma signal pathways, *Phytother Res 23*, 262-266.

226. Zhang, Y., Proenca, R., Maffei, M., Barone, M., Leopold, L., and Friedman, J. M. (1994) Positional cloning of the mouse obese gene and its human homologue, *Nature 372*, 425-432.
227. Ingalls, A. M., Dickie, M. M., and Snell, G. D. (1950) Obese, a new mutation in the house mouse, *J Hered 41*, 317-318.
228. Steinberg, G. R., Rush, J. W., and Dyck, D. J. (2003) AMPK expression and phosphorylation are increased in rodent muscle after chronic leptin treatment, *Am J Physiol Endocrinol Metab 284*, E648-654.
229. Minokoshi, Y., Kim, Y. B., Peroni, O. D., Fryer, L. G. D., Muller, C., Carling, D., and Kahn, B. B. (2002) Leptin stimulates fatty-acid oxidation by activating AMP-activated protein kinase, *Nature 415*, 339-343.
230. Yamauchi, T., Kamon, J., Minokoshi, Y., Ito, Y., Waki, H., Uchida, S., Yamashita, S., Noda, M., Kita, S., Ueki, K., Eto, K., Akanuma, Y., Froguel, P., Foufelle, F., Ferre, P., Carling, D., Kimura, S., Nagai, R., Kahn, B. B., and Kadowaki, T. (2002) Adiponectin stimulates glucose utilization and fatty-acid oxidation by activating AMP-activated protein kinase, *Nature Medicine 8*, 1288-1295.
231. Arita, Y., Kihara, S., Ouchi, N., Takahashi, M., Maeda, K., Miyagawa, J., Hotta, K., Shimomura, I., Nakamura, T., Miyaoka, K., Kuriyama, H., Nishida, M., Yamashita, S., Okubo, K., Matsubara, K., Muraguchi, M., Ohmoto, Y., Funahashi, T., and Matsuzawa, Y. (1999) Paradoxical decrease of an adipose-specific protein, adiponectin, in obesity, *Biochem Biophys Res Commun 257*, 79-83.
232. Tomas, E., Tsao, T. S., Saha, A. K., Murrey, H. E., Zhang Cc, C., Itani, S. I., Lodish, H. F., and Ruderman, N. B. (2002) Enhanced muscle fat oxidation and glucose transport by ACRP30 globular domain: acetyl-CoA carboxylase inhibition and AMP-activated protein kinase activation, *Proc Natl Acad Sci U S A 99*, 16309-16313.
233. Kubota, N., Yano, W., Kubota, T., Yamauchi, T., Itoh, S., Kumagai, H., Kozono, H., Takamoto, I., Okamoto, S., Shiuchi, T., Suzuki, R., Satoh, H., Tsuchida, A., Moroi, M., Sugi, K., Noda, T., Ebinuma, H., Ueta, Y., Kondo, T., Araki, E., Ezaki, O., Nagai, R., Tobe, K., Terauchi, Y., Ueki, K., Minokoshi, Y., and Kadowaki, T. (2007) Adiponectin stimulates AMP-activated protein kinase in the hypothalamus and increases food intake, *Cell Metab 6*, 55-68.
234. Zhou, L., Deepa, S. S., Etzler, J. C., Ryu, J., Mao, X., Fang, Q., Liu, D. D., Torres, J. M., Jia, W., Lechleiter, J. D., Liu, F., and Dong, L. Q. (2009) Adiponectin activates AMP-activated protein kinase in muscle cells via APPL1/LKB1-dependent and phospholipase C/Ca2+/Ca2+/calmodulin-dependent protein kinase kinase-dependent pathways, *J Biol Chem 284*, 22426-22435.
235. Iwabu, M., Yamauchi, T., Okada-Iwabu, M., Sato, K., Nakagawa, T., Funata, M., Yamaguchi, M., Namiki, S., Nakayama, R., Tabata, M., Ogata, H., Kubota, N., Takamoto, I., Hayashi, Y. K., Yamauchi, N., Waki, H., Fukayama, M., Nishino, I., Tokuyama, K., Ueki, K., Oike, Y., Ishii, S., Hirose, K., Shimizu, T., Touhara, K., and Kadowaki, T. (2010) Adiponectin and AdipoR1 regulate PGC-1alpha and mitochondria by Ca(2+) and AMPK/SIRT1, *Nature 464*, 1313-1319.
236. Miller, R. A., Chu, Q., Le Lay, J., Scherer, P. E., Ahima, R. S., Kaestner, K. H., Foretz, M., Viollet, B., and Birnbaum, M. J. (2011) Adiponectin suppresses gluconeogenic gene expression in mouse hepatocytes independent of LKB1-AMPK signaling, *J Clin Invest 121*, 2518-2528.
237. Anderson, K. A., Ribar, T. J., Lin, F., Noeldner, P. K., Green, M. F., Muehlbauer, M. J., Witters, L. A., Kemp, B. E., and Means, A. R. (2008) Hypothalamic CaMKK2 contributes to the regulation of energy balance, *Cell Metab 7*, 377-388.

238. Kohno, D., Gao, H. Z., Muroya, S., Kikuyama, S., and Yada, T. (2003) Ghrelin directly interacts with neuropeptide-Y-containing neurons in the rat arcuate nucleus: Ca2+ signaling via protein kinase A and N-type channel-dependent mechanisms and cross-talk with leptin and orexin, *Diabetes 52*, 948-956.
239. Kim, M. S., and Lee, K. U. (2005) Role of hypothalamic 5'-AMP-activated protein kinase in the regulation of food intake and energy homeostasis, *J Mol Med (Berl) 83*, 514-520.
240. Steinberg, G. R., Watt, M. J., Fam, B. C., Proietto, J., Andrikopoulos, S., Allen, A. M., Febbraio, M. A., and Kemp, B. E. (2006) Ciliary neurotrophic factor suppresses hypothalamic AMP-kinase signaling in leptin-resistant obese mice, *Endocrinology 147*, 3906-3914.
241. Lee, W. J., Song, K. H., Koh, E. H., Won, J. C., Kim, H. S., Park, H. S., Kim, M. S., Kim, S. W., Lee, K. U., and Park, J. Y. (2005) Alpha-lipoic acid increases insulin sensitivity by activating AMPK in skeletal muscle, *Biochem Biophys Res Commun 332*, 885-891.
242. Watt, M. J., Dzamko, N., Thomas, W. G., Rose-John, S., Ernst, M., Carling, D., Kemp, B. E., Febbraio, M. A., and Steinberg, G. R. (2006) CNTF reverses obesity-induced insulin resistance by activating skeletal muscle AMPK, *Nat Med 12*, 541-548.
243. Carey, A. L., Steinberg, G. R., Macaulay, S. L., Thomas, W. G., Holmes, A. G., Ramm, G., Prelovsek, O., Hohnen-Behrens, C., Watt, M. J., James, D. E., Kemp, B. E., Pedersen, B. K., and Febbraio, M. A. (2006) Interleukin-6 increases insulin-stimulated glucose disposal in humans and glucose uptake and fatty acid oxidation in vitro via AMP-activated protein kinase, *Diabetes 55*, 2688-2697.
244. Yang, Z., Kahn, B. B., Shi, H., and Xue, B. Z. (2010) Macrophage alpha1 AMP-activated protein kinase (alpha1AMPK) antagonizes fatty acid-induced inflammation through SIRT1, *J Biol Chem 285*, 19051-19059.
245. Neumann, D., Woods, A., Carling, D., Wallimann, T., and Schlattner, U. (2003) Mammalian AMP-activated protein kinase: functional, heterotrimeric complexes by co-expression of subunits in Escherichia coli, *Protein Expression and Purification 30*, 230-237.
246. Webb, M. R., Reid, G. P., Munasinghe, V. R., and Corrie, J. E. (2004) A series of related nucleotide analogues that aids optimization of fluorescence signals in probing the mechanism of P-loop ATPases, such as actomyosin, *Biochemistry 43*, 14463-14471.
247. Jameson, D. M., and Eccleston, J. F. (1997) Fluorescent nucleotide analogs: synthesis and applications, *Methods in Enzymology 278*, 363-390.
248. Webb, M. R., and Corrie, J. E. T. (2001) Fluorescent Coumarin-Labeled Nucleotides to Measure ADP Release from Actomyosin, *Biophysical Journal 81*, 1562-1569.
249. Avery, J. S. (1966) Resonance energy transfer and spontaneous photon emission, *Proceedings of the Physical Society 88*, 559.
250. Storer, A. C., and Cornish-Bowden, A. (1976) Concentration of MgATP2- and other ions in solution. Calculation of the true concentrations of species present in mixtures of associating ions, *Biochem J 159*, 1-5.
251. Lawrie, A. M., Noble, M. E., Tunnah, P., Brown, N. R., Johnson, L. N., and Endicott, J. A. (1997) Protein kinase inhibition by staurosporine revealed in details of the molecular interaction with CDK2, *Nature Structural Biology 4*, 796-801.
252. Huang, D., Zhou, T., Lafleur, K., Nevado, C., and Caflisch, A. (2010) Kinase selectivity potential for inhibitors targeting the ATP binding site: a network analysis, *Bioinformatics 26*, 198-204.

253. Iyer, G. H., Taslimi, P., and Pazhanisamy, S. (2008) Staurosporine-based binding assay for testing the affinity of compounds to protein kinases, *Analytical Biochemistry 373*, 197-206.
254. Engh, R. A., and Bossemeyer, D. (2002) Structural aspects of protein kinase control-role of conformational flexibility, *Pharmacol Ther 93*, 99-111.
255. Martinez. S, P. E., Drexler. C, Préaudat. M, Steger. K,. HTRF® KinEASE™ : Development of sensitive, reliable Aurora A and AMPK kinase inhibitory assays, http://www.htrf.com/files/resources/KinEASE.pdf.
256. Hsiao. K, Z. H., Vidugiriene. J, Goueli. S,. ADP-Glo™: AMPK Kinase Assay, http://kbadminga.knowledgebase.net/pf/10537/webfiles/AMPK1.pdf.
257. Futer, O., Saadat, A. R., Doran, J. D., Raybuck, S. A., and Pazhanisamy, S. (2006) Phosphoryl transfer is not rate-limiting for the ROCK I-catalyzed kinase reaction, *Biochemistry 45*, 7913-7923.
258. Zhang, B., Zhang, Y., Wang, Z., and Zheng, Y. (2000) The role of Mg2+ cofactor in the guanine nucleotide exchange and GTP hydrolysis reactions of Rho family GTP-binding proteins, *J Biol Chem 275*, 25299-25307.
259. Weiss, J. N. (1997) The Hill equation revisited: uses and misuses, *FASEB J 11*, 835-841.
260. Williamson, D. H., Lund, P., and Krebs, H. A. (1967) The redox state of free nicotinamide-adenine dinucleotide in the cytoplasm and mitochondria of rat liver, *Biochem J 103*, 514-527.
261. Yamada, K., Hara, N., Shibata, T., Osago, H., and Tsuchiya, M. (2006) The simultaneous measurement of nicotinamide adenine dinucleotide and related compounds by liquid chromatography/electrospray ionization tandem mass spectrometry, *Analytical Biochemistry 352*, 282-285.
262. Cohen, P. (2001) The role of protein phosphorylation in human health and disease. The Sir Hans Krebs Medal Lecture, *Eur J Biochem 268*, 5001-5010.
263. Huang, C. Y., and Ferrell, J. E., Jr. (1996) Ultrasensitivity in the mitogen-activated protein kinase cascade, *Proc Natl Acad Sci U S A 93*, 10078-10083.
264. Adams, J. A. (2001) Kinetic and catalytic mechanisms of protein kinases, *Chem Rev 101*, 2271-2290.
265. Hardie, D. G., Salt, I. P., Hawley, S. A., and Davies, S. P. (1999) AMP-activated protein kinase: an ultrasensitive system for monitoring cellular energy charge, *Biochem J 338 (Pt 3)*, 717-722.
266. Davies, S. P., Carling, D., and Hardie, D. G. (1989) Tissue distribution of the AMP-activated protein kinase, and lack of activation by cyclic-AMP-dependent protein kinase, studied using a specific and sensitive peptide assay., *European Journal of Biochemistry 186*, 123-128.
267. Dale, S., Wilson, W. A., Edelman, A. M., and Hardie, D. G. (1995) Similar substrate recognition motifs for mammalian AMP-activated protein kinase, higher plant HMG-CoA reductase kinase-A, yeast SNF1, and mammalian calmodulin-dependent protein kinase I, *FEBS Letters 361*, 191-195.
268. Scott, J. W., Norman, D. G., Hawley, S. A., Kontogiannis, L., and Hardie, D. G. (2002) Protein kinase substrate recognition studied using the recombinant catalytic domain of AMP-activated protein kinase and a model substrate, *Journal of Molecular Biology 317*, 309-323.
269. Cook, P. F., Neville, M. E., Jr., Vrana, K. E., Hartl, F. T., and Roskoski, R., Jr. (1982) Adenosine cyclic 3',5'-monophosphate dependent protein kinase: kinetic mechanism for the bovine skeletal muscle catalytic subunit, *Biochemistry 21*, 5794-5799.

270. Corton, J. M., Gillespie, J. G., and Hardie, D. G. (1994) Role of the AMP-activated protein kinase in the cellular stress response, *Current Biology 4*, 315-324.
271. Overton, J. D., Adams, G. S., McCall, R. D., and Kinsey, S. T. (2009) High energy phosphate concentrations and AMPK phosphorylation in skeletal muscle from mice with inherited differences in hypoxic exercise tolerance, *Comp Biochem Physiol A Mol Integr Physiol 152*, 478-485.
272. Kunzelmann, S., and Webb, M. R. (2010) A fluorescent, reagentless biosensor for ADP based on tetramethylrhodamine-labeled ParM, *ACS Chem Biol 5*, 415-425.
273. Ozalp, V. C., Pedersen, T. R., Nielsen, L. J., and Olsen, L. F. (2010) Time-resolved measurements of intracellular ATP in the yeast Saccharomyces cerevisiae using a new type of nanobiosensor, *J Biol Chem 285*, 37579-37588.
274. Chen, Z. P., McConell, G. K., Michell, B. J., Snow, R. J., Canny, B. J., and Kemp, B. E. (2000) AMPK signaling in contracting human skeletal muscle: acetyl-CoA carboxylase and NO synthase phosphorylation, *Am J Physiol Endocrinol Metab 279*, E1202-1206.
275. Hellsten, Y., Richter, E. A., Kiens, B., and Bangsbo, J. (1999) AMP deamination and purine exchange in human skeletal muscle during and after intense exercise, *J Physiol 520 Pt 3*, 909-920.
276. Clark, S. A., Chen, Z. P., Murphy, K. T., Aughey, R. J., McKenna, M. J., Kemp, B. E., and Hawley, J. A. (2004) Intensified exercise training does not alter AMPK signaling in human skeletal muscle, *Am J Physiol Endocrinol Metab 286*, E737-743.
277. Roepstorff, C., Thiele, M., Hillig, T., Pilegaard, H., Richter, E. A., Wojtaszewski, J. F., and Kiens, B. (2006) Higher skeletal muscle alpha2AMPK activation and lower energy charge and fat oxidation in men than in women during submaximal exercise, *J Physiol 574*, 125-138.
278. Khan, M. M., and Martell, A. E. (1966) Thermodynamic quantities associated with the interaction of adenosine triphosphate with metal ions, *Journal of the American Chemical Society 88*, 668-671.
279. Veech, R. L., Lawson, J. W., Cornell, N. W., and Krebs, H. A. (1979) Cytosolic phosphorylation potential, *Journal of Biological Chemistry 254*, 6538-6547.
280. McConell, G. K., Lee-Young, R. S., Chen, Z. P., Stepto, N. K., Huynh, N. N., Stephens, T. J., Canny, B. J., and Kemp, B. E. (2005) Short-term exercise training in humans reduces AMPK signalling during prolonged exercise independent of muscle glycogen, *J Physiol 568*, 665-676.
281. Beeler, T., Bruce, K., and Dunn, T. (1997) Regulation of cellular Mg2+ by Saccharomyces cerevisiae, *Biochim Biophys Acta 1323*, 310-318.
282. Fryer, L. G., Parbu-Patel, A., and Carling, D. (2002) The Anti-diabetic drugs rosiglitazone and metformin stimulate AMP-activated protein kinase through distinct signaling pathways, *J Biol Chem 277*, 25226-25232.
283. Koshland, D. E., Jr., Goldbeter, A., and Stock, J. B. (1982) Amplification and adaptation in regulatory and sensory systems, *Science 217*, 220-225.
284. Goldbeter, A., and Koshland, D. E., Jr. (1984) Ultrasensitivity in biochemical systems controlled by covalent modification. Interplay between zero-order and multistep effects, *Journal of Biological Chemistry 259*, 14441-14447.
285. Krishnan, V. V., and Rupp, B. (2001) Macromolecular Structure Determination: Comparison of X-ray Crystallography and NMR Spectroscopy, In *eLS*, John Wiley & Sons, Ltd.
286. Orlova, E. V., and Saibil, H. R. (2011) Structural analysis of macromolecular assemblies by electron microscopy, *Chem Rev 111*, 7710-7748.

287. McCoy, A. (2010) Protein Crystallography with Coffee – An Introduction to Biomolecular Crystallography, In *BCA Protein Crystallography Summer School 2010*, Oxford.
288. Sherwood, D., and Cooper, C. (2011) *Crystals, X-rays and Proteins – Comprehensive Protein Crystallography*, first ed., Oxford University Press, Oxford.
289. Yee, A. A., Savchenko, A., Ignachenko, A., Lukin, J., Xu, X., Skarina, T., Evdokimova, E., Liu, C. S., Semesi, A., Guido, V., Edwards, A. M., and Arrowsmith, C. H. (2005) NMR and X-ray crystallography, complementary tools in structural proteomics of small proteins, *J Am Chem Soc 127*, 16512-16517.
290. Otwinowski, Z., and Minor, W. (1993) in Data Collection and Processing, *SERC Daresbury Laboratory, Warrington*.
291. McCoy, A. J., Grosse-Kunstleve, R. W., Adams, P. D., Winn, M. D., Storoni, L. C., and Read, R. J. (2007) Phaser crystallographic software, *J Appl Crystallogr 40*, 658-674.
292. Adams, P. D., Grosse-Kunstleve, R. W., Hung, L. W., Ioerger, T. R., McCoy, A. J., Moriarty, N. W., Read, R. J., Sacchettini, J. C., Sauter, N. K., and Terwilliger, T. C. (2002) PHENIX: building new software for automated crystallographic structure determination, *Acta Crystallographica D - Biological Crystallography 58*, 1948-1954.
293. (1994) The CCP4 suite: programs for protein crystallography, *Acta Crystallographica D - Biological Crystallography 50*, 760-763.
294. Emsley, P., and Cowtan, K. (2004) Coot: model-building tools for molecular graphics, *Acta Crystallographica D - Biological Crystallography 60*, 2126-2132.
295. Nijegorodov, N. I., and Downey, W. S. (1994) The Influence of Planarity and Rigidity on the Absorption and Fluorescence Parameters and Intersystem Crossing Rate Constant in Aromatic Molecules, *Journal of Physical Chemistry 98*.
296. Hedbacker, K., and Carlson, M. (2008) SNF1/AMPK pathways in yeast, *Front Biosci 13*, 2408-2420.
297. Carlson, M. (1999) Glucose repression in yeast, *Curr Opin Microbiol 2*, 202-207.
298. Vallier, L. G., and Carlson, M. (1994) Synergistic release from glucose repression by mig1 and ssn mutations in Saccharomyces cerevisiae, *Genetics 137*, 49-54.
299. Sanz, P. (2003) Snf1 protein kinase: a key player in the response to cellular stress in yeast, *Biochemical Society Transactions 31*, 178-181.
300. Woods, A., Munday, M. R., Scott, J., Yang, X. L., Carlson, M., and Carling, D. (1994) Yeast SNF1 is functionally related to mammalian AMP-activated Portein-Kinase and regulates Acetyl-CoA carboxylase in-vivo., *Journal of Biological Chemistry 269*, 19509-19515.
301. Shirra, M. K., Patton-Vogt, J., Ulrich, A., Liuta-Tehlivets, O., Kohlwein, S. D., Henry, S. A., and Arndt, K. M. (2001) Inhibition of acetyl coenzyme A carboxylase activity restores expression of the INO1 gene in a snf1 mutant strain of Saccharomyces cerevisiae, *Molecular and Cellular Biology 21*, 5710-5722.
302. Mayordomo, I., Estruch, F., and Sanz, P. (2002) Convergence of the target of rapamycin and the Snf1 protein kinase pathways in the regulation of the subcellular localization of Msn2, a transcriptional activator of STRE (Stress Response Element)-regulated genes, *Journal of Biological Chemistry 277*, 35650-35656.
303. Alepuz, P. M., Cunningham, K. W., and Estruch, F. (1997) Glucose repression affects ion homeostasis in yeast through the regulation of the stress-activated ENA1 gene, *Molecular Microbiology 26*, 91-98.
304. Celenza, J. L., and Carlson, M. (1989) Mutational analysis of the Saccharomyces cerevisiae SNF1 protein kinase and evidence for functional interaction with the SNF4 protein, *Mol Cell Biol 9*, 5034-5044.

305. Elbing, K., Rubenstein, E. M., McCartney, R. R., and Schmidt, M. C. (2006) Subunits of the Snf1 kinase heterotrimer show interdependence for association and activity, *Journal of Biological Chemistry 281*, 26170-26180.
306. Celenza, J. L., and Carlson, M. (1984) Structure and expression of the SNF1 gene of Saccharomyces cerevisiae, *Molecular and Cellular Biology 4*, 54-60.
307. Rudolph, M. J., Amodeo, G. A., Bai, Y., and Tong, L. (2005) Crystal structure of the protein kinase domain of yeast AMP-activated protein kinase Snf1, *Biochemical and Biophysical Research Communications 337*, 1224-1228.
308. Jiang, R., and Carlson, M. (1997) The Snf1 protein kinase and its activating subunit, Snf4, interact with distinct domains of the Sip1/Sip2/Gal83 component in the kinase complex, *Molecular and Cellular Biology 17*, 2099-2106.
309. Crute, B. E., Seefeld, K., Gamble, J., Kemp, B. E., and Witters, L. A. (1998) Functional domains of the alpha 1 catalytic subunit of the AMP-activated protein kinase, *Journal of Biological Chemistry 273*, 35347-35354.
310. Estruch, F., Treitel, M. A., Yang, X., and Carlson, M. (1992) N-terminal mutations modulate yeast SNF1 protein kinase function, *Genetics 132*, 639-650.
311. Hardie, D. G., Carling, D., and Carlson, M. (1998) The AMP-activated/SNF1 protein kinase subfamily: Metabolic sensors of the eukaryotic cell?, *Annual Review of Biochemistry 67*, 821-855.
312. Vincent, O., Townley, R., Kuchin, S., and Carlson, M. (2001) Subcellular localization of the Snf1 kinase is regulated by specific beta subunits and a novel glucose signaling mechanism, *Genes & Development 15*, 1104-1114.
313. Vincent, O., and Carlson, M. (1999) Gal83 mediates the interaction of the Snf1 kinase complex with the transcription activator Sip4, *EMBO J 18*, 6672-6681.
314. Wiatrowski, H. A., Van Denderen, B. J., Berkey, C. D., Kemp, B. E., Stapleton, D., and Carlson, M. (2004) Mutations in the gal83 glycogen-binding domain activate the snf1/gal83 kinase pathway by a glycogen-independent mechanism, *Mol Cell Biol 24*, 352-361.
315. Mangat, S., Chandrashekarappa, D., McCartney, R. R., Elbing, K., and Schmidt, M. C. (2010) Differential roles of the glycogen-binding domains of beta subunits in regulation of the Snf1 kinase complex, *Eukaryot Cell 9*, 173-183.
316. Lu, J. Y., Lin, Y. Y., Sheu, J. C., Wu, J. T., Lee, F. J., Chen, Y., Lin, M. I., Chiang, F. T., Tai, T. Y., Berger, S. L., Zhao, Y., Tsai, K. S., Zhu, H., Chuang, L. M., and Boeke, J. D. (2011) Acetylation of yeast AMPK controls intrinsic aging independently of caloric restriction, *Cell 146*, 969-979.
317. Celenza, J. L., Eng, F. J., and Carlson, M. (1989) Molecular analysis of the SNF4 gene of Saccharomyces cerevisiae: evidence for physical association of the SNF4 protein with the SNF1 protein kinase, *Mol Cell Biol 9*, 5045-5054.
318. Carlson, M., Osmond, B. C., Neigeborn, L., and Botstein, D. (1984) A suppressor of SNF1 mutations causes constitutive high-level invertase synthesis in yeast, *Genetics 107*, 19-32.
319. Adams, J., Chen, Z. P., Van Denderen, B. J., Morton, C. J., Parker, M. W., Witters, L. A., Stapleton, D., and Kemp, B. E. (2004) Intrasteric control of AMPK via the gamma1 subunit AMP allosteric regulatory site, *Protein Science 13*, 155-165.
320. Hedbacker, K., and Carlson, M. (2006) Regulation of the nucleocytoplasmic distribution of Snf1-Gal83 protein kinase, *Eukaryot Cell 5*, 1950-1956.
321. Hong, S. P., Momcilovic, M., and Carlson, M. (2005) Function of mammalian LKB1 and Ca2+/calmodulin-dependent protein kinase kinase alpha as Snf1-activating kinases in yeast, *J Biol Chem 280*, 21804-21809.

322. Nath, N., McCartney, R. R., and Schmidt, M. C. (2003) Yeast Pak1 kinase associates with and activates Snf1, *Molecular and Cellular Biology 23*, 3909-3917.
323. Sutherland, C. M., Hawley, S. A., McCartney, R. R., Leech, A., Stark, M. J., Schmidt, M. C., and Hardie, D. G. (2003) Elm1p is one of three upstream kinases for the Saccharomyces cerevisiae SNF1 complex, *Current Biology 13*, 1299-1305.
324. Hedbacker, K., Hong, S. P., and Carlson, M. (2004) Pak1 protein kinase regulates activation and nuclear localization of Snf1-Gal83 protein kinase, *Mol Cell Biol 24*, 8255-8263.
325. Elbing, K., McCartney, R. R., and Schmidt, M. C. (2006) Purification and characterization of the three Snf1-activating kinases of Saccharomyces cerevisiae, *Biochem J 393*, 797-805.
326. McCartney, R. R., and Schmidt, M. C. (2001) Regulation of Snf1 kinase. Activation requires phosphorylation of threonine 210 by an upstream kinase as well as a distinct step mediated by the Snf4 subunit, *Journal of Biological Chemistry 276*, 36460-36466.
327. Ludin, K., Jiang, R., and Carlson, M. (1998) Glucose-regulated interaction of a regulatory subunit of protein phosphatase 1 with the Snf1 protein kinase in Saccharomyces cerevisiae, *Proc Natl Acad Sci U S A 95*, 6245-6250.
328. Jiang, R., and Carlson, M. (1996) Glucose regulates protein interactions within the yeast SNF1 protein kinase complex, *Genes & Development 10*, 3105-3115.
329. Dombek, K. M., Voronkova, V., Raney, A., and Young, E. T. (1999) Functional analysis of the yeast Glc7-binding protein Reg1 identifies a protein phosphatase type 1-binding motif as essential for repression of ADH2 expression, *Mol Cell Biol 19*, 6029-6040.
330. Sanz, P., Alms, G. R., Haystead, T. A., and Carlson, M. (2000) Regulatory interactions between the Reg1-Glc7 protein phosphatase and the Snf1 protein kinase, *Molecular and Cellular Biology 20*, 1321-1328.
331. Tabba, S., Mangat, S., McCartney, R., and Schmidt, M. C. PP1 phosphatase-binding motif in Reg1 protein of Saccharomyces cerevisiae is required for interaction with both the PP1 phosphatase Glc7 and the Snf1 protein kinase, *Cellular Signalling 22*, 1013-1021.
332. Ruiz, A., Xu, X., and Carlson, M. (2011) Roles of two protein phosphatases, Reg1-Glc7 and Sit4, and glycogen synthesis in regulation of SNF1 protein kinase, *Proc Natl Acad Sci U S A 108*, 6349-6354.
333. Wilson, W. A., Hawley, S. A., and Hardie, D. G. (1996) Glucose repression/derepression in budding yeast: SNF1 protein kinase is activated by phosphorylation under derepressing conditions, and this correlates with a high AMP:ATP ratio, *Current Biology 6*, 1426-1434.
334. Mashego, M. R., Jansen, M. L., Vinke, J. L., van Gulik, W. M., and Heijnen, J. J. (2005) Changes in the metabolome of Saccharomyces cerevisiae associated with evolution in aerobic glucose-limited chemostats, *FEMS Yeast Res 5*, 419-430.
335. Alterthum, F., Dombek, K. M., and Ingram, L. O. (1989) Regulation of Glycolytic Flux and Ethanol Production in Saccharomyces cerevisiae: Effects of Intracellular Adenine Nucleotide Concentrations on the In Vitro Activities of Hexokinase, Phosphofructokinase, Phosphoglycerate Kinase, and Pyruvate Kinase, *Appl Environ Microbiol 55*, 1312-1314.
336. Walther, T., Novo, M., Rossger, K., Letisse, F., Loret, M. O., Portais, J. C., and Francois, J. M. (2010) Control of ATP homeostasis during the respiro-fermentative transition in yeast, *Mol Syst Biol 6*, 344.